IMPROVED LOAD DISTRIBUTION FOR LOAD RATING OF LOW-FILL BOX STRUCTURES

By

Raju Acharya

Submitted to the graduate degree program in the Department of Civil, Environmental, and Architectural Engineering and the Graduate Faculty of the University of Kansas in partial fulfillment of the requirements for the degree of Master of Science.

……..

Chairperson, Dr. Jie Han

..……..

Dr. Robert L. Parsons

...……

Dr. Anil Misra

Date Defended: 12/04/2012

The Thesis Committee for Raju Acharya certifies that this is approved version of the following thesis:

IMPROVED LOAD DISTRIBUTION FOR LOAD RATING OF LOW-FILL BOX STRUCTURES

.....
Dr. Jie Han, Chairperson

Date approved: 12/04/2012

Abstract

Reinforced concrete box culverts are mostly used at shallow depths. Periodic evaluation of their load carrying capacities is required for load rating of the culvert by determining a rating factor (RF) or truck tonnage of a HS truck. The rating factor is defined as the capacity of the structure minus the dead load demand, and then divided by the live load demand. All the state DOTs are required to inspect and assess culvert conditions and capacities by load rating in every two years.

The distribution of live loads on the top slab of a box culvert plays a major role in determining the rating factor of the culvert. The current AASHTO guidelines do not consider the effects of pavements present above the fill while determining the load distribution. The distribution of the wheel load through a pavement may be different from that suggested by the current AASHTO guidelines. In addition to the pavement effect, the fill conditions (i.e., fill thickness and fill modulus) may affect the load distribution. Currently, there is lack of a design method to address the load distribution when a pavement is present above the fill.

In this research, two field tests were carried out on the culverts under rigid and flexible pavements respectively. The finite difference numerical models of the test culverts were created in the Fast Lagrangian Analysis of Continua in 3 Dimensions (FLAC3D) software and were verified against the field test results. The verified finite difference models of the culverts were used for a parametric study to analyze the effects of pavement type (i.e., flexible and rigid pavement), pavement thickness, fill depth, and culvert span on the pressure distribution. The material properties and boundary conditions used in the models for the parametric study were similar to the verified models.

The parametric study demonstrated that the intensity of vertical pressure on the top slab of the culvert gradually decreased as the pavement thickness increased. The vertical pressure under a rigid pavement was lower than that under a flexible pavement at the same pavement thickness. Within the range of the fill depth covered in this study, the intensity of vertical pressure decreased gradually with an increase of the fill depth over the culvert. The effect of the traffic load on the vertical pressure on the culvert was more significant at the lower fill depth and gradually decreased with the increase of the fill depth. The distribution of the vertical pressure at the fill depth of 0.6 m was characterized by a peak pressure under the wheel load and the peak pressure shifted to the middle of the axle at the fill depth of 1.2 m and greater. There was little interaction between the wheels at the fill depth of 0.6 m and, the interaction between the wheel loads was fully developed for the fill depth of 1.2 m and greater. The calculated vertical pressure decreased by increasing the culvert span from 1.8 to 5.4 m when the top slab thickness of the culvert was the same. However, when the top slab thickness increased, the vertical pressure at the larger span was close to that at the small span. The effect of the culvert span on the vertical pressure was negligible if the thickness of the top slab was properly designed.

The maximum vertical pressure obtained from the numerical analysis was compared with those by the distribution formulae in the AASHTO guidelines. The comparison showed that the current AASHTO guidelines over-estimated the pressure for low-fill culverts under a pavement. Simplified methods were developed in this study to estimate the vertical pressures under rigid and flexible pavements. In the case of the culvert under a rigid pavement, the total wheel load is distributed uniformly over the combined area with the extremities of the distributed areas by individual wheels. In the case of the culvert under a flexible pavement, the vertical pressure within the overlapped area is obtained by the superposition of the pressures due to individual

wheels. The calculated vertical pressures by the simplified methods were in good agreement with the maximum vertical pressures obtained by the numerical method.

Dedicated to my parents,

Mr. Narayan Prasad Acharya and Mrs. Kamala Acharya

Acknowledgements

First of all, I would like to express my great gratitude to my research advisor, Dr. Jie Han, for giving me the opportunity to complete my Master's thesis at the University of Kansas under his direction. Without his guidance, support, encouragement, and the excellent research environment, this thesis would not be possible. I appreciate the time he afforded for discussing my research and providing me with the invaluable suggestions for my future career. I am also grateful to my graduate advisory committee members, Dr. Robert L. Parsons, and Dr. Anil Misra, for their valuable comments and suggestions during the research and in the completion of this thesis.

This research was supported by Kansas Department of Transportation (KDOT). I would like to thank KDOT for sponsoring this study and making this thesis possible. Furthermore, I would like to appreciate Mr. James Brennan and his team at KDOT for their help during the field testing of the box culverts and obtaining of the test samples.

I would like to thank Mr. Jim Weaver and Mr. Matthew Maksimowicz for their technical supports. Besides, I am honored to be part of the Kansas University Geotechnical Society (KUGS) and I am grateful to its members including my colleagues and visiting scholars for their great support during this research. Their contributions to this research mean a lot to me. Finally, I would like to thank my parents for their continuous encouragement and endless love and support throughout my life.

Table of Contents

List of Tables

List of Figures

Chapter 1 Introduction

1.1 Background

Culverts are the structures constructed below highways and railways to provide access to the natural drainage across them. They are also constructed sometimes to provide the access to the animals across the road. The opening of the culvert is determined based on the waterway required to pass the design flood, whereas the thickness of the culvert section is designed based on the loads applied on the culvert. Historically different materials have been used in the construction of culverts and stone culverts were the pioneers in history of culverts. Culverts of different materials, ranging from rigid concrete to flexible thermal plastics came into use as buried or underground drainage structures in civil engineering. At present reinforced concrete culverts, steel culverts, and thermal plastics culverts are popular in practice. Circular, rectangular, and arch are the mostly used culvert shapes and the culverts with these shapes are called pipe culverts, box culverts, and arch culverts respectively. Culverts and bridges often serve the same purpose; however, they differ on the size of the structure. The Federal Highway Administration (FHWA) considers the drainage structure constructed across the road having a total span less than 6 m (20 ft) as culverts and above 6 m as bridges.

Culverts are classified as rigid, semi rigid or flexible based on material type, how they carry load, and to what degree they rely on the soil surrounding them. The capacity of a culvert to carry imposed loads depends on many factors including the type and age of the material, the size and shape of the culvert, and the supporting materials surrounding the culvert. Its capacity gradually decreases mainly due to aging and degradation of the material after repeated loading of the culvert by heavy trucks. The rate of the capacity reduction can be more significant if the fill

thickness over the culvert is small and/or the culvert is frequently subjected to heavy trucks. Reinforced concrete box culverts are most common type used at shallow depths than other culverts. Periodic assessment of their capacities is important for prolonged life of the culverts. The live load carrying capacity of the culvert is determined by load rating of the culvert. Load rating of a culvert is often done by evaluating a rating factor (RF) or truck tonnage of a HS truck. HS truck is the design truck specified by AASHTO. The rating factor is defined as the capacity of the structure minus the dead load demand, and then divided by the live load demand. In other words, the structure must have enough capacity after the dead load is subtracted to support the live load. If the rating factor falls below 1, the live load on the culvert should be reduced to maintain the culvert in a serviceable condition. The process of establishing the reduced live load on the culvert is called posting. All the state DOTs are required to inspect and assess culvert conditions and capacities in every two years by load rating.

The American Association of State Highway and Transportation Officials (AASHTO) provides three methods of determining load rating, namely Allowable Stress Rating (ASR), Load Factor Rating (LFR), and Load and Resistance Factor Rating (LRFR). Regardless of the rating method employed in load rating, the distribution of live loads on the top slab of the box culvert plays a major role in determining the rating factor of the culvert. AASHTO Standard Specifications and LRFD Code provide guidelines for determining the live load distribution on the culvert. The existing guidelines have been evolved through contributions of many researchers working on the load distribution on culverts in different eras. Recently more research has been carried out to modify the existing guidelines to provide more rational ways of load distribution over culverts.

1.2 Problem Statement

Culverts are installed at grade to different depths. The effect of the live load becomes more significant when they are installed at shallow depths. As load rating of culverts depends on how the live load is distributed on the culvert, a more rational approach of live load distribution over such a shallow fill culvert is important in determining its live load capacity. AASHTO Standard Specification for Highway Bridges (1992) considers the wheel load as a point load on the surface and distributes it on a square area having a width of 1.75 times the fill depth, H, above the culvert as shown in Figure 1.1. Whereas the AASHTO LRFD Code (2007) applies the wheel load on a rectangular area (t_l x t_w) of 0.5 m x 0.25 m on the surface as a tire footprint and distributes it on the culvert by increasing the tire footprint by H or 1.15 H depending on the type of fill as shown in Figure 1.2.

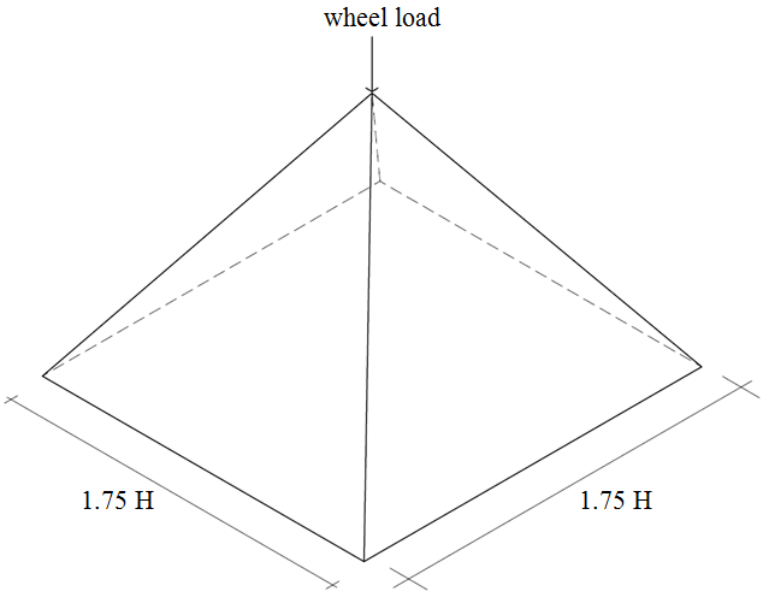

FIGURE 1.1 Wheel load distribution per AASHTO Standard Specifications

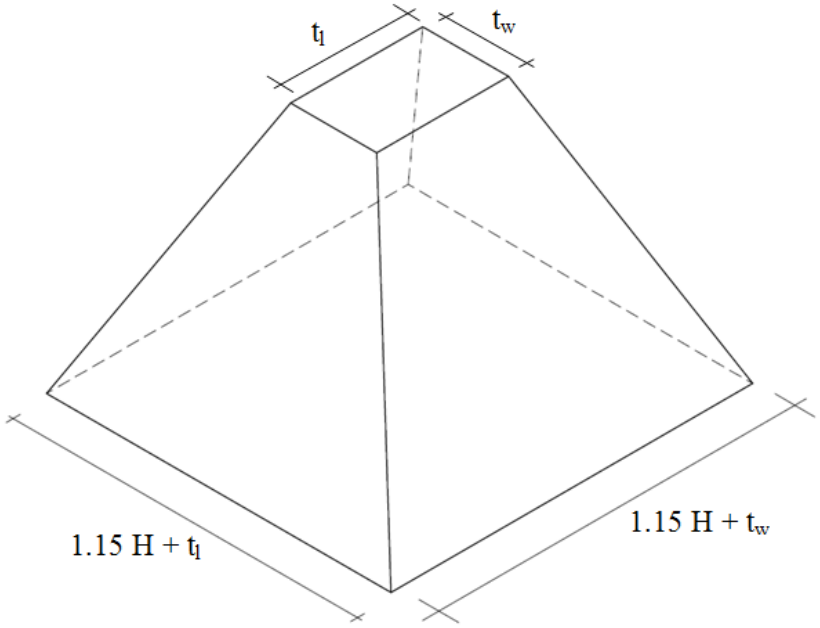

(a) For select granular backfill

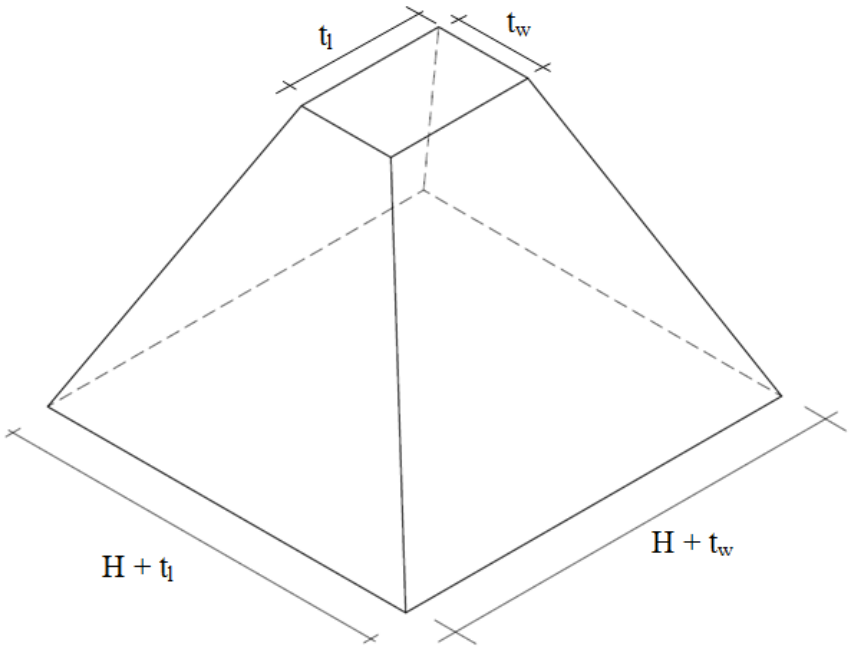

(b) For soils other than select granular backfill

FIGURE 1.2 Wheel load distribution per AASHTO LRFD Code

However, the current AASHTO guidelines do not consider the effects of pavements present above the fill while determining the load distribution. This distribution is valid for the design of the culvert when there is no pavement present above the fill, which more often occurs during construction. But in the case of load rating of existing culverts, pavements (rigid or flexible pavements) often exist above the fill. The distribution of the wheel load through a pavement may be different from that suggested by the current AASHTO guidelines. In addition to the pavement effect, the fill conditions (i.e., fill thickness and fill modulus) may affect the load distribution. Currently, there is lack of a design method to address the load distribution when a pavement is present above the fill.

1.3 Research objective

The objective of this research is to study the distribution of live load on the top slab of the low-fill concrete box culvert by considering the effects of pavement type (i.e., flexible and rigid pavements), pavement thickness, fill thickness, and span of the culvert. The test data and numerical results obtained from this research would provide a basis for the development of new load distribution guidelines for load rating of low-fill concrete box culverts with rigid or flexible pavements.

1.4 Research Methodology

The research methodology adopted in this research includes a comprehensive literature review of the research in this flied, two field tests on low-fill box structures (one under a rigid pavement and another one under a flexible pavement) using loaded trucks, calibration of numerical models in Fast Lagrangian Analysis of Continua in 3 Dimensions (FLAC3D) based on the field test results, a 3D numerical parametric study, and development of a design guideline for load

distribution considering the existence of a pavement. The following influence factors were investigated within typical design ranges in the parametric study: (1) flexible and rigid pavements, (2) pavement thickness, (3) fill thickness, and (4) culvert span. In the numerical analysis, pavements, box culverts, and all the soils were modeled as elastic materials.

1.5 Organization of Thesis

This thesis is divided into six chapters. Chapter One presents the background, problem statement, research objective, and research methodology. Chapter Two describes present state of knowledge in load distribution and load rating of box culverts and a literature review on wheel load distribution on low-fill box structures. The field testing of culverts and lab testing of the pavement materials and fill materials to determine their properties are presented in Chapter Three. Chapter Four presents the calibration and validation of the FLAC3D numerical models of the tested culverts. The parametric study carried out to determine the effects of different influence factors in load distribution is presented in Chapter Five. Conclusions and recommendations for future work are given in Chapter Six.

Chapter 2 Literature Review

This chapter presents a literature review on relevant topics of this research. It begins with the classification of box culverts as outlined in the literature, which is followed by descriptions on load rating, different levels and methods of load rating, and posting policy. Then, the AASHTO guidelines for load distribution for culverts are discussed in conjunction with the previous studies. Influence factors in load rating of box culverts are discussed thereafter. Finally, constitutive models for soil are discussed.

2.1 Classification of Box Culverts

Kansas Department of Transportation classifies box culverts in three categories based on the span: bridge box, 10 ft to 20 ft structure (3 m to 6 m structure), and road culvert (KDOT,2011). The KDOT Bridge Design Manual (2011) defines a bridge box as a structure having a width greater than 6 m measured along the centerline of the roadway from the inside faces of both exterior walls (including all span widths and the thicknesses of all interior walls). A box culvert with a total width of 3 m or greater (measured perpendicular to the centerline of box) but less than or equal to 6 m (measured along the centerline of the roadway)is considered as a 10 ft to 20 ft structure (3 m to 6 m structure). And, a road culvert is defined as a structure having a length of less than 3 m from the inside faces of both exterior walls measured perpendicular to the centerline of the box. The manual further classifies the box culverts as reinforced concrete box (pinned) and rigid frame box (fixed) based on wall to slab connection. A box designed with walls and slabs that are assumed to be simple spans (independent of one another) is a pinned box. A box designed with walls and slabs that are assumed to be continuous or connected to each other is called a fixed box. According to the type of installation, box culverts can also be

classified in three categories: embankment culvert, trench culvert, and imperfect trench culvert (Lawson et al. 2010, Yoo 2005, and Kang et al. 2008). Besides these methods, tunneling is also recognized as a method of installation of buried culverts (Sandford, 2010). Culverts installed on existing soil or fill and then covered by backfill as shown in Figure 2.1 are referred as embankment culverts. In such culverts even the well-compacted surrounding soil mass is less stiff than the combined culvert and soil column. Therefore, the backfill material around the culvert has tendency to settle more than the soil directly above the culvert. The relative stiffness of the combined culvert and soil column to the surrounding soil controls the magnitude and distribution of vertical pressures on structures (Lawson et al. 2010, Sun et al. 2011).

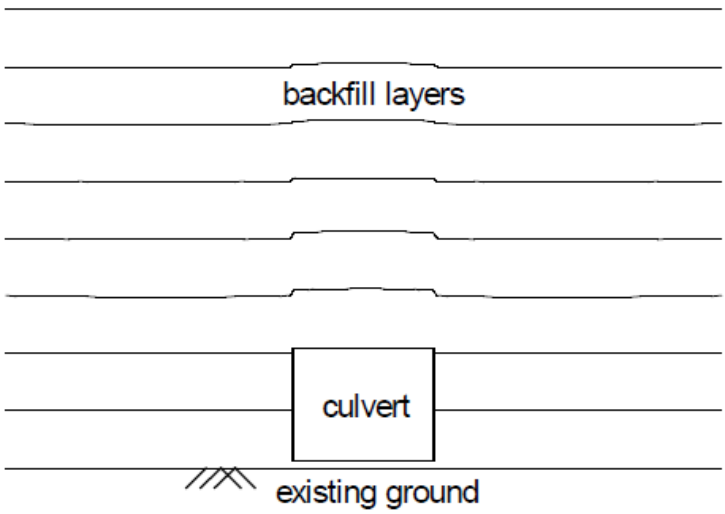

FIGURE 2.1 Embankment culvert (Lawson et al., 2010)

Figure 2.2 illustrates the trench installation. Trench installation culvert is mostly adopted in actual construction in field. Here the backfilled soil is less stiff than the surrounding in-situ soil and undergoes more settlement relative to the in-situ soil.

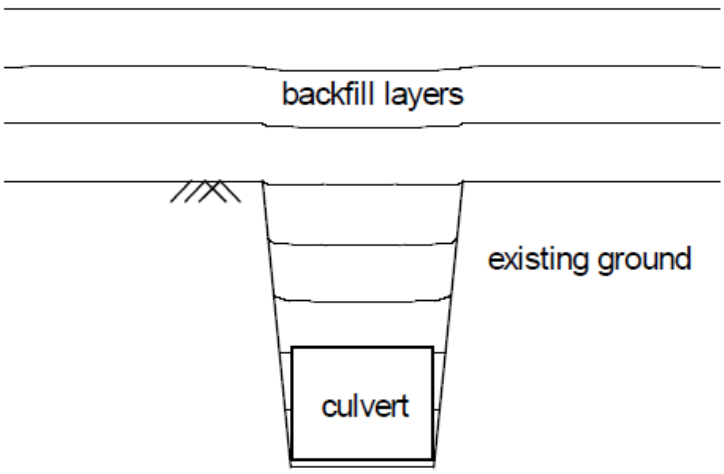

FIGURE 2.2 Trench culvert (Lawson et al., 2010)

Figure 2.3 shows an imperfect trench culvert, which is still a subject of research. Therefore it is not that popular in construction field as embankment and trench installation culverts. This kind of culvert is installed in a similar way as an embankment culvert with an exception that a layer of compressible material, such as geofoam, straw or compressive soil, is placed directly above the culvert. The remaining part of embankment is backfilled to the final level and compacted with a typical procedure. The compressible layer reduces the stiffness of the soil column to be less than that of the surrounding soil. Consequently, the settlement becomes comparable to the trench culvert and an imperfect trench culvert has the same load reduction behavior as the trench culvert (Kim and Yoo 2005, Kang et al. 2008, Lawson et al. 2010). An instrumented field test carried out by Sun et al. (2011) found that the vertical stresses were greatly reduced by using the imperfect trench technique. The vertical stresses acting on the culvert were only about 9% to 11% of those occurring on the portion of the culvert where an imperfect trench was not used.

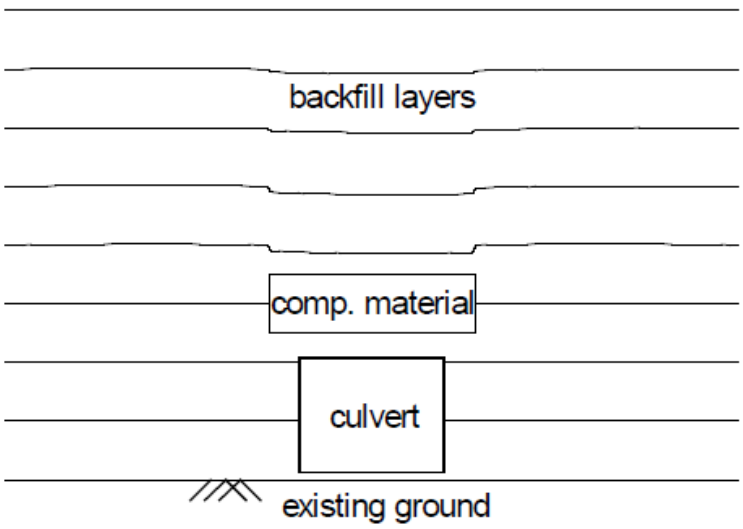

FIGURE 2.3 Imperfect trench culvert (Lawson et al., 2010)

2.2 Load Rating

On December 15, 1967, the Silver Bridge on the U.S. 35 Highway between Point Pleasant in West Virginia and Gallipolis in Ohio collapsed, which killed 46 people and injured 9. The investigation revealed that a cracked eyebar created extra stress on other members of the bridge, which ultimately caused the collapse. The incident raised national concern on the condition of bridges, which led to the establishment of the National Bridge Inspection Standards (NBIS) in early 1970s (Jaramilla and Huo 2005). Since then the Federal Highway Administration (FHWA), the American Association of State Highway and Transportation Officials (AASHTO), and other agencies have developed guidelines for inspecting and maintaining existing bridges. The idea of the load rating of the bridges evolved from there.

Load rating, in general, involves the determination of live load capacities of culverts or bridges. The American Association of State Highway and Transportation Officials (AASHTO) defines load rating as the maximum truck tonnage, expressed in terms of HS load designation, permitted

across a culvert. KDOT Bridge Design Manual (2011) describes load rating as the analysis of culverts and bridges performed to determine the live load that structures can safely carry.

The culvert load rating process is part of the regular inspection process. It involves the process of determining the safe load-carrying capacity of the culvert structure, and finding whether design, legal or permit vehicles can safely cross the culvert, thus determining if the culvert needs to be restricted and if so, what level of load posting is required. Load rating is carried out based on the current culvert condition and needs analysis and engineering judgment by comparing the culvert structure's capacity and dead load demand to live load demand (Lawson et al., 2009). A complete description of an as-built bridge, modifications since it was built, and its present condition are the necessary information required to load rate a bridge (KDOT, 2011). Load rating engineer performs a detailed inspection of the culvert beforehand. If the plans are not available, a set of measurements become necessary to determine the dimensions of the culvert that are needed in capacity and demand calculations. Actual conditions of the culvert are represented in the calculations by considering reduction in the section, if any, and reduced resistance of the materials. Areas of deterioration become a special concern during field inspection because a member reduced in its section may control the capacity of the structure.

Jaramilla and Huo (2005) pointed out three major needs for a bridge owner to carry out load rating. Firstly, the culverts deteriorate gradually during their long service life, thus accessing their reduced capacities becomes important to ensure that the culverts can perform safely under current traffic loads. Secondly, all existing culverts were constructed using different design loads, material strengths, and design methods at different times based on the design standards evolved at that time. So it becomes necessary to load rate them for the current traffic condition and using the current specifications. Lastly, permit rating is required for the culvert carrying a

load more than the legal load. Heavy or frequent permit vehicles can cause permanent damage to the structure if its capacity is not determined appropriately.

Numerical analysis is carried out to find the structural response at critical sections based on loading. The outcome of the analysis will be used as an input to the load rating equation to determine the appropriate load rating. Results obtained from load rating provide information whether the culvert needs to be restricted to reduced loads, help identify culvert components that require rehabilitation, or help devise retrofitting measures to avoid the posting of the culvert (KDOT, 2011). If a culvert is not safe enough to carry the loads allowed by State Statute, it is posted at lower capacity. Kansas State Statutes permits a gross vehicle weight of 80,000 pounds (355 kN) on the Interstate and 85,500pounds (380 kN) on other highways without a special permit.

2.2.1 Levels of Load Rating

Bridges are load rated at two different levels, referred to as "Inventory Rating" and "Operating Rating" (KDOT, 2011). Inventory Rating is the load level which a structure can safely withstand for an indefinite period of time. And, Operating Rating is the absolute maximum permissible truck load that may be on the culvert. Thus, the Inventory load level is approximately comparable to the design load level for normal service conditions and Operating Rating is indicative of the capacity of the structure for occasional use. If unlimited numbers of vehicles are allowed on the structure at the operating level, it will reduce its service life. This value is typically used when evaluating overweight permit.

AASHTO Bridge Evaluation Manual (2011) suggests the equation for the rating factor as follows:

$$RF = \frac{C - A_1\ D}{A_2\ L(1 + I)} \tag{2.1}$$

where: RF = the rating factor

C = the structural capacity of the member

D = the dead load effect on the member

L = the live load effect on the member

I = the impact factor

A_1 = factor for dead loads

A_2 = factor for live loads

Equation 2.1 clearly indicates that the main factors for load rating are the culvert capacity, the dead load demand, and the live load demand. AASHTO policy provides guidelines for calculating the section capacity considering the reduction in the material capacity based on age and condition of deterioration of culvert components. Whereas dead load and live load demands are determined by computer analyses. This simple load rating equation offers a real challenge to obtain reliable values for each of these governing factors. It is because AASHTO has not suggested any particular tool for analysis of dead load and live load effects. And the output of the analysis varies with the simulation technique used. It is compulsory to determine rating factors using Equation 2.1 for each critical section of the culvert like corners, mid-spans, top and bottom slabs, and interior and exterior walls, for each demand type (moment, shear, and thrust), for maximum and minimum load envelopes at both inventory and operating rating levels. Critical sections of a culvert for moment are shown in Figure 2.4. Of all the computed rating factors, the

lowest inventory rating factor and the lowest operating rating factor control the load rating for the culvert (Lawson et al., 2009).

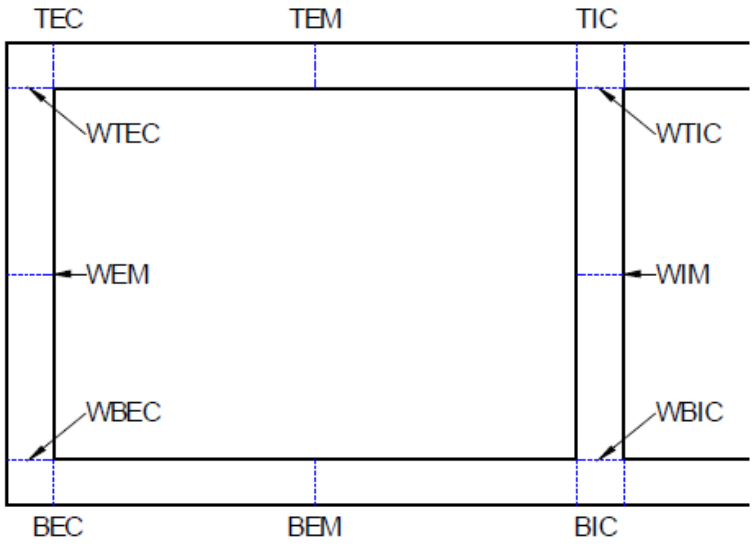

FIGURE 2.4 Moment critical sections for a culvert without haunches (Lawson et al, 2010)

Abbreviations for the typical critical sections shown in Figure 2.4, listed clockwise, are: top exterior corner (TEC), top exterior mid-span (TEM), top interior corner (TIC), top interior mid-span (TIM), wall top interior corner (WTIC), wall interior mid-span (WIM), wall bottom interior corner (WBIC), bottom interior mid-span (BIM), bottom interior corner (BIC), bottom exterior mid-span (BEM), bottom exterior corner (BEC), wall bottom exterior corner (WBEC), wall exterior mid-span (WEM), and wall top exterior corner (WTEC). For multiple-span box culverts, the sections are designated as per the culvert span, e.g., TIC1, TIC2, BIC1, BIC2, etc.

Variability in the way of assessing the culvert capacity, dead load demands, and live load demands leads to varying rating factors. Original construction documents and the material property assumptions used in the design provide bases for calculating the capacity. But they need to be used in conjunction with visual inspection of culvert conditions. The demand

calculation process is carried out through analytical modeling. The AASHTO guidelines provide values for all input parameters, such as soil unit weight, equivalent fluid weight for lateral loads, and live load distributions through the soil. But AASHTO guidelines are not specific on the analytical model and the way of applying the loads to the model. Thus load rating engineers should make decisions about modeling practices and procedures. And the assumptions, simplifications and mathematical structures of demand modeling tools can have a significant effect on the culvert load rating analysis (Lawson et al., 2009).

A bridge's response depends not only upon the total weight from a vehicle, but also upon the axle configuration and the distribution of loads between the axles (KDOT, 2011). Since it is not pragmatic to rate a bridge for countless number of possible axle configurations, KDOT has a policy to load rate highway bridges for eight standard vehicles which closely represent the actual vehicles on highways. These are called the rating trucks and are divided into five categories as shown in Table 2.1. The KDOT manual also stresses on requirements to load rate all the bridges for the same trucks to achieve the consistency on the local and state system bridges. The standard truck is the "H" truck, which is a design truck."T-3", "T3S2", and "T3-3" are recommended by AASHTO. FHWA requires the "HS". The "T130" and "T170" are used for special permits on state highways. And, the heavy equipment transport (HET) truck is required by KDOT (KDOT, 2011).

TABLE 2.1 Trucks being used for load rating KDOT bridges (KDOT, 2011)

	Max gross weight (tons)	Posting weight (tons)	Location on posting sign
Single Truck:			Top
H Unit	20.0	12.5	
Type 3 Unit:	27	25	
Truck-tractor Semi-Trailer			Middle
HS Unit	36.0	22.5	
Type 3S2 Unit	36.0	36	
Truck Trailer and LCV's:			Bottom
Type 3-3 Unit	40	40	
Permit:			N/A
Type T130 Unit	65.0		
Type 170 Unit	85.0		
Special Kansas:			N/A
Heavy Equipment Transport:	109.9		

The choice of KDOT on Standard Load Rating Trucks is based on several years of truck weight data collected in Kansas and also based on the recommended AASHTO Maintenance Rating Trucks (KDOT, 2011). The KDOT manual (2011) explains two reasons for using H-Trucks and HS-Trucks for load rating - one is their familiarity in design and other is conservative. The maximum axle loads allowed on the Kansas highway system are 10 tons for a single axle and 17 tons for a dual axle, with a maximum weight not to exceed 42.75 tons (40 tons on the Interstate), without special permits. The weight on a group of axles is limited by Kansas statutes K.S.A. 8-1908 and 8-1909.

2.2.2 Load Rating Methods

Load rating methods include load testing and analysis (KDOT, 2011). Load testing of the culvert for load rating is not economic. Therefore load testing is carried out only in special conditions

where an analytical method cannot be used due to some specific difficulties. In the analysis method of load rating, commercially available software are used to determine the live load and the dead load demands for each of the culvert responses (moment, shear, and thrust). Culverts can also be load rated by load testing and calibrating the finite element/difference model and subsequently carrying out analysis for load demands (Yost et al. 2005, and Chajes and Shenton2005). Load testing method helps to eliminate the unreliable conditions. Approximately 95% of bridges out of more than 200 bridges analyzed by Yost et al. (2005) obtained higher load rating by load testing method. Schulz et al. (1995) also stated that this method could increase the rating of the bridges but they also presented an example showing where the rating decreased. Load testing method is more convenient for steel structures than concrete structures. Chajes and Shenton (2005) outlined four important factors load testing method could establish that affect load rating, including (1) lateral load distribution, (2) support fixity, (3) composite action, and (4) effects of secondary members.

The Manual for Bridge Evaluation (AASHTO, 2011) included three methods of analysis to load rate a structure, i.e., load and resistance factor rating (LRFR), allowable stress rating, and load factor rating (LFR). KDOT design manual (2011) included two methods of analysis used to load rate structures: the Load Factor Rating (LFR) method and the Load and Resistance Factor Rating (LRFR) method. Working stress method is also used by some DOTs to load rate their bridges (DelDOT Manual, 2005). KDOT used the Load Factor Rating Method to load rate bridges since 1988. The philosophy of LFR method is to use smaller factors of safety for more predictable loads (such as dead loads) and higher factors of safety for less predictable loads (such as live loads). The introduction of new criteria, such as load modifiers, multiple presence factors, change in distribution of live loads and dynamic load allowance, in the LRFR method sometimes

produces a rating factor less than 1.0 for the bridges which passed the criteria in the LFR method (NCHRP,2011).

The introduction of the LRFD specification for highway bridges by AASHTO in 1994 made it necessary to develop a new bridge evaluation manual to be consistent with the specification. NCHRP Project 12-46 was initiated in March 1997 to develop a new AASHTO LRFR manual for bridge evaluation (Shivakumar, 1999). The AASHTO Manual for Bridge Evaluation (2011) incorporated the load and resistance factor methodology for load rating of bridges. This method needs the use of site specific information to support an Engineer's judgment on the safe rating level for a particular bridge. Under this specification, a bridge's rating may be improved by making use of options related to thorough inspection and maintenance or control of heavy overloads (KDOT, 2011).

The current policy at KDOT is to load rate all structures using the LFR method. However, a structure designed or rehabilitated with the Load and Resistance Factor Design (LRFD) is also rated using the LRFR Specification. For purposes of reporting to FHWA, the HS-type truck is used for LFR rating and HL-93 loading is used for LRFR (KDOT, 2011).

Rund and McGrath (2000) compared all the provisions from the AASHTO standard specifications and the AASHTO LRFD code for precast concrete box culverts. The analysis conducted on several combinations of box culvert sizes and fill depths under both specifications revealed that the provisions from the LRFD code yielded higher design loads and therefore required more area of steel reinforcement. More steel was particularly required by the low-fill culverts having fill 2 ft (0.6 m) or lower. Thus the low-fill culverts constructed according to LRFD code yield higher capacities and hence higher load rating than that from the LFD method.

2.2.3 Analytical Steps for Load Rating

The analytical steps that are followed to load rate each member are similar and independent of the type of member and the role played by the member in the overall structure. The method of analysis varies with any of the steps for each member, depending on the member and the choice of LFR or LRFR, but the function of the calculations is the same. KDOT's Design Manual (2011) summarizes the following analytical steps:

1. Determination of section properties.

2. Determination of allowable and/or yield stresses.

3. Calculation of section capacity.

4. Determination of dead load effect.

5. Calculation of dead load portion of section capacity.

6. Calculation of live load effect.

7. Calculation of live load impact and distribution.

8. Calculation of allowable live load

2.2.4 Posting Policy

The 1995 FHWA publication Recording and Coding Guide of the Structure Inventory and Appraisal of the Nation's Bridges states: "Although posting a bridge for load-carrying capacity is required only when the maximum legal load exceeds the operating rating, highway agencies may choose to post at a lower level." This statement means, although posting becomes necessary when one or more of the legal trucks give lower operating rating than its own legal weight, this

statement gives freedom to local authority to post the bridge at an appropriate level depending on engineering judgment and/or the recommendation of their consultant. However, posting of culvert at particular level should not shorten the life of the culvert and the level of posting must be less than or equal to the operating rating. KDOT commonly employs a level of posting that is approximately midway between inventory and operating rating. The public authority responsible for inspection and maintenance of the structure has the authority to post anywhere within this range. It may not be wise or advisable to commonly post the culvert near the operating rating (KDOT, 2011).

The KDOT manual (2011) also indicates an option of posting a speed limit. Reduced speed reduces the impact and raises or eliminates the need for posting. This alternative is not generally considered feasible and has not been used by KDOT. If a bridge is not capable of carrying three tons at the operating level, KDOT closes that bridge. As per the manual, if a structural rating is low, the Local Authority should consider using the Load Factor Method and post the culvert at the operating rating as the maximum posting value. However posting the culvert at operating rating should be employed only with more frequent inspections, for short term or until repair or rehabilitation can be done.

If the inventory and operating rating factors are greater than 1.0, the culvert will be unrestricted (Lawson et al., 2010). Because the culvert load rating is obtained by multiplying the rating factors by the tractor tonnage (i.e., 20 tons for HS-20 trucks) to determine the operating (OR) and inventory (IR) load ratings. On the other hand, if either of the inventory rating factor or operating rating factor is less than 1.0, the culvert may be subjected to load posting. In some cases the load rater may prefer to perform the analysis again using a higher level of model sophistication to avoid posting as an alternative.

2.3 AASHTO Guidelines for Load Distribution

AASHTO Standard Specifications for Highway Bridges and AASHTO LRFD code are two main documents which provide the guidelines about the live loads in the design of the box culverts. The same guidelines are being used for the load rating application too. AASHTO introduced the Load and Resistance Factor Design (LRFD) Bridge Design Specification methodology in 1994. Before the introduction of the LRFD code, the Standard Specifications was the only guideline for determining the live loads on the culverts. The aim of the LRFD code is to provide a reliability-based code which can offer more consistent level of safety than the existing Standard Specifications. Both guidelines used load factors and strength reduction factors. The LRFD specification not only included load factors and strength reduction factors but also added provisions for load modifiers, multiple presence factors, design vehicle loads, distribution of live loads through fill, and dynamic load allowance.

A load factor accounts for the uncertainty inherent in the specific load or combination of loads whereas the load modifiers relate mainly to ductility, redundancy and importance of a particular component of the structure or the structure as a whole. The Standard Specification did not use the concept of the load modifiers, even though it included the provision of load factors. The LRFD code used a load factor of 1.75 as compared with the load factor of 2.17 used by the Standard Specification. However, this change in the load factor in the code is covered by the introduction of multiple presence factors. The values of the multiple presence factors depend on the numbers of loaded lanes. According to the LRFD Specification, the multiple presence factor is 1.2 for a single loaded lane, 1.0 for two loaded lanes, 0.85 for 3 loaded lanes, and 0.65 for 4 or more loaded lanes.

The design vehicle load was another important factor changed from the Standard to the LRFD code. Design truck and design tandem are two design vehicles specified by the LRFD code. Design truck is the same as the HS20 truck as specified in the standard specification. The axle load for the design tandem is increased from 24 to 25 kip (107 to 111 kN) from standard specification to LRFD code. Figures 2.5 and 2.6 show the design truck and design tandem respectively. Furthermore, the LRFD code specifies that both the design truck and design tandems should be accompanied with the design lane load of intensity 640 lb/ft (8 kN/m) uniformly distributed over a lane width of 10 feet (3 m).

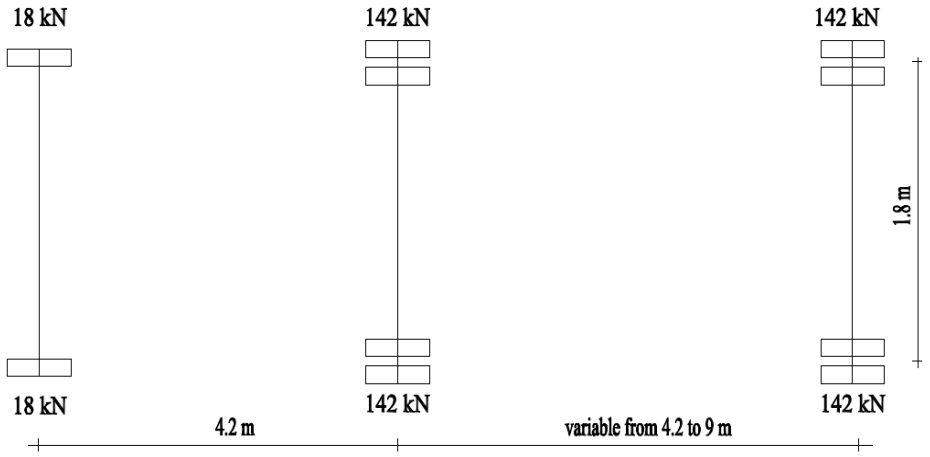

FIGURE 2.5 Design truck HS20 (AASHTO, 2007)

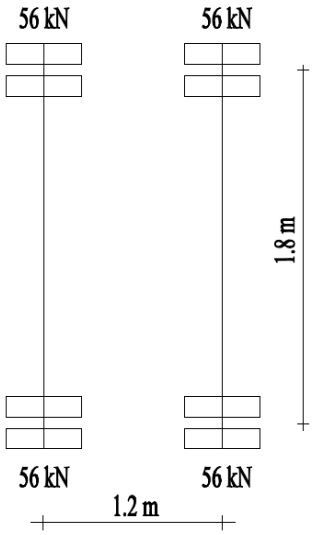

FIGURE 2.6 Design tandem (AASHTO, 2007)

The AASHTO LRFD code (2007) defines the tire contact area of a wheel consisting of one or two tires to be a single rectangle, whose width and length are 20 in (0.5 m) and 10 in (0.25 m), respectively. The tire pressure is assumed to be uniformly distributed over a contact area.

2.3.1 Dead Loads

AASHTO provides the guidelines for the dead load to be used in load rating. AASHTO has modified its guidelines over the years to impose more load on culverts. In-service culverts, which were built many years ago, must be reanalyzed using the current AASHTO methods. Many researchers, for example M. K. Tadros, T. J. McGrath, A. M. Abdel-Karim, have contributed to the determination of the loads on culvert top, base and sides.

The development of the AASHTO provision for culvert design began with the American Association of State Highway Officials' (AASHO) standard specification for highway bridges in 1949. AASHO (1949) adopted the unit weight of compacted sand, earth, gravel or ballast as 120 pcf (18.85 kN/m^3). According to AASHO (1949), the earth load on a culvert could be computed

ordinarily as the weight of earth directly above the slab. AASHO (1949) allowed the effective weight of the soil to be taken as 70% of its actual load to calculate the design load on the culvert.

In 1983, the AASHTO standard specifications defined the effective horizontal unit weight as 30 pcf (4.7 kN/m^3). All the AASHTO standard specifications before 1987 allowed the use of verticalsoil pressure of 0.7 times the pressure due to equivalent fluid having unit weight of 120 pcf (18.85 kN/m^3) and horizontal soil pressure due to equivalent fluid having unit weight of 30 pcf (4.7 kN/m^3) (Abdel-Karim et al., 1993). Tadros et al. (1987) concluded that the earlier AASHTO specifications were unconservative for the soil loads. The AASHTO interim report released in 1987 to update the 1983 standard specifications revised the lateral soil pressure to vary from pressure due to equivalent fluid having unit weight of 30 to 60 pcf (4.7 to 9.4 kN/m^3). This report also removed the vertical pressure reduction factor of 0.7 (Abdel-Karim et al. 1993, Kim and Yoo 2005). In 1990, the AASHTO standard specifications was further updated by including an equation for calculating the earth pressure on the reinforced concrete box structures, which included a soil-structure interaction factor for embankment and trench installations. It was the first time when the soil-structure interaction of reinforced concrete box culverts was addressed by the AASHO standard specifications. This method for determining the soil pressure was continued in the later editions of the AASHTO standard specifications (Lawson et al., 2010). Culvert load rating parameters associated with these installation methods should be used as specified by the AASHTO Manual for Bridge Evaluation.

A lateral dead load is applied as a pressure from equivalent fluid on the side walls of the culvert. Any of the AASHTO standard specifications does not include any provision for the requirement and geometry of the side fill for box culverts. However, the Yoo et al. (2005) study showed that compaction of the side fill had a significant effect on the behavior of the box culvert. According

to Lawson et. al. (2009), current AASHTO standard specification requires using a lateral pressure of equivalent fluid having a unit weight of 60 pcf (9.4 kN/m^3) for total load case and 30 pcf (4.7 kN/m^3) for reduced load case. The total load case generates the maximum axial and shear demands in all components of the culvert whereas it creates the maximum moments in all critical sections except the top and bottom slab mid-spans. The reduced lateral load case is analyzed to determine the maximum moments at positive moment sections. This load creates a worst case loading for the slabs by reducing the deflection of the walls caused by the lateral loads. Lateral live load surcharge is not considered in this case to further reduce the amount of the lateral pressure.

Yoo et al. (2005) stressed that the behavior of the box culvert was dependent largely on the method of installation than the yielding or unyielding type of the foundation. Furthermore, Lawson et al. (2010) stated soil arching and culvert deformation as two primary factors that determine the magnitude and distribution of soil loads on a culvert. Soil arching, which is the result of the differential settlement in soil, has an indeterminate effect on soil load. When one section of soil settles more than its adjacent section, shear stresses develop to resist the settlement. Soil arching on the culvert depends primarily on the type of culvert installation.

Negative arching effect occurs in embankment installation culvert. In embankment installation culvert, the combined column of culvert and soil is stiffer than the surrounding soil. When the surrounding soil settles more than the soil above the culvert, shear planes develop along the interface between soil and culvert. These shear forces transfer some of the adjoining soil weight onto the culvert. As a result, the culvert carries the weight of the soil column directly above it as well as some of the surrounding soil weight. Figure 2.7 shows this negative soil arching effect. As the soil continues to settle over time the load will continue to increase. Some studies

suggested that the increased load might be as much as twice the weight of the in-situ soil column (Tadros 1986, Yang 1997, Yang1999, Kang et al.2008, Sandford2010).

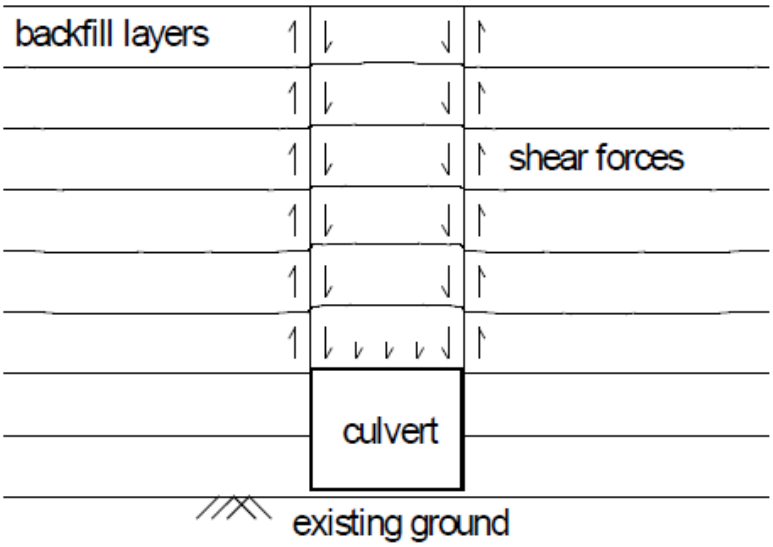

FIGURE 2.7 Embankment culvert installation (Lawson et al., 2010)

Positive arching occurs in trench installation culverts and imperfect trench culverts, in which the combined culvert-soil column becomes less stiff and has a larger settlement than the adjoining soil. Therefore the shear stress and load changes are in the opposite direction than those in the embankment installation culvert. The resulting load reduction can be less than half the weight of the soil column. Figure 2.8 shows this positive soil arching effect (Dasgupta and Sengupta1991, Vaslestad et al. 1993).

To account for the soil structure interaction, AASHTO LRFD code (2007) allows the use of the soil structure interaction factor F_e. Soil structure interaction factor as given in equation 2.2 incorporates the increase in the soil load due to negative arching in embankment installation culverts. A relatively lower value of F_e is suggested if the soil is compacted. The soil structure

interaction coefficient is 1.15 for installation with compacted backfill or 1.4 if the fill is uncompacted along the sides of the box section.

$$F_e = 1 + \frac{0.2\ H}{B_c} \tag{2.2}$$

where F_e= soil-structure interaction coefficient for embankment installation culvert

H= fill depth above the culvert

B_c= outside width of the culvert

The soil-structure interaction coefficient for a trench installation culvert, where positive arching occurs, is given by Equation 2.3.

$$F_t = \frac{C_d\ B_d^2}{H\ B_c} \leq F_e \tag{2.3}$$

where F_t= soil-structure interaction coefficient for a trench installation culvert

B_d= width of the trench

C_d= load coefficient for trench installation culvert

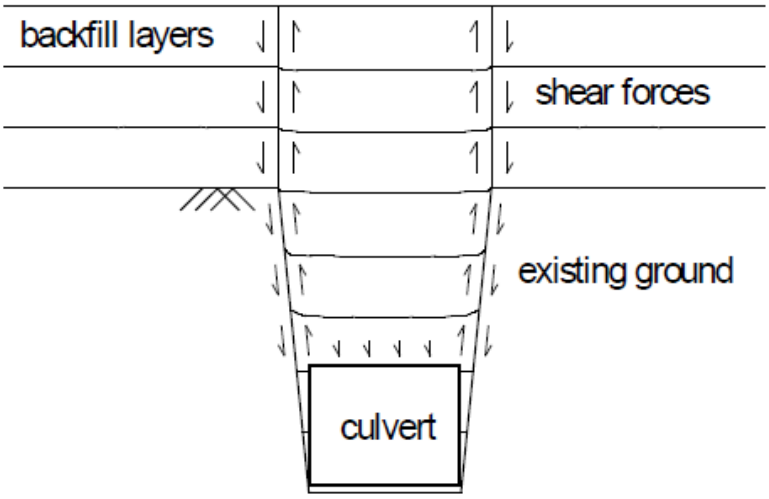

FIGURE 2.8 Trench installation culvert (Lawson et al., 2010)

The nature of the deflection of the culvert also affects the load acting on the culvert. This is also indeterminacy in the soil-culvert system. When the top and bottom slabs of the culvert deflect, the soil begins to transfer the load away from the center of the span to the outside of the culvert. The stress transfer causes a decreased load in the mid-span and an increased load near the supports. As a result, the moment at the mid-span decreases. As shown in Figure 2.9, the actual pressure distribution was found to be parabolic instead of uniform (Katona and Vittes1982, Dasgupta and Sengupta1991, Lawson et al. 2010). Oswald (1996) indicated the possibility of load redistribution resulting from creep.

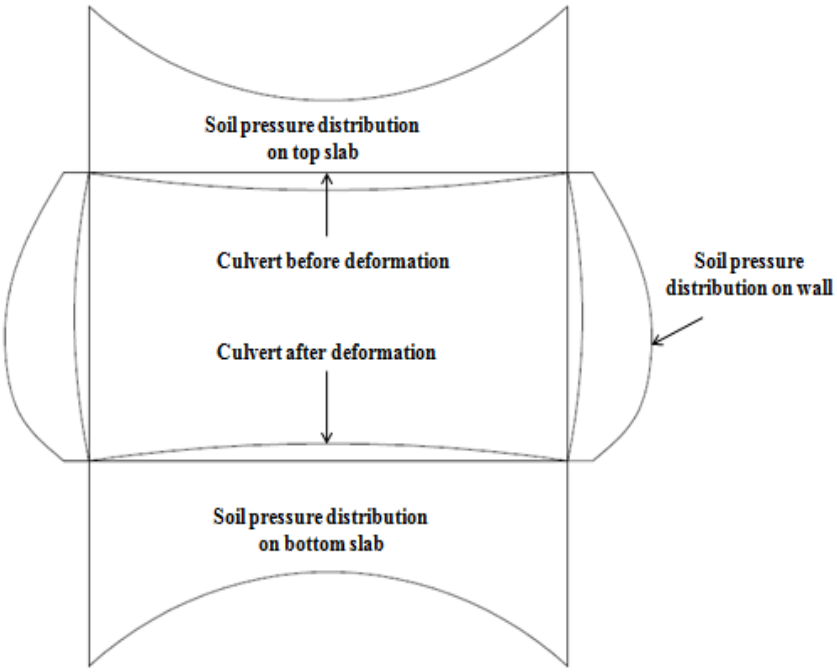

FIGURE 2.9 Culvert deflection and resulted pressure distribution (Lawson et al., 2010)

Lateral loads also produce deflections of the culvert members, which affect the loads around the culvert. Nature of such deflection is opposite to that induced by the vertical pressure (see Figure 2.10). This effect causes decreases in moments in the top and bottom slabs but increases in the walls (Awwad, 2000). Yang et al. (1999) carried out two field tests on culverts to study the earth pressures on the culvert roofs and walls and carried out a parametric analysis using the finite element method. This study revealed that the prevailing AASHTO (1996) load distribution factors for the soil load were unconservative. The lateral soil pressure was found to be dependent on backfill modulus with a higher modulus yielding a higher pressure. Relatively higher pressures were observed near the base of the culvert, which induced a high shear stress on the bottom of the wall.

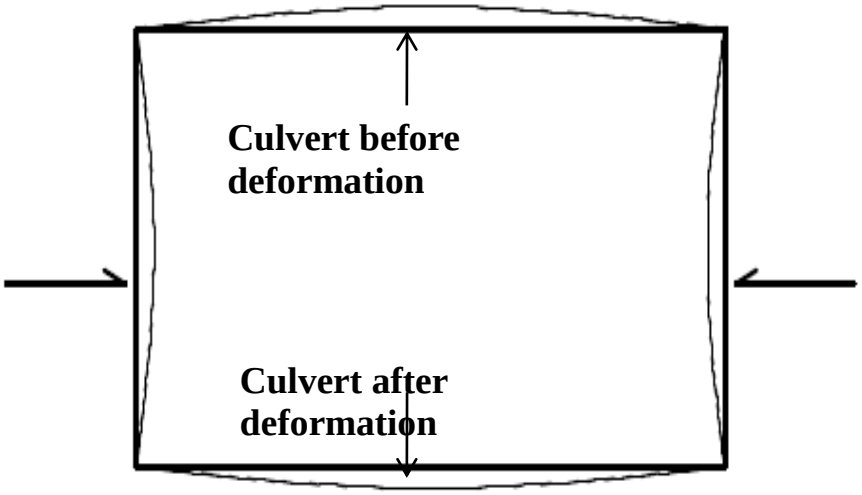

FIGURE 2.10 Deflection of culvert under lateral loads (Lawson et al., 2010)

From the literature, it becomes apparent that the AASHTO guidelines for the soil loads in embankment culverts are un-conservative, and those for the trench and imperfect trench culverts are over-conservative. Lawson et al. (2010) indicated the possibility for trench and imperfect trench culverts that a more refined analysis could minimize the over-conservatism in load ratings and still maintain an acceptable factor of safety. However, this approach may not be applicable for very old culverts because the soil overburden stresses may become stable over time and do not have any installation effect on soil pressure. As far the load rating is concerned, consideration should be taken on the effect of the culvert deflection on the soil pressure.

2.3.3 Impact Factors

The AASHTO Standard Specification for Highway Bridges (1992) allows the live loads to be increased by an improvement factor to consider the dynamic, vibratory and impact effects. This specification limits the impact factor only to the culverts with a fill depth up to 3 ft (0.9 m) and allows the impact to be reduced by steps as shown in Table 2.2. It is recommended that the impact factor be 20% for a fill depth ranging from 1’-0” to 1’-11” (0.3 m to 0.6 m), 10% for a fill

depth from 2’-0” to 2’-11” (0.6 m to 0.9 m), and 0% for a fill depth 3’-0” (0.9 m) or greater. On the other hand, the Article 3.6.6.2 of AASHTO LRFD code (2007) suggests increasing loads for impact effects by 33% for a zero fill depth. The effect does not drop to 0% until the fill depth is 8 ft (2.4 m). At fill depths of 2 to 4 ft (0.6 to 1.2 m), the AASHTO LRFD code (2007) suggests the loads about 15 to 20% higher than the AASHTO standard specifications (NCHRP, 2010).

TABLE 2.2 Impact factors given by AASHTO standard specification (AASHTO, 1992)

Fill depth	Impact Factor (I)
0' to 1'-0"	30%
1'-1" to 2'-0"	20%
2'-1" to 2'-11"	10%
$\geq$ 3’	0

However KDOT uses a straight line interpolation for this impact, as given in Equation 2.4, to avoid the severe jumps in the live load moments caused by the steps shown in the AASHTO standard specifications.

$$\% \text{ Impact: } 0 < 30 - [(F - 1) \times 10] < 30 \qquad (2.4)$$

where F = fill depth in feet

2.3.2 Live Loads

Both the AASHTO standard specifications (1992) and AASHTO LRFD code (2007) indicate that for culverts with less than 2 ft (0.6 m) of fill, the soil does not distribute the wheel load considerably and suggest that the culvert should be designed as a direct slab for the fill depth less than 2 ft (0.6 m). Several researchers have expressed their concerns about the inconsistencies

that this assumption creates and indicated that the AASHTO guidelines greatly underestimate actual soil pressures (for example, Tadros et al. 1989, Abdel-Karim et al.1990, Yang1999). The provision for the distribution of the live load was also changed from the AASHTO Standard specification (1992) to the LRFD code (2007). Both AASHTO guidelines use the equivalent strip method for a fill depth less than 2 ft (0.6 m). Article 3.24.3.2 of the AASHTO standard specifications (1992) provides a single equation (Equation 2.5) for the distribution width, E, for a single wheel load on the top slab of a box culvert for a fill depth less than 2 ft (0.6 m). A distribution width of 2E is used for the calculation of pressure for the axle load (McGrath et al., 2005).

$$E = 1.2m + 0.018\,S \leq 2.1m \quad for\ H < 0.6\,m \tag{2.5}$$

where E is the distribution width and S is the effective span length in meter

The AASHTO LRFD code (2007) on the other hand provides a separate distribution width for the positive moment and negative moment as shown in Equations 2.6 and 2.7 respectively. Table 4.6.2.1.3-1 of the LRFD code provides distribution width, which depends on the span of the culvert, for an axle load.

$$E = 0.65\,m + 1.98\,S \quad for\ positive\ moment \tag{2.6}$$

$$E = 1.2\,m + 0.9\,S\ for\ negative\ moment \tag{2.7}$$

The above equations are valid only for a span less than or equal to 15 ft (4.5 m). For box sections with spans greater than 15 ft (4.5 m), Article 4.6.2.3 of AASHTO LRFD code (2007) provides the distribution width which depends on the span of the box and the total length of the bridge as well as shown in Equation 2.8.

$$E = 0.25\,m + (0.09SW_1)^{0.5} \quad (2.8)$$

where, W1 is the modified edge-to-edge width of the bridge in meter, which is limited to a maximum value of 60 feet (18 m) for multiple lane loading and 30 feet (9 m) for single lane loading.

Calculations using the above equations for a fill depth less than 2 ft (0.6 m) show that the AASHTO LRFD provision (2007) for spans greater than 15 ft (4.5 m) give similar distribution widths to the AASHTO standard provision (1992). However, for the span lengths less than 15 ft (4.5 m) the AASHTO LRFD provision gives smaller distribution widths. Therefore, the AASHTO LRFD provisions are more conservative than the AASHTO Standard provisions for spans less than 10 ft (0.3 m) (McGrath et al., 2005).

According to the AASHTO LRFD code (2007), for a depth of fill of 2 ft (0.6 m) and greater, a wheel load acts over the tire footprint area of 20 in x 10 in (0.5 m x 0.25 m). The wheel load distribution on the culvert is calculated by increasing the tire footprint dimensions by 1.15 times the depth of fill for a select granular backfill and by 1.0 times the depth of fill for all other soil types. On the other hand, the AASHTO standard specifications(1992) considers the wheel load acting as a point load and distributes it over a square area with a side dimension of 1.75 times the depth of fill. When the fill depth increases to the depth that the distribution areas from two or more tires overlap, the interacting tire loads are added together to calculate the total load, which is considered uniformly distributed over the area defined by the outside limits of the individual areas. The AASHTO LRFD code (2007) yields more pressure than the Standard Specification (1992) and the difference in pressure is much more at shallow depths (Cook et al, 2002).

KDOT Manual (2011) recommends the wheel load distribution width on an under fill structure be calculated as the maximum of the above formula (equation 2.5) for less than 2 ft (0.6 m) fill structures given by the AASHTO standard specification (1992) or 1.75 times the fill depth.

Seed and Raines (1988) provided an equivalent line load equation to determine the axle load for a two dimensional finite element analysis. Tadros and Benak (1989), Abdel-Karim et al. (1990), and Awwad (2000) believe the AASHTO square area distribution is conservative. They also agreed that beyond a 10 ft (3 m) fill depth the truck load became negligible as compared to the earth pressure loads. Abdel-Karim et al. (1990) suggested including the distributive effect of the road bed. Flexible pavements are suggested to treat as just additional fill depth. For rigid pavement structures the load can be distributed through the pavement according to Boussinesq's equations. Another option would be to develop an equivalent depth for rigid pavements (Abdel-Karim et al. 1990).

Possible methods to minimize over-conservatism in load ratings include more accurate modeling of distribution of the applied loads through finite element analysis or Boussinesq's equations, and by considering the load-distribution effects of pavement stiffness (Lawson et al. 2010). The Petersen et al. (2008) study showed that the pavement reduced the distributed vertical stress due to a live load considerably. They also suggested that both the distribution factors of 1.75 and 1.15 are un-conservative.

Awwad et al. (2000) carried out a finite element analysis of culverts with different sizes under fill depths ranging from 0 to 10 ft (0 to 3 m) at an interval of 2 ft (0.6 m). They concluded that the wheel load effect was dominant within the fill depth of 3 ft (0.9 m). Both the soil load and wheel load affect the culvert response when the fill depth is between 3 to 7 ft (0.9 to 2.1 m).

They further indicated that the effect of a wheel load was negligible for more than 7 ft (2.1 m) deep fill and found that the effect of reduction in the maximum positive moment on the top slab due to lateral pressure decreased with an increase in the span of the culvert.

Bloomquist and Gutz (2002) carried out research in relation to the distribution of live load through earth fill and reported the development of equations for calculating the distribution of wheel loads through fill above the precast concrete box culvert. They aimed at devising a new distribution method and developing a single design equation for the live load distribution on the top slab of the precast concrete box culvert.

Live load Surcharge

Article 3.20.3 in the AASHTO standard specification (1992) requires using additional 2 feet (0.6 m) of surcharge to the lateral load to consider the near-structure lateral live load due to approaching vehicles. This load is constant regardless of the number of trucks that are passing over the culvert. However, this load is not considered in the reduced load case while the maximum positive moments on the top and bottom slabs are calculated. KDOT manual (2011) also uses a lateral live load surcharge pressure equal to 2 ft (0.6 m) of earth fill to all culvert structures.

Although AASHTO has provided the guidelines for load rating, some state DOTs still have tendency to use their own methods and policies for load rating of culverts. Lawson et al. (2010) carried out a survey in 2009 to find the policies used by different states for load rating of culverts. The survey revealed that only 21 out of 32 states who completed the survey applied loads following the AASTHO guidelines. Table 2.3 shows the distribution of the load application policies used by the responding states to load rate concrete box culverts. Among

these 32 loading practices, only 15 incorporate soil-structure interaction and only 7 consider the effects of varying soil conditions. Lawson et al. (2010) also found that two of the responding states that claimed to use the load application on culverts per AASHTO specifications came with different answers to the questions about whether their procedure accounted for soil-structure interaction and varying soil conditions. This fact implies the existence of some level of confusion to what the AASHTO specifications and conditions should be accounted for. However, this problem is not a new one. A similar survey carried out by Tadros et al. (1987) found the variations in the loading policy from state to state. They also raised the question of adequacy of the AASHTO provisions then. Because of the confusion created by the existence of the AASHTO standard and the LRFD specification some state DOTs have two different loading guidelines (Iowa DOT, 2005).

TABLE 2.3 Load application policies used by different state DOTs (Lawson et al. 2010)

AASHTO	Custom	Other
21	9	2

2.4 Influence Factors for Load Rating

There are different independent variables which affect the load rating of culverts with changes in their values. Some of them have significant effects and some do not cause any considerable change on the overall Inventory Rating and Operating Rating. Soil modulus, depth of fill, modulus of subgrade reaction, Poisson's ratio are among the important parameters that should be supplied as inputs to the numerical models used to analyze the culvert to determine live load and dead load demands. Therefore, the knowledge about the sensitivity of different input parameters would be beneficial to load rating engineers. Variability in the load rating is not limited to the

input parameters only. There are many analytical tools available in practice with different level of model sophistication. Different analytical tools yield different rating values for same parameters. The numerical models with a lower level of model sophistication are more conservative than one with a higher level of sophistication. Thus the rating of a culvert is also dependent on the level of effort put on during the load rating calculation. Lawson et al. (2010) carried out a regression analysis between the six independent variables (modulus of subgrade reaction, Poisson's ratio, multi-barrel effects, lateral earth pressure, modulus of elasticity, and depth of fill) and the actual inventory ratings for seven selected culverts in Texas. These culverts had been designed and constructed at different time using the design philosophy prevailing at that particular design era. Their analysis showed that the depth of the fill is the most significant parameter in the load rating calculation and found that there was no significant relationship between the number of spans, the barrel height or the span length and the load rating. However, the relationship between the load rating and the depth of fill showed higher load rating at the higher fill. Some of the findings from their work are discussed below.

2.4.1 Modulus of Subgrade Reaction

Modulus of subgrade reaction, k, is the measure of the soil support to the bottom slab of a culvert. The analysis using the k values of 75, 150 and 250 pci (20.36×10^3, 40.72×10^3 and 67.88×10^3 kN/m^3) showed that the change in the k value had little effect in the inventory rating.

2.4.2 Poisson's Ratio

Poisson's ratio is the ratio between the transverse strain and longitudinal strain. The analysis using Poisson's ratios of 0.5, 0.3 and 0.1 at the soil modulus of 20 ksi (138 MPa) showed that the slope of the change in the load rating with respect to Poisson's ratio was small (i.e., less than

10% change across the range of Poisson's ratio). This result showed that the inventory rating was not sensitive to Poisson's ratio. For most of the cases, typical Poisson's ratio of 0.3 provided suitable results. However, if tall culverts were backfilled with poor materials like highly plastic clays, the sensitivity of Poisson's ratio increased.

2.4.3 Multi-barrel Effects

Lawson et al. (2010) compared the inventory ratings of five, six, and seven barrel culverts with those of four barrel culverts. The results showed a small slope of the change in the load rating with respect to the number of barrels. The percent difference between the inventory ratings was less than 10%. This result also showed that the inventory rating for four barrel culverts was the lowest and most conservative.

2.4.4 Lateral Earth Pressure

Lateral earth pressures act on the end walls of the culverts. The soil was assumed as an equivalent fluid and the distribution of the lateral earth pressure was triangular. The equivalent fluid weight depended on the soil properties and the stress history of the soil. The inventory ratings were determined using the lateral earth pressure values ranging from 40 pcf to 100 pcf (6.3 kN/m^{3}to 18.9 kN/m^3) at 20 pcf (3.15 kN/m^3) increments. It was shown that the inventory rating was less sensitive to the lateral earth pressure for typical culverts. However, it became sensitive for the tall culverts because the critical section moved to the mid-spans of the exterior wall. Lawson et al. (2010) further considered the current AASHTO (2007) requirement for the lateral earth pressure as logical and reasonable.

2.4.5 Modulus of Elasticity

The analysis carried out using a modulus of elasticity ranging from 4 ksi to 40 ksi (27.5 MPa to 275 MPa) at increments of 4 ksi (27.5 MPa) showed that the culverts with a greater depth of fill were more sensitive to the elastic modulus. This finding suggested the importance of accurately accessing the elasticity of the soil for deeper culverts. They further indicated that it was reasonable to use the elastic modulus of the soil within $\pm$200 psi (1380 kPa) for fill depths greater than 6 ft (1.8 m) and $\pm$1000 psi (6896 kPa) for smaller depths. The modulus of elasticity significantly affected the inventory rating, especially at higher fill depths. Since soil is highly variable and its strength is dependent on the stress level and time, the selection of soil modulus for culvert load rating purposes can induce higher uncertainty into the calculation.

2.4.6 Depth of Fill

The depth of fill represents the overburden pressure acting on the top of the culvert. Culverts are considered being subjected to direct traffic when the depth of fill is less than 0.6 m. Inventory ratings are higher at minimum and maximum depths. At an intermediate depth, the rating is between minimum and maximum ratings. Lawson et al. (2010) revealed that the highest rating occurred at the maximum design depth. Although a culvert's rating factor was found to be more than one for high fill, it did not necessarily be more than one at low fill. Although at low fill the dead load became considerably small, the traffic load became much higher as a result of the minimum distribution of live loads.

Lawson et al. (2010) regarded the depth of fill and the elastic modulus of the soil as "very sensitive" to the inventory rating and other parameters as "not sensitive".

2.5 Constitutive Models of Soil

Constitutive model, also referred as constitutive equation, is a mathematical approximation of the stress-strain behavior of a material. A constitutive model is an essential and important part of finite element and finite difference analyses. Since the stress-strain behavior of soil is dependent on many factors, such as stress level, soil type, saturation condition, level of compaction, and others, a number of soil constitutive models have been developed and are available for finite element/difference analyses. Lade (2005) summarized a number of available constitutive models. Each model has its own capability and requirements for experimental data for calibration. One constitutive model cannot represent all soil behavior; however each model captures part of important behavior of a particular type of soil. Simulating the response of a buried structure to live loads acting on the surface in a finite element/difference analysis requires a soil constitutive model that best captures the soil-culvert interaction. Linearly elastic soil models have been used by many researchers in their studies (for example, Moore and Brachman1994, Fernando and Carter 1998, NCHRP 2010). Nonlinear models including nonlinear elastic models, perfectly plastic models, and plastic models with hardening have been also used by researchers (for example, Pang 1999). Stress-dependent stiffness and shear failure have been found to be important characteristics for an analysis using soil models. The Duncan-Chang hyperbolic model has such features (Selig1988), which has been implemented in the finite element programs CANDE and SPIDA to analyze soil-structure interaction problems for culverts.

For computationally intensive 3D models it becomes important to select a simplest soil model that is suitable for the soil-structure interaction problems for load rating of culverts. The linearly elastic model and the Mohr-Coulomb model have been used in soil-structure interaction analyses

of buried culverts (NCHRP 2010, Lawson et al. 2010). The linearly elastic model provides the most basic soil behavior; however, it does not consider nonlinear stress-strain behavior or plasticity at failure. For linearly elastic isotropic soil behavior, there are four elastic constants (i.e., modulus of elasticity, Poisson's ratio, bulk modulus, and shear modulus); however, any two of the four constants are independent. In reality, these elastic constants vary with stress level. Some analyses used elastic properties that vary with depth (for example, NCHRP 2010). The stress-strain relationship of a linearly elastic isotropic model can be expressed as Equation 2.9. An elastic model simulates recoverable deformation of soil; however, complicated soil behavior cannot be captured by the elastic model in most of the cases.

$$\varepsilon_{11} = \frac{1}{E}[\sigma_{11} - \upsilon(\sigma_{22} + \sigma_{33})]$$

$$\varepsilon_{22} = \frac{1}{E}[\sigma_{22} - \upsilon(\sigma_{11} + \sigma_{33})]$$

$$\varepsilon_{33} = \frac{1}{E}[\sigma_{33} - \upsilon(\sigma_{11} + \sigma_{22})] \qquad (2.9)$$

$$\varepsilon_{12} = \frac{\sigma_{12}}{2G}$$

$$\varepsilon_{13} = \frac{\sigma_{13}}{2G}$$

$$\varepsilon_{23} = \frac{\sigma_{23}}{2G}$$

The Mohr-Coulomb model (also known as the linearly elastic perfectly plastic model) is one of the simplest elastoplastic models. In this model, Mohr-Coulomb's yield criterion and a non-

associated flow rule for shear failure are used. Equation 2.10 shows the simple form of Mohr-Coulomb's yield criterion.

$$\tau = c + \sigma \tan(\phi) \tag{2.10}$$

where τ and σ are the shear stress and normal stress on the plane, on which a slip is initiated and c and ø are respectively the cohesion and the internal friction of the soil. In terms of maximum and minimum principle stresses, the Mohr-Coulomb yield criterion can be expressed as follows:

$$\frac{\sigma_1 - \sigma_3}{2} = \frac{\sigma_1 + \sigma_3}{2} \sin(\phi) + c \cos(\phi) \tag{2.11}$$

Studies have found the Mohr-Coulomb model was effective in modeling shear strengths of soils and rocks. However, this model uses soil elasticity constants, which is not stress dependent.

NCHRP (2010) carried out a detailed study on live load distribution to buried structures and used most frequently adopted software in practice for culvert modeling. Soil-structure interaction, sequential model development, structure/soil interface modeling, 3D analysis, structural analysis capabilities, built-in soil models were the major criteria for selecting the software to use in their study. The Fast Lagrangian Analysis of Continua in 3 Dimensions (FLAC3D) was selected since it met most of their requirements. FLAC3D is a finite difference program, which was developed for simulating three-dimensional geotechnical engineering problems and is suitable for solving nonlinear and large displacement problems. This program has 11 built-in constitutive models for modeling various types of geomaterials and can model reinforcement and structural features.

The NCHRP (2010) study analyzed over 830 3D models of culverts including box culverts. The Mohr-Coulomb model for soils was used. However, the elastic model was used for the top thin layer to prevent the failure of the soil under the wheel load and used for the pavement.

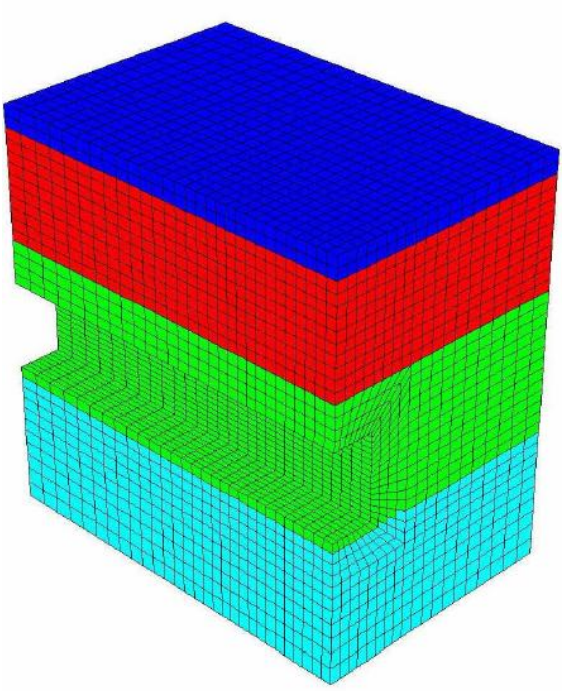

FIGURE 2.11 Typical box culvert model in FLAC3D (NCHRP, 2010)

2.6 Summary

This chapter reviewed in culvert classification, load rating of culverts, AASHTO guidelines for load distribution, influence factors in load rating, and constitutive models of soils. This literature review provided helpful understandings and ideas on the problems of the current study. Conclusions from this literature review can be summarized below:

1) Vertical stresses due to soil loads on the top slab are higher in embankment installation culverts and lower in trench installation and imperfect trench installation culverts than the weight of the soil above the culverts. This increase/decrease in vertical stresses due to

the soil loads are significant for newly installed culverts. This effect gradually decreases with the age of the culvert and can be ignored in old culverts.

2) Live load and dead load demands, and hence the load rating, of the culvert are dependent on the level of model sophistication used in analyzing these demands. A higher level of model sophistication yields higher load rating. Therefore the higher level of model sophistication can capture the soil-structure interaction more precisely than the lower one.
3) AASHTO Standard and LRFD Specifications provide the guidelines for load distribution over culverts under dead and live loads. These guidelines do not consider the effect of a pavement present over the fill, which is a controlling case in design considering the loads during construction. However, the actual stress distribution on the culvert under the pavement, which is the case in load rating, may not be truly represented by the current AASHTO distribution.
4) Depth of fill and soil modulus are the two sensitive parameters for load rating.
5) FLAC3D finite difference modeling technique can more accurately simulate the three-dimensional load distribution in culverts. Elastic model and Mohr-Coulomb model can be used for modeling soils in around culverts.

Chapter 3 Field Tests and Material Properties

This chapter presents two field tests carried out on box culverts under flexible and rigid pavements in field and the laboratory tests conducted to characterize the pavement layers and the natural subgrade soil samples obtained from the field. The field tests were conducted on two low-fill box culverts using a low boy truck carrying a backhoe as a test truck. The soil, concrete, and asphalt samples taken from the field were tested in the lab to determine the characteristics of each material.

3.1 Statistical Study of Culverts

A statistical study of box culverts in Kansas having a span greater than 3.6 m and a fill depth up to 0.6 m was carried out before the selection of the test culverts. Three hundred and five culverts met these criteria. Figure 3.1 shows box bridges with a span of 3.6 or 4.2 m were the most common and those with a span of 4.8, 5.4, and 6m were common as well. Figure 3.2 shows the number of boxes with different spans. Since some of the box bridges had more than one cell, the number of boxes and the number of bridges was different. Although the box bridges having 4.2 m span cells were slightly more than those having 3.6 m span cells in Figure 3.1, 3.6 m cells outnumbered the 4.2 m cells in Figure 3.2. Figure 3.3 shows that the most common fill depth in these culverts were either 0.3 or 0.6 m. The culverts having fill depths ranging from 0.42 to 0.48 m were also in significant numbers. Some of these culverts had multiple spans. For simplicity, single span culverts with simple geometry were selected for testing. After field visits at several possible culverts in Kansas, the culverts on US50 Highway and KS148 (All American Drive) were selected. Both of the culverts had the fill depth of nearly 0.6 m. The culvert on US50 was

under the rigid pavement and that on KS148 was under the flexible pavement. They had spans of 3.6 and 5.4 m respectively.

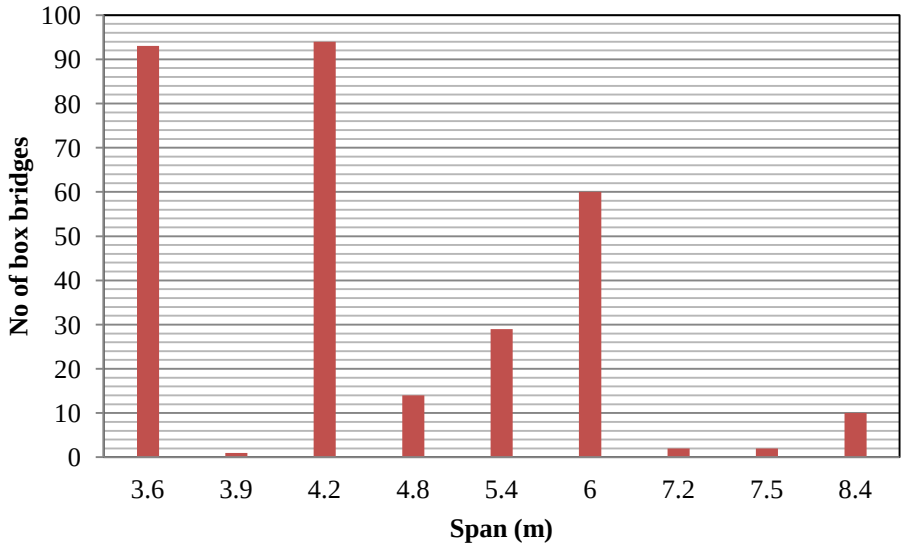

FIGURE 3.1 Span distribution of low-fill culverts in Kansas

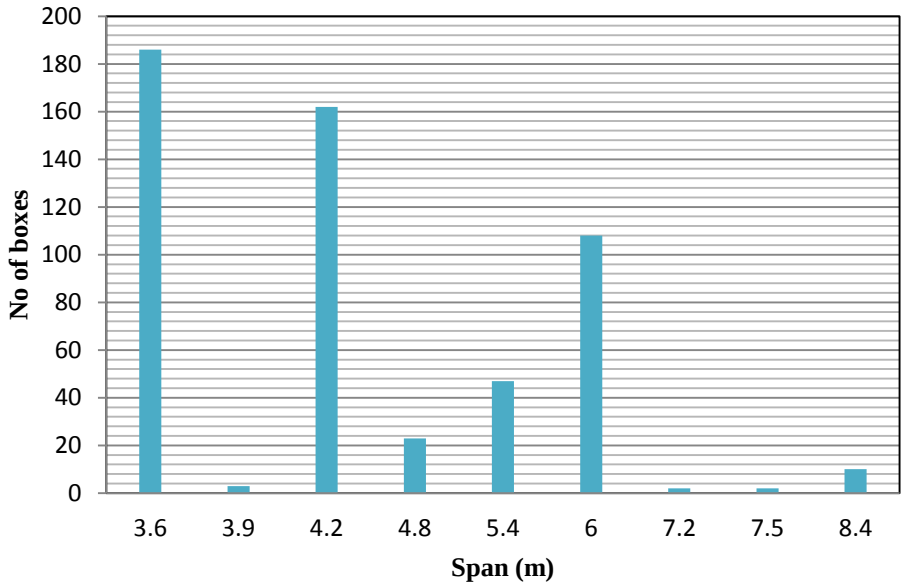

FIGURE 3.2 Span distribution of low-fill boxes in Kansas

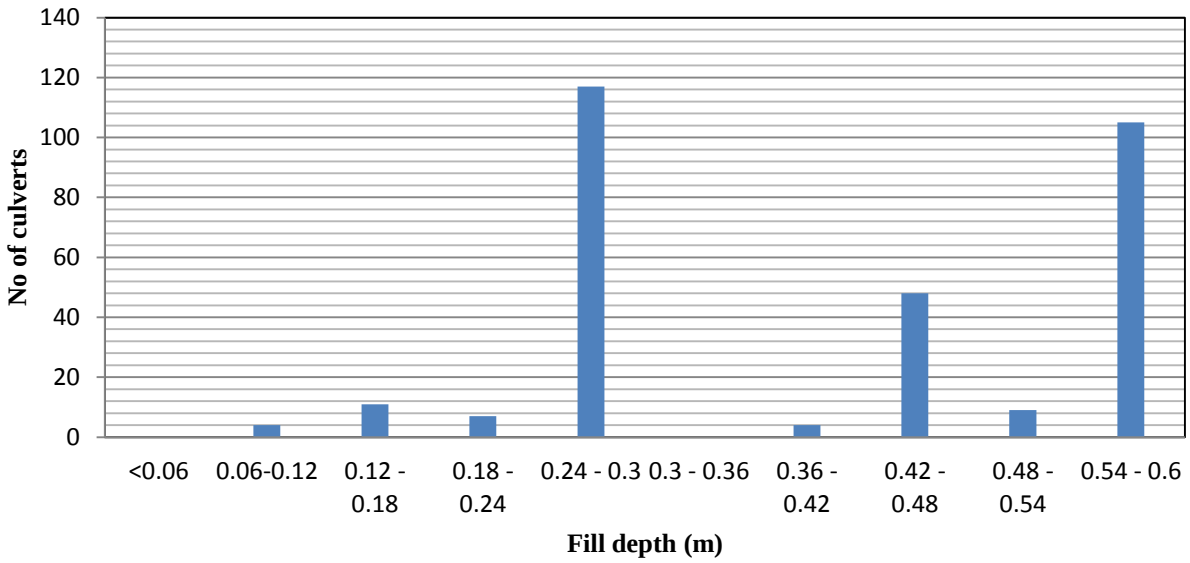

FIGURE 3.3 Fill depth distribution of low-fill boxes in Kansas

3.2 Field Test on Culvert under Rigid Pavement

3.2.1 Site Condition

The culvert selected for the field test was a single span reinforced concrete box culvert located at milepost 399 on US 50 Highway, west of Emporia, Kansas. The culvert was a rigid frame box (RFB). The cross section of the culvert and the interior of the culvert are shown in Figures 3.4 and 3.5 respectively. The inside dimensions of the culvert were 3.6 m wide and 3 m high. The culvert was aligned perpendicularly to the highway. The fill height up to the riding surface of the concrete pavement was 0.65m from the top of the culvert roof. The overall length of the culvert was 27.6 m, of which13.2 was under the concrete pavement and the concrete shoulders. The width of the concrete pavement in each lane was 3.6 m while the width of each shoulder was 3 m. The culvert extended under an unsurfaced embankment area on each side of the road. The pavement, shoulder and unsurfaced area over the culvert are shown in Figure 3.6. The embankment was composed of high-plasticity clay. The concrete pavement was 0.25 m thick,

which was placed over a 0.1 m thick cement-treated aggregate base course. The base course was underlain by a 0.15 m thick lime-treated subgrade, which overlaid a 0.15 m thick soil layer. The soil layer had a liquid limit of 59, plastic limit of 30, plasticity index of 29, and specific gravity of 2.68 placed immediately above the culvert. The shoulder portion also consisted of similar layers with the only difference being the concrete shoulder thickness that was 0.2 m thick. The culvert had 0.3 m wide haunches at the corners.

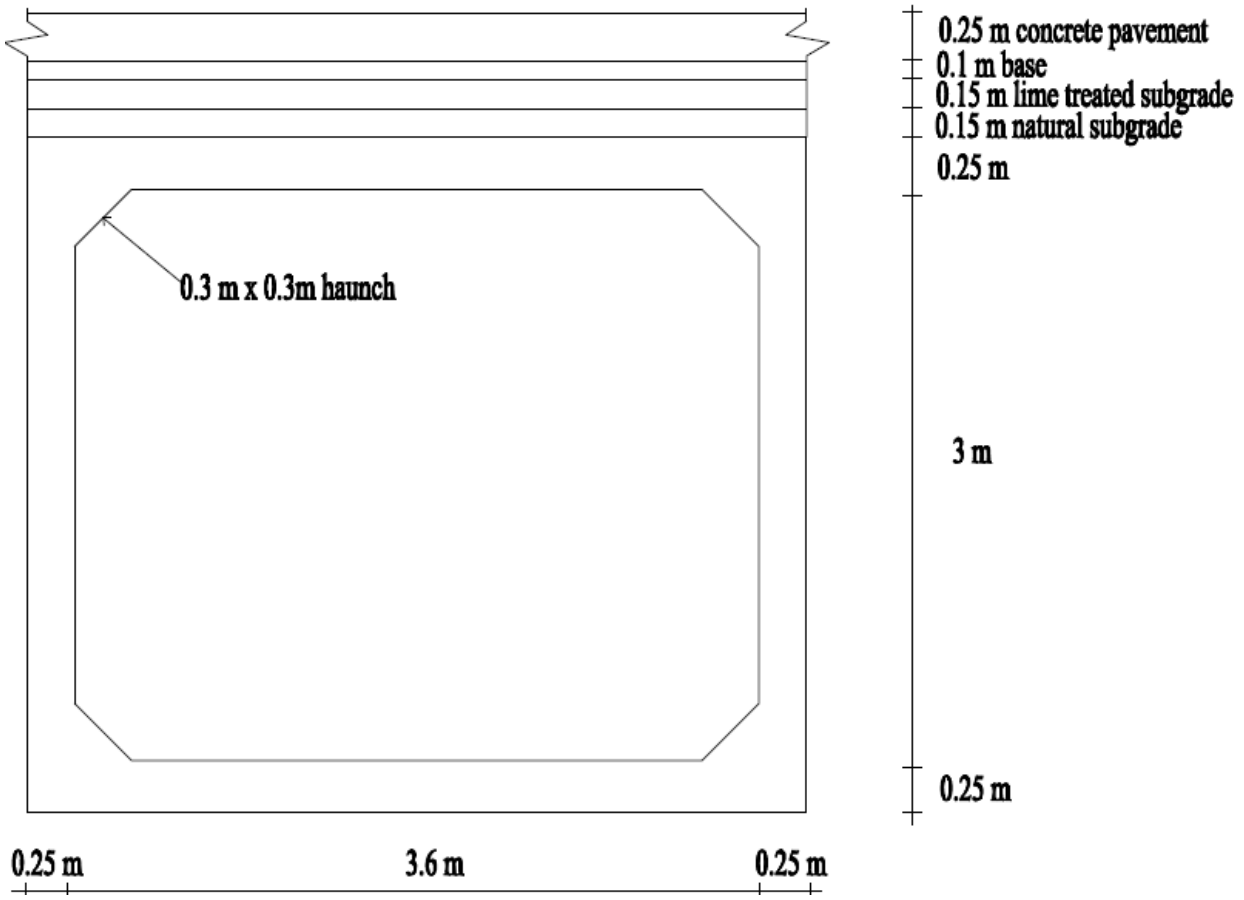

FIGURE 3.4 Cross section of the culvert and pavement layers

FIGURE 3.5 Interior of the test culvert

FIGURE 3.6 Concrete pavement, concrete shoulder, and unsurfaced sections over the culvert

3.2.2 Test Devices and Instrumentations

To evaluate the performance of the culvert under the variable loading conditions, a series of test devices and instrumentations were used during the experiment. Only one half of the culvert was instrumented with displacement transducers, earth pressure cells, and strain gages under the eastbound portion of the highway. Displacement transducers were used to measure the vertical deflections of the culvert roof slab while pressure cells were used to measure the vertical pressures on the culvert. Strain gages were installed to measure the strain in the surface of the top slab at different locations during the loading.

Displacement Transducers

The displacement transducers used in this research were strain gauge-type sensors manufactured by Tokyo Sokki Kenkyujo, Co., Ltd., Japan. They had two displacement ranges: 0 to 100 mm (Model: CDP-100) and 0 to 50 mm (Model: CDP-50).The accuracy of the transducers was 0.01 mm. The locations of the displacement transducers are shown in Figure 3.7. Three displacement transducers of 100 mm limit, labeled as L1, L2 and L3, were installed under the pavement section. Two displacement transducers of 50 mm limit, labeled as L4 and L5, were installed under the shoulder and the unsurfaced section respectively. Displacement transducers L2, L4 and L5 were right below the center of the pavement, shoulder and unsurfaced sections respectively along the culvert axis. Displacement transducer L3 was also installed along the same axis but was right below the outer wheel of the test truck during loading. Displacement transducer L1 was the only transducer placed at the quarter span to monitor the deflection along the transverse direction. More displacement transducers were installed under the pavement section because the expected deformation was small there. Metal frames of approximately 2.8 m

height were used to support and fix the displacement transducers in position as shown in Figure 3.8. The frames were stabilized by sand bags at the base.

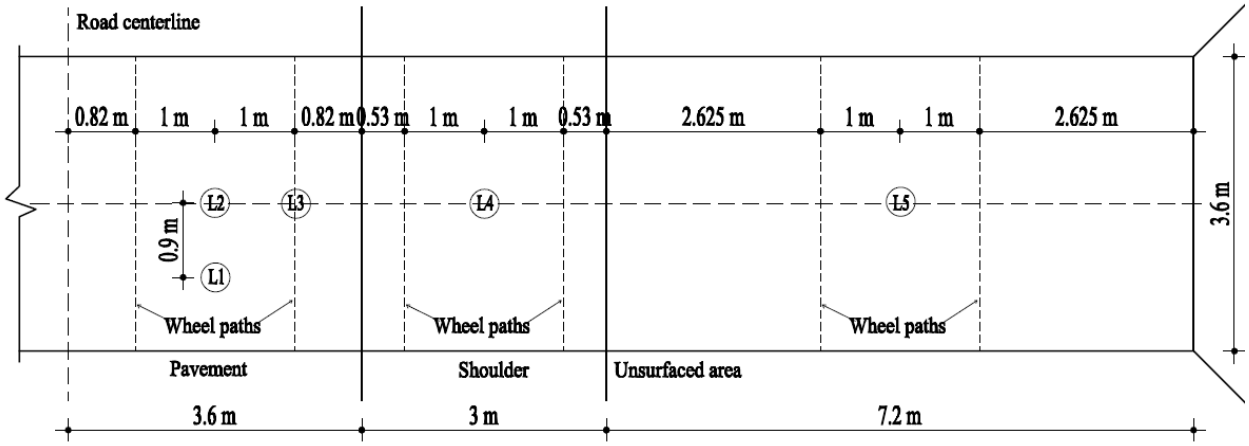

FIGURE 3.7 Schematic of the displacement transducer locations

FIGURE 3.8 Displacement transducers and supporting frames

Earth Pressure Cells

The earth pressure cells used in this research were strain gauge-type soil pressure gauges, which were manufactured by Tokyo Sokki Kenkyujo Co., Ltd. in Japan. They had two capacity ranges: 200 (Model: KDE-200KPA) and 500kPa (Model: KDE-500KPA). The pressure cells were made of stainless steel and can work at a temperature range from -20˚C to 60˚C. Each cell had a thickness of 11.3 mm, an outer diameter of 50 mm with a sensing area diameter of 46 mm, and a total weight of 160 g. It had minute displacement of pressure-sensitive area due to a double diaphragm structure and nonlinearity of 1% RO (random occurrence). These pressure cells are suitable for measuring earth pressure under dynamic loading.

Four earth pressure cells were installed in the unsurfaced portion of the culvert to measure the vertical stresses at the interface between soil and culvert top slab. Four holes were dug at the locations shown in Figure 3.9 for the placement of the pressure cells. The pressure cells, labeled as E1, E2, E3, and E4, were placed at depths of 0.45, 0.4, 0.375 and 0.35 m respectively, due to the slope of the ground surface. Pavement and shoulder sections were not instrumented with pressure cells due to the difficulty of installation. Pressure cells E1 and E4 were placed at 1.8 m apart and were intended to be below the wheels during loading. However, the actual distance between the wheels of the truck from center to center was 2 m as shown in Figure 3.9. As a result, only pressure cell E4 was below the wheel while E1, though it was below the wheel, was 0.15 m off the center of the wheel during loading. E2 was in the middle between E1 and E4 while E3 was in the middle between E2 and E4. Holes were filled and compacted with the same soil excavated after the placement of the pressure cells. The same amount of the soil was excavated and compacted back to the same hole to the same elevation to ensure the same density before and after the installation of pressure cells.

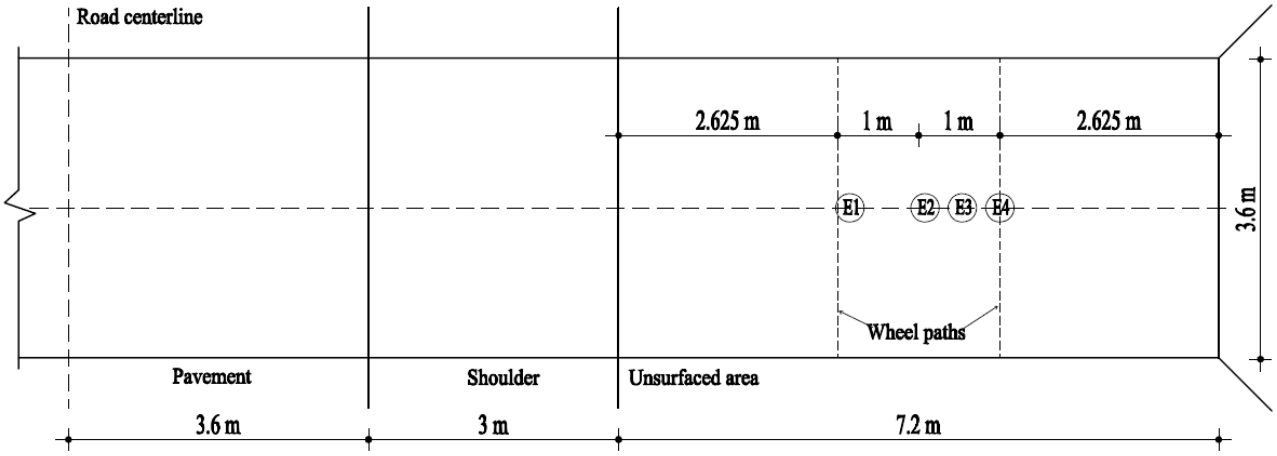

FIGURE 3.9 Schematic of the pressure cells location

FIGURE 3.10 Installation of earth pressure cell on the top of the culvert slab

Strain Gages

Strain gages were installed to measure the strain on the bottom surface of the top slab at different locations during the loading. The strain gages used in this research were N2A-06-40CBT-350 strain gages, manufactured by Micro-Measurements, Vishay Precision Group, USA, which are suitable for use on concrete surface. The strain gages had grid resistance of 350 ± 0.2% in ohms, a gage factor at 24˚C of 2.1 ± 0.5%, and a gage length of 100 mm.

The locations to be installed with strain gages were marked with a permanent marker. Surface preparation was carried out on a marked rectangular area. CSM-2 degreaser was first applied to the marked surface and scrubbed with a stiff-bristled brush to remove any loose soil and surface irregularities. The loose dust on the surface was blown out and rinsed thoroughly with clean water. The water on the surface was wiped out using gauze sponges. M-Prep Conditioner A was generously applied to the surface and the surface was again scrubbed with the bristled brush. The contaminated conditioner was blotted using gauze sponges. The surface was again cleaned thoroughly with clean water. Thereafter, M-Prep Neutralizer 5A was applied and then scrubbed with the stiff bristled brush. The contaminated neutralizer was blotted using gauze sponges and the surface was rinsed again with clean water and then scrubbed with 320 grit abrasive paper. The Neutralizer 5A was applied for the third time, cleaned using gauze sponges and rinsed using clean water. Propane torch was used to evaporate all the water from the surface and to make the surface completely dry and the surface was allowed to cool down before placing strain gages.

FIGURE 3.11 Surface preparation and installation of strain gage

Following the preparation of the surface, a glass plate was cleaned with CSM-2 Degreaser to create an alcoholic environment. The strain gages were put on the glass plate using the PCT-2M gage installation tape. Then a calibrated dropper was used to measure the curing agent 10 to be filled exactly to the number 10 and it was dispensed into the center of the jar of Resin AE. The curing time of the resin was 6 hours at 70˚F. The cured resin allows 6% elongation capacity to the strain gage. The bottle of the curing agent 10 was immediately capped and the dropper was discarded. The mixture was thoroughly stirred for five minutes using a plastic stirring rod. The mixed adhesive was allowed to stand for 5 minutes before being used. The life of the pot after mixing was only 15 to 20 minutes. After the mixture standing for 5 minutes, the adhesive was applied onto the surface of the strain gage using a cotton swab. Then, strain gages were bonded to the prepared surface aligning in the earlier marked direction. To have better bonding, the strain gage was pressed gently using the gauze sponge. The strain gages were then allowed to cure.

FIGURE 3.12 Strain gages attached to a glass plate and concrete surface

Twelve strain gages were installed on the bottom surface of the top slab of the culvert, with four strain gages under pavement, shoulder and unsurfaced sections each. The locations of the strain gages are shown in Figure 3.13. At each section two strain gages were positioned along the culvert axis and three perpendicular to the culvert axis. Strain gages S2, S6, and S10 were at the quarter span and S1, S5, and S11 were at the edge of the haunch. All the strain gages were aligned perpendicular to the culvert axis.

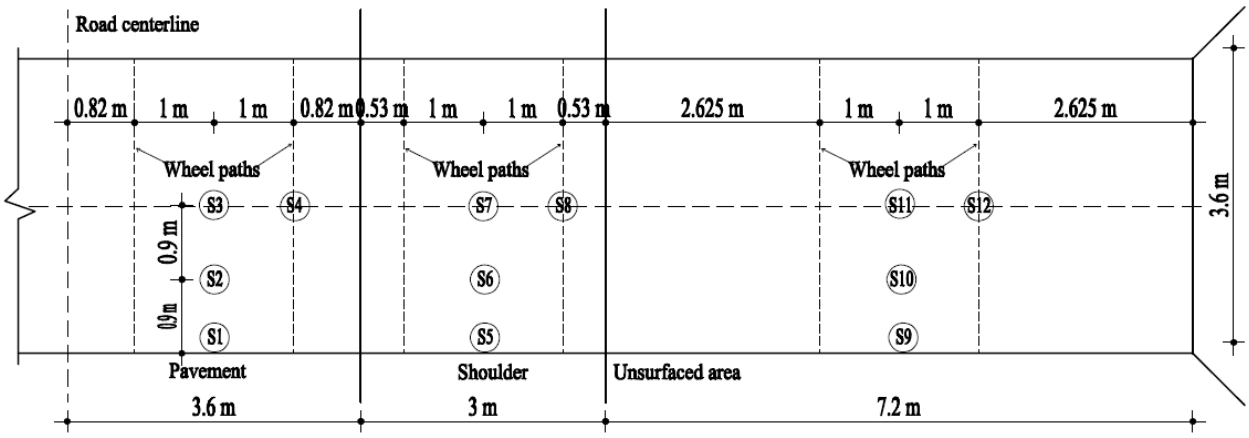

FIGURE 3.13 Locations of strain gages

Data Acquisition

Smart Dynamic Strain Recorder DC-204R manufactured by Tokyo Sokki Kenkyujo, Co., Ltd., Japan was used to record the data from displacement transducers, earth pressure cells, and strain gages. There were four recorders used during the tests. One data recorder and a computer were used to record the earth pressure cell data. Remaining three recorders were used to obtain the data from displacement transducers and strain gages using the second computer. Among these three recorders one data recorder served as a master recorder and the remaining two served as slaves, which were synchronized with the master recorder during connections. Each recorder had four connection ports to strain gauge sensors. A manual data recorder was also used because the number of strain gages and displacement transducers were more than the available ports in the data recorder. Therefore, a connection was made between DC-204R and a manual data recorder. The power to the recorders and computers were supplied using batteries and inverters.

Load Scheme

A low-boy loaded with a backhoe was used as the test truck. The truck consisted of six physical axles: a front steering axle, middle tandem axles, and triple axles at the end. However, seven axle positions were adopted in this study. The axle configuration and the load on each axle are shown on Figure 3.14 while Figure 3.15 shows a picture of the truck. Table 1 shows the calculated contact area for each wheel load. The load of the front steering axle was 49 kN. The second axle from the front of the truck shown in the photo of Figure 3.15 did not touch the ground; therefore, it is not counted. The center of the tandem axles was 4.8 m from the front axle and had a 105 kN load on each axle. The center of the triple axles was 12.3 m behind the center of the tandem axles. Each axle of the triple provided 80.5 kN load. The center to center distance between wheels on the same axle was 2 m.

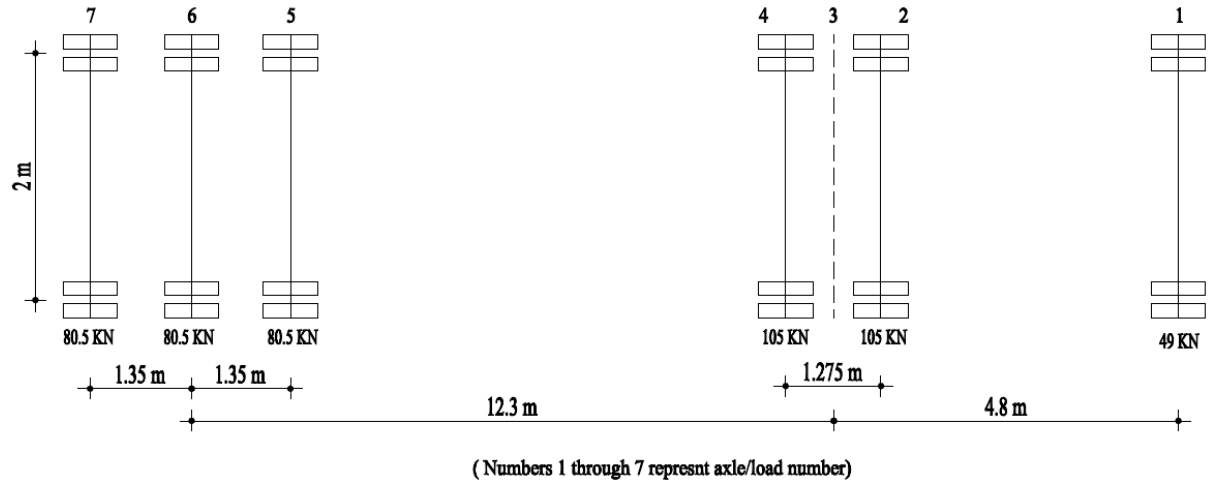

FIGURE 3.14 Axle loads and configuration

FIGURE 3.15 Test truck

TABLE 3.1 Calculated contact area for each axle load

Axle no.	Axle load (kN)	Tire Pressure (kPa)	Calculated wheel contact area (m^2)
1	49	760	0.064
2	105	760	0.138
3	0	760	0
4	105	760	0.138
5	80.5	760	0.105
6	80.5	760	0.105
7	80.5	760	0.105

The culvert was tested for static loading and traffic loading as well. The axis of the culvert was marked with color spray on the surface to determine the position of each axle during static loading. Also the intended lateral positions of the wheels were marked along the same line in each of the three sections as shown in Figure 3.6. Seven load combinations were obtained through applying static loading at each section by placing six axles of the truck over the marked line in turn. One more combination was obtained by assuming one dummy axle in the middle of the tandem axle. This dummy axle also provided one more symmetric load. The numbering of each axle load combination is shown in Figure 3.14.

Static loading was first applied at each section beginning with the unsurfaced section. Desired positions of axles were achieved by guiding the truck on the points previously marked. All the seven axles, including the dummy axle, were placed on the marks in turn to create seven loading positions (referred as Loads 1 to 7) as shown in Figure 3.16. Pressure and deflection readings

were recorded using the data acquisition systems. A similar procedure was repeated on the shoulder and the pavement for static loading. Traffic loading was applied only on the pavement section by moving the truck at three predetermined speeds: 25, 45, and 65 mph.

FIGURE 3.16 Seven load combinations

3.2.3 Field Test Results

The test data collected through displacement transducers and earth pressure cells were analyzed and presented in tabular forms and graphically in this section. Strain gage data were not recorded by the automatic recorder; therefore, no strain gage result is presented.

Displacement Results

The measured deflections of the culvert at each displacement transducer locations are shown in Figure 3.17 and Table 2. The deflections at L1, L2, and L3 were measured when the concrete pavement was loaded. The deflections at L4 were measured when the concrete shoulder was loaded. The deflections at L5 were measured when the unsurfaced section was loaded. Figure 3.17 shows that the deflections under the unsurfaced section (i.e., at L5) were much larger than

those under the pavement and shoulder sections (i.e., at L1, L2, L3, and L4). The deflections at L2 under the pavement and L4 under the shoulder were almost the same under each axle load. This comparison implies that the concrete pavement and the concrete shoulder had similar performance. However, displacement transducer L1, placed at the quarter span of the culvert, measured the least deflections. The deflections of the culvert under the unsurfaced section were 2 to 3 times larger than those under the concrete pavement and shoulder sections because the pavement and shoulder sections consisted of pavement layers with much higher stiffness than the natural soil in the unsurfaced section.

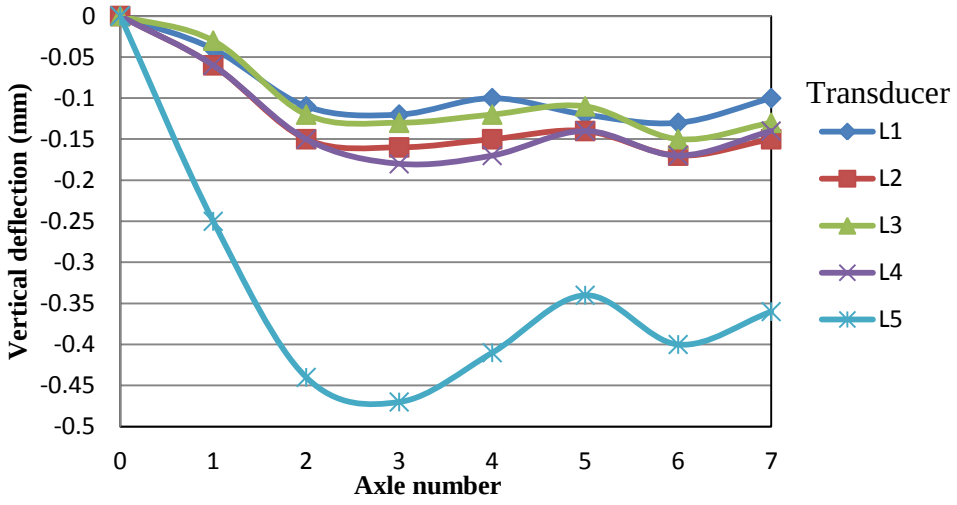

FIGURE 3.17 Measured vertical deflections under different axles

Figure 3.18 shows the profiles of the vertical deflections under the culvert from the centerline of the two-lane highway when the loads were applied on the unsurfaced, shoulder, and pavement sections, respectively. The maximum deflection for each test section occurred at the point of the wheel load. The arrows represent the locations of the axle loads. The vertical deflections under the load on the shoulder were nearly symmetric along the center of the load.

The front steering axle, the tandem axles, and the triple axles shown in inset in Figure 3.19 had a gross load of 49, 219, and 241.5kN, respectively. These axle loads became symmetric with regard to the culvert axis at Loads 1, 3, and 6, respectively. Figure 3.19 also shows that the vertical deflection generally increased with an increase of the gross load of the axle; however, there was a slight reduction when the triple axles were applied instead of the tandem axles.

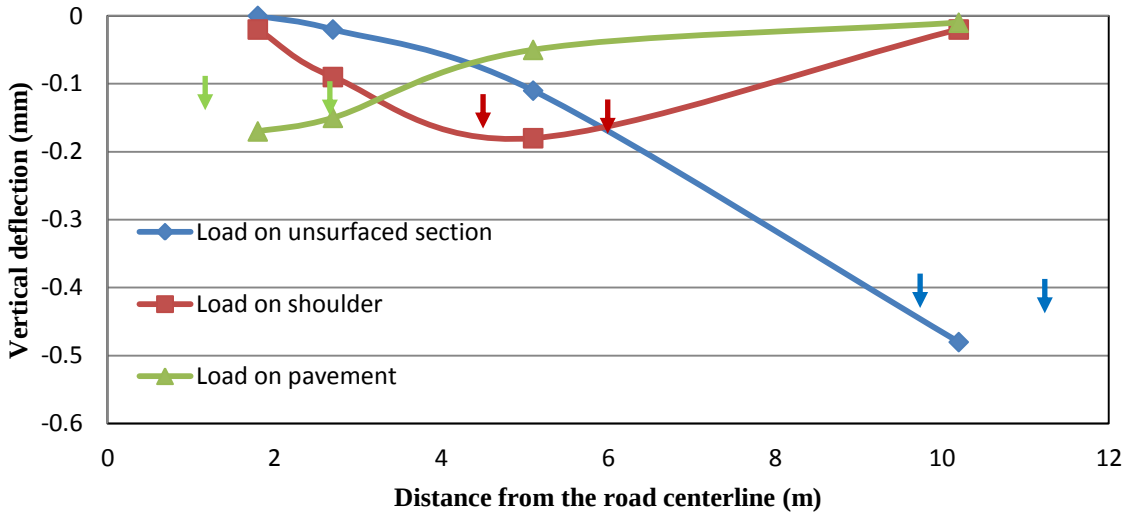

FIGURE 3.18 Deflection of culvert along culvert axis for load on different section

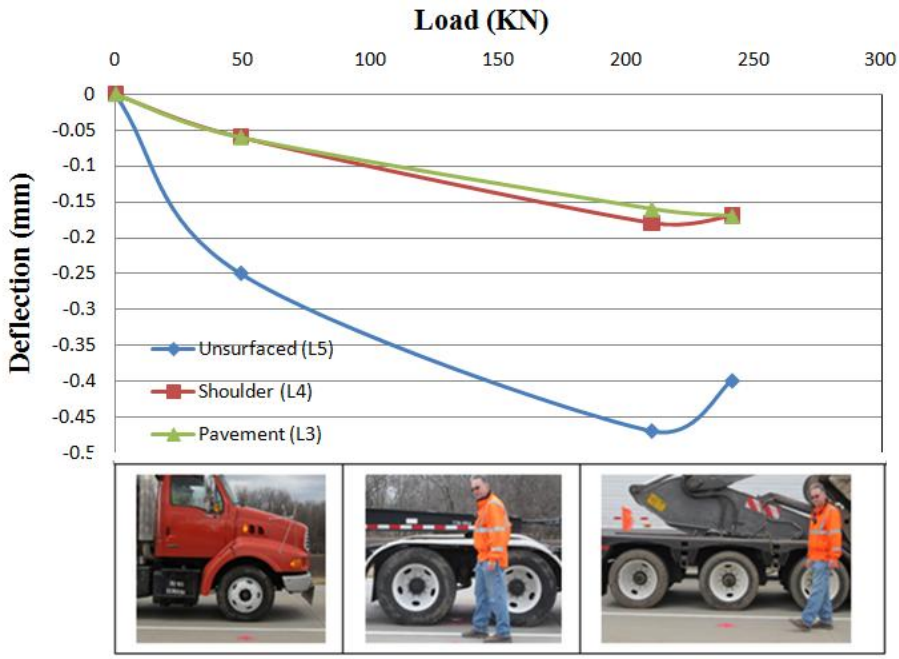

FIGURE 3.19 Maximum deflections at different section under a symmetric load

The culvert was also tested for a moving load by driving the test truck at approximately 25, 45 and 65 mph on the pavement section. Figure 3.20 shows the maximum deflections of the culvert at three locations. The general trend of the plot shows that the deflection at location L1 decreased by a small amount from static loading to traffic loading at the speed of 25 mph. Then it increased with the increasing speed. The general trend of the deflection at Location L2 was also increasing with an increase of the speed. The larger deflection might be accumulated by the deflection induced by the front axle followed by the rear axle. The vertical deflections at L3 had a continuous decrease with an increase of the speed.

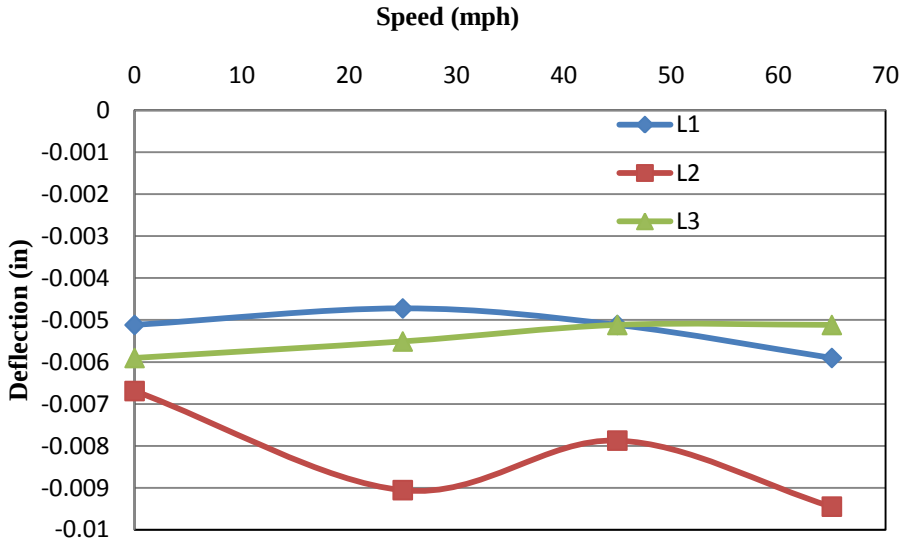

FIGURE 3.20 Maximum vertical deflections at different speeds

TABLE 3.2 Measured pressures and deflections at different axle loads and locations

Static Loading							
Axle Load	Deflection (mm)					Pressure(kPa)	
	Pavement			Shoulder	Unsurfaced Area		
	L1	L2	L3	L4	L5	E1	E4
1	-0.04	-0.06	-0.05	-0.06	-0.25	32	175
2	-0.11	-0.15	-0.12	-0.15	-0.44	118	180
3	-0.12	-0.16	-0.13	-0.18	-0.47	0	0
4	-0.1	-0.15	-0.12	-0.17	-0.41	122	220
5	-0.12	-0.14	-0.11	-0.14	-0.34	86	65
6	-0.13	-0.17	-0.15	-0.17	-0.4	118	165
7	-0.1	-0.15	-0.13	-0.14	-0.36	86	140

Pressure Results

Figure 3.21 shows the variation of the measured vertical pressure on the top of the culvert with the axle load applied on the unsurfaced area. The measured vertical pressures at different locations are also summarized in Table 3.2. The maximum measured pressure was measured by

pressure cell E4 when it was under Axle Load 4, which was approximately 29% of the tire pressure. The measured pressure was zero at Axle 3. Pressure cell E2 did not measure any pressure during loading. This result implies that the distribution of the wheel load through the soil did not reach this point, which was located at a distance of 0.9 m from the center of the wheels. Pressure cell E3 located at 0.45 m from the center of the wheels recorded lower pressure than those by Pressure cells E4 and E1. Since pressure cell E4 was right below the wheels, it measured the highest pressure as compared with pressure cells E1, E2, and E3 under the same load except for Axle 5. The reason for the lower pressure measured by cell E4 at Axle 5 is not clear. The measured pressures at Axle 6 were higher than those at Axles 5 and 7 because of the influence by Axles 5 and 7.

Figure 3.22 shows the distribution of the measured pressure with the distance at different axle load. The highest pressure developed at the center of wheels and decreased with an increase of the distance. The rates of pressure reduction at Loads 1 and 4 were higher than those at other axle loads. The measured pressure by cell E1 was lower than that by cell E4 because the pressure cell E1 was 0.15 m away from the center of the wheel and the fill depth at E1 was approximately 0.1 m more than that at E4 due to the sloping ground.

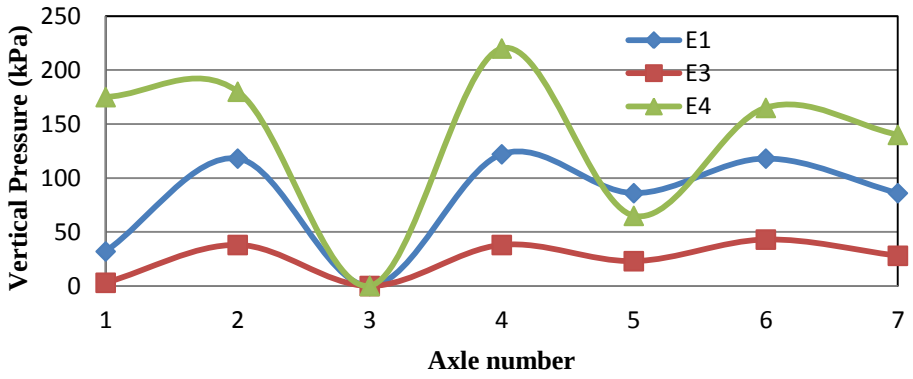

FIGURE 3.21 Measured pressures under different axles

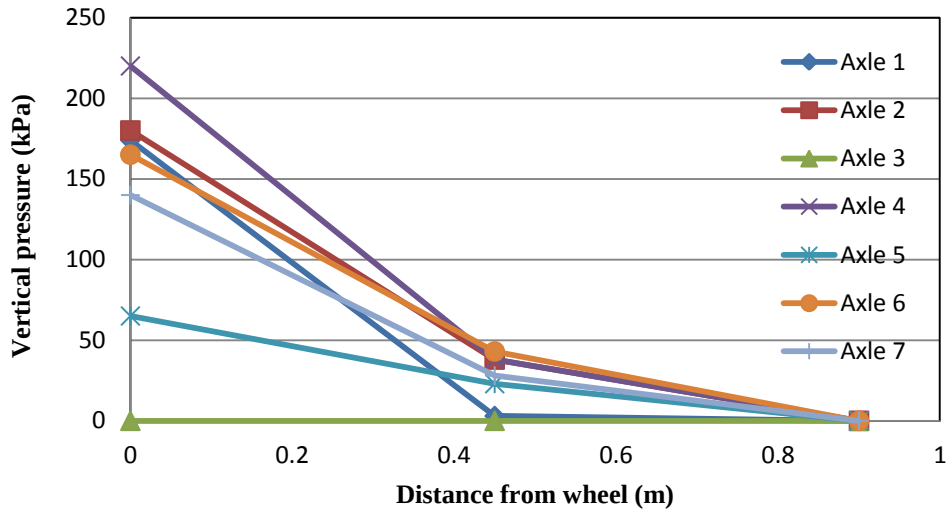

FIGURE 3.22 Pressure distributions with the distance under different axle load

3.3 Laboratory Tests

After the loading test on the culvert was finished, samples of the pavement layers along with the natural backfill soil around the culvert were obtained by KDOT from three boreholes: one borehole was drilled above the culvert and two boreholes were drilled in the unsurfaced section. The first borehole was located at 0.27 m west of the axis of the box and 2.19 m south of the centerline of the US50 highway. The second borehole was located at 3.42 m west of the culvert axis and 9.93 m south of the centerline of the US50 highway. The third borehole was located at 1.02 south of the second borehole. The truck used in the drilling operation is shown in the Figure 3.23. The borehole above the culvert confirmed the pavement layers as presented in Figure 3.4.They consisted of 0.25 m thick concrete at the top surface, 0.1 m thick cement-treated base course, 0.15 m thick lime-treated subgrade, and 0.15 m thick natural backfill soil on the top of the culvert. Five Shelby tube samples were obtained from the boreholes. The Shelby tube obtained from over the culvert recovered the lime-treated subgrade and the natural backfill soil.

The remaining four Shelby tube samples, which were taken from the borehole in the unsurfaced section, recovered the natural soil samples at the depths of 1.8 m and 3.9 m. Both boreholes in the unsurfaced section were advanced down to 4.5 m depth. Grayish brown, moist, firm silty clay fill existed with the top 1.5 m. The soil at the depth from1.5 m to 3.66 was the dark gray, moist and firm clay fill with small trace roots. The soil at the depth from3.66 m to 4.5 m was the moist, firm gray clay with trace brown mottling. The Shelby tubes were capped, sealed, and labeled with borehole and sample numbers after they were taken out.

FIGURE 3.23 Core drilling on the pavement and the truck used in drilling

3.3.1 Compressive Strength Test of the Concrete Sample

The core obtained from the pavement consisted of 250 mm thick concrete and113 mm thick cement-treated base. The cement-treated base was separated from the sample by sawing. The diameter of the concrete cylinder was measured to be 101.2 mm with the help of a vernier caliper. The concrete sample was sawed into 200 mm long to maintain the ratio of sample height to diameter to approximately 2:1. The density of the concrete sample was measured to be 2243 kg/m^3. This sample was tested in a compressive testing machine. The load was applied at the rate of 245 kPa (35 psi) per second as specified in ASTM C39/C39M-11a until the failure of the sample. Figure 3.24 shows the machine and setup for the compressive strength test of the concrete cylinder. The compressive strength of the pavement concrete was found to be 12.44 MPa.

FIGURE 3.24 Compressive strength test of concrete sample

3.3.2 Compressive Strength Test of the Base Material

The cement-treated base sample was separated from the pavement concrete sample by sawing. The base sample had the diameter and length of 101.2 and 113 mm respectively and a density of 1986 kg/m^3. The top and bottom ends of the sample were smoothened out by sulfur capping. This sample was placed in the curing room overnight and then tested in a compressive testing machine as shown in Figure 3.25. The load was applied at the rate of 245 kPa (35 psi) per second as specified in ASTM C39/C39M-11a until the failure of the sample. Dial gage readings along with the corresponding load readings were taken manually during the test. The stress-strain curve of the base sample is shown in Figure 3.26. The compressive strength of the cement-treated base sample was found to be 15.5 MPa and the elastic modulus was 180 MPa.

FIGURE 3.25 Compressive strength test of the base material

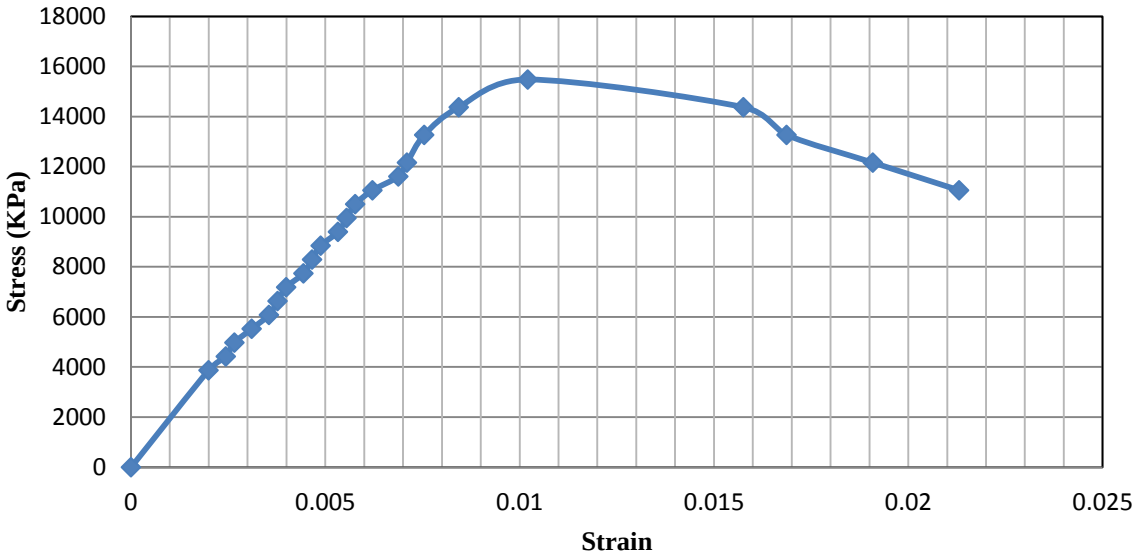

FIGURE 3.26 Stress-strain curve of the cement-treated base

3.3.3 Laboratory Tests on the Backfill Soil

The undisturbed soil samples in the Shelby tubes obtained from the field were extruded using a Shelby tube sample extractor as shown in Figure 3.27. The extrusion was carried out at a very slow rate so as to minimize disturbance to the soil sample. One of the undisturbed soil samples after extrusion is shown in Figure 3.28. The soil sample was then trimmed to a required size of diameter 71 mm and length 142 mm for the triaxial test as shown in Figure 3.29. The soil obtained during trimming of the sample was used to measure moisture content and carry out Atterberg limit and specific gravity tests. The moisture contents of the soil samples from different tubes were between 28 to 30%.

FIGURE 3.27 Extruding sample from Shelby tube

FIGURE 3.28 Undisturbed soil sample obtained from Shelby Tube

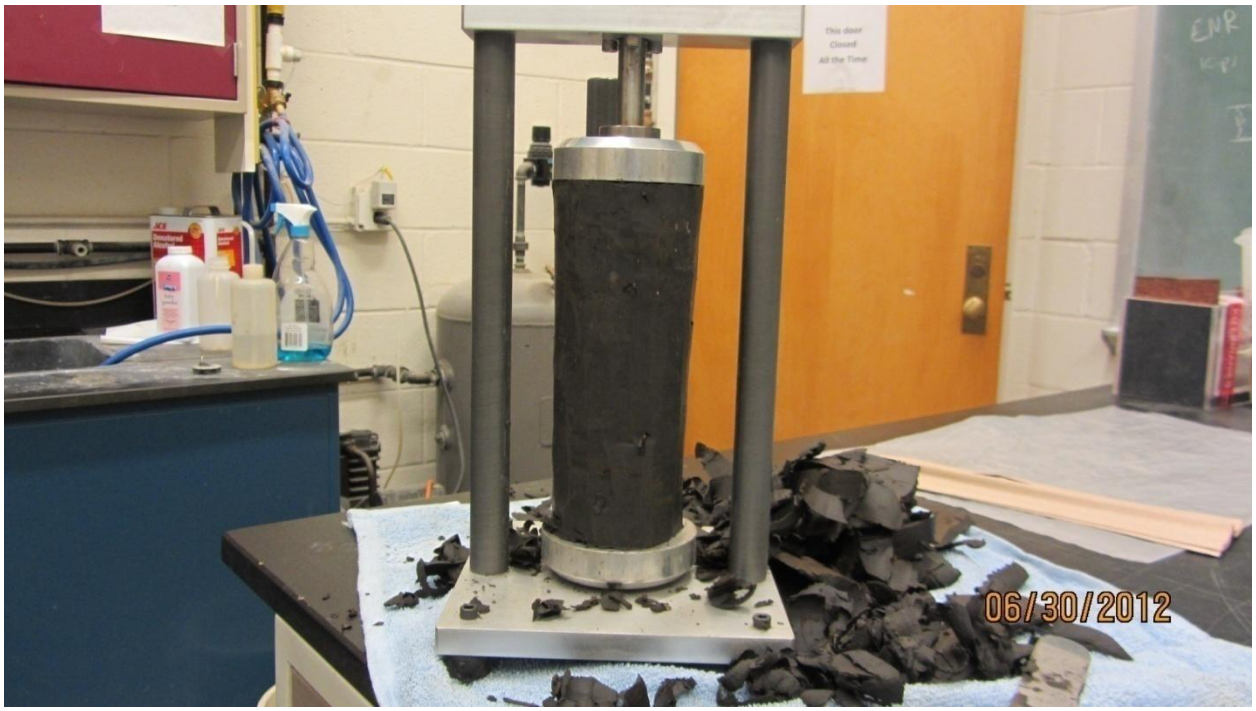

FIGURE 3.29 Trimming of the sample

The Atterberg limit tests were carried out in accordance with ASTM D4318-05 on the soil obtained from trimming of the undisturbed soil sample to determine the liquid and plastic limits. Figures 3.30 and 3.31 show the pictures taken during the liquid limit and plastic limit tests. To determine the liquid limit of the backfill soil, a flow curve was developed by plotting the data from four liquid limit tests using the Casagrande apparatus at different moisture contents in Figure 3.32. From the flow curve the liquid limit was found to be 59. The plastic limit test determined the plastic limit of 30. Therefore, the plasticity index of the backfill soil was 29. Based on unified soil classification system (USCS), the soil was classified as CH (high plasticity clay).

FIGURE 3.30 Casagrande's apparatus for liquid limit test

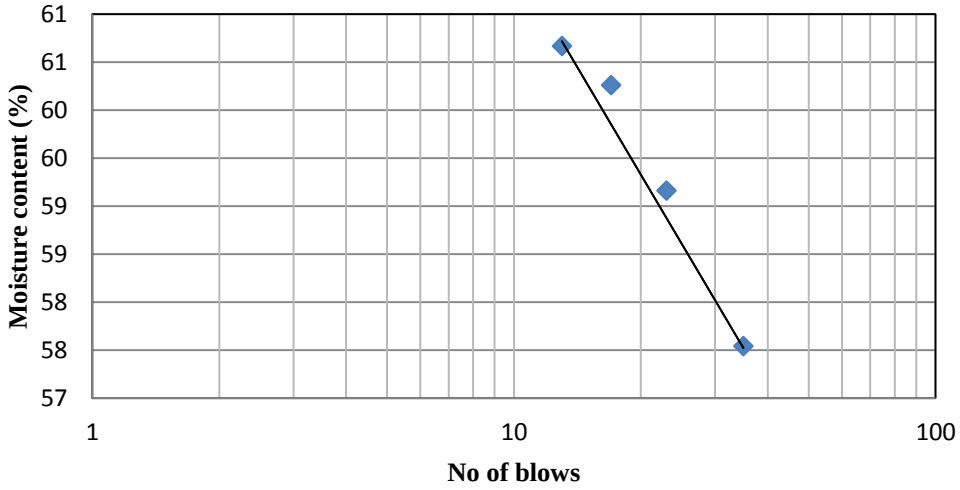

FIGURE 3.31 Flow curve of the soil

FIGURE 3.32 Plastic limit test

A specific gravity test was conducted in accordance with ASTM D854-10. Figure 3.33 shows a picture taken during the specific gravity test. The specific gravity of the soil was obtained to be 2.67. Specific gravity is useful in determining the soil parameters such as degree of saturation and void ratio.

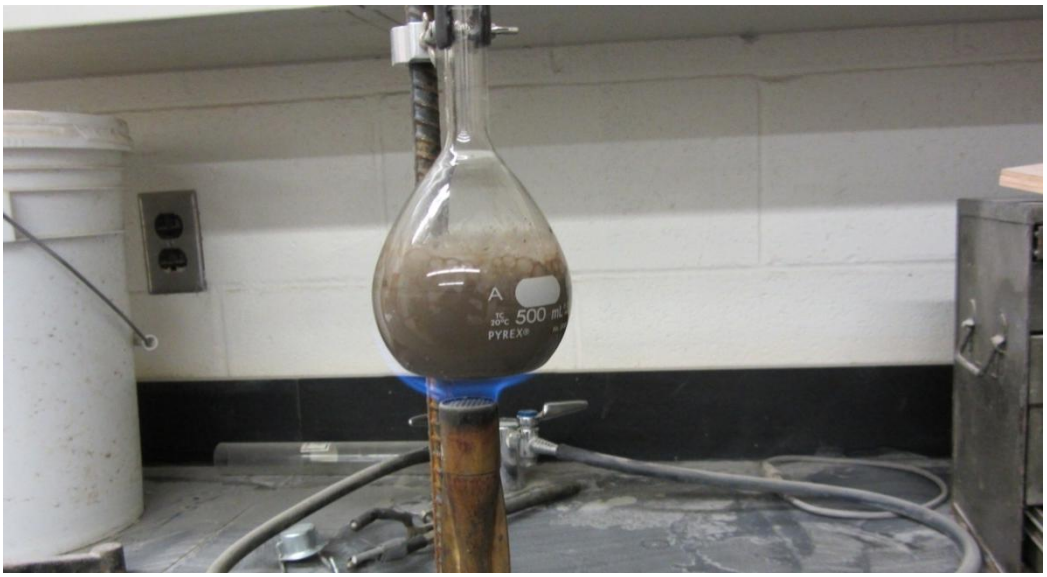

FIGURE 3.33 Boiling the soil slurry in a pycnometer

Triaxial tests of the soil samples were carried out in natural condition to determine the elastic modulus, cohesion, and friction angle of the soil. The soil samples extruded from the Shelby tubes had 100 mm in diameter. Therefore, the samples were trimmed into 2.8 in (71 mm) in diameter and 2.6 in (65 mm) in height as shown in Figure 3.34. The triaxial tests were conducted on three specimens at different confining pressures of 80, 45, and 10 kPa respectively. Figure 3.35 shows the sample after being sheared, which clearly showed the development of a shear plane at failure. Figure 3.36 shows the stress-strain plots obtained from these three tests. The elastic moduli of the soil sample were calculated as secant moduli at 50% peak strength as 15.0, 9.8 and 10.1 MPa at the confining stresses of 80, 45 and 10 kPa respectively, with an average modulus of 12.9 MPa. The total stress envelope was drawn based on the test results as shown in Figure 3.37 and resulted in a cohesion of 55 kPa and a friction angle of 13^{o}.

FIGURE 3.34 Trimmed sample

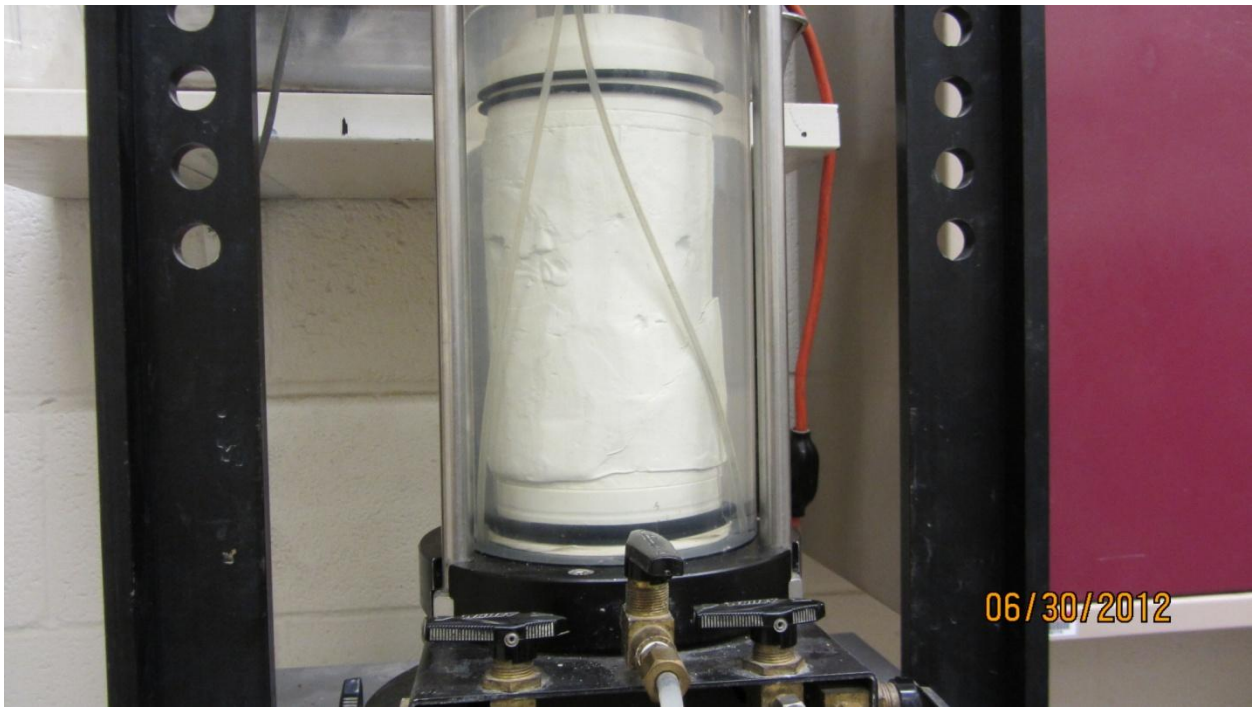

FIGURE 3.35 Shearing of the sample in triaxial test

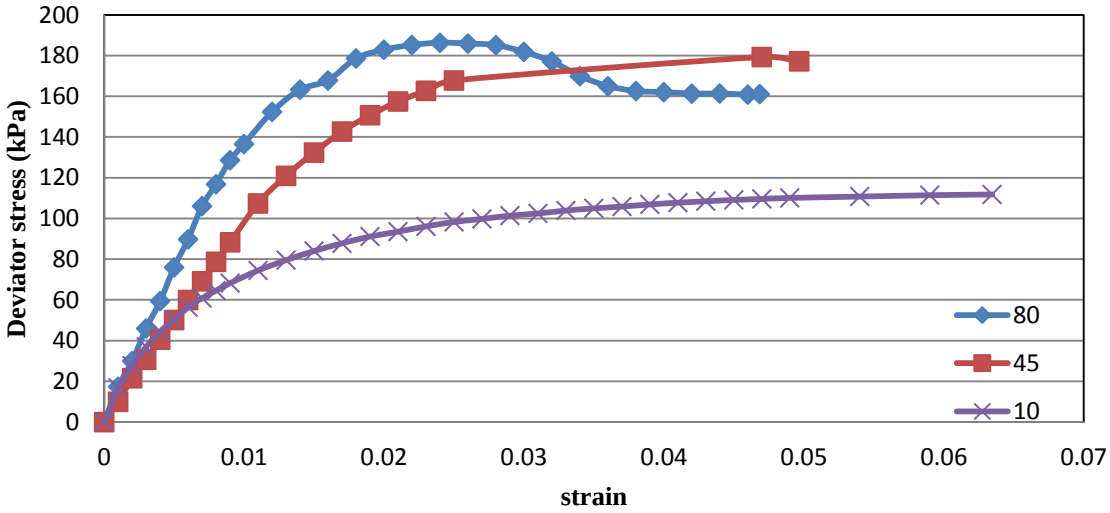

FIGURE 3.36 Stress-strain curve at different confining pressure

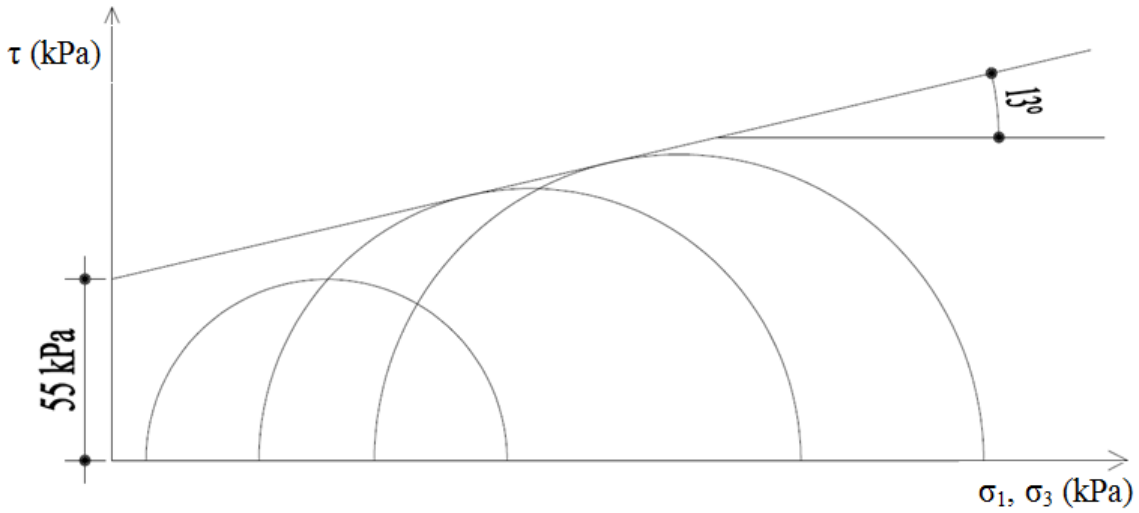

FIGURE 3.37 Total stress envelope of the soil

3.3.4 Summary of Experimental Study on Culvert under Rigid Pavement

This section summarizes the field test on a low fill box culvert under a rigid pavement under static and moving traffic loads and the laboratory tests on the samples obtained from the field. The data obtained from these tests will be used to verify and calibrate the numerical models created in this study. The following conclusions can be drawn from the test results:

1) The deflections of the culvert under static loading varied with the magnitude and position of the axle load and the type of the test section (concrete pavement, shoulder, or unsurfaced area). The higher axle load resulted in a larger deflection of the culvert. The culvert under the unsurfaced area deformed the most while that under the pavement deformed the least. This result implies that the distribution of the wheel loads through the pavement onto the culvert was to a wider area than those through the shoulder and the unsurfaced area.

2) The maximum deflection happened in the mid-span of the culvert when the load was applied at that location. The deflection decreased longitudinally and transversely with a distance. This result implies a two-way slab action.
3) In general, the observed deflections were higher for moving loads than static loads.
4) The pressure cell results showed that the wheel load was distributed onto the culvert within an area. The maximum pressure occurred beneath the point of wheel loading.
5) Compressive strength test was carried out on the samples cored from the concrete pavement and cement treated base courses. The compressive strength of the pavement concrete was 12.44 MPa, which was relatively lower than the typical concrete compressive strength used for pavements. The cement stabilized base course had compressive strength of 16.03 MPa and elastic modulus of 138 MPa. Both values were less than the typical values for the cement treated base course.
6) The backfill soil around the culvert was a high plasticity clay (CH), which had a liquid limit of 59, a plastic limit of 30, and a plasticity index of 29. The specific gravity of the soil was 2.67. The soil had an average elastic modulus of 12.9 MPa, cohesion of 55 kPa, and a friction angle of 13^{o} as determined from the triaxial tests.

3.4 Field Test on Culvert under Flexible pavement

3.4.1 Site Condition

The culvert selected for the field test was a single span reinforced concrete box culvert located at milepost 68.7 on K-148 highway over Mercer creek drainage near Barnes, Kansas. The culvert was a rigid frame box. The cross section of the culvert and the picture of the culvert are shown in Figures 3.38and 3.39respectively. The inside dimensions of the culvert were 5.4 m wide and 3

m high. The culvert was aligned perpendicularly to the highway. The fill depth from the riding surface of the asphalt concrete pavement was 600 mm from the top of the culvert roof. The overall length of the culvert was 10.35 m. There were two lanes of 3.3 m each. The culvert backfill was composed of dark brown low plasticity clay. The soil layer had liquid limit of 43, plastic limit of 20, plasticity index of 23, and specific gravity of 2.71. The hot mixed asphalt layer at the top surface was 475 mm thick, which was placed over a 125 mm thick lime stabilized subgrade. The culvert had 300 mm wide haunches at the corners.

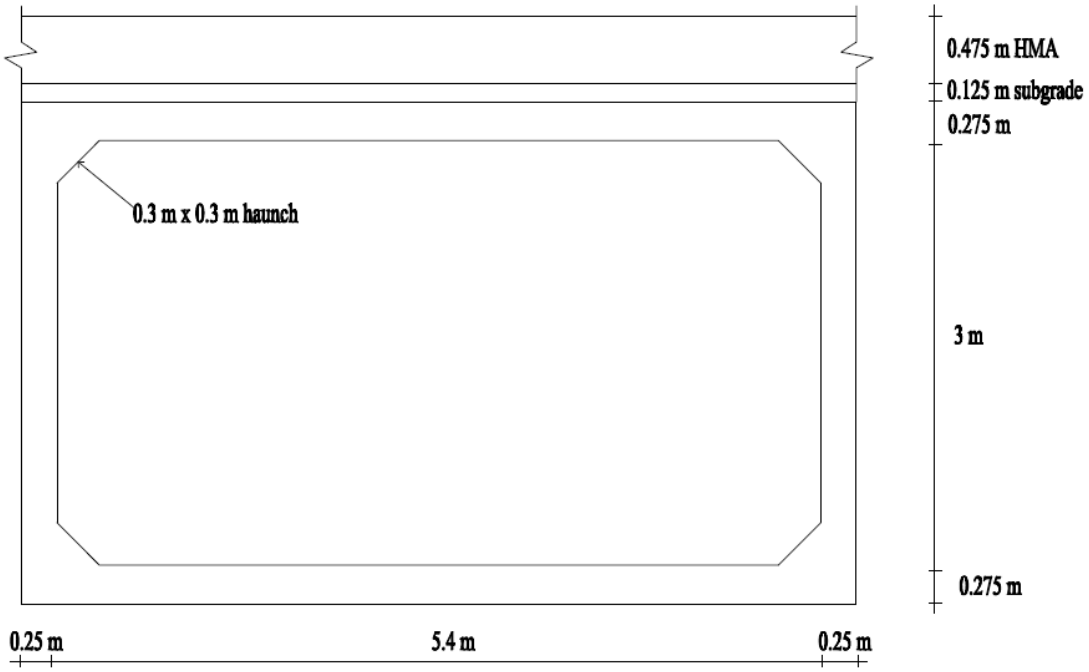

FIGURE 3.38 Cross-section of culvert and pavement layers

FIGURE 3.39 Test culvert

3.4.2 Test Devices and Instrumentations

To evaluate the performance of the culvert under the variable loadings, a series of test devices and instrumentations were used during the experiment. The culvert was instrumented with displacement transducers and strain gages under the southbound lane of the highway. Only one transducer was used under the northbound lane. Displacement transducers were used to measure the vertical deflections of the culvert roof slab. Strain gages were installed to measure the strain in the surface of the top slab at different locations during the loading.

Displacement Transducers

The displacement transducers used in this experiment were similar as explained in section 3.2.2.1. The layout of the displacement transducers are shown in Figure 3.40. Six transducers were used to capture the deflection response of the culvert under loading. Four displacement

transducers labeled as L1, L2, L3, and L4, were installed along the box axis to obtain the deflection profile along the centerline of the culvert whereas transducers L2, L5, and L6 were installed along the culvert span. Five out of six transducers were installed under the southbound lane of the highway and remaining one was placed under the northbound lane. The layout of the displacement transducers were planned to utilize the symmetry of the culvert about centerline of the road so that deflection profile can be drawn for a longer length of culvert. Also the three transducer located along a line perpendicular to the culvert axis can give deflection profile along the span for symmetric load about culvert axis. Transducers L1 and L3 were planned to be located right below the wheels and L2 to be under the middle of the axle. Load was applied at both northbound and southbound lanes. When load was applied in northbound lane, transducer L4 was serving as transducer L3 when southbound lane was loaded. Similarly, the deflection measured at transducers L1 and L2 during northbound lane loading could be considered as the deflection at respective locations under northbound lane while loading southbound lane. Metal frames of approximately 2.8 m height were used to support and fix the displacement transducers in position as shown in Figure 3.41. The frames were stabilized by sand bags at the base.

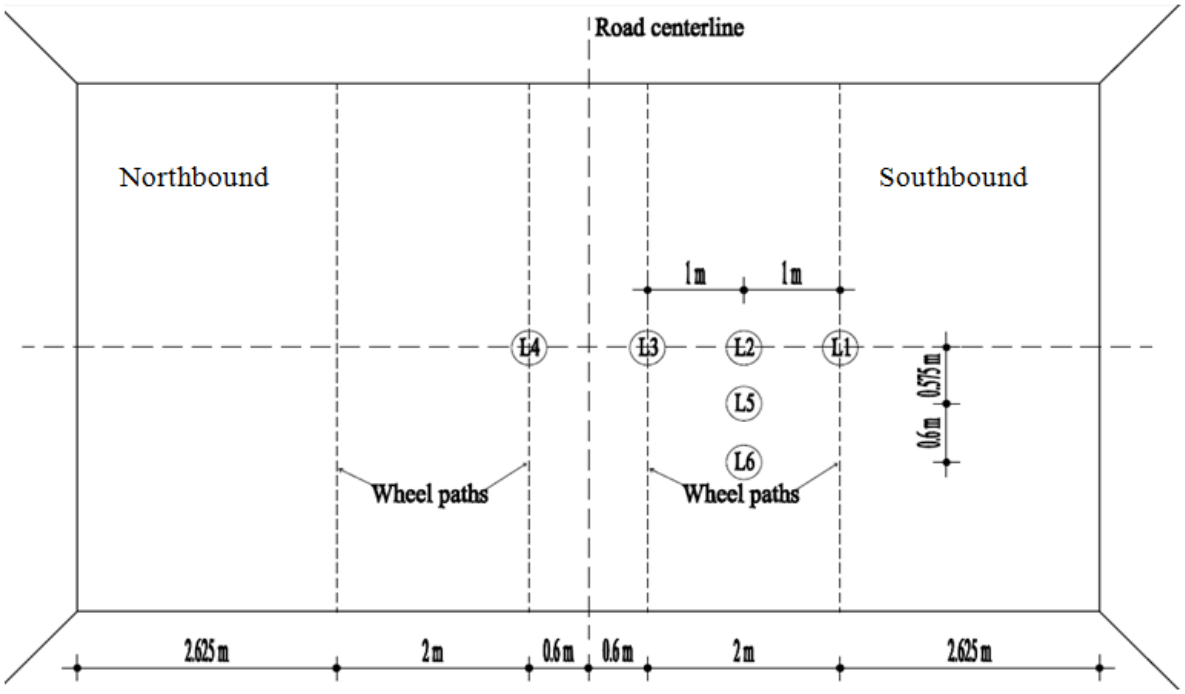

FIGURE 3.40 Layout of displacement transducers

FIGURE 3.41 Metal frames used to support displacement transducers

Strain Gages

Strain gages were installed to measure the strain on the bottom surface of the top slab at different locations during the loading. The strain gages used in this research and installation procedure were similar as explained in section 3.2.2.3.

Five strain gages were installed on the bottom surface of the top slab, with all of them installed under the southbound lane. The layout of the strain gages are shown in Figure 3.42. Three strain gages were positioned along the culvert axis and three perpendicular to the culvert axis. Strain gages S1 and S3 were intended to measure the strain right below the wheels, whereas strain gage S2 was located to be under the middle of the axle during loading. Strain gages S2, S4 and S5 were installed along the culvert span.

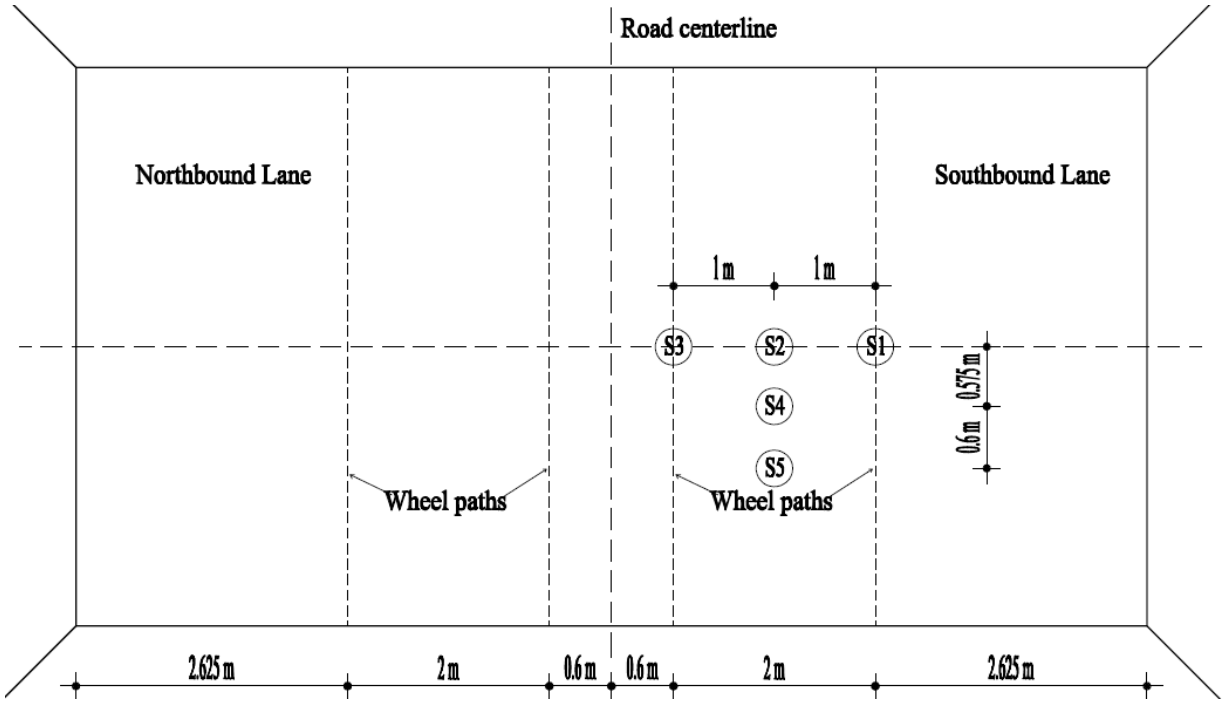

FIGURE 3.42 Layout of strain gages

Data Acquisition

Smart Dynamic Strain Recorder DC-204R manufactured by Tokyo Sokki Kenkyujo, Co., Ltd., Japan was used to record the data from displacement transducers, and strain gages. There were three recorders used during the tests. Among the three recorders one data recorder served as a master recorder and the remaining two served as slaves, which were synchronized with the master recorder during connections. Each recorder had four connection ports to sensors. The power to the recorders and computers were supplied using batteries and inverters. The set up of the data acquisition system is shown in Figure 3.43.

FIGURE 3.43 Data acquisition system

Load Scheme

A low-boy loaded with a backhoe was used as the test truck. The truck consisted of six physical axles: a front steering axle, middle tandem axles, and triple axles at the end. However, seven

load positions were adopted in this study. The axle configuration and the load on each axle are shown on Figure 3.44 while Figure 3.45 shows a picture of the truck used in this experiment. Table 3 shows the calculated contact area for each wheel load. The load of the front steering axle load was 57 kN. The center of the tandem axles was 4.8 m from the front axle and had a 98 kN load on each axle. The center of the triple axles was 12.3 m behind the center of the tandem axles. Each axle of the triple provided a 80.5 kN load. The center to center distance between wheels on the same axle was 2 m.

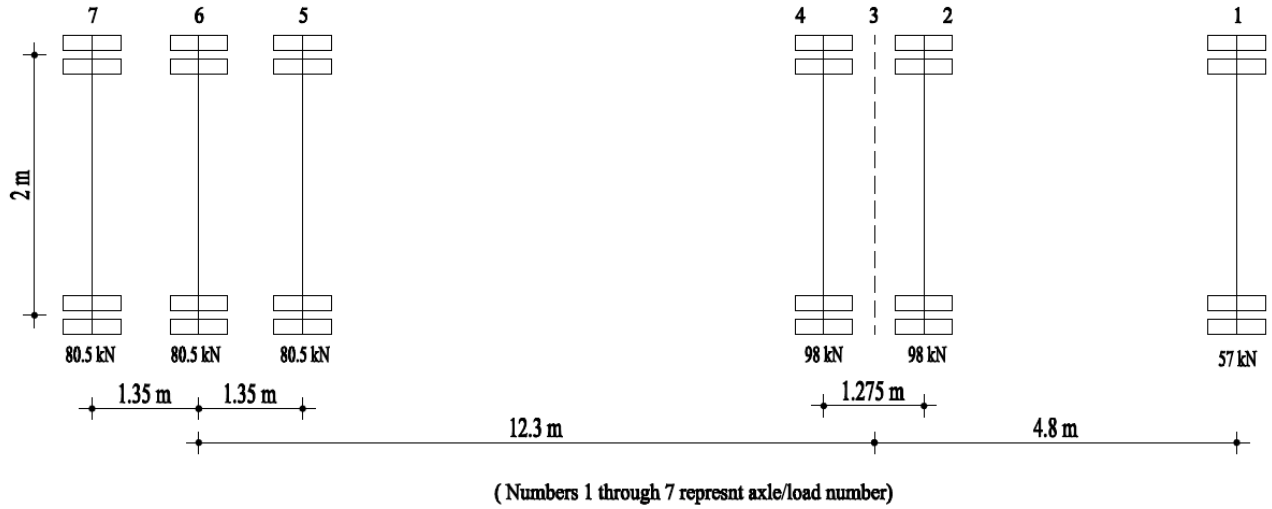

FIGURE 3.44 Axle load and configuration of the test truck

FIGURE 3.45 Test truck used in loading the culvert

TABLE 3.3 Calculated contact area for each axle load

Axle no.	Axle load (kN)	Tire Pressure (kPa)	Calculated wheel contact area (m^2)
1	57	760	0.075
2	98	760	0.129
3	0	760	0
4	98	760	0.129
5	80.5	760	0.106
6	80.5	760	0.106
7	80.5	760	0.106

The response of the culvert was measured under static and traffic loading condition. Static and traffic loadings were applied at both southbound and northbound lanes. The axis of the culvert was marked with color sprayer on the surface to determine the position of each axle during static loading as shown in Figure 3.46. Also the intended lateral positions of the wheels were marked along the same line in both lanes. Seven load combinations were obtained through applying static loading at each section by placing six axles of the truck over the marked line in turn. One more combination was obtained by assuming one dummy axle in the middle of the tandem axle. This dummy axle also provided one more symmetric load. The numbering of each axle load combination is shown in Figure 3.44.

FIGURE 3.46 Marks along the axis of the culvert for wheel position

Static loading was first applied at southbound lane then to northbound lane. Desired positions of axles were achieved by guiding the truck on the points previously marked on the pavement. All the seven axles, including the dummy axle, were placed on the marks in turn to create seven

loading positions (referred as Loads 1 to 7) as shown in Figure 3.47. Pressure and deflection readings were recorded using the data acquisition systems. Later, similar procedure was followed on the northbound lane for static loading. Traffic loading was applied on both lanes by moving the truck at six predetermined speeds: 10 to 60 mph at an increment of 10 mph.

FIGURE 3.47 Seven load combinations used in static lading on the culvert

3.4.3 Field Test Results

The test data collected through displacement transducers and strain gages were analyzed and are presented below in tabular forms and graphically.

Displacement Results

The measured deflections of the culvert at the displacement transducer locations, when the load was applied on the southbound lane, are shown in Figure 3.48 and Table 3.4. The deflections observed at transducers L1, L2, L3, and L5 were almost equal. However, transducer L2, which was at the middle of the axle, recorded the maximum deflection. Displacement transducer L4 installed below the northbound lane recorded the minimum deflection during the southbound

lane loading. The deflection at the quarter span of the culvert was also considerably lower than the deflections at other locations.

TABLE 3.4 Deflections during southbound lane loading

Deflection (mm)						
Axle	L1	L2	L3	L4	L5	L6
0	0	0	0	0	0	0
1	-0.09	0.04	-0.07	-0.05	-0.09	-0.08
2	-0.47	-0.41	-0.43	-0.27	-0.48	-0.41
3	-0.53	-0.53	-0.49	-0.31	-0.52	-0.41
4	-0.51	-0.51	-0.49	-0.31	-0.47	-0.35
5	-0.46	-0.44	-0.43	-0.27	-0.47	-0.4
6	-0.58	-0.58	-0.55	-0.36	-0.57	-0.45
7	-0.47	-0.47	-0.46	-0.3	-0.43	-0.31

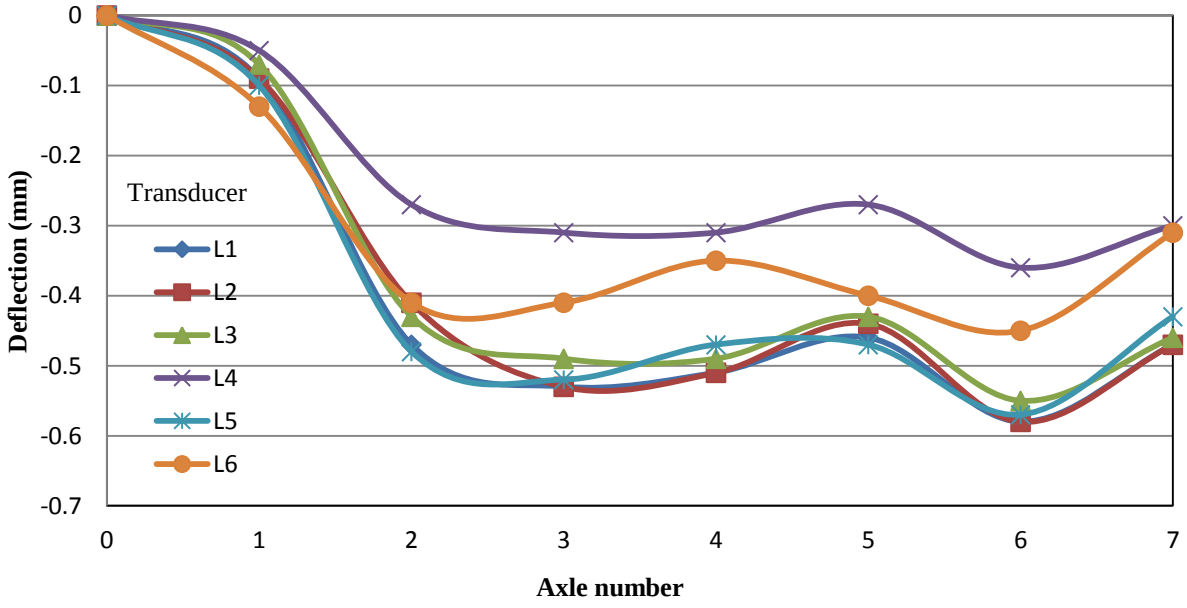

FIGURE 3.48 Deflections during southbound lane loading

The measured deflections of the culvert at the displacement transducer locations, when the load was applied on the northbound lane, are shown in Figure 3.49 and Table 3.5. The maximum deflection was observed at transducer L4 and the minimum deflections were observed at L6 and L1. The deflections observed at transducers L2 and L5 were almost equal.

TABLE 3.5 Deflections during northbound lane loading

Deflection (mm)						
Axle	L1	L2	L3	L4	L5	L6
0	0	0	0	0	0	0
1	-0.01	-0.03	-0.06	-0.13	-0.02	0
2	-0.09	-0.17	-0.28	-0.46	-0.14	-0.09
3	-0.11	-0.2	-0.32	-0.54	-0.17	-0.11
4	-0.1	-0.18	-0.32	-0.52	-0.17	-0.11
5	-0.09	-0.16	-0.27	-0.46	-0.14	-0.08
6	-0.12	-0.22	-0.38	-0.6	-0.2	-0.13
7	-0.11	-0.19	-0.33	-0.53	-0.18	-0.13

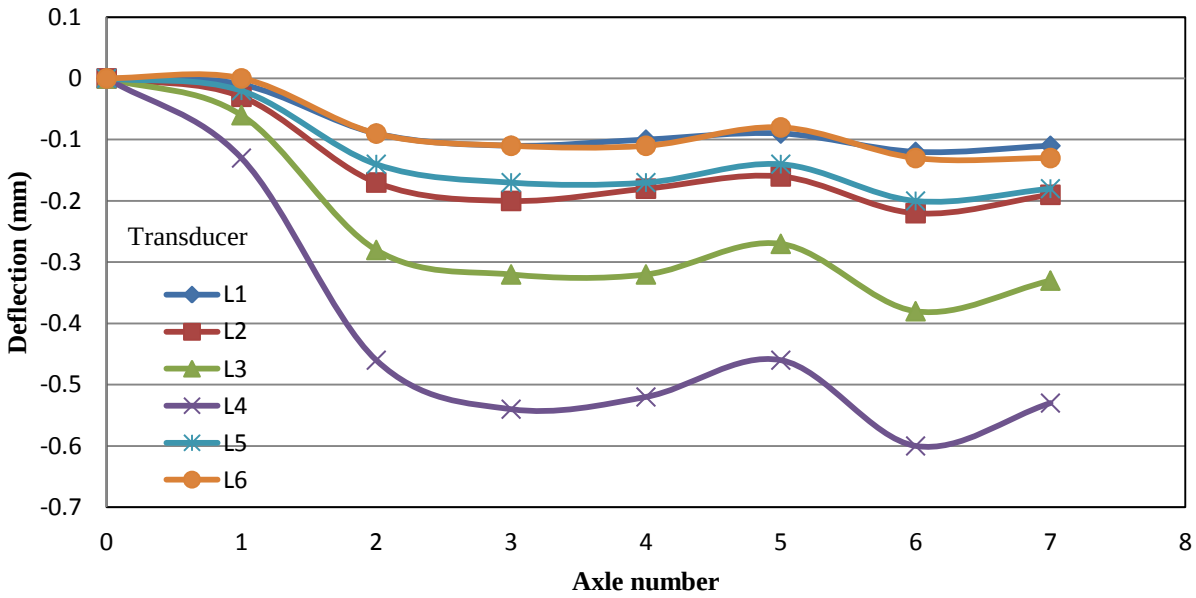

FIGURE 3.49 Deflections during northbound lane loading

Deflection transducer L4 was at a distance of 1.2 m from the inner wheel of the truck when the load was applied at the southbound lane. Similarly deflection transducer L3 was at a distance of 1.2 m from the inner wheel of the truck when the load was applied at the northbound lane. Therefore the observed deflections at those locations during southbound and northbound lane loadings were nearly interchangeable. Because of the relative locations of the displacement transducers during southbound and northbound lane loadings, it was possible to plot the deflection profile along the culvert axis even under the northbound lane. The resulting deflection profiles under each axle load during southbound lane loading are shown in Figure 3.50. While these deflection profiles were drawn, the deflections recorded at L1, and L2 were assumed to be equal to the deflections at the corresponding locations under the northbound lane. Axle 6 produced the maximum deflections at all locations whereas Axle 1 produced the least deflections.

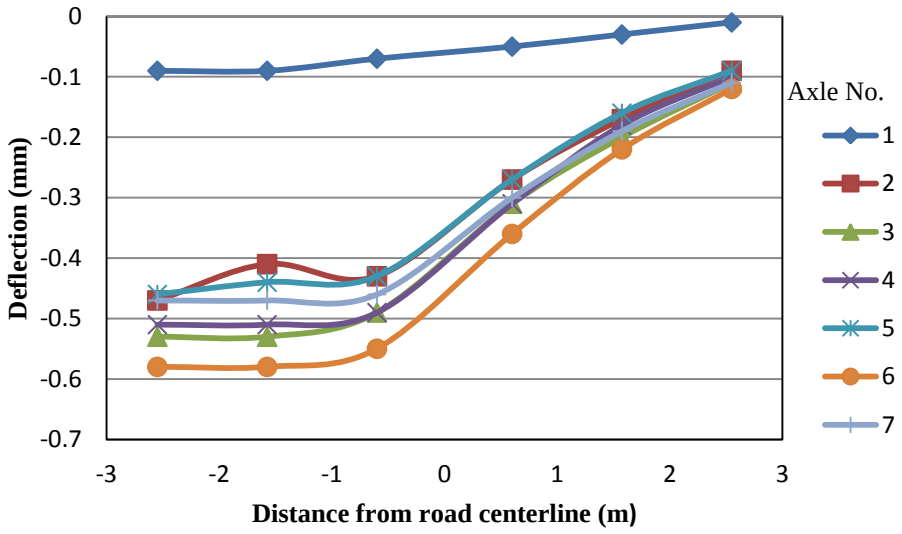

FIGURE 3.50 Deflection profiles along the culvert axis during southbound lane loading

The loading was symmetric about the culvert axis when the axles 1, 3, and 6 were at the marked locations. Therefore the deflections observed at L5 and L6 can be assumed to be equal to those at the corresponding locations of the symmetric half of the culvert. Under this assumption the deflection curve can be plotted as shown in Figure 3.51. However, the recorded deflections under Axle 1 loading show a curvature in the opposite direction.

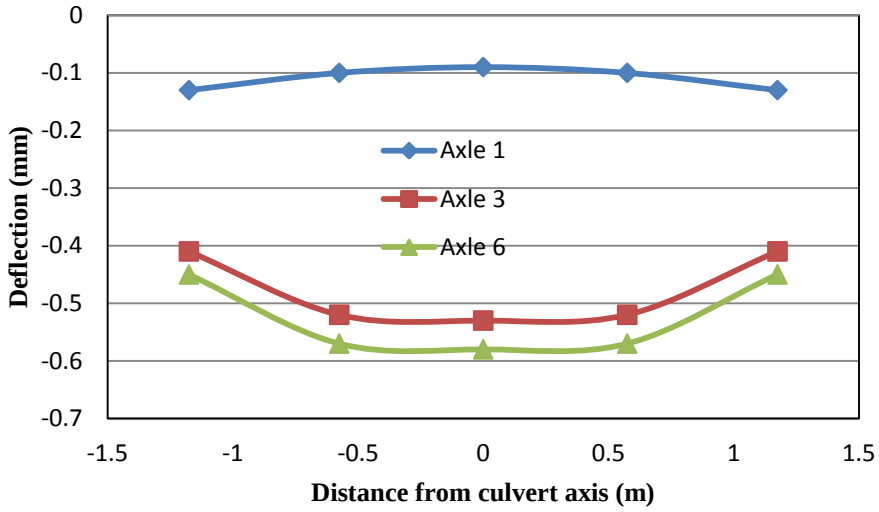

FIGURE 3.51 Deflection profiles perpendicular to the culvert axis during southbound lane loading

The front steering axle, the tandem axles, and the triple axles as shown in Figure 3.52 had gross loads of 57, 196, and 241.5 kN, respectively. The axle loads became symmetric with regard to the culvert axis at Axles 1, 3, and 6, respectively. Figure 3.52 also shows that the vertical deflection generally increased with an increase of the gross load of the axle. Here the deflections were taken from southbound lane loading for L1, L2 and L3 and from northbound lane loading for L4. The deflections for L1 and L2 were equal for all the loads; therefore they are overlapping.

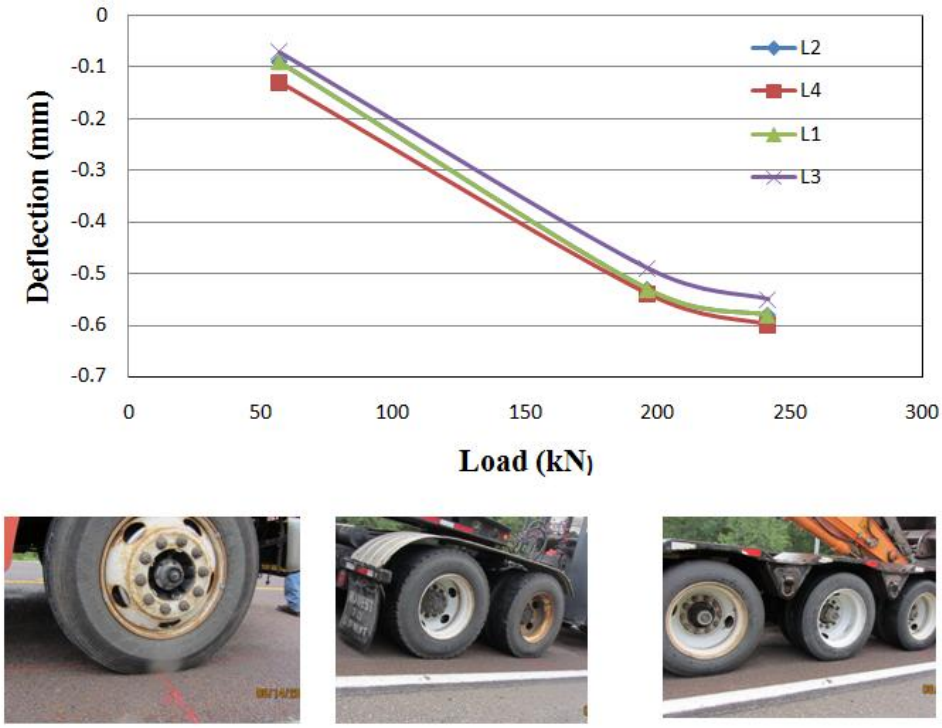

FIGURE 3.52 Deflections at different sections under a symmetric load

The culvert was also tested for a moving load by driving the test truck at speeds varying from approximately 10 mph to 60 mph with an increment of 10 mph. The moving load was applied to both lanes. The resulting maximum deflections at all the locations are shown in Tables 3.5 and 3.6 and Figures 3.53 and 3.54 for southbound lane loading and northbound lane loading respectively. The general trend of the plot shows that the deflections decreased gradually with an increase in speed from 10 to 40 mph. Beyond the speed of 40 mph the deflection remained almost unchanged.

TABLE 3.6 Maximum deflections due to moving load for southbound lane loading

Deflection (mm)						
Speed (mph)	L1	L2	L3	L4	L5	L6
10	-0.41	-0.41	-0.33	-0.22	-0.37	-0.28
20	-0.41	-0.36	-0.3	-0.21	-0.33	-0.25
30	-0.37	-0.34	-0.32	-0.18	-0.31	-0.24
40	-0.35	-0.37	-0.26	-0.23	-0.31	-0.25
50	-0.36	-0.36	-0.31	-0.22	-0.33	-0.25
60	-0.39	-0.41	-0.33	-0.23	-0.35	-0.27

TABLE 3.7 Maximum deflections due to moving load for northbound lane loading

Deflection (mm)						
Speed (mph)	L1	L2	L3	L4	L5	L6
10	-0.12	-0.22	-0.23	-0.33	-0.16	-0.12
20	-0.1	-0.2	-0.21	-0.3	-0.15	-0.11
30	-0.11	-0.18	-0.24	-0.29	-0.13	-0.11
40	-0.1	-0.15	-0.19	-0.23	-0.12	-0.09
50	-0.1	-0.15	-0.19	-0.3	-0.17	-0.11
60	-0.1	-0.13	-0.2	-0.3	-0.12	-0.12

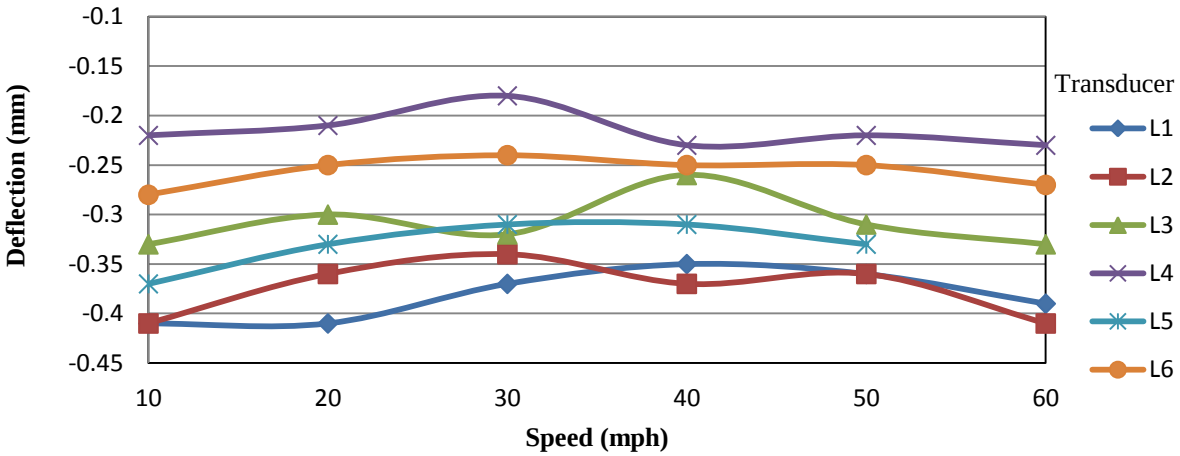

FIGURE 3.53 Maximum deflections due to moving load for southbound lane loading

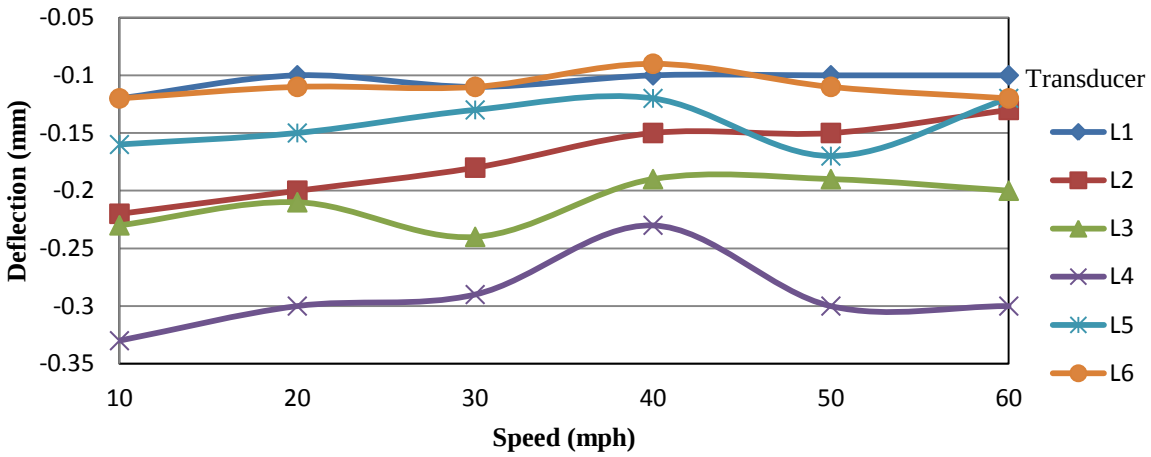

FIGURE 3.54 Maximum deflections due to moving load for northbound lane loading

Strain results

Strains were recorded under both static and moving loads. However, the recorded strains were small and within the magnitude of noise. Therefore, they are not meaningful to be reported and useful for the calibration of the numerical model.

3.5 Laboratory Tests of Samples

After the field loading test on the culvert, the samples of the pavement layers along with the natural backfill soil were obtained from two boreholes: one borehole was drilled above the culvert and another borehole was drilled on the side of the culvert. Both boreholes were drilled on the southbound lane, which were 1.5 m west from the centerline of the road. All the samples taken from the field are shown in Figure 3.55. Two asphalt cores and four Shelby tube samples were obtained after the drilling operation. Both asphalt cores were 475 mm thick. The Shelby tubes, which were pushed inside the borehole on the side of the culvert, recovered the natural soil samples at four depths1, 2, 3, and 4 m respectively. The borehole located at the side of the

culvert was advanced down to 5.9 m deep. Below the asphalt layer there was a dark brown gray fill containing a silty clay with some sand, asphalt, and wood particles down to 4 m deep. The ground water table was at the depth of 3.8 m below the pavement surface. Weathered limestone was found from 4.3 m to 4.7 m deep. From the depths of 4.7 m to 5.9 m there was brown mottled dark gray shale, which was firm and moist. Hard and dense limestone was found at the depth of 5.9 m.

FIGURE 3.55 Shelby tube samples and asphalt cores obtained from drilling

FIGURE 3.56 Core drilling above the culvert

3.5.1 Rebound Test of Asphalt Sample

The core obtained from the pavement consisted of 475 mm thick asphalt concrete. The diameter of the concrete sample was measured with the help of Vernier caliper and found to be 98 mm. The 475 mm high samples were sawed into the samples with a height-to-diameter ratio of 2:1. The heights of the samples were approximately 200 mm after sawing. The density of the sample measured before testing was 2138 kg/m^3. A rebound test was conducted to estimate the elastic modulus of the asphalt concrete. Figure 3.57 shows the dial gage arrangement and test setup for a rebound test of the asphalt sample. The gage length for the deformation measurement was 150 mm. The compressive load was applied up to 5.33 kN at the rate of 0.5% strain per second. The corresponding maximum compressive stress was 690 kPa, which was nearly equal to the tire contact pressure applied by the test truck. The dial gage reading was taken immediately after the

applied pressure reached the maximum value and the maximum compression was 0.114 mm. Then the applied load was released and the specimen was allowed to rebound. The dial gage reading after the rebound was 0.038 mm; therefore, the total rebound was 0.076 mm. The elastic modulus of the asphalt concrete was determined to be 1,827 MPa.

FIGURE 3.57 Rebound test of the asphalt cylinder

3.5.2Laboratory Tests on Backfill Soil

The undisturbed soil samples in the Shelby tubes obtained from the field were extruded using the Shelby tube sample extractor as shown in Figure 3.27. The soil sample was then trimmed to required size for the triaxial test. The soil obtained during trimming of the sample was used to measure moisture content and carry out Atterberg limit and specific gravity tests. The moisture contents of the soil samples from different tubes were between 18 to 20%.

The Atterberg limit tests were carried out in accordance with ASTM D4318-05 on the soil obtained from trimming of the undisturbed soil sample to determine the liquid and plastic limits. To determine the liquid limit of the backfill soil, a flow curve was developed by conducting three liquid limit tests using the Casagrande apparatus at different moisture contents as shown in Figure 3.58. From the flow curve the liquid limit was found to be 43% and the plastic limit test showed the plastic limit of 20%. Therefore, the plasticity index of the backfill soil was 23. According to USCS the soil was classified as low plasticity clay (CL).

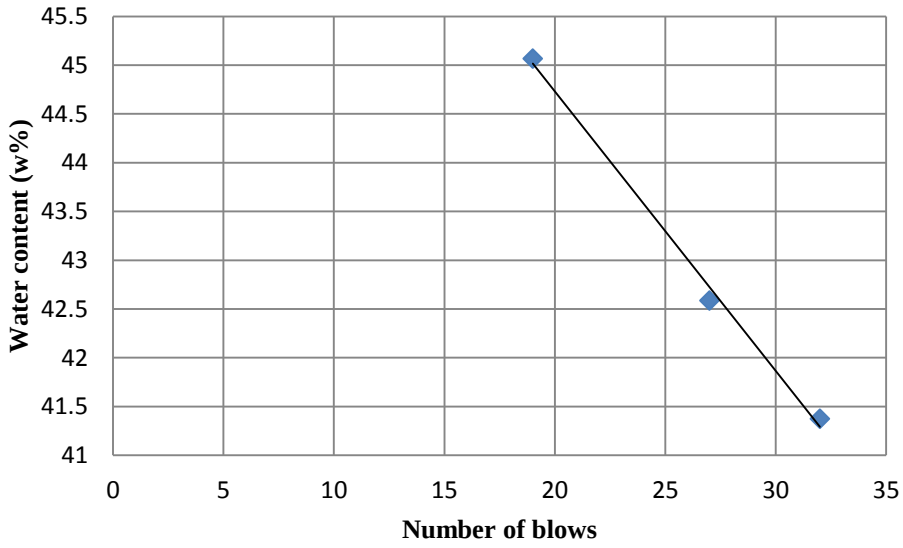

FIGURE 3.58 Flow curve of the soil

A specific gravity test was conducted in accordance with ASTM D854-10. The specific gravity of the soil was determined to be 2.71.

Triaxial tests of the soil samples were carried out in natural condition to determine the elastic modulus, cohesion, and friction angle of the soil. The soil sample extruded from the Shelby tubes had 100 mm in diameter. The samples were trimmed into the ones with 2.8 in (71 mm) in diameter and 5.6 in (142 mm) in height. Figure 3.59 shows the soil sample inside the membrane

resting on the bottom pedestal of the triaxial chamber. The triaxial tests were conducted on three samples at different confining pressures of 80, 45, and 10kPa respectively. Figure 3.60 shows the entire triaxial test setup. Figure 3.61 shows the stress-strain curves obtained from the three tests. The elastic modulus of the soil was calculated as a secant modulus at 50% the peak strength. The elastic moduli of the soil were found to be 12.3, 9.1 and 10.8 MPa at the confining stresses of 80, 45, and 10 kPa respectively with an average value of 10.7 MPa. The total stress envelope drawn using the test results is shown in Figure 3.62. It resulted in cohesion of 44 kPa and friction angle of 22^{o}.

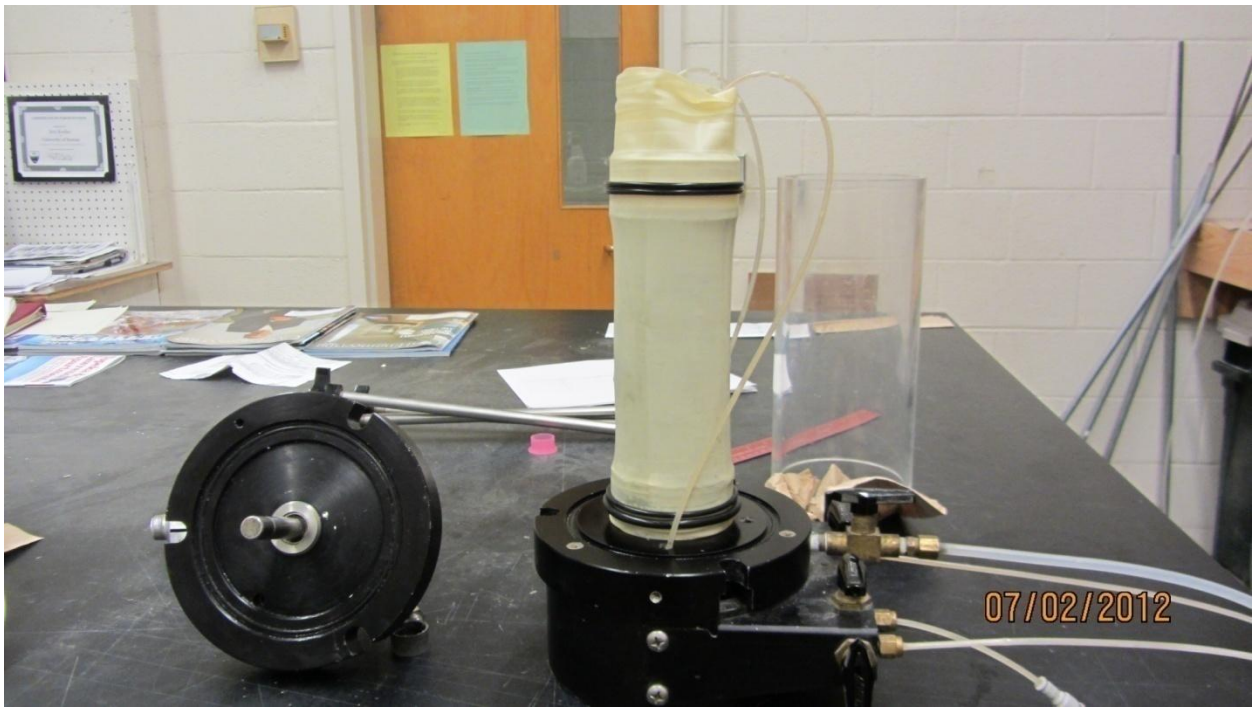

FIGURE 3.59 Soil sample placed inside the membrane

FIGURE 3.60 Loading frame and pressure control system for the triaxial test

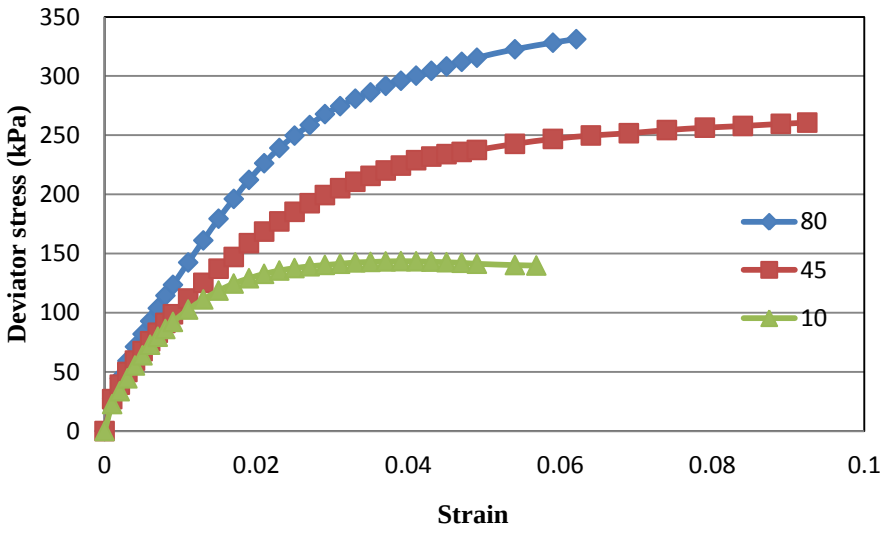

FIGURE 3.61 Stress-strain curves for samples tested at different confining pressures

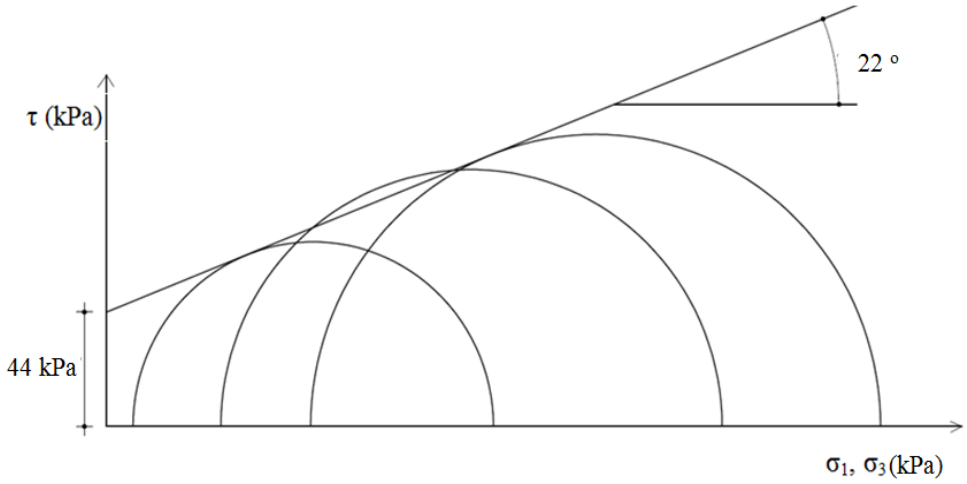

FIGURE 3.62 Total stress envelope

3.5.3 Summary of Experimental Study on Culvert under Flexible Pavement

This section summarizes the field test on a low fill box culvert under a flexible pavement under static and moving traffic loads and the laboratory tests on the samples obtained from the field. The following conclusions can be drawn from the test results:

1) The deflections of the culvert under static loading varied with the magnitude and position of axle load. The higher axle load resulted in a larger deflection of the culvert.
2) The maximum deflection happened in the mid-span of the culvert when the load was applied at that location. The deflection decreased longitudinally and transversely with the distance. This result implies a two-way slab action.
3) In general, the observed deflections were smaller under moving loads than under static loads.
4) The rebound test was carried out on the asphalt concrete sample to determine the elastic modulus of the asphalt concrete to 1,827 MPa.

5) The backfill soil around the culvert was a natural clay soil having a liquid limit of 43, a plastic limit of 20, and a plasticity index of 23. The specific gravity of the soil was 2.71. The backfill soil had an average elastic modulus of 10.7 MPa, cohesion of 44 kPa, and a friction angle of 22^{o} as determined from the triaxial tests.

Chapter 4 Verification of Numerical Model

4.1 Introduction

To study the load distribution on the culverts, a parameter study was carried out using the commercial software, Fast Lagrangian Analysis of Continua in 3 Dimensions (FLAC3D). A true representation of the culvert response under loading becomes important before carrying out the study on the effects of different influence factors on load distribution. In this chapter two culverts that were tested under truck loads as presented in Chapter 3 were modeled and calibrated in FLAC3D.

4.2 FLAC3D

FLAC3D is a finite difference program, which is specially designed for simulating three-dimensional geotechnical engineering problems. This program is suitable for solving nonlinear and large displacement problems and has 11 built-in constitutive models for various types of geomaterials. With this program it is possible to model reinforcement and structural features along with appropriate soil models. This software also provides users the facility to create their own constitutive model, which is also called user defined model (UDM). However, the user defined model should be programmed with C++ and compiled to a DLL file to make it work with FLAC3D.

4.3 Culvert under Rigid Pavement

4.3.1 Material Models and Parameters

The pavement-culvert system involved different materials. The pavement consisted of plain cement concrete (PCC), under which there were cement treated base course, lime-treated

subgrade, and a natural subgrade above the top slab of the culvert. The culvert was made of reinforced cement concrete. The backfill around the culvert was a natural soil. The dimensions of the culvert and pavement layers were described in Chapter 3. All the layers were modeled as elastic materials with different properties.

The compressive strength of the concrete pavement as determined in the lab was 12.44 MPa (1,804 psi). This strength value was low compared to a typical value of 15 to 40 MPa (2 to 6 ksi) (Sidney et al. 2003). The lower strength of the test sample might be attributed to possible sample damage during coring and boundary effects. The typical concrete pavement design strength by KDOT is 26.9 MPa (3,900 psi). The compressive strength of the concrete can be used to determine its elastic modulus using the correlation given in Equation 4.1 as given by ACI 318-11 in Section 8.5.

$$E_c = 57000\sqrt{f'_c} \tag{4.1}$$

where E_c = elastic modulus of the concrete in psi;

f'_c = compressive strength of the concrete in psi.

The calculated elastic modulus of the concrete based on the typical concrete pavement design strength by KDOT was 24,545 MPa (3,560 ksi), which was adopted for the numerical analysis. In addition, Poisson's ratio of concrete of 0.15 was used in the model calibration.

The elastic modulus of the cement-treated base course as described in Chapter 3 was 180 MPa (26 ksi), which was much lower than the typical value (500 to 1000 ksi) for cement aggregate mixture provided by the AASHTO Guide for Design of Pavement Structures (1993). The lower modulus of the test sample might also be attributed to possible sample damage during coring and

boundary effects. Therefore, the average elastic modulus of 5171 MPa (750 ksi) based on the typical value was used in the calibration of the model with Poisson's ratio of 0.3.

The AASHTO Guide for Design of Pavement Structures (1993) also suggested a typical value of elastic modulus for lime-treated subgrade ranging from 138 to 483 MPa (20 to 70 ksi). Therefore, an average value of 310 MPa (45 ksi) was adopted for the calibration of the numerical model. Poisson's ratio of 0.3 was used for the lime-treated subgrade. The average elastic modulus of the soil obtained from the triaxial test was 12.9 MPa, which was used for the unsurfaced section including the natural subgrade and the backfill soil. Poisson's ratio of 0.3 was used for soils.

It was assumed that the concrete had a typical compressive strength of 4500 psi. Considering 1% of the steel reinforcement with an elastic modulus of 29,000 MPa, the elastic modulus of the reinforced concrete was determined to be 27,580 MPa (4,000 ksi). Poisson's ratio of the concrete was assumed at 0.15. The summary of the material properties used in the numerical analysis is listed in Table 4.1.

Axles 1, 3 and 6 provided symmetric loads with respect to the culvert axis. Therefore, Axle 6 was used to calibrate the model and the computed deflections using the calibrated model with Axles 1 and 3 will be compared with those from the field study.

TABLE 4.1 Summary of the material properties used in the model calibration

Material	Elastic modulus (MPa)	Poisson's ratio
Pavement concrete	24545	0.15
Cement treated base course	5171	0.3
Lime treated subgrade	310	0.3
Natural subgrade and backfill soil	12.9	0.3
Culvert concrete	27580	0.15

4.3.2 Numerical Mesh and Boundary Conditions

Only half of the culvert was modeled to utilize the symmetry condition as shown in Figure 4.1. Unyielding foundation conditions were assumed for the model. Therefore the vertical movement at the bottom of the culvert was restricted. All vertical boundaries were restrained for horizontal movement except for the free boundary of the box culvert in the y direction. The horizontal displacement of the culvert was restrained at the symmetry plane (yz plane). Rollers were used at the symmetrical boundary, which allowed vertical movement but restrained horizontal movement. The boundary conditions are shown in Figure 4.2.

The length, width, and height of the model were 28 m, 6.75 m, and 4.15 m respectively. The numbers of zones were 123,436, 117,088 and 119,986 when Axles 1, 3, and 6 were applied in the model respectively. The reason for the difference in the number of zones for different axles is that each axle had a different contact area of the load, which required changing the size of the mesh on the surface where the load was applied. Finer zones were used near the culvert and the zone density gradually decreased away from the culvert. The load was applied as a pressure on the surface of the pavement, the shoulder, and the unsurfaced area in turns. The number and size of zones required to apply the pressure were calculated as shown in Table 4.2 so that the total wheel load was equal to that in the field test while the contact pressure was close to that in the field test.

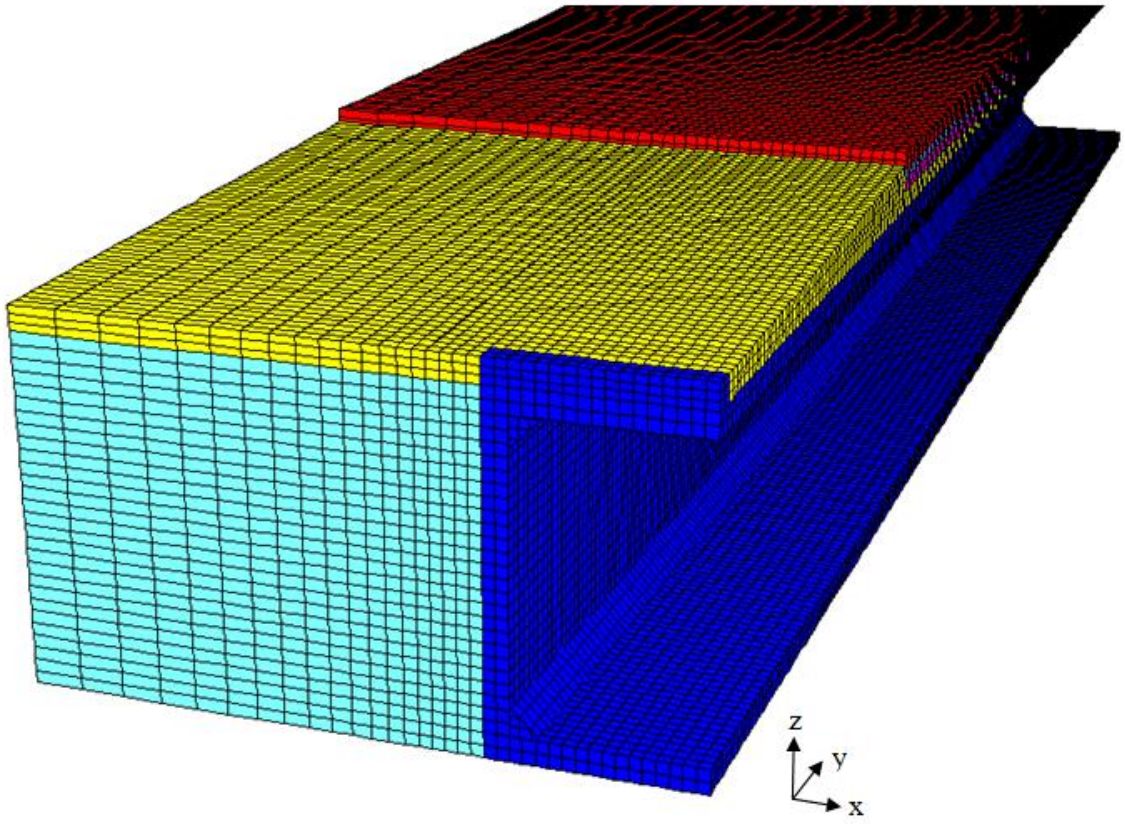

(a)

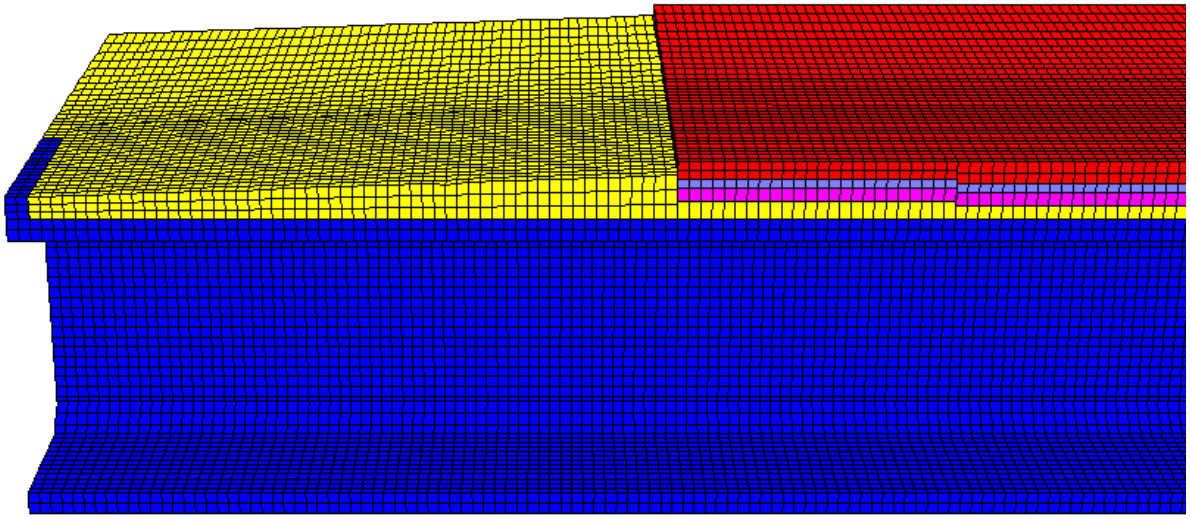

(b)

FIGURE 4.1 FLAC3D model of the culvert

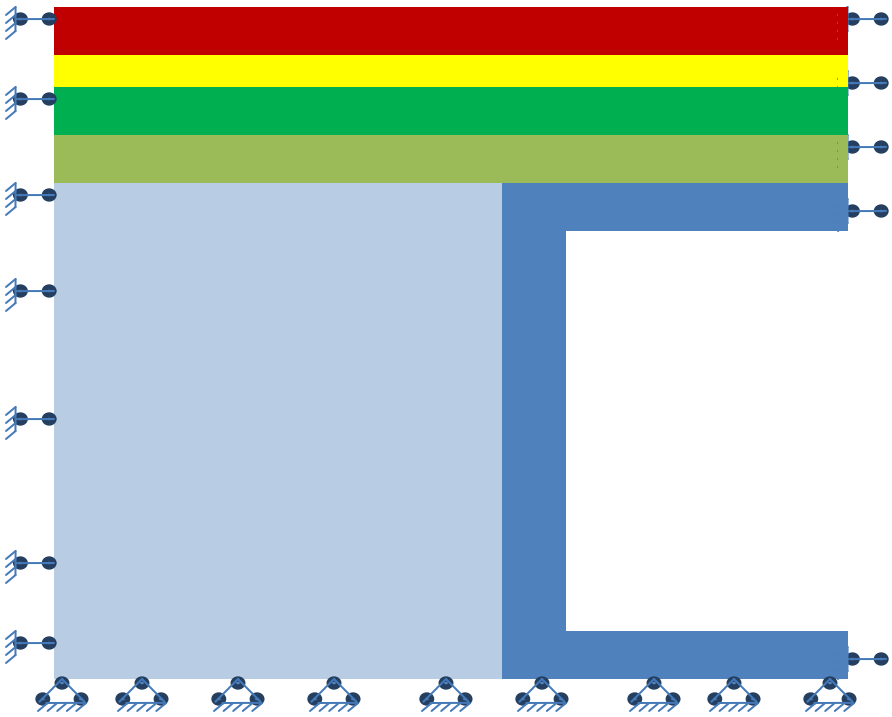

FIGURE 4.2 Boundary conditions used in the model

TABLE 4.2 Calculation of pressure and number of zones to apply pressure

Axle No.	Single wheel load (kN)	Actual tire pressure in field (kPa)	Contact area (m^2)	Area of each zone (m^2)	Number of zones	Applied pressure in model (kPa)
1	24.5	760	0.032	0.010	4	613
2	52.5	760	0.069	0.016	4	840
3	0	0	0	0.000	0	0
4	52.5	760	0.069	0.016	4	840
5	40.25	760	0.052	0.013	4	805
6	40.25	760	0.052	0.013	4	805
7	40.25	760	0.052	0.013	4	805

When Axle 1 was applied in the model, each wheel only had two zones due to the symmetry condition as shown in Figure 4.3. Axle 3 did not have its own load. However, when Axle 3 was in place, the wheel loads used for Axles 2 and 4 were applied on the culvert. Due to the symmetry, only one of the wheel loads was applied in the model as shown in Figure 4.4.

Similarly, when Axle 6 was on place, the wheel loads for Axles 5 and 7 were also applied on the culvert. However, half of the load from Axle 6 and a full load from Axle 5 or 7 were applied to the model as shown in Figure 4.5.

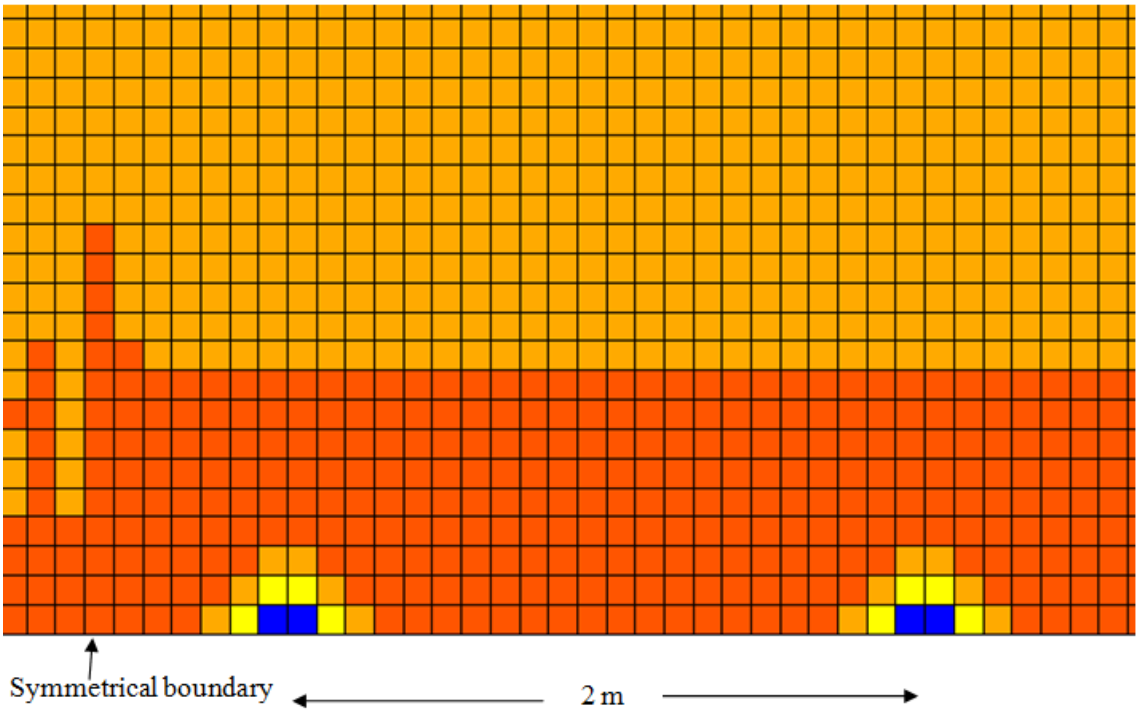

FIGURE 4.3 Axle 1 load applied as pressure on the top surface of the pavement

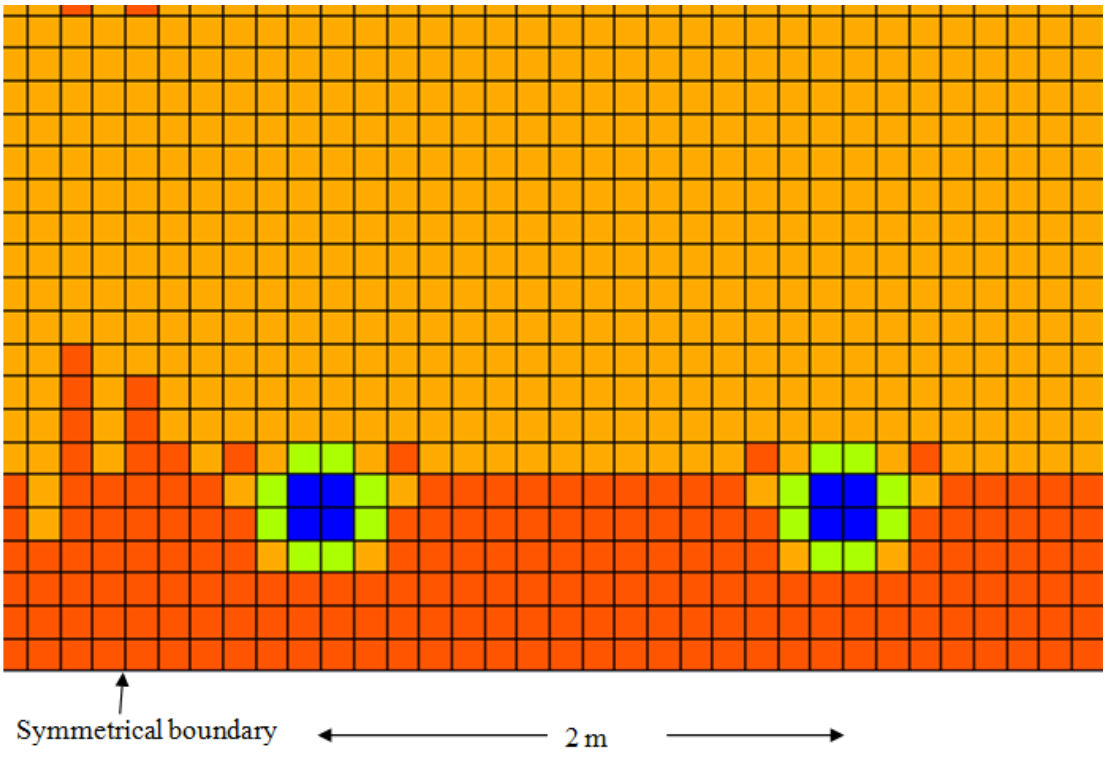

FIGURE 4.4 Axle 3 applied on the top surface of the pavement

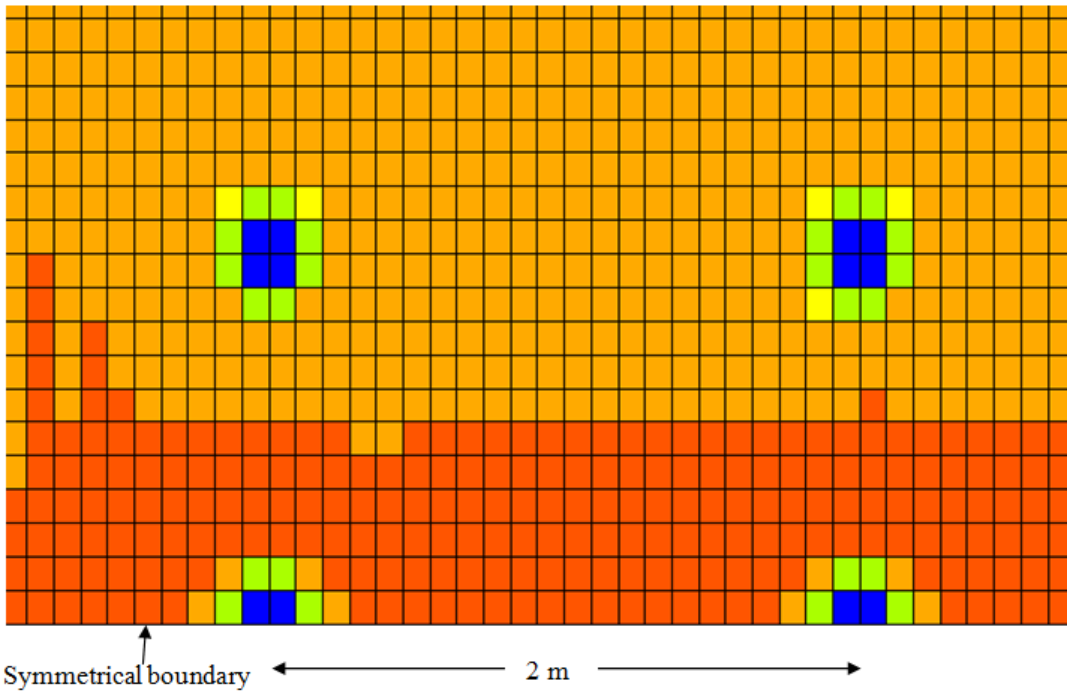

FIGURE 4.5 Axle 6 applied on the top surface of the pavement

4.3.2 Deflections of Culvert Top Slab

The measured deflections at Locations L1through L5 are compared with the computed ones from FLAC3D. Table 4.3 and Figure 4.6 show the measured deflections compared with the computed ones from FLAC3D when Axle 1 was applied on different test sections. Figure 4.6 (a) shows that the measured deflections at all the locations reasonably matched the computed ones from FLAC3D when Axle 1 was applied on the unsurfaced section. The difference in their deflections was more significant near the point of the load application and gradually decreased with an increase of the distance. Similarly, Figure 4.6 (b) shows a reasonable comparison of the measured and computed deflections when Axle 1 was applied on the shoulder. Figure 4.6 (c) shows a better comparison of the measured and computed deflections when Axle 1 was applied on the pavement section. Overall, the computed deflection profiles had similar shapes to the measured ones but the measured deflections were larger or smaller than the computed ones depending on the test sections. Their differences were most obvious when Axle 1 was applied on the shoulder and was smallest when Axle 1 was applied on the concrete pavement. Both the measurement and the numerical method had the maximum deflections when Axle 6 was applied on the unsurfaced section.

TABLE 4.3 Measured and Computed Deflections under Axle 1on Different Test Sections

Transducer location	Load on unsurfaced section		Load on shoulder		Load on pavement	
	Measured	Computed	Measured	Computed	Measured	Computed
L1	0	-0.01	0	-0.01	-0.04	-0.05
L2	0	0	-0.01	-0.02	-0.06	-0.06
L3	-0.01	0	-0.03	-0.04	-0.05	-0.06
L4	-0.04	-0.01	-0.06	-0.08	-0.01	-0.02
L5	-0.25	-0.14	-0.01	-0.04	0	0

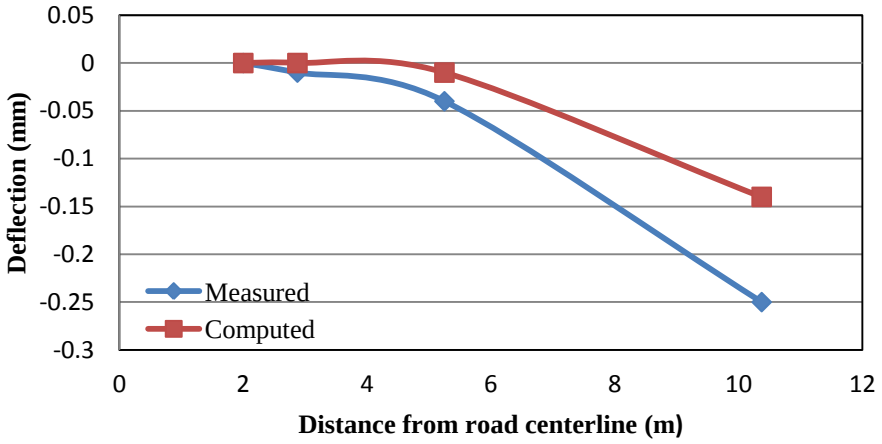

(a) Unsurfaced section

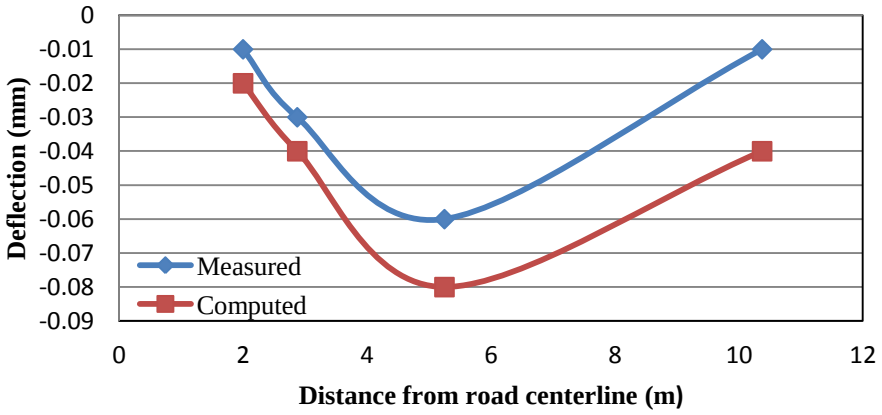

(b) Shoulder

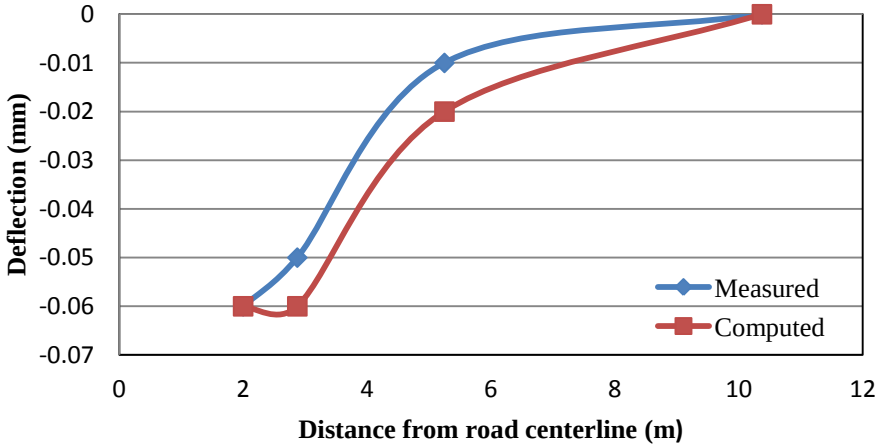

(c) Pavement

FIGURE 4.6 Measured and computed deflections under Axle 1 applied on different test sections

Table 4.4 and Figure 4.7 show the comparisons of the measured deflections with the computed ones from FLAC3D when Axle 3 was applied on different test sections. Obviously, Axle 3 resulted in higher deflections than Axle 1. Figures 4.7(a), (b), and (c) show the measured and computed deflections when Axle 3 was applied on the unsurfaced, shoulder, and pavement sections. The comparisons between the measured and computed deflections are similar to those in Figure 4.6.

TABLE 4.4 Deflection under axle 3 applied at each section

Transducer Location	Load on unsurfaced section		Load on shoulder		Load on pavement	
	Measured	FLAC3D	Measured	FLAC3D	Measured	FLAC3D
L1	0	0	-0.04	-0.06	-0.12	-0.19
L2	0	0	-0.05	-0.07	-0.16	-0.21
L3	-0.01	0	-0.08	-0.13	-0.13	-0.19
L4	-0.03	-0.02	-0.18	-0.25	-0.05	-0.06
L5	-0.47	-0.4	-0.03	-0.02	-0.01	0

The deflection caused by the axle 6 was found to be almost similar to the deflection caused by the axle 3 with axle 3 producing little more deflection. Table 4.5 and Figure 4.8 show the comparisons of the measured and computed deflections when Axle 6 was applied on different test sections. Their deflections were similar but slightly less than those when Axle 1 was applied on the same test section.

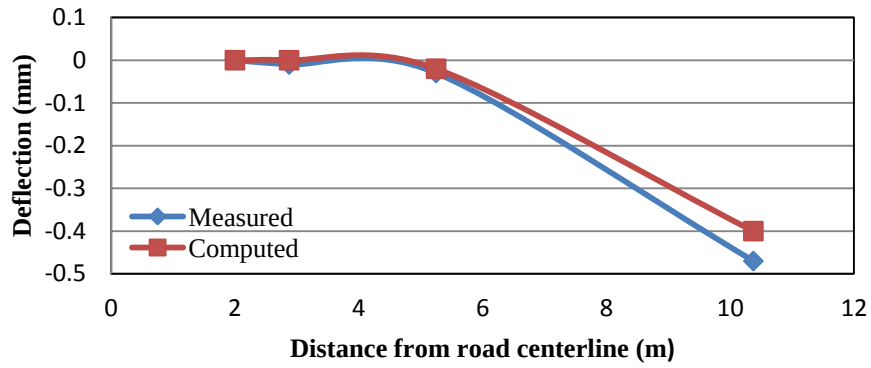

(a) Unsurfaced section

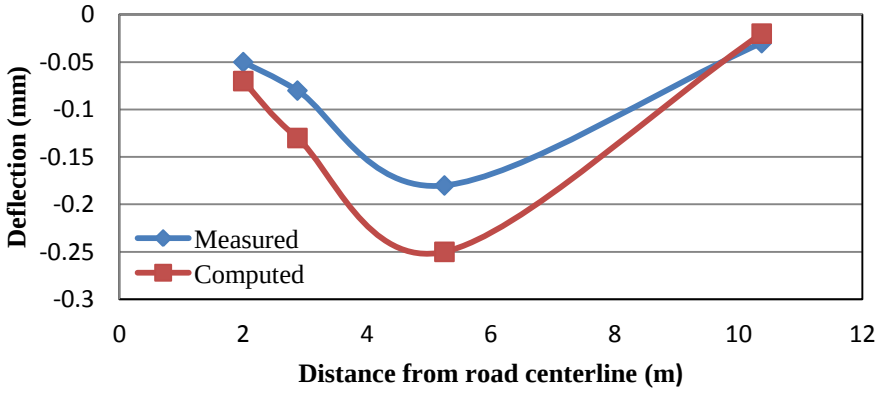

(b) Shoulder

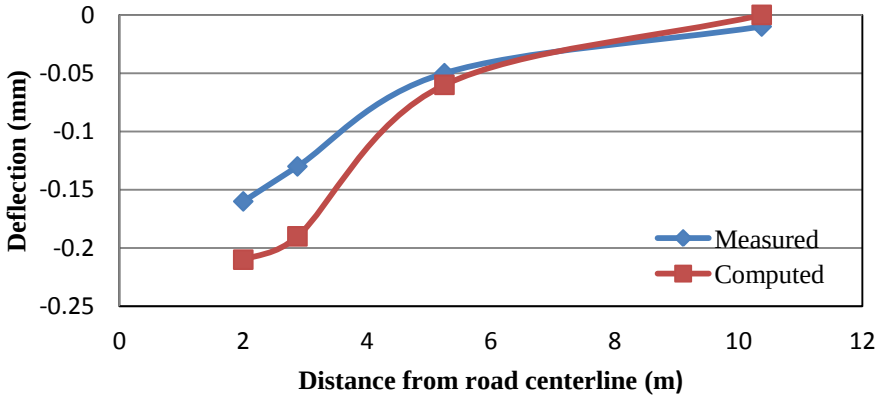

(c) Pavement

FIGURE 4.7 Measured and computed deflections under Axle 3 applied at different test sections

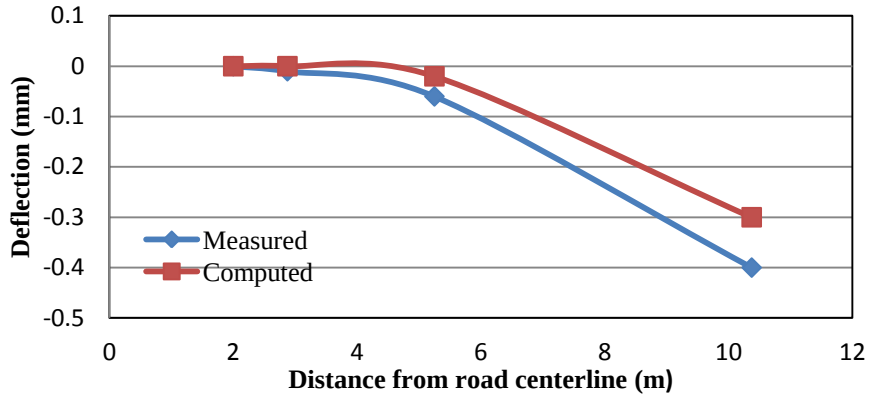

(a) Unsurfaced section

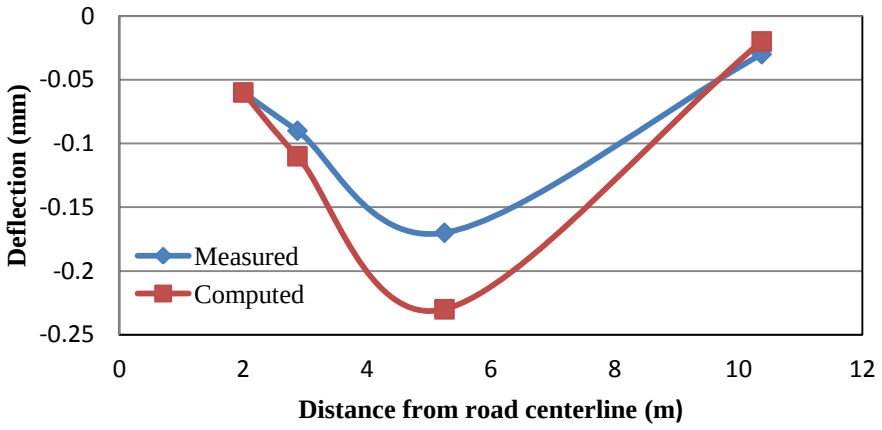

(b) Shoulder

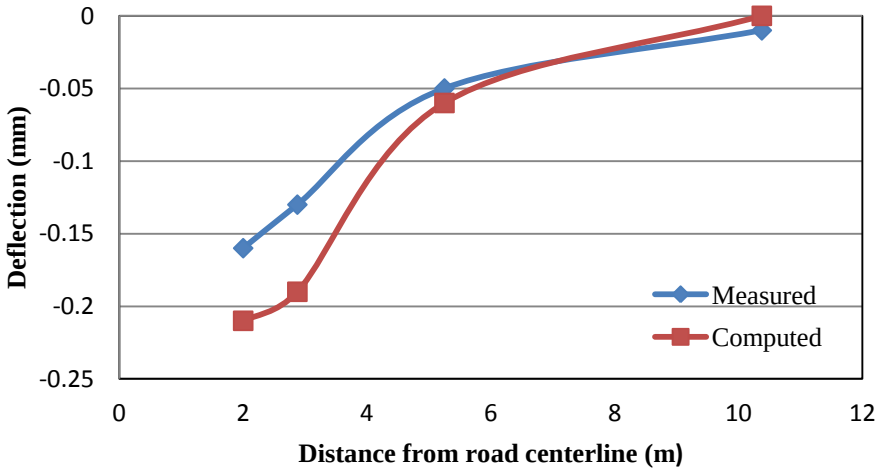

(c) Pavement

FIGURE 4.8 Measured and computed deflections under Axle 6 applied on different test sections

TABLE 4.5 Deflections under Axle 6 applied at different test sections

Transducer Location	Load on unsurfaced section		Load on shoulder		Load on pavement	
	Measured	FLAC3D	Measured	FLAC3D	Measured	FLAC3D
L1	0	0	-0.05	-0.05	-0.13	-0.17
L2	0	0	-0.06	-0.06	-0.17	-0.19
L3	-0.01	0	-0.09	-0.11	-0.15	-0.18
L4	-0.06	-0.02	-0.17	-0.23	-0.16	-0.07
L5	-0.4	-0.3	-0.03	-0.02	-0.01	0

The above comparisons demonstrate that the numerical model could reasonably simulate the behavior of the box culvert when an axle load was applied on the unsurfaced, shoulder, and pavement. Therefore, similar material properties, boundary conditions, and mesh densities were adopted for the numerical analysis in the parameter study to be discussed in the following chapter.

4.3.3 Earth Pressures above Culvert

The measured and computed vertical earth pressures on the top of the culvert under different axle loads on the unsurfaced section are shown in Table 4.6. Table 4.6 shows reasonable comparisons of the measured and computed values. Figures 4.9, 4.10, and 4.11 show the vertical earth pressure contours above the culvert under Axle 1, Axle 2 or 4, and Axle 6 and Axle 5 or 7, respectively. Clearly, the wheel loads were distributed to the top of the culvert. The vertical pressure on the top of the culvert found from FLAC3D due to outer wheel of axle 1 was 131kPa and that for the inner wheel was 43kPa. But the vertical pressures measured at those locations during the field test were 175 and 32 kPa respectively. Figure 4.9 shows the contour of vertical pressure on the top of the culvert due to axle 1.

TABLE 4.6 Comparison of measured and computed pressures

Axle No.	Pressure (kPa)			
	E1 (inner wheel)		E4 (outer wheel)	
	Measured	Computed	Measured	Computed
1	32	43	175	131
2	118	185	180	235
4	122	185	220	235
5	86	113	65	198
6	118	148	165	198
7	68	113	140	198

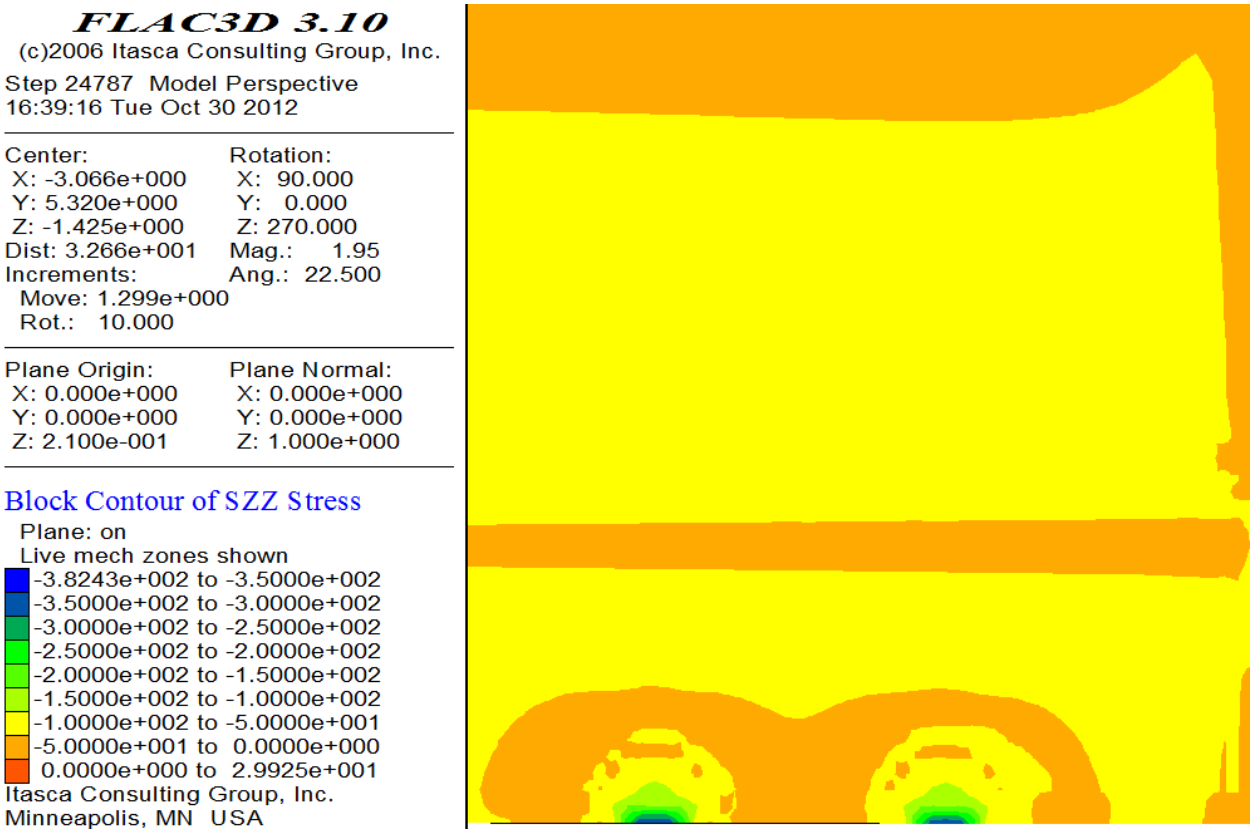

FIGURE 4.9 Vertical earth pressure contour on the top of the culvert due to Axle 1

The vertical pressure on the top of the culvert found from FLAC3D due to outer wheel of axle 2/4 was 235 kPa and that for the inner wheel was 185kPa. But the vertical pressure measured at

these locations during the field test due to axle 2 were 180 and 118 kPa respectively and that from axle 4 were 220 and 122 kPa respectively. Figure 4.10 shows the contour of vertical pressure on the top of the culvert due to axle 2/4.

The vertical pressure on the top of the culvert found from FLAC3D due to outer wheel of axle 6 was 198 kPa and that for the inner wheel was 148 kPa. But the vertical pressure measured at these locations during the field test due to axle 6 were 165 and 118 kPa respectively. Also the vertical pressure on the top of the culvert found from FLAC3D due to outer wheel of axle 5/7 was 198 kPa and that for the inner wheel was 113 kPa. But the measured vertical pressure at those locations from axle 5 were 65 and 86 kPa respectively and that for axle 7 were 140 and 86 kPa respectively. Figure 4.11 shows the contour of vertical pressure on the top of the culvert due to axles 6 and 5/7.

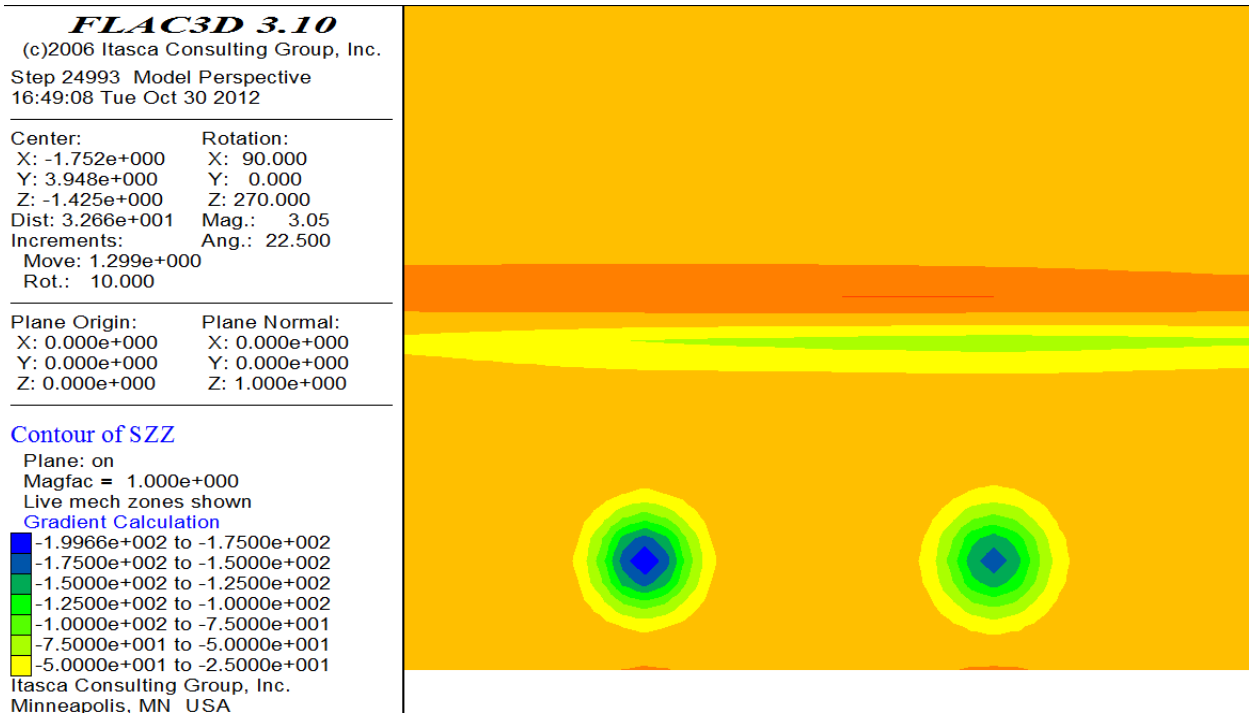

FIGURE 4.10 Vertical earth pressure contour on the top of the culvert due to Axle 2 or 4

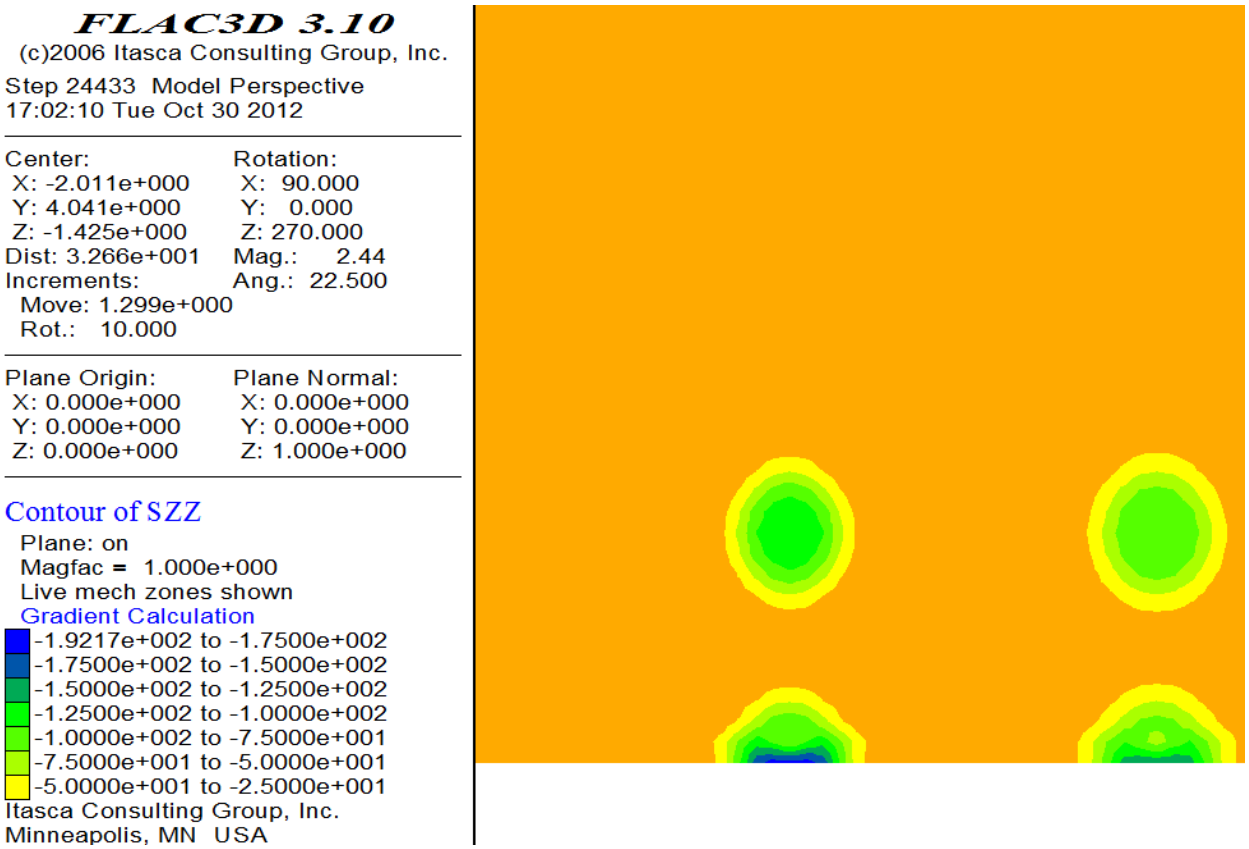

FIGURE 4.11 Vertical earth pressure contour on the top of the culvert due to Axle 6 and Axle 5 or 7

4.4 Culvert under Flexible Pavement

4.4.1 Material Models and Parameters

The flexible pavement on the top of the culvert consisted of two layers. The surface course of the pavement consisted of hot mixed asphalt (HMA) layer, under which there was lime treated subgrade. The culvert was made of reinforced concrete. The backfill around the culvert was a natural soil. The dimensions of the culvert and pavement layers were described in Chapter 3. Elastic constitutive model were used for all the materials with different properties.

The elastic modulus of the asphalt layer as obtained from the rebound test was 1827 MPa, which was used along with Poisson's ratio of 0.3 for the model calibration. The AASHTO Guide for Design of Pavement Structures (1993) suggested a typical value of elastic modulus for lime-treated subgrade ranging from 138 to 483 MPa (20 to 70 ksi). Therefore, an average value of 310 MPa (45 ksi) was adopted for the calibration of the numerical model. Poisson's ratio of 0.3 was used for the lime-treated subgrade. The average elastic modulus of the soil obtained from the triaxial test was 10.7 MPa, which was used for the natural subgrade including the backfill soil. Poisson's ratio of 0.3 was used for soils.

It was assumed that the concrete had a typical compressive strength of 4500 psi. Considering 1% of the steel reinforcement with an elastic modulus of 29,000 MPa, the elastic modulus of the reinforced concrete was determined to be 27,580 MPa (4,000 ksi). Poisson's ratio of the concrete was assumed at 0.15. The summary of the material properties used in the numerical analysis is listed in Table 4.7.

Axles 1, 3 and 6 provided symmetric loads with respect to the culvert axis. Therefore, Axle 6 was used to calibrate the model and the computed deflections using the calibrated model with Axles 1 and 3 will be compared with those from the field study.

TABLE 4.7 Summary of the material properties used in model calibration

Material	Elastic modulus (Mpa)	Poisson's ratio
Asphalt concrete	1827	0.3
Lime treated subgrade	310	0.3
Natural subgrade and backfill soil	10.73	0.3
Culvert concrete	27580	0.15

4.3.2 Numerical Mesh and Boundary Conditions

Only half of the culvert was modeled to utilize the symmetry condition as shown in Figure 4.12. Unyielding foundation conditions were assumed for the model. Therefore the vertical movement at the bottom of the culvert was restricted. All vertical boundaries were restrained for horizontal movement except for the free boundary of the box culvert in the y direction. The horizontal displacement of the culvert was restrained at the symmetry plane (yz plane). Rollers were used at the symmetrical boundary, which allowed vertical movement but restrained horizontal movement. The boundary conditions are shown in Figure 4.2.

The length, width, and height of the model were 10.5 m, 7.5 m, and 4.225 m respectively. The numbers of zones were 87864, 80304, and 84924 when Axles 1, 3, and 6 were applied in the model respectively. The reason for the difference in the number of zones for different axles is that each axle had a different contact area of the load, which required changing the size of the mesh on the surface where the load was applied. Finer zones were used near the culvert and the zone density gradually decreased away from the culvert. The load was applied as a pressure on the surface of the pavement. The number and size of zones required to apply the pressure were calculated as shown in Table 4.8 so that the total wheel load was equal to that in the field test while the contact pressure was close to that in the field test.

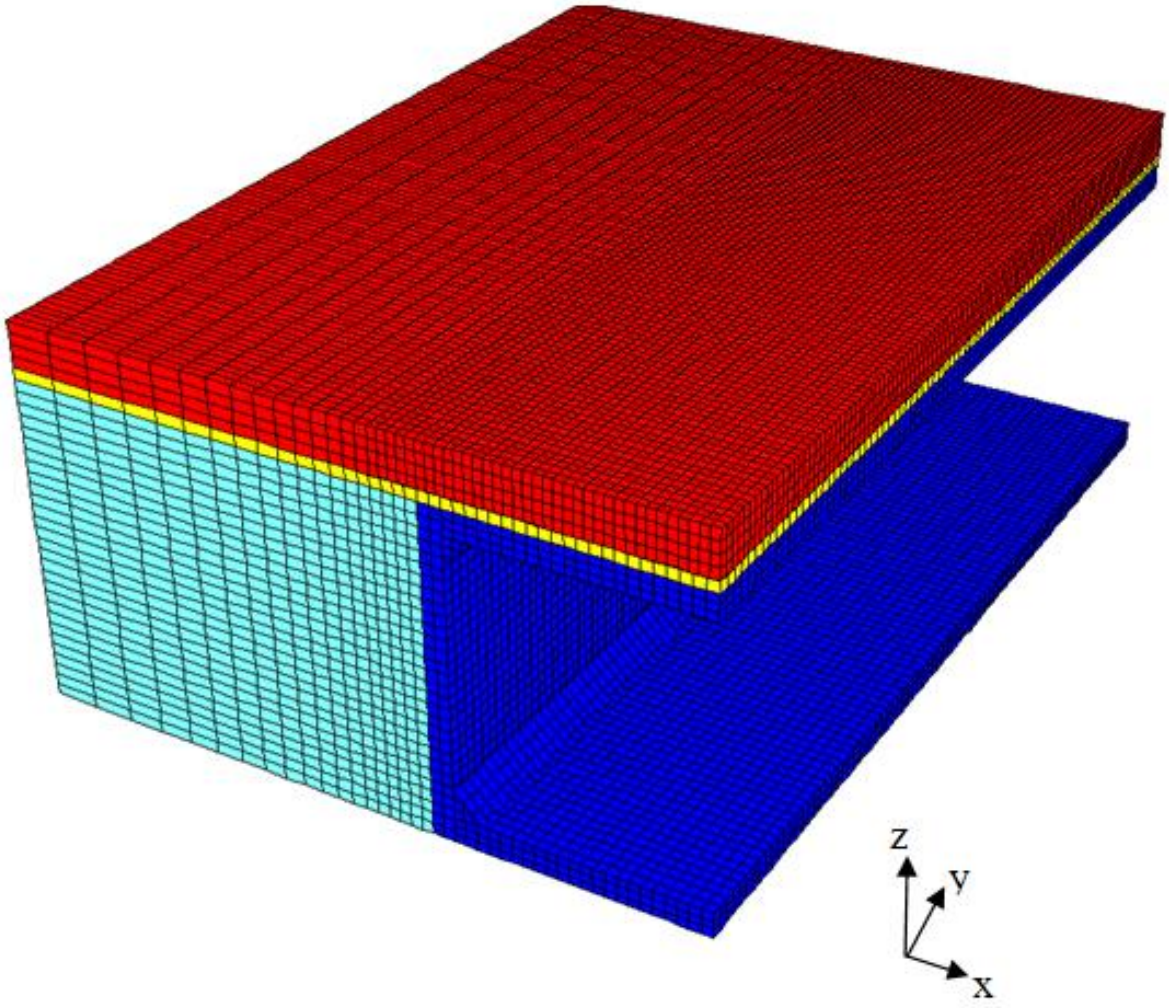

FIGURE 4.12 FLAC3D model of the culvert

TABLE 4.8 Calculation of pressure and number of zones to apply pressure

Axle No.	Single wheel load (kN)	Actual tire pressure (kPa)	Contact area (m^2)	Area of each zone (m^2)	Number of zones	Applied pressure (kPa)
1	28.5	760	0.038	0.010	4	700
2	49	760	0.064	0.016	4	784
3	0	0	0	0.000	0	0
4	49	760	0.064	0.016	4	784
5	40.25	760	0.052	0.013	4	805
6	40.25	760	0.052	0.013	4	805
7	40.25	760	0.052	0.013	4	805

When Axle 1 was applied in the model, each wheel only had two zones due to the symmetry condition as shown in Figure 4.3. Axle 3 did not have its own load. However, when Axle 3 was in place, the wheel loads used for Axles 2 and 4 were applied on the culvert. Due to the symmetry, only one of the axle loads was applied in the model as shown in Figure 4.4. Similarly, when Axle 6 was on place, the wheel loads for Axles 5 and 7 were also applied on the culvert. However, half of the load from Axle 6 and a full load from Axle 5 or 7 were applied to the model as shown in Figure 4.5.

4.3.2 Deflections of Culvert Top Slab

The measured deflections at Locations L1 through L6 are compared with the computed ones from FLAC3D. Table 4.9 and Figures 4.13 and 4.14 show the measured deflections compared with the computed ones from FLAC3D when Axles 1, 3 and 6 were applied on the pavement. Figures 4.13 (a) and 4.14 (a) show that the measured deflections at all the locations reasonably matched the computed ones from FLAC3D when Axle 1 was applied on the pavement. The difference in their deflections was more significant near the point of the load application and gradually decreased with an increase of the distance. Similarly, Figure 4.13 (b) and 4.14 (b) show a reasonable comparison of the measured and computed deflections when Axle 3 was applied on the pavement. Figure 4.13 (c) and 4.14 (c) show a better comparison of the measured and computed deflections when Axle 6 was applied on the pavement. Overall, the computed deflection profiles had similar shapes to the measured ones but the measured deflections were larger or smaller than the computed ones depending on the axles. Their differences were most obvious when Axle 1 was applied on the pavement and was smallest when Axle 6 was applied.

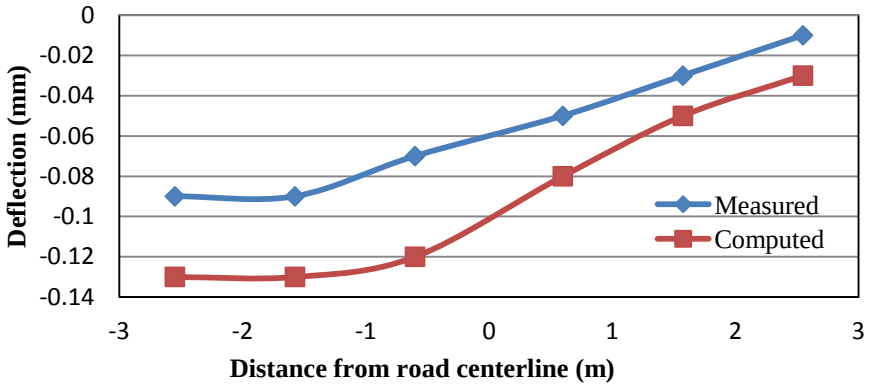

(a) Axle 1

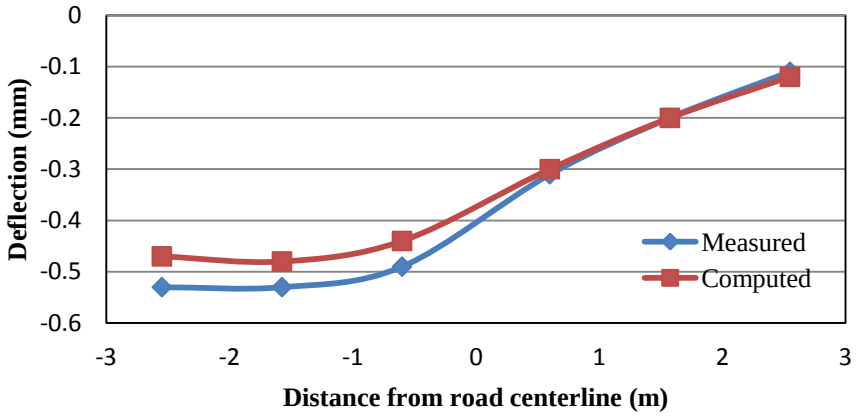

(b) Axle 3

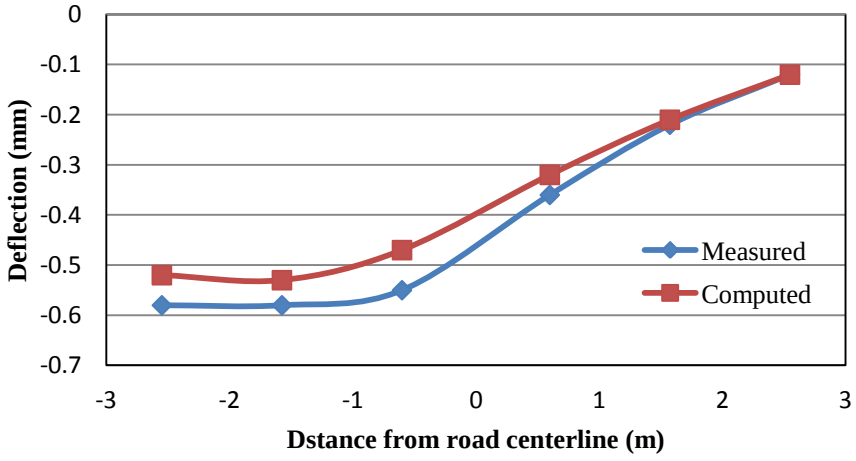

(c) Axle 6

FIGURE 4.13 Measured and computed deflections along culvert axis

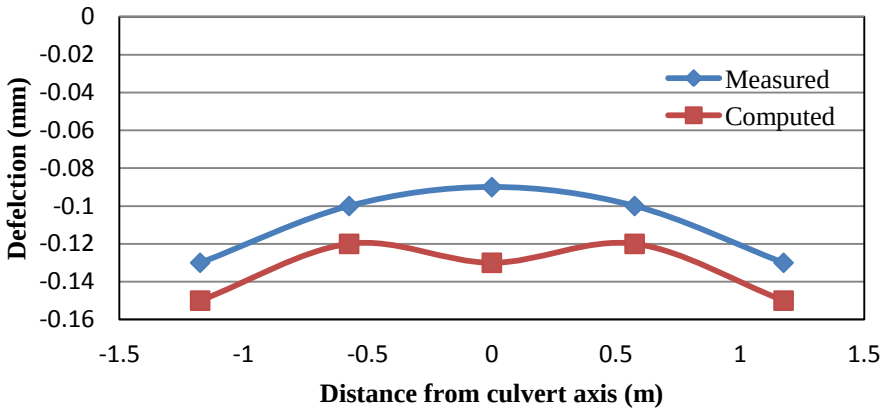

(a) Axle 1

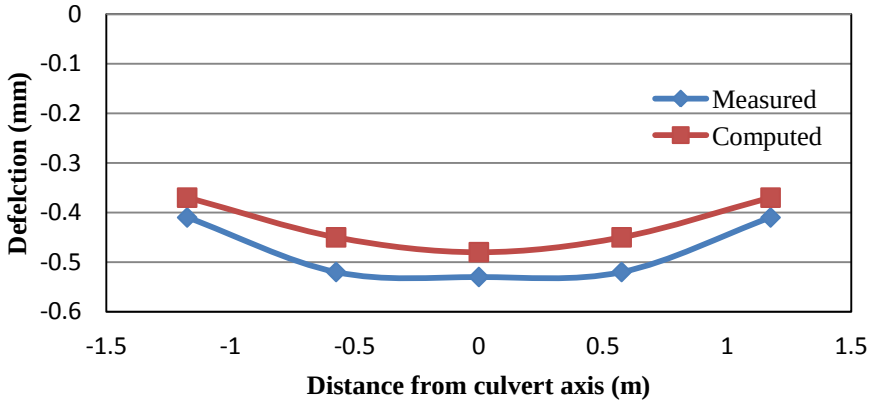

(b) Axle 3

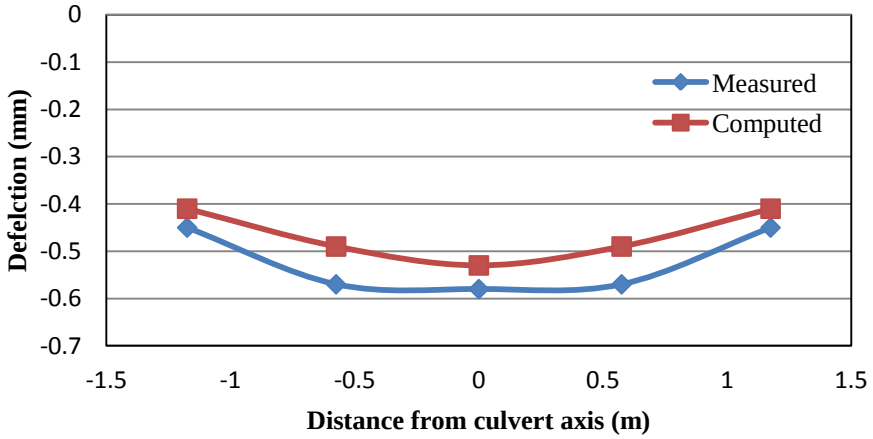

(c) Axle 6

FIGURE 4.14 Measured and computed deflections along culvert span

TABLE 4.9 Comparison of measured and computed deflection

Transducer Location	Axle 1		Axle 3		Axle 6	
	Measured	Computed	Measured	FLAC3D	Measured	FLAC3D
L1	-0.09	-0.13	-0.53	-0.47	-0.58	-0.52
L2	-0.09	-0.13	-0.53	-0.48	-0.58	-0.53
L3	-0.07	-0.12	-0.49	-0.44	-0.55	-0.47
L4	-0.05	-0.08	-0.31	-0.3	-0.36	-0.32
L5	-0.1	-0.12	-0.52	-0.45	-0.57	-0.49
L6	-0.13	-0.15	-0.41	-0.37	-0.45	-0.41

The above comparisons demonstrate that the numerical model could reasonably simulate the behavior of the box culvert when an axle load was applied on the unsurfaced, shoulder, and pavement. Therefore, similar material properties, boundary conditions, and mesh densities were adopted for the numerical analysis in the parameter study to be discussed in the following chapter.

4.4 Summary

This chapter describes the development of the numerical models for culverts under rigid and flexible pavements subjected to static axle loading. All the materials modeled in this study were linearly elastic because the stress levels of load rating as compared with the strengths of materials are usually low. The numerical models created using the finite difference program FLAC3D were validated using the data obtained from the field tests. A few conclusions can be drawn from this study:

1) Elastic model were used for all the materials. This study showed that the assumption of linear elastic models for the all the materials is valid for culverts under pavements.

2) The elastic moduli of the reinforced concrete culvert, plain cement concrete pavement, cement-treated base, lime treated subgrade, and asphalt concrete pavement used in the numerical modeling were 27,580, 24,545, 5,171, 310, and 1,827 MPa, respectively. The analyses showed that the selected modulus values were appropriate for respective materials.
3) The deflections computed by the numerical method were in good agreement with those observed in the field tests for both culverts.
4) Pressure applied on the specified contact area of the tire can simulate the wheel load very well.

Chapter 5 Parametric Study

5.1 Introduction

Based on the numerical models created for their verification with the field performance of the culverts, a simplified model was created for a parametric study. The parametric study was performed to investigate the influence of pavement type, pavement thickness, fill depth, and culvert span on the load distribution over the culvert under wheel loads. The constitutive model, boundary condition, and material properties were similar to those used in the model verification in the previous sections except for the soil elastic moduli. Since the soil elastic moduli obtained from the triaxial tests on the samples obtained from two culvert test sites were different, 12 MPa was used for the elastic modulus of soil for simplicity in the parametric study. A total of ninety-six culvert models were analyzed for the parametric study, among which forty-eight culverts each were under rigid and flexible pavements.

Figure 5.1 shows the schematic plan of the culvert modeled for the parametric study. Each modeled case consisted of a two-lane road having a lane width of 3.75 m, which had a 3 m wide unsurfaced shoulder on each side. The culvert was symmetrical about both the road centerline and the culvert axis. Therefore only a quarter of the culvert was modeled to utilize the symmetry of the culvert and also to minimize the time required for the numerical analysis. Figure 5.1 shows the limit of the culvert actually modeled and the coordinate system. The intersection point between the road centerline and the culvert axis was considered as the origin. For all the subsequent discussion in this study, the distance is considered from the origin as shown in Figure 5.1.

Figures 5.2 and 5.3 show the typical cross sections of the culvert models under rigid and flexible pavements respectively. Similar to the culvert model under the rigid pavement used for the verification, the culvert models with rigid pavements for the parametric study also consisted of a top concrete layer, a cement-treated base layer, a lime-treated subgrade layer, and a natural subgrade layer. The thicknesses of the cement-treated base layer and the lime-treated subgrade layer were fixed at 100 mm and 150 mm respectively for all the models. However, the flexible pavement consisted of a hot mix asphalt layer, a lime-stabilized subgrade layer, and a natural subgrade layer, in which the lime-treated subgrade was 150 mm thick. The thicknesses of the concrete layer, the asphalt layer, and the natural subgrade layer were varied during the parametric study. All the box culverts modeled had 250 mm thick walls and top and bottom slabs. The clear height of each culvert was fixed at 3 m. The span of the culvert was one of the variables for the parametric study. The width of the backfill beyond the culvert was fixed at 4.625 m for all the culverts analyzed in this study, which is far enough to avoid the boundary effect. Figures 5.4 and 5.5 show two typical numerical models for the culverts under rigid and flexible pavements respectively. Finer zones were used near the culvert and the zone density gradually decreased away from the culvert.

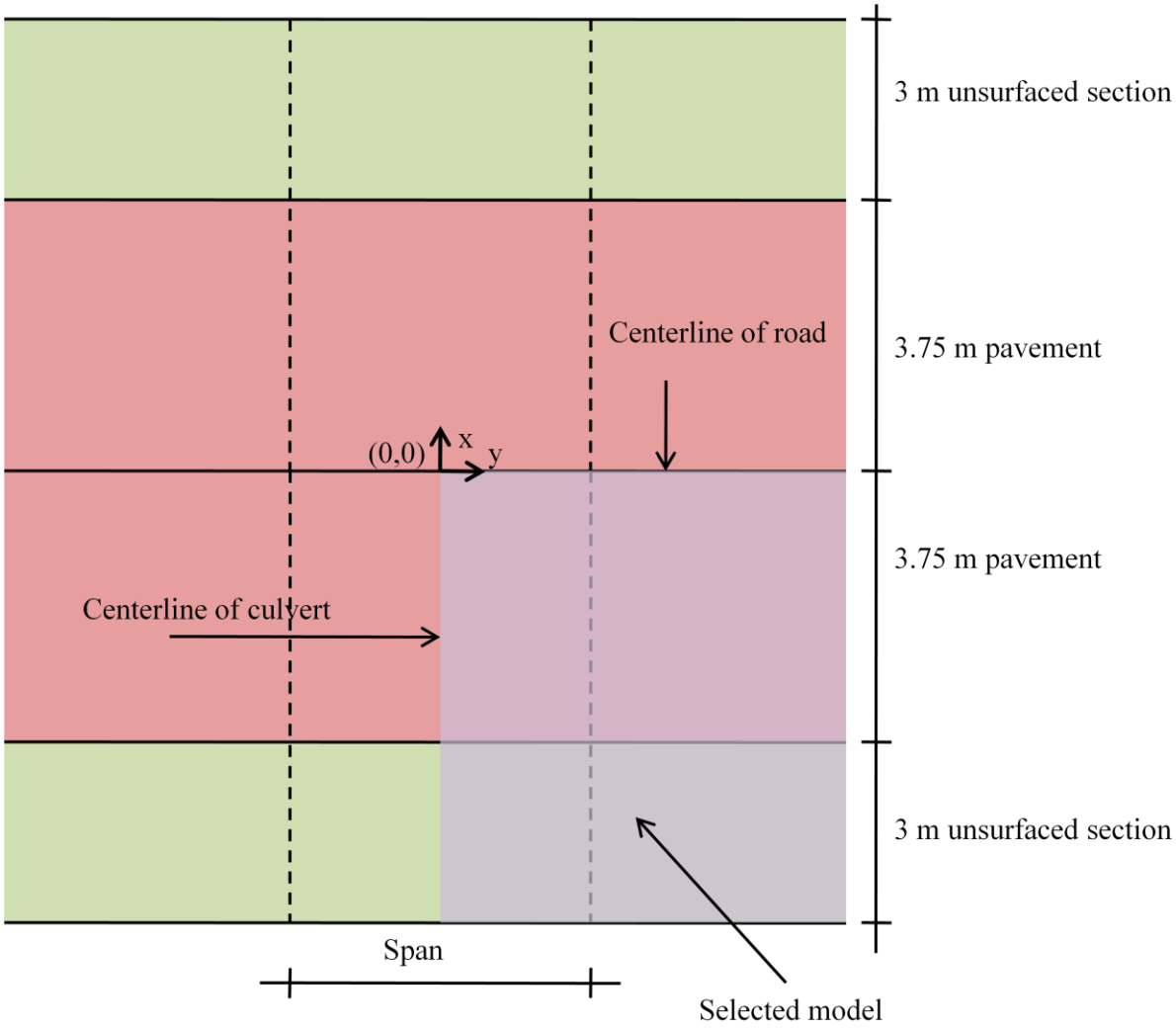

FIGURE 5.1 Schematic plan of the culvert modeled for the parametric study

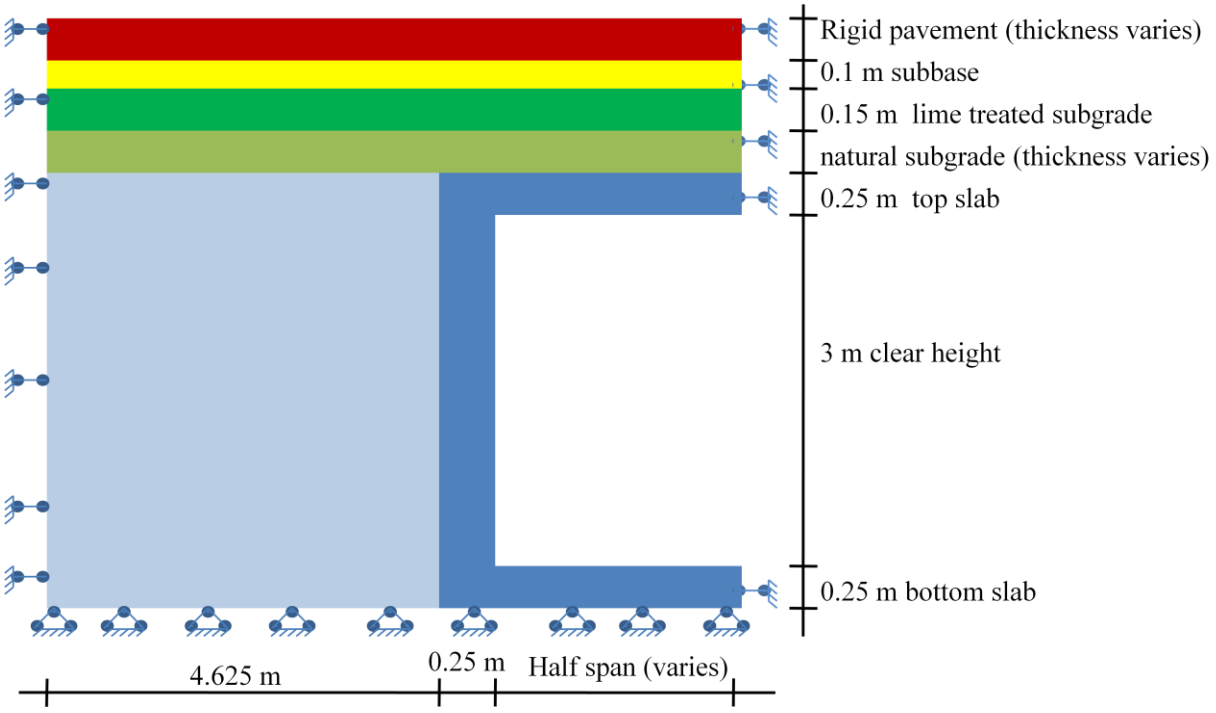

FIGURE 5.2 Typical cross-section of the culvert model under a rigid pavement

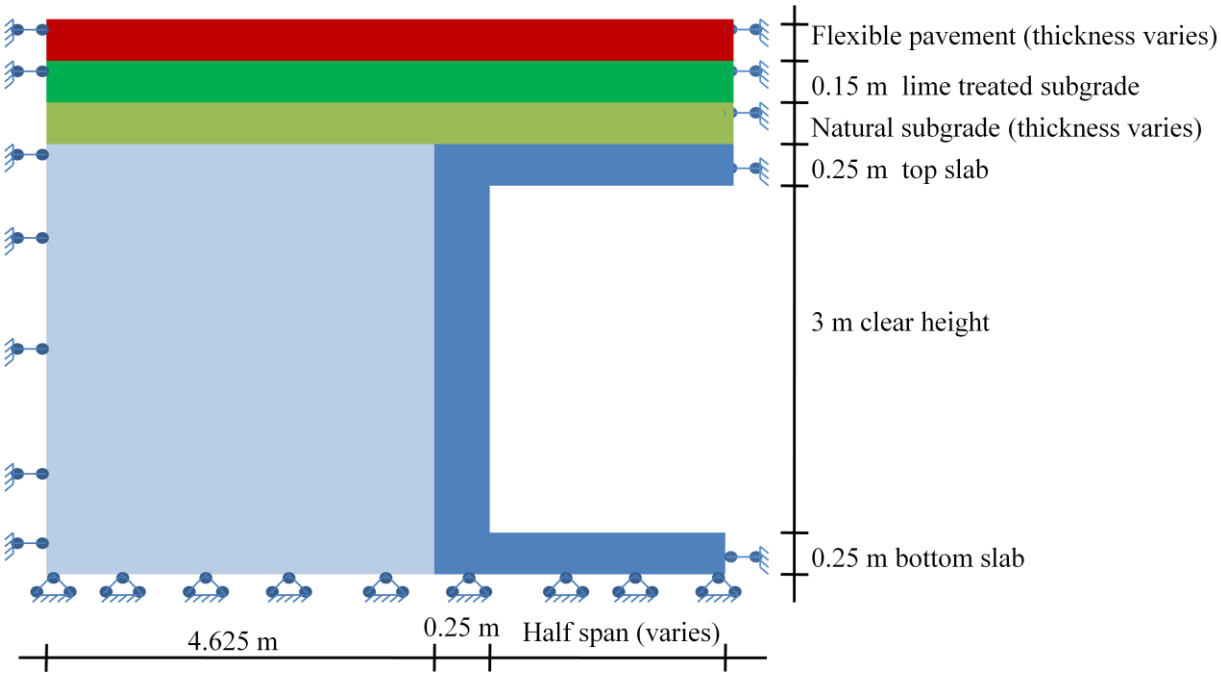

FIGURE 5.3 Typical cross-section of the culvert model under a flexible pavement

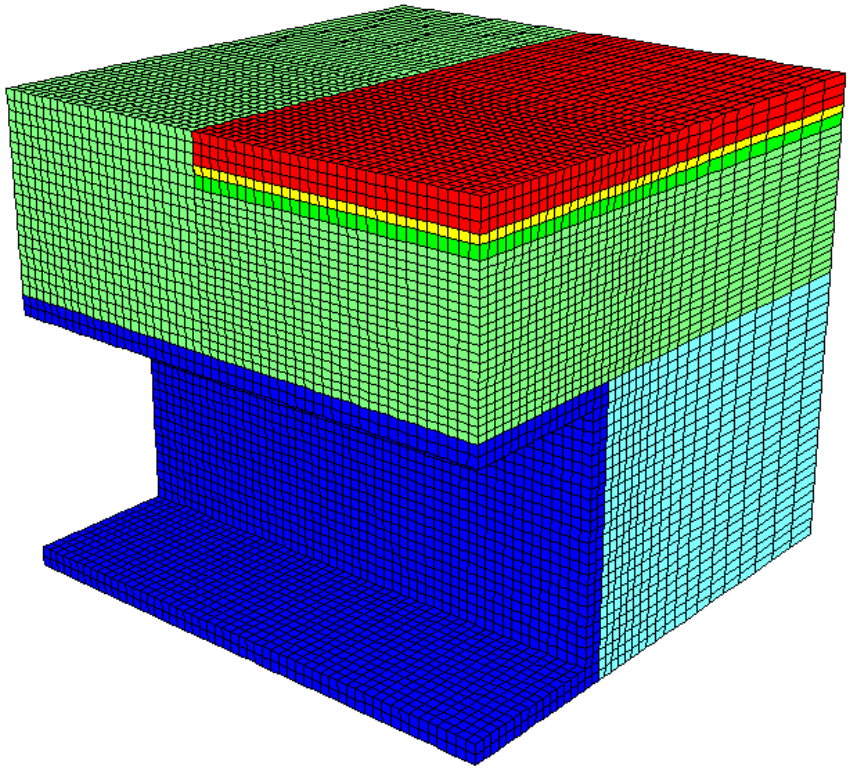

FIGURE 5.4 typical numerical model for the culvert under a rigid pavement

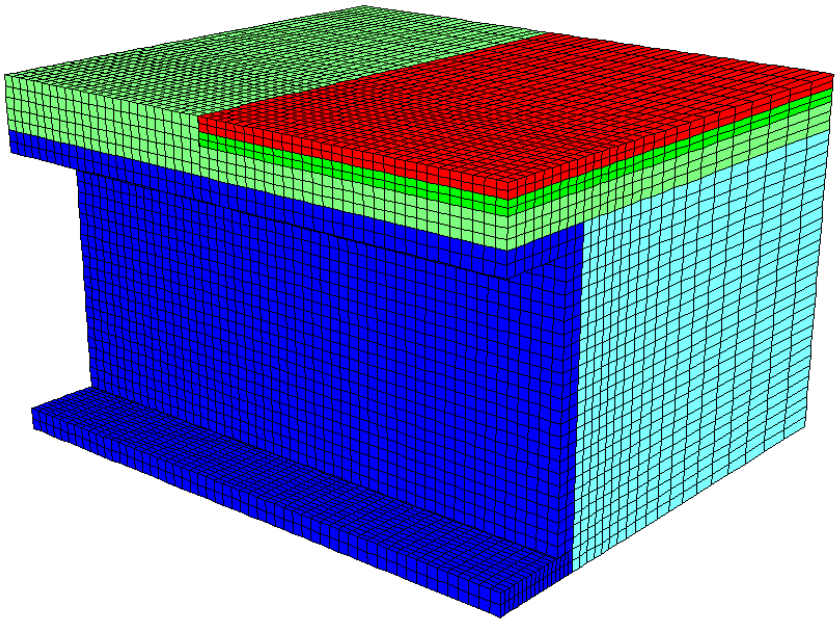

FIGURE 5.5 Typical numerical model for the culvert under a flexible pavement

Due to the symmetry of the problem, one fourth of the model was created in FLAC3D as shown in Figure 5.4. The boundary conditions included the vertical and horizontal displacements fixed at the bottom boundary and the lateral displacements fixed at the four-side boundaries. The load was applied on the pavement as a pressure in an area equal to the tire footprint area of 0.5 m x 0.25 m as specified in AASHTO LRFD code (AASHTO, 2007). Figure 5.6 shows the application of the wheel loads on the culvert. Because of the symmetry of the model created for the parametric study only half of one wheel load was applied to the model in an area of 0.5 m x 0.125 m. A typical tire contact pressure of 550 kPa was used.

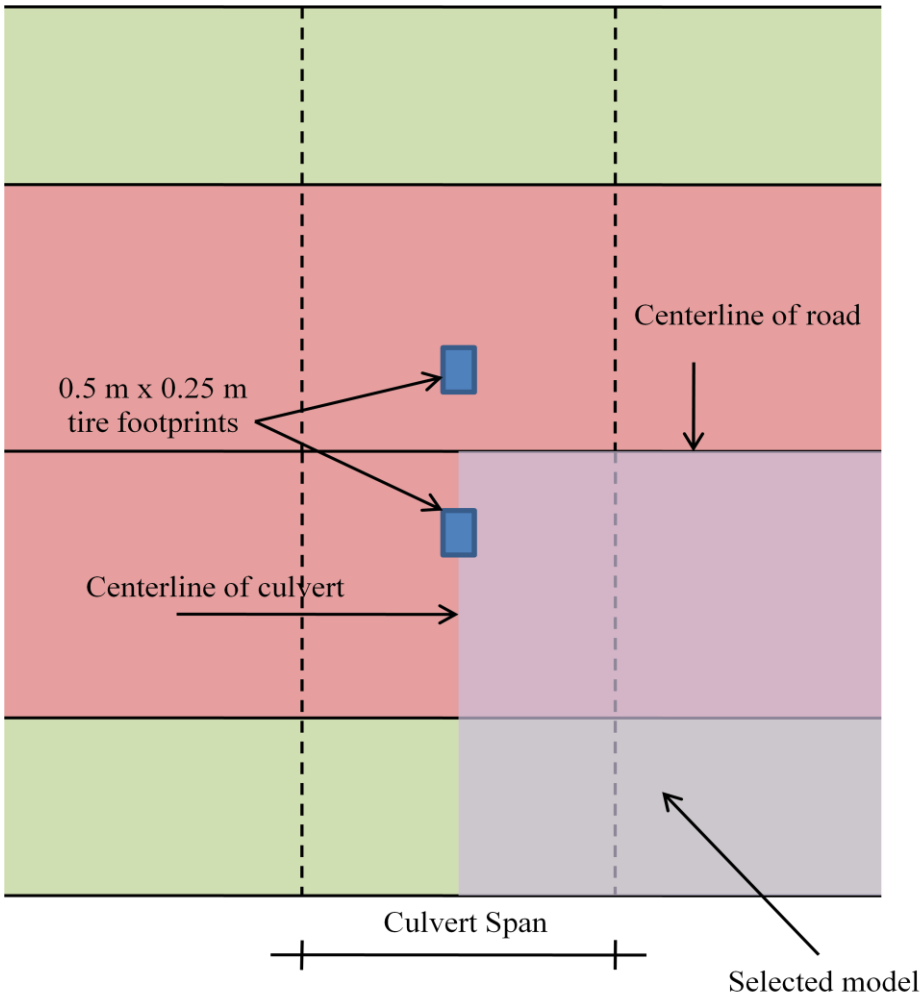

FIGURE 5.6 Application of the load on the culvert model

Each culvert model was solved and saved at two stages. The culvert model was first solved and saved when the initial equilibrium was reached at the maximum unbalanced force ratio of 10^{-5} under the self-weight. Then the wheel load was applied on the pavement as the pressure and the model was again stepped to the equilibrium and saved after the equilibrium. The additional pressure on the culvert due to the applied load was obtained by deducting the pressure at the final equilibrium condition to that at the initial equilibrium condition under the self-weight.

5.2 Influence Factors

Different factors play different roles in the distribution of the load through the pavement onto the culvert. Three key influence factors were considered in the parametric study. These factors were varied within the practical ranges to evaluate the effects of (a) pavement thickness, (b) fill depth, and (c) span for culverts under both rigid and flexible pavements.

5.3 Rigid Pavement

Forty-eight culvert models under rigid pavements were created to study the effects of the influence factors mentioned above. Analyses were carried out in three categories based on the spans of 1.8 m, 3.6 m and 5.4 m. In each category, fill depths above the culverts at 0.6 m, 1.2 m, 1.8 m, and 2.4 m were considered. For each fill depth, the thickness of the concrete pavement layer was varied from 0.2 m to 0.35 m at an increment of 0.05 m. Because of this variation, the thickness of the natural subgrade was also changed to meet the total fill depth. The vertical pressure distribution on the top of the culvert was monitored along the axis and span of the culvert through the origin of the coordinate system (referred as the center herein).

5.3.1 Effect of Concrete Pavement Thickness

Figures 5.7 and 5.8 show the variations of vertical pressure distributions on the culvert along and perpendicular to the culvert axis with the thickness of the concrete pavement thickness at different fill depths, respectively. All these distributions are presented at the culvert span of 1.8 m. These figures clearly indicate that the intensity of the vertical pressure on the culvert decreased gradually with the increase of the concrete pavement thickness. A similar trend was observed at the culvert spans of 3.6 m and 5.4 m. However, there was one exception where the intensity of the vertical pressure increased with the thickness of the concrete pavement. This case occurred when the fill depth was 0.6 m and the concrete pavement thickness was 0.35 m (i.e., there was no soft natural subgrade above the culvert). All the layers above the culvert had relatively higher elastic moduli; therefore, the applied load was distributed to a smaller area, which resulted in higher vertical pressure.

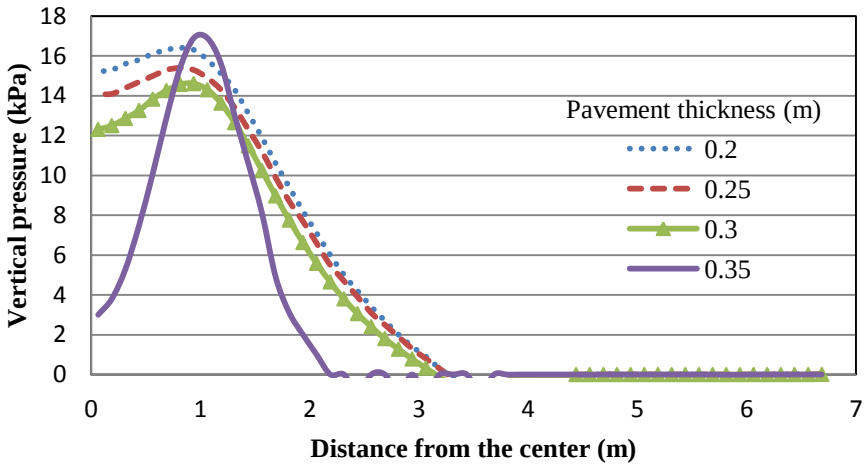

(a) Fill depth =0.6 m

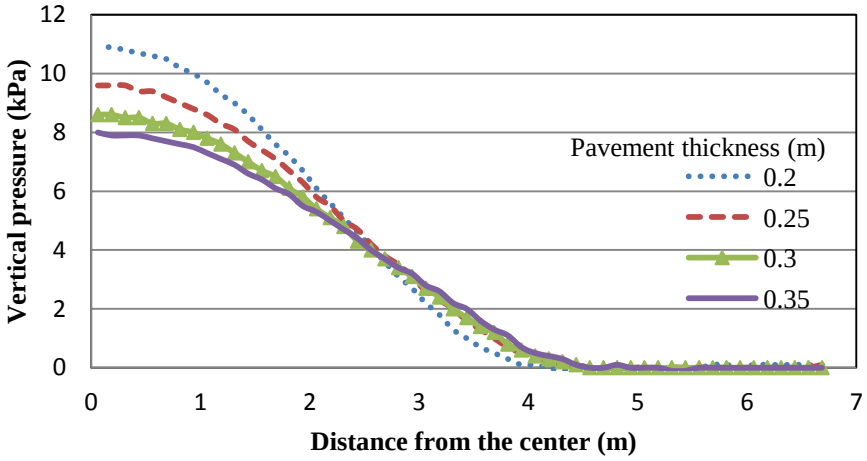

(b) Fill depth =1.2 m

FIGURE 5.7 Vertical pressure distribution on the culvert along the culvert axis at different concrete pavement thickness and fill depth (culvert span = 1.8 m)

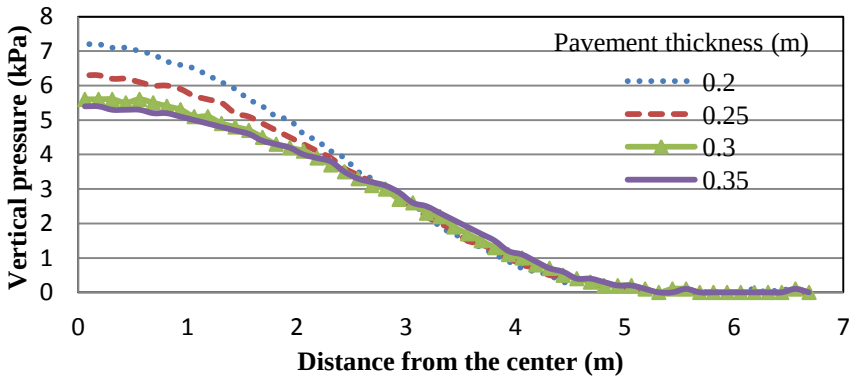

(c) Fill depth =1.8 m

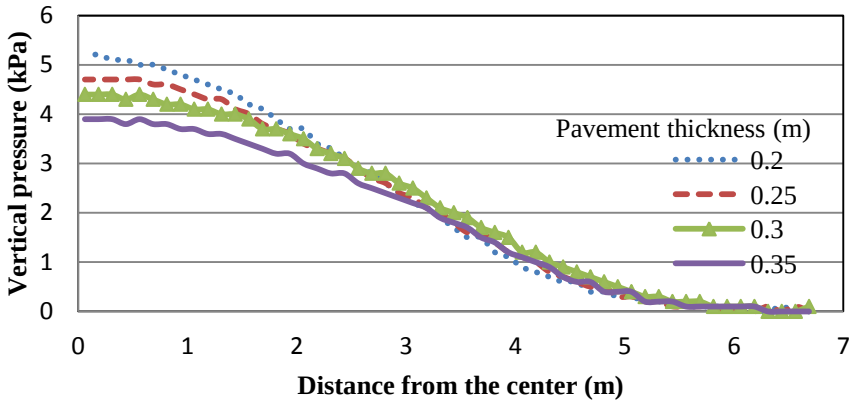

(d) Fill depth =2.4 m

FIGURE 5.7 Vertical pressure distribution on the culvert along the culvert axis at different concrete pavement thickness and fill depth (culvert span = 1.8 m) (continued)

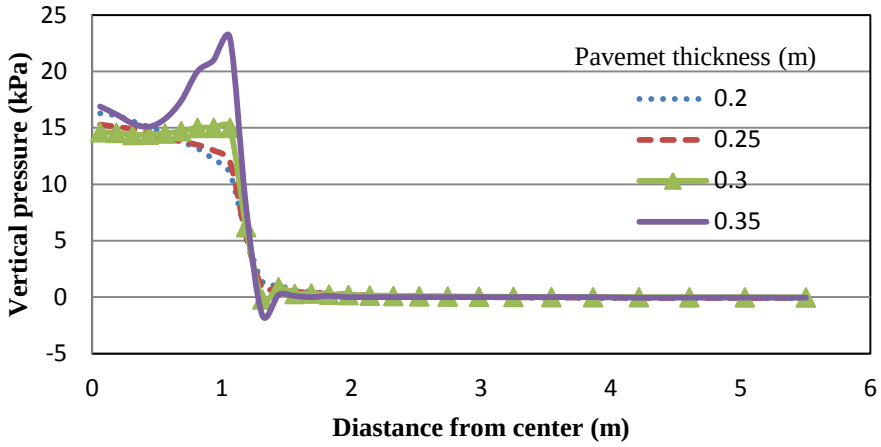

(a) Fill depth = 0.6 m

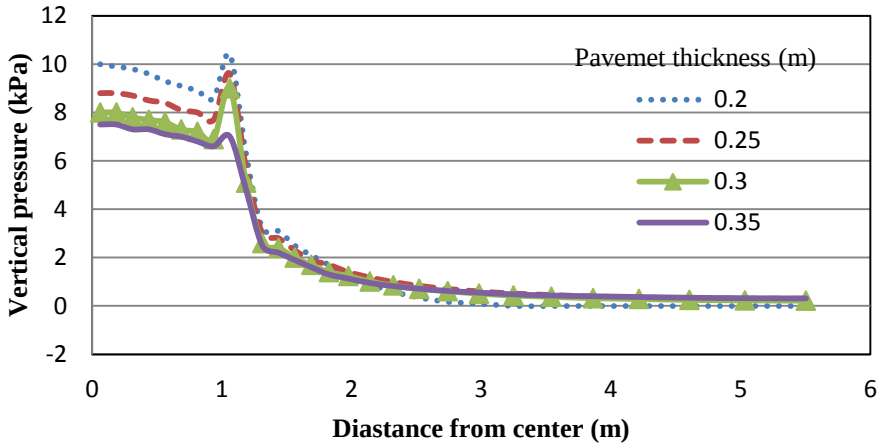

(b) Fill depth = 1.2 m

FIGURE 5.8 Vertical pressure distribution on the culvert perpendicular to the culvert axis at different concrete pavement thickness and fill depth (culvert span = 1.8 m)

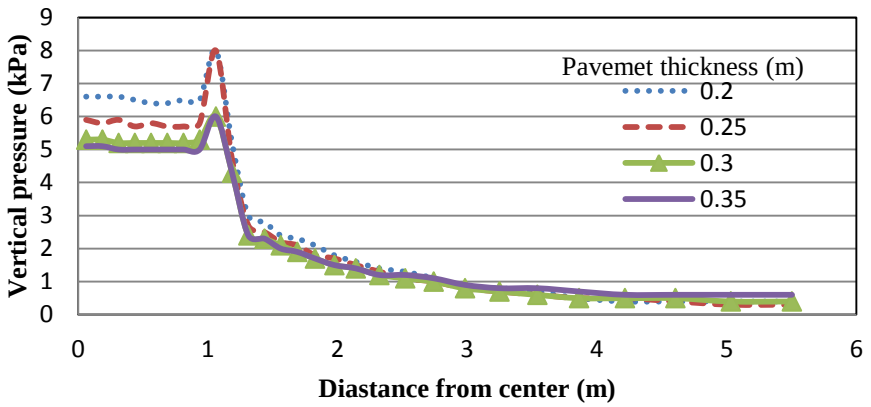

(c) Fill depth = 1.8 m

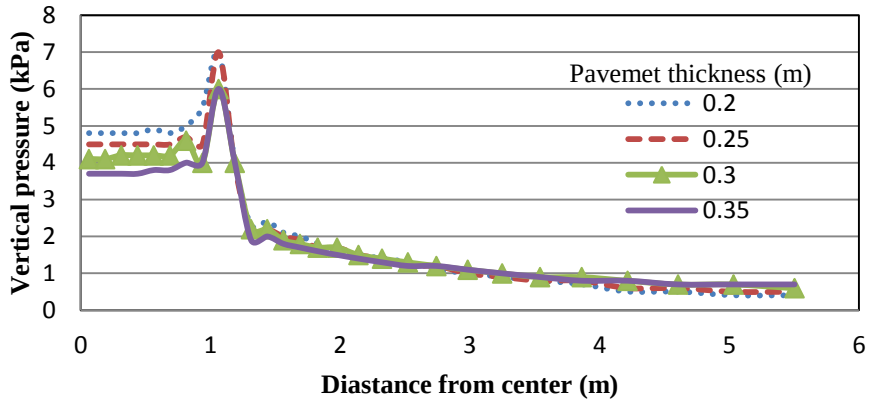

(d) Fill depth = 2.4 m

FIGURE 5.8 Vertical pressure distribution on the culvert perpendicular to the culvert axis at different concrete pavement thickness and fill depth (culvert span = 1.8 m) (continued)

Figure 5.9 shows the variations of the maximum vertical pressure on the culvert with the concrete pavement thickness at different fill depth for the culvert spans of 1.8 m, 3.6 m, and 5.4 m. This figure also indicates that the maximum vertical pressure on the culvert decreased gradually with the increase in the concrete pavement thickness. This trend was valid for all cases except for the case with 0.6 m fill depth and 0.35 m pavement thickness because of the absence of the soft natural subgrade layer above the culvert.

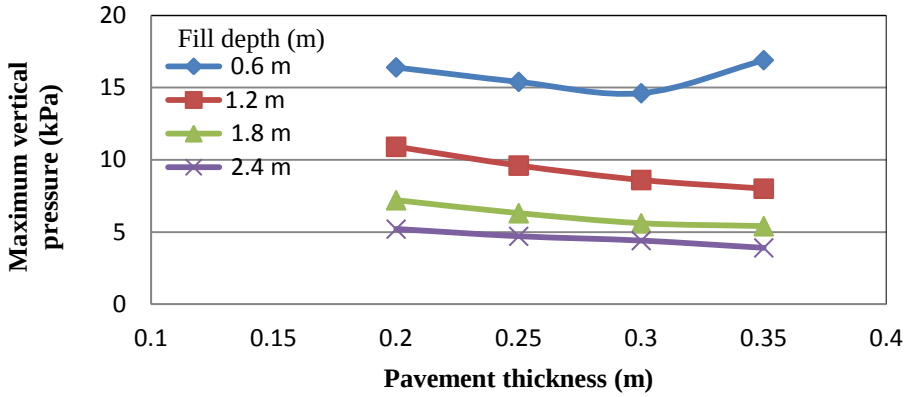

(a) Span = 1.8 m

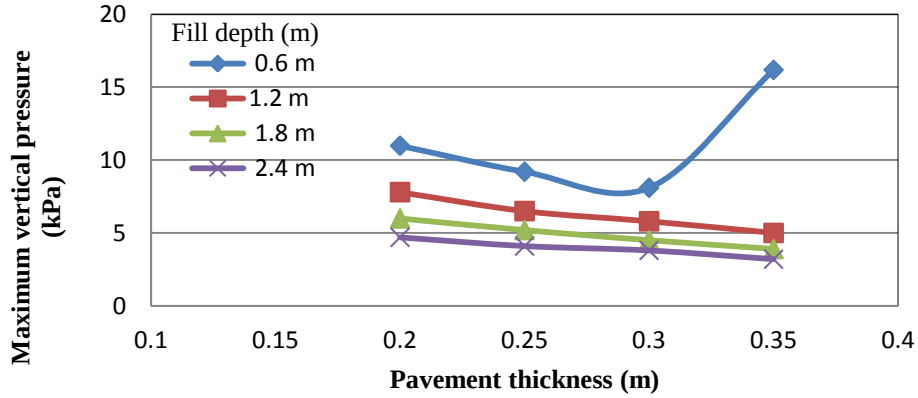

(b) Span = 3.6 m

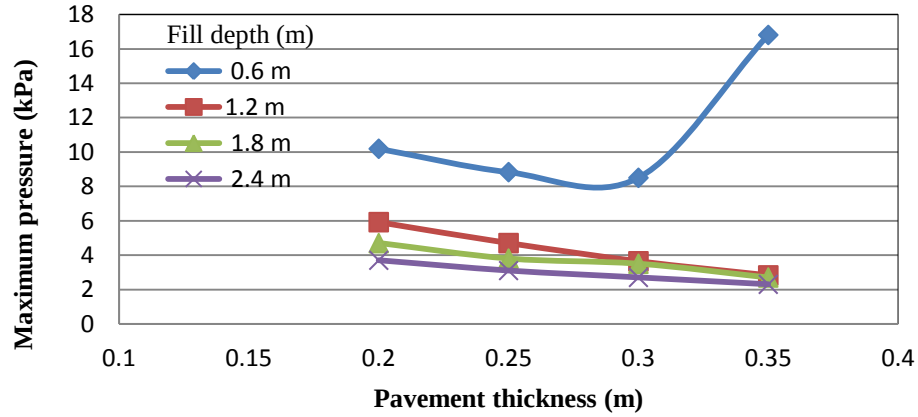

(c) Span = 5.4 m

FIGURE 5.9 Variation of the maximum vertical pressure on the culvert with the concrete pavement thickness at different fill depth and culvert span

5.3.2 Effect of Fill Depth

Figures 5.10 and 5.11 show the variations in the vertical pressure distributions on the culvert along and perpendicular to the culvert axis with the fill depth at different concrete pavement thickness. These figures clearly indicate that the intensity of the vertical pressure on the culvert decreased gradually with the increase in the fill depth. A similar trend was observed for the culverts with spans of 1.8 m and 5.4 m. However, the locations of the maximum vertical pressures were not consistent for all fill depths. Along the culvert axis, the maximum vertical stress was located below the wheel load for the case with 0.6 m fill but at the middle of the axle load for the case with 1.2 m or more fill depth. Along the culvert span, the locations of the maximum vertical pressures were either at the middle of the axle load or at the edge of the culvert wall.

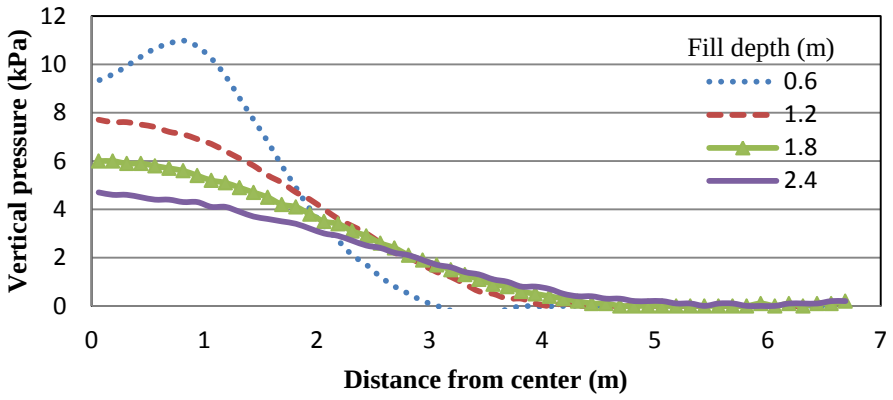

(a) Concrete pavement thickness = 0.2 m

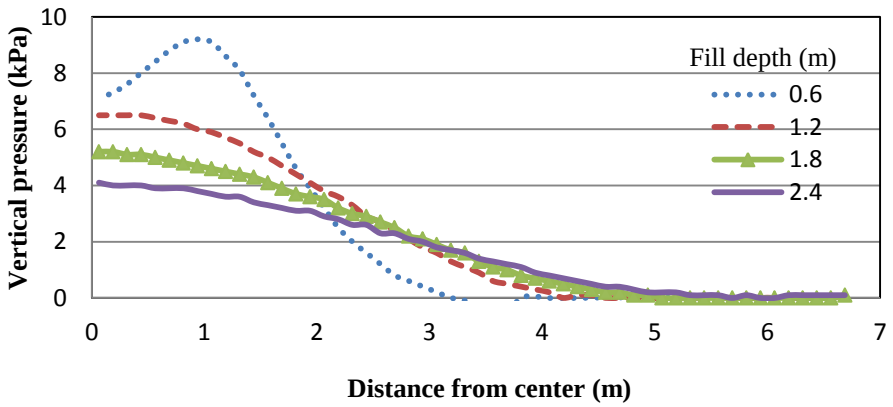

(b) Concrete pavement thickness = 0.25 m

FIGURE 5.10 Vertical pressure distribution on the culvert along the culvert axis at different fill depth and concrete pavement thickness (culvert span = 3.6)

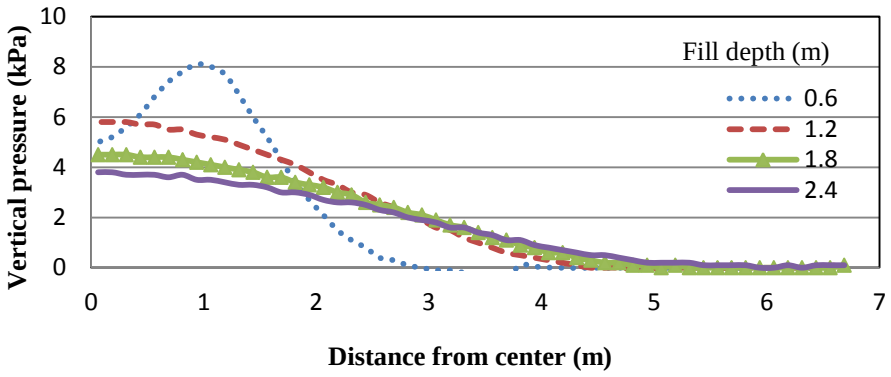

(c) Concrete pavement thickness = 0.3 m

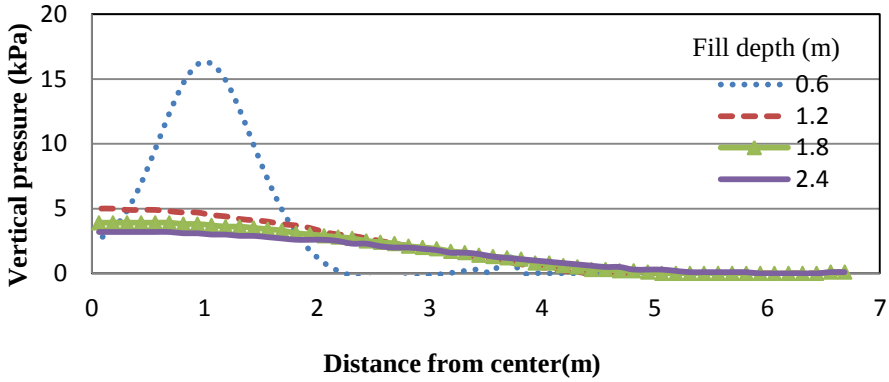

(d) Concrete pavement thickness = 0.35 m

FIGURE 5.10 Vertical pressure distribution on the culvert along the culvert axis at different fill depth and concrete pavement thickness (culvert span = 3.6) (continued)

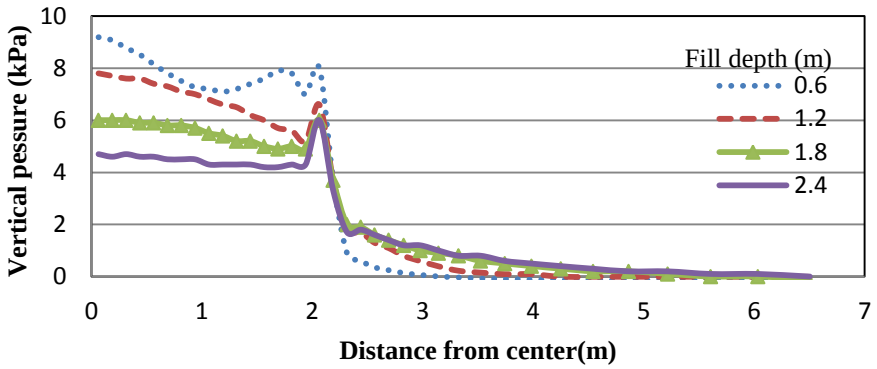

(a) Concrete pavement thickness = 0.2 m

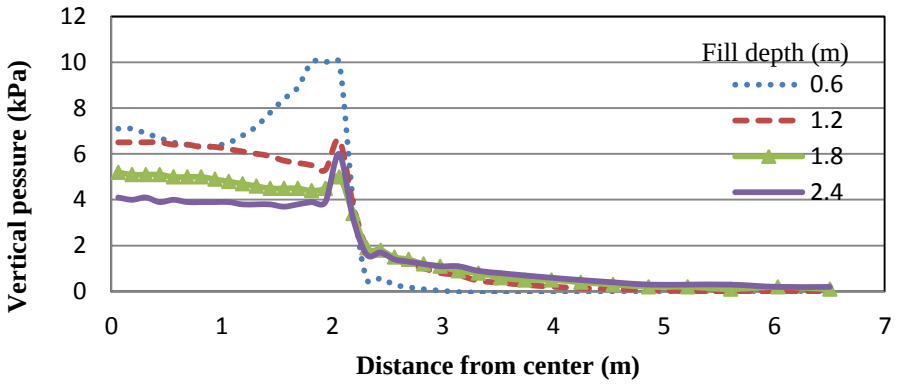

(b) Concrete pavement thickness = 0.25 m

FIGURE 5.11 Vertical pressure distribution on the culvert perpendicular to the culvert axis at different fill depth and concrete pavement thickness (culvert span = 3.6 m)

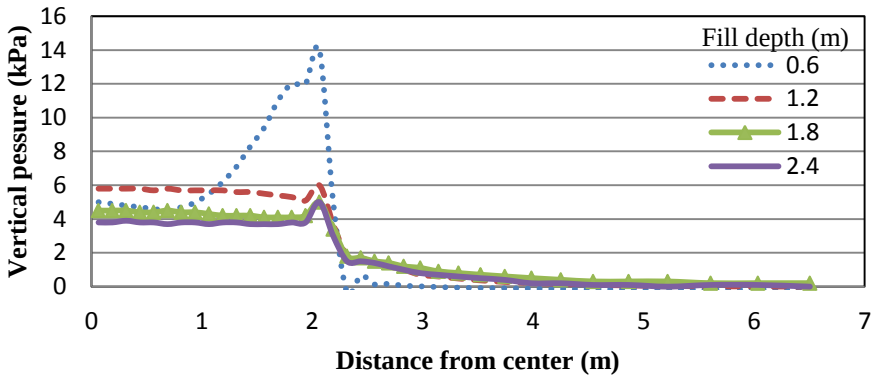

(c) Concrete pavement thickness = 0.3 m

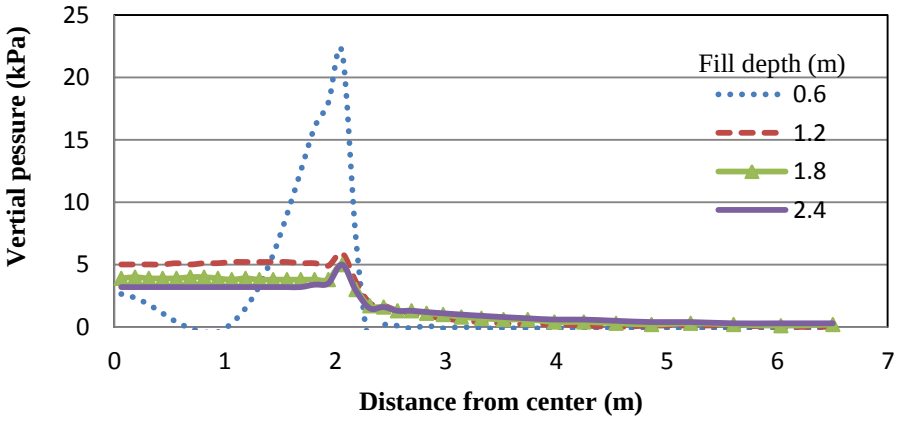

(d) Concrete pavement thickness = 0.35 m

FIGURE 5.11 Vertical pressure distribution on the culvert perpendicular to the culvert axis at different fill depth and concrete pavement thickness (culvert span = 3.6 m) (continued)

Figure 5.12 shows the variations of the maximum vertical pressures on the culverts with different span, fill depth, and concrete pavement thickness. It is shown that the change of the maximum vertical pressure with the fill depth was higher at a low fill depth and the rate of the change gradually decreased at a higher fill depth. This similar trend was observed for each pavement thickness.

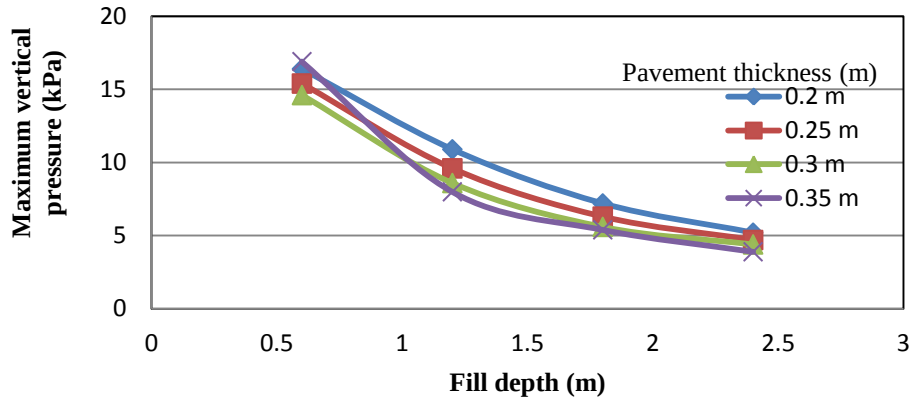

(a) Culvert span = 1.8 m

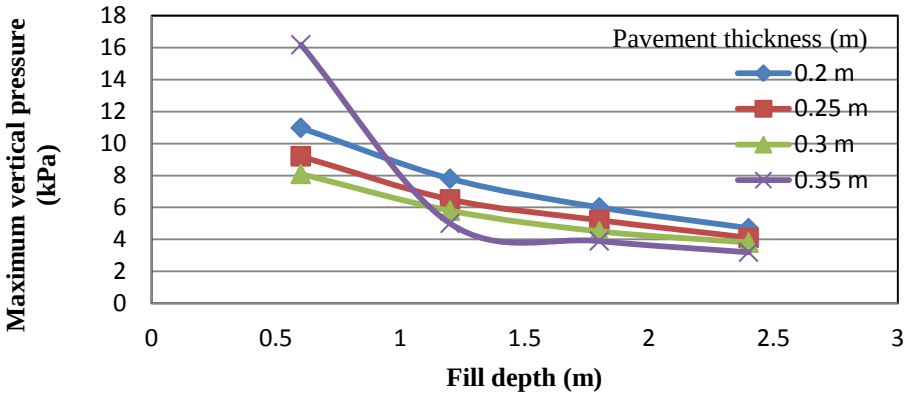

(b) Culvert span = 3.6 m

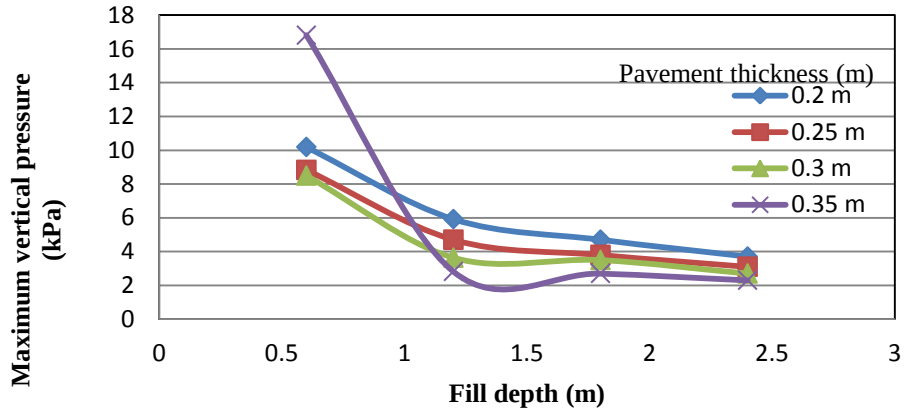

(c) Culvert span 5.4 m

FIGURE 5.12 Variation of the maximum vertical pressure on the culvert with different span, fill depth, and concrete pavement thickness

5.3.3 Effect of Span

Figure 5.13 shows the variation of the vertical pressure distribution on the culvert along the culvert axis with the span at the fill depth of 1.2 m and different concrete pavement thickness. Figure 5.14 shows the variation of the vertical pressure distribution on the culvert along the culvert axis at different fill depth and the pavement thickness of 0.25 m. These figures clearly indicate that the intensity of the vertical pressure on the culvert decreased gradually with the increase of the culvert span.

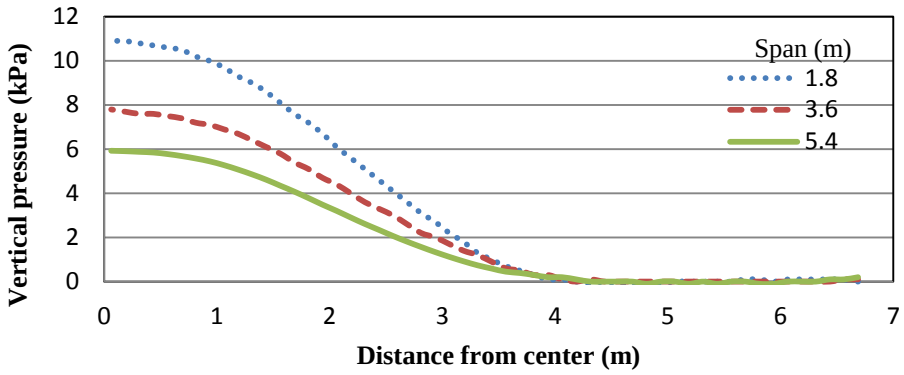

(a) Concrete pavement thickness = 0.2 m

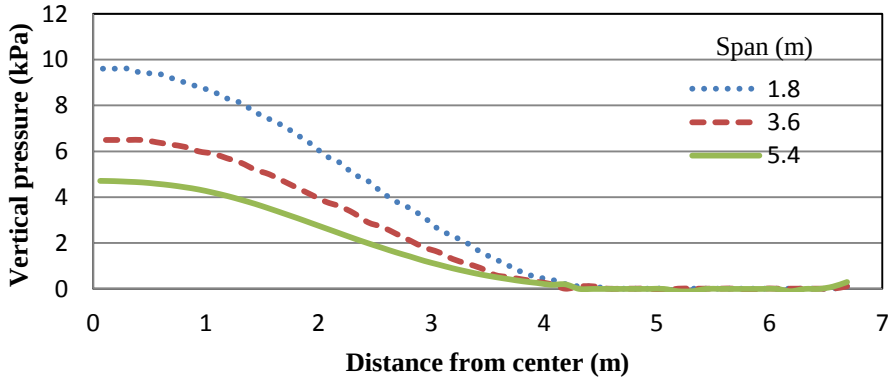

(b) Concrete pavement thickness = 0.25 m

FIGURE 5.13 Vertical pressure distribution on the culvert along the culvert axis at different span and concrete pavement thickness (fill depth = 1.2 m)

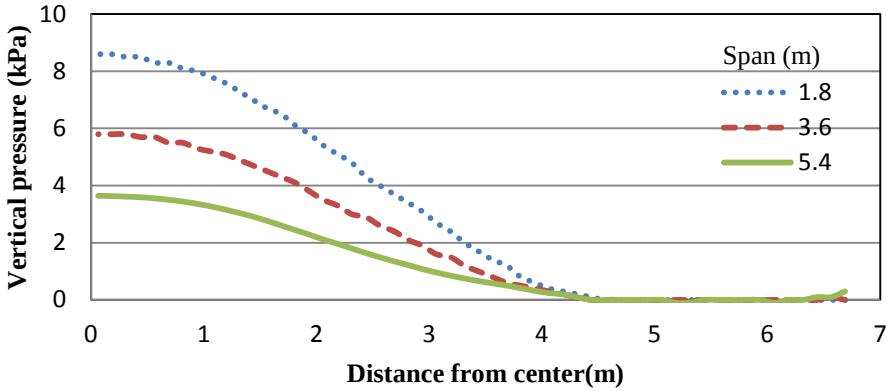

(c) Concrete pavement thickness = 0.3 m

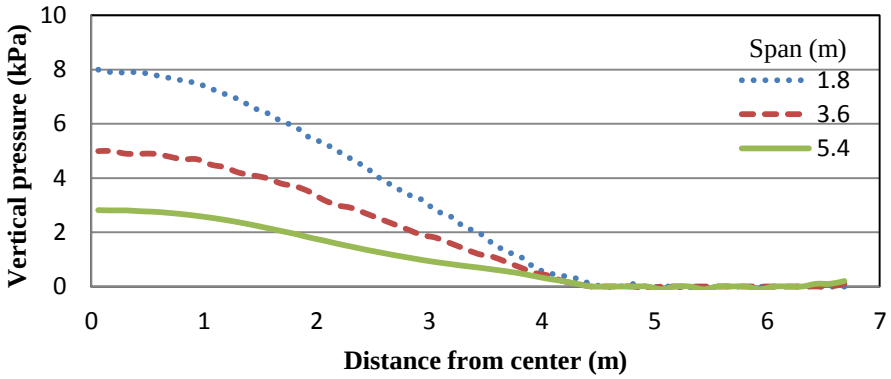

(d) Concrete pavement thickness = 0.35 m

FIGURE 5.13 Vertical pressure distribution on the culvert along the culvert axis at different span and concrete pavement thickness (fill depth = 1.2 m) (continued)

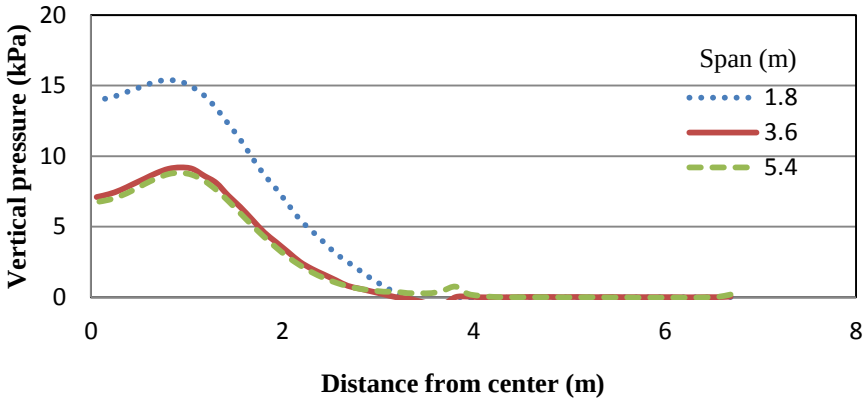

(a) Fill depth = 0.6 m

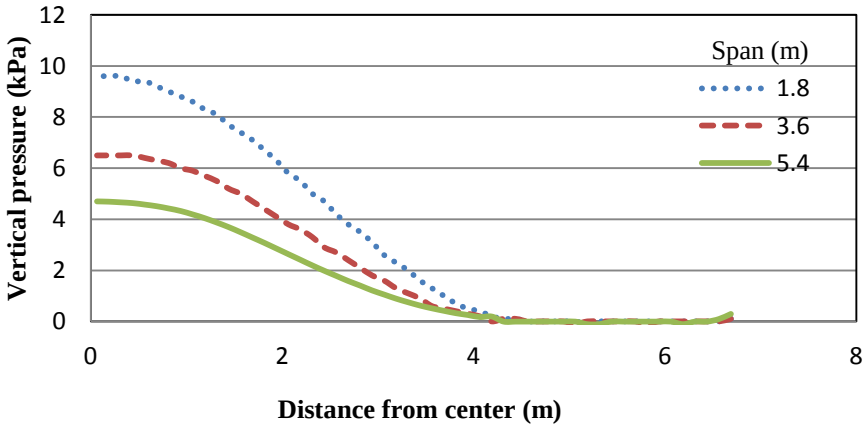

(b) Fill depth = 1.2 m

FIGURE 5.14 Vertical pressure distribution on the culvert along the culvert axis at different span and fill depth (concrete pavement thickness = 0.25 m)

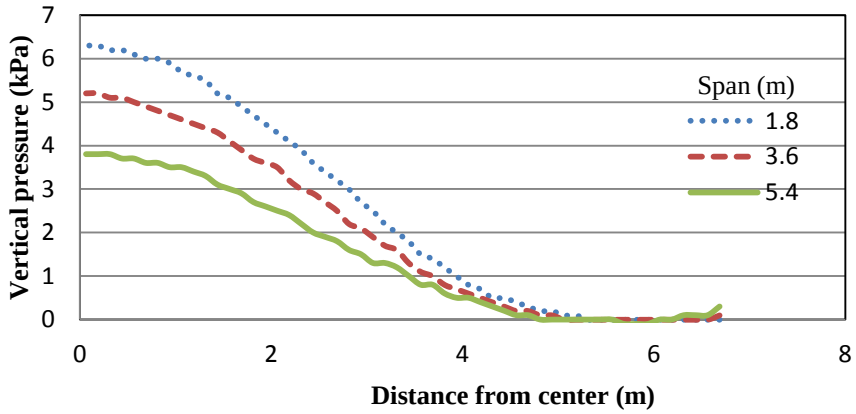

(c) Fill depth = 1.8 m

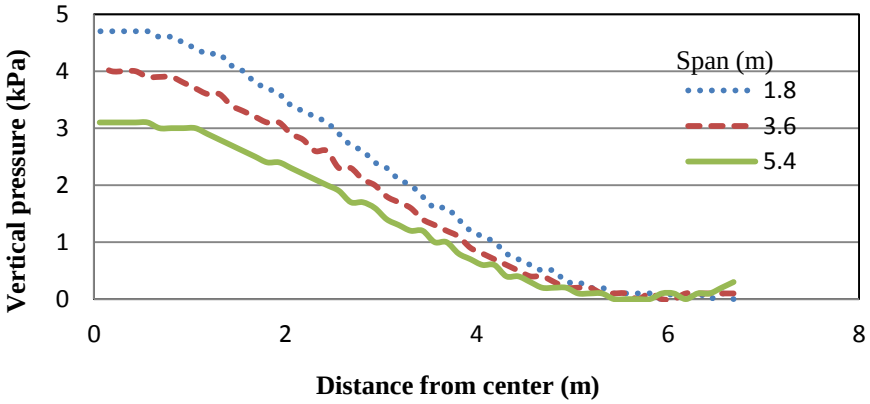

(d) Fill depth = 2.4 m

FIGURE 5.14 Vertical pressure distribution on the culvert along the culvert axis at different span and fill depth (concrete pavement thickness = 0.25 m) (continued)

Figure 5.15 shows the variation of the maximum vertical pressure on the culvert with the span at different fill depth and concrete pavement thickness. The figure shows that the change in the culvert span had more effect on the vertical pressure distribution at a low fill depth. The vertical pressure on the culvert increased with the decrease in the span. At the lower fill depth the change in the vertical pressure when the span was varied from 1.8 m to 3.6 m was more

significant than that when the span was varied from 3.6 m to 5.4 m. At the higher fill depth, however, the rate of change for the maximum vertical pressure with the span was uniform over all spans considered.

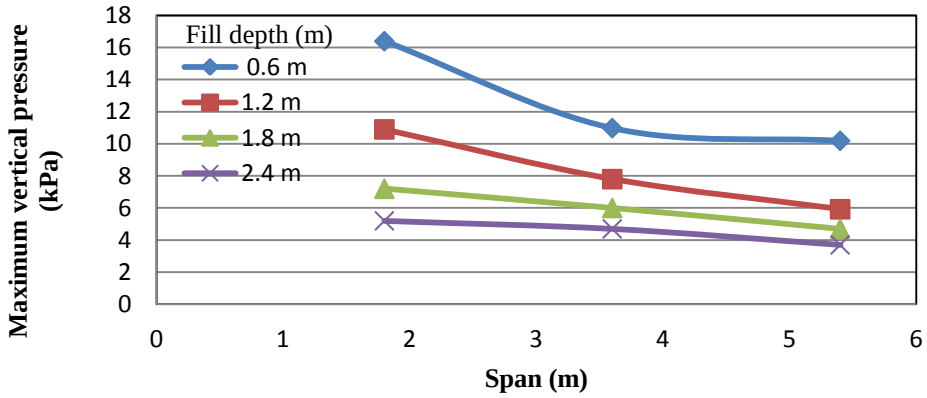

(a) Concrete pavement thickness = 0.2 m

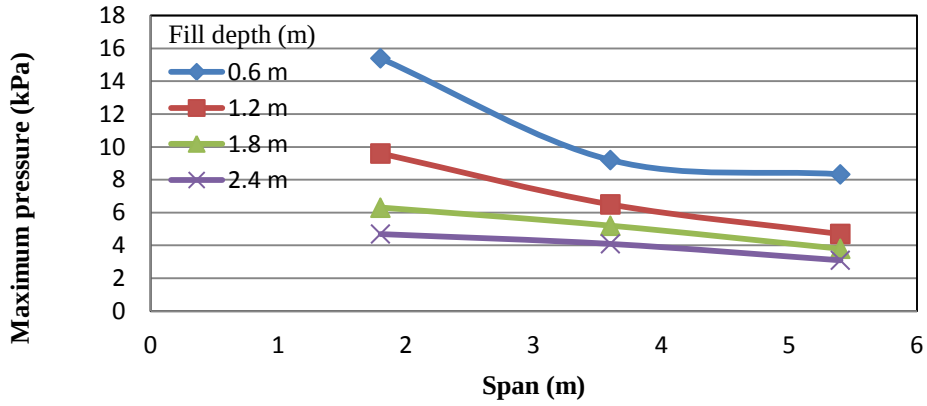

(b) Concrete pavement thickness = 0.25 m

FIGURE 5.15 Variation in the maximum vertical pressure on the culvert with the span at different fill depth and concrete pavement thickness

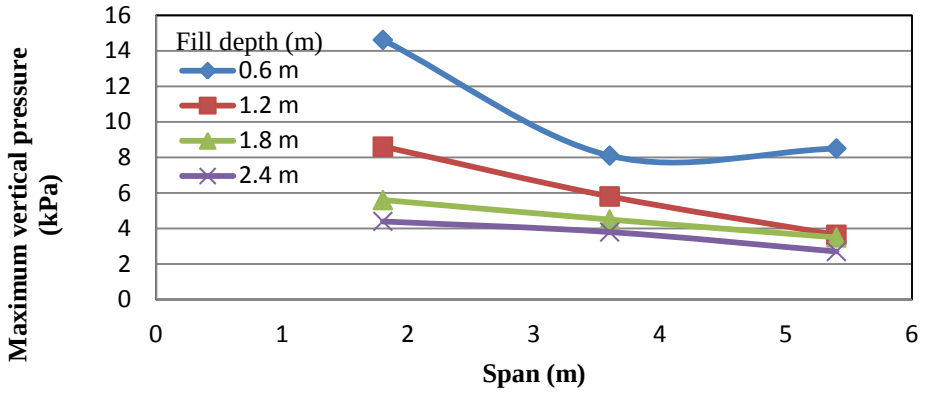

(c) Concrete pavement thickness = 0.3

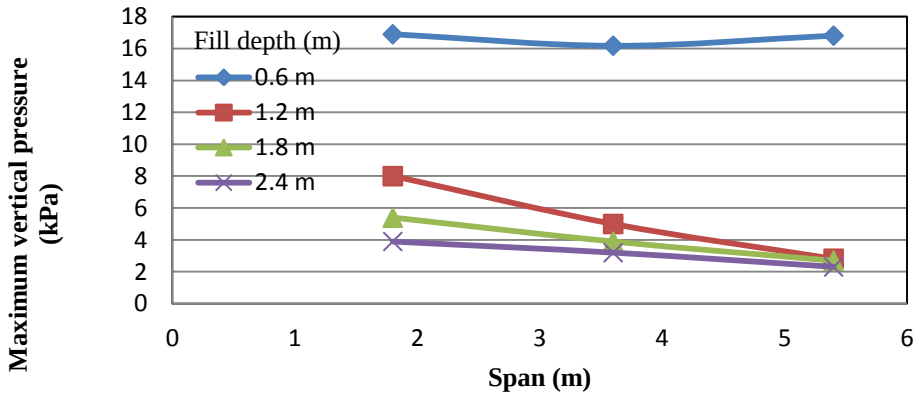

(d) Concrete pavement thickness = 0.35 m

FIGURE 5.15 Variation in the maximum vertical pressure on the culvert with the span at different fill depth and concrete pavement thickness (continued)

Since the thickness of the top slab used in the numerical model for all the three culvert spans was same, the culverts with a larger span were more flexible than those with a smaller span thus having more deflections as shown in Figure 5.16. The deflections might have affected the magnitudes of the vertical pressure on the culverts with a larger span. To investigate this effect, a separate model was created for a 5.4 m span culvert under a 1.2 m fill depth and a 0.2 m thick

pavement by doubling the top slab thickness (i.e., 0.50 m) as the original thickness. Figure 5.17 shows the distributions of the vertical pressure along the culvert axis for the 1.8 m span culvert and the 5.4 m span culverts with 0.25 m and 0.50 m thick top slabs. It is clearly shown that the increase of the slab thickness increased the vertical pressure on the culvert and the increased vertical pressure for the larger span was closer to that for the smaller span. In practice, thicker top slabs are always used to reduce deflections for larger span culverts. Therefore, it is conservative not to consider the vertical pressure reduction due to the increase of the culvert span.

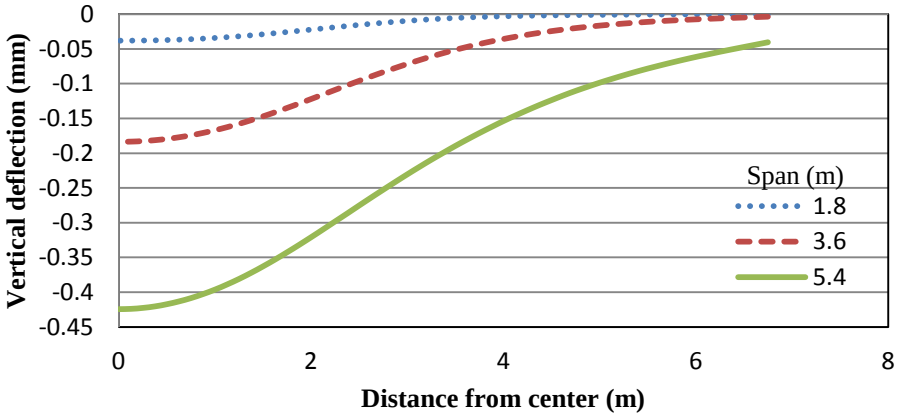

FIGURE 5.16 Deflection of slab at different span

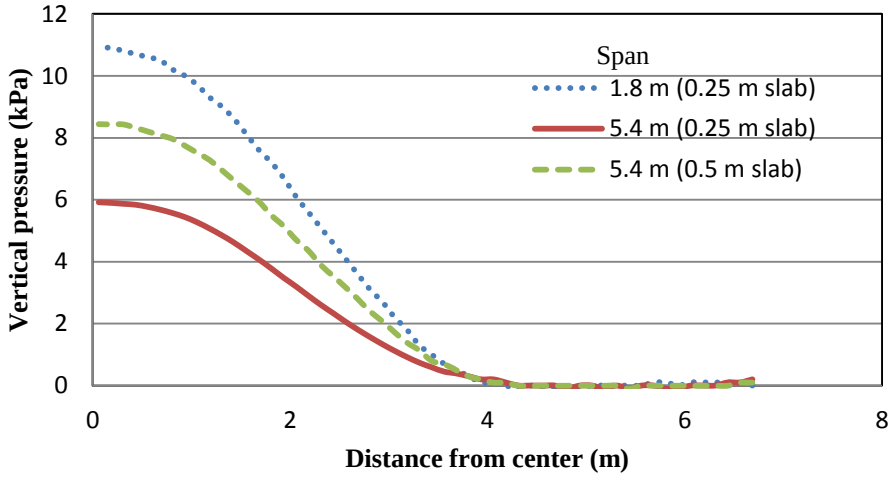

FIGURE 5.17 Effect of the top slab thickness on the vertical pressure distribution

5.3.4 Summary

The distribution of the vertical pressure due to a wheel load on the top slab of the low-fill box culvert under a rigid pavement was investigated using the 3D finite difference method in FLAC3D. Three key influence factors including the pavement thickness, fill depth, and culvert span, were considered. Before this parametric study, the finite difference model was verified against the field test data. The following conclusions can be made based on the parametric study:

1) The intensity of the vertical pressure on the top slab of the culvert gradually decreased as the increase of the concrete pavement thickness because the wheel load was distributed over a wider area.
2) The intensity of the vertical pressure gradually decreased with the increase of the fill depth over the culvert also because the wheel load was distributed over a wider area.
3) The location of the maximum vertical pressure was below the wheel load when the fill depth was 0.6 m. However, the maximum vertical pressure was located below the middle of the axle load at the fill depth of 1.2 m and larger.
4) The vertical pressure on the top slab of the culvert decreased with the increase of the culvert span. The influence of the span was more at a lower fill depth. The rate of change in the vertical pressure on the top slab of the culvert with the span decreased with the increase of the culvert span. The increase of the slab thickness increased the maximum vertical pressure on the culvert.

5.4 Flexible Pavement

Forty-eight culvert models under flexible pavements were created to study the effects of the influence factors mentioned above. Analyses were carried out in three categories based on the spans of 1.8 m, 3.6 m and 5.4 m. In each category, fill depths above the culverts at 0.6 m, 1.2 m, 1.8 m, and 2.4 m were considered. For each fill depth, the thickness of the asphalt pavement layer was varied at 0.15, 0.23, 0.30, and 0.38 m. Because of this variation, the thickness of the natural subgrade was also changed to meet the total fill depth. The vertical pressure distribution on the top of the culvert was monitored along the axis and span of the culvert through the center.

5.4.1 Effects of Asphalt Pavement Thickness

Figures 5.18 and 5.19 show the variations of vertical pressure distributions on the culvert along and perpendicular to the culvert axis with the thickness of the asphalt pavement thickness at different fill depths, respectively. All these distributions are presented at the culvert span of 1.8 m. These figures clearly indicate that the intensity of the vertical pressure on the culvert decreased gradually with the increase of the asphalt pavement thickness. A similar trend was observed at the culvert spans of 3.6 m and 5.4 m.

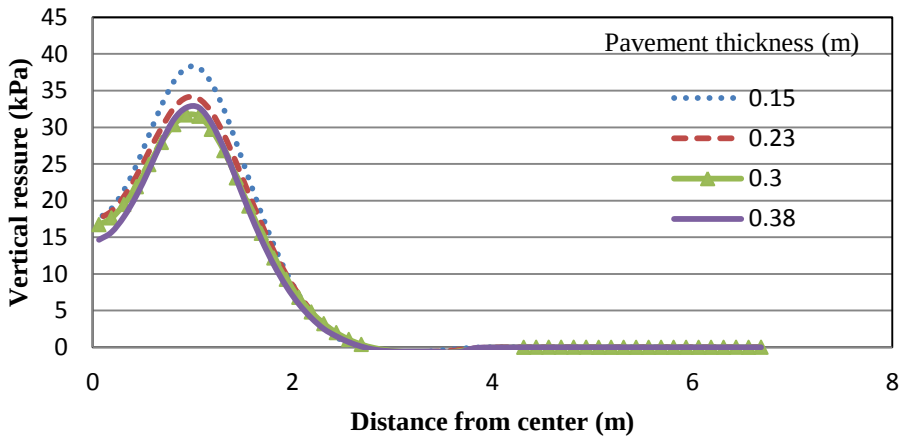

(a) Fill depth = 0.6 m

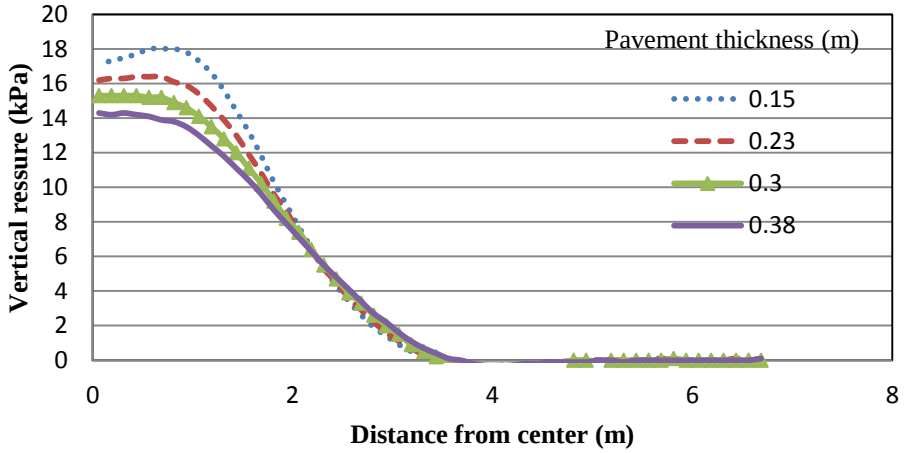

(b) Fill depth = 1.2 m

FIGURE 5.18 Vertical pressure distribution on the culvert along the culvert axis at different asphalt pavement thickness and fill depth (culvert span = 1.8 m)

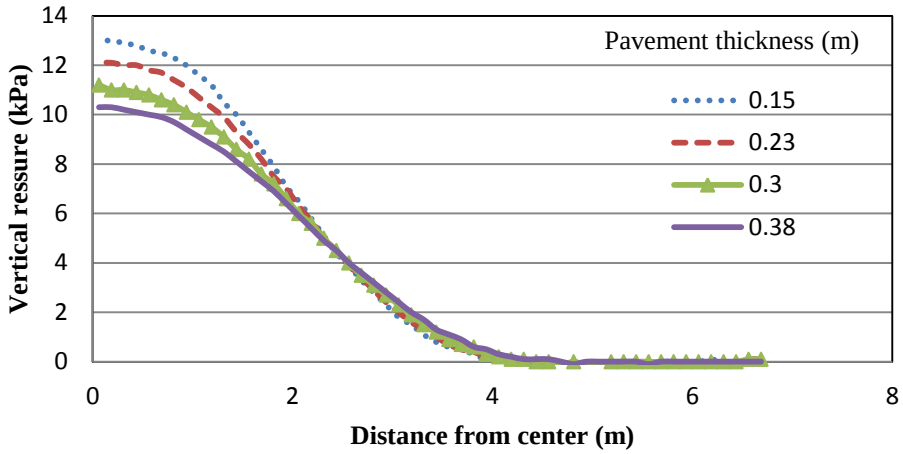

(c) Fill depth = 1.8 m

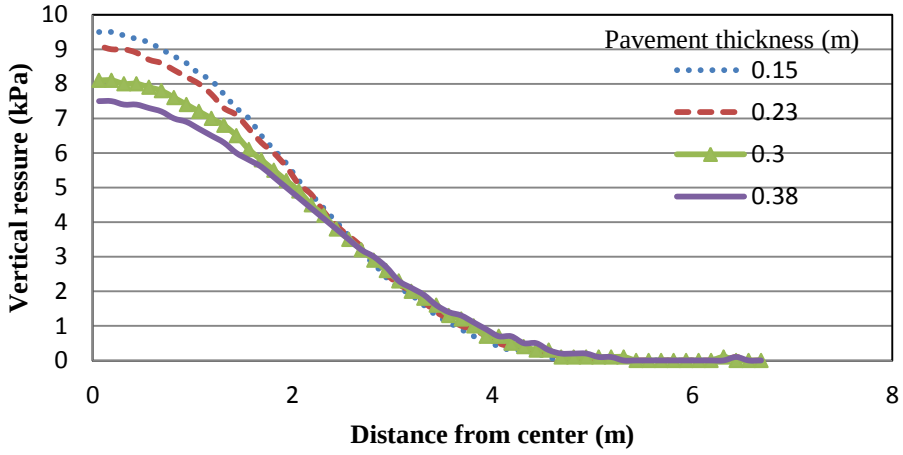

(d) Fill depth = 2.4 m

FIGURE 5.18 Vertical pressure distribution on the culvert along the culvert axis at different asphalt pavement thickness and fill depth (culvert span = 1.8 m) (continued)

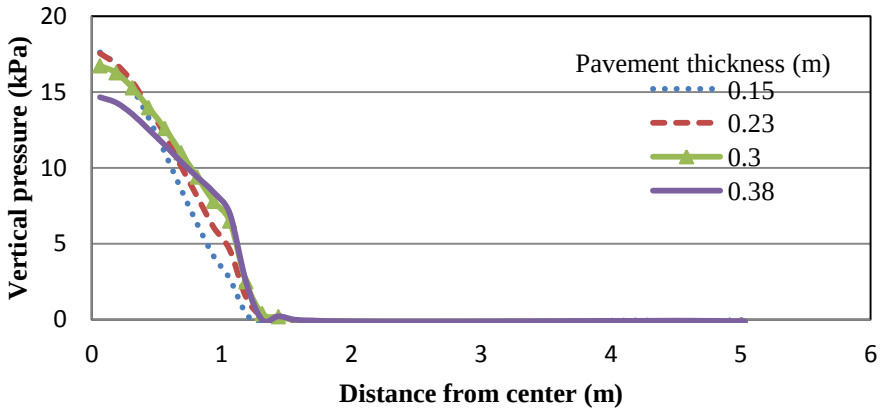

(a) Fill depth = 0.6 m

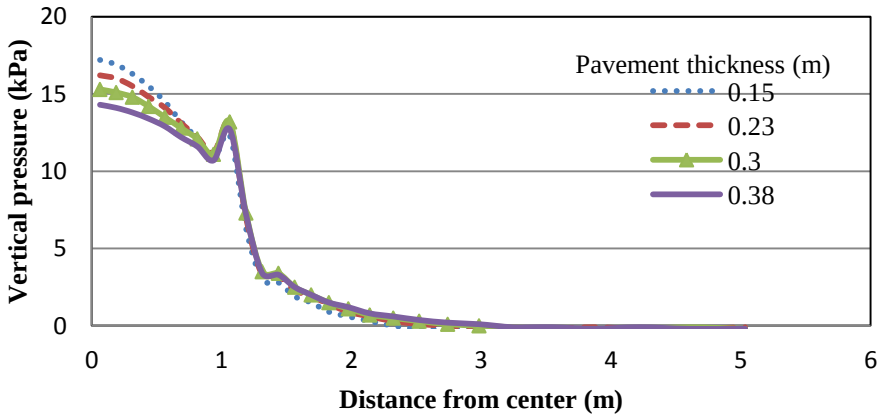

(b) Fill depth = 1.2 m

FIGURE 5.19 Vertical pressure distribution on the culvert perpendicular to the culvert axis at different asphalt pavement thickness and fill depth (culvert span = 1.8 m)

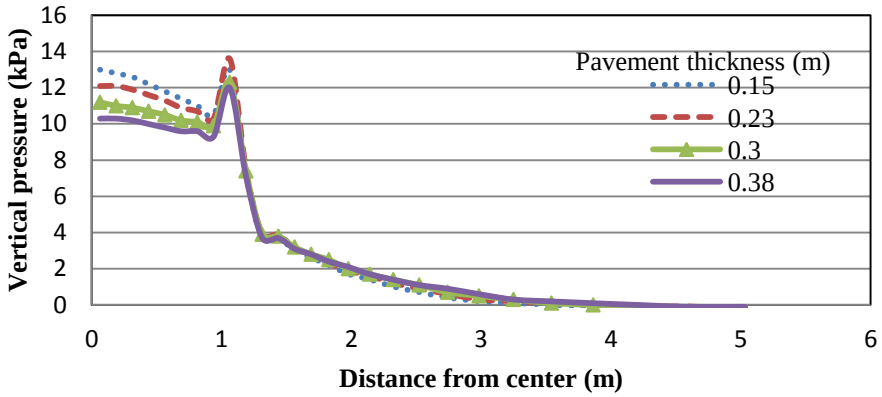

(c) Fill depth = 1.8 m

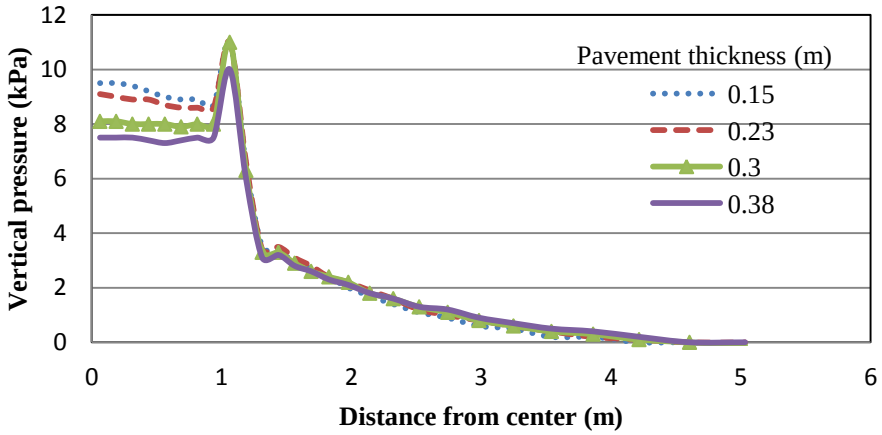

(d) Fill depth = 2.4 m

FIGURE 5.19 Vertical pressure distribution on the culvert perpendicular to the culvert axis at different asphalt pavement thickness and fill depth (culvert span = 1.8 m) (continued)

Figure 5.20 shows the variations of the maximum vertical pressure on the culvert with the asphalt pavement thickness at different fill depth for the culvert spans of 1.8 m, 3.6 m, and 5.4 m. This figure also indicates that the maximum vertical pressure on the culvert decreased gradually with the increase in the concrete pavement thickness.

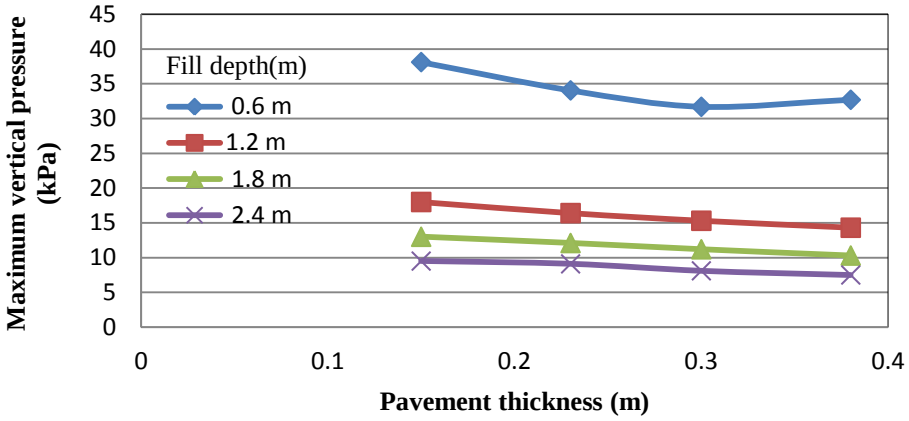

(a) Span =1.8 m

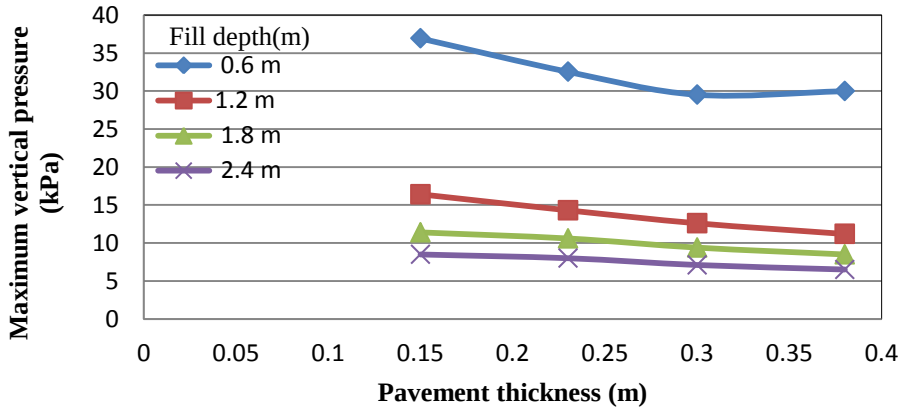

(b) Span =3.6 m

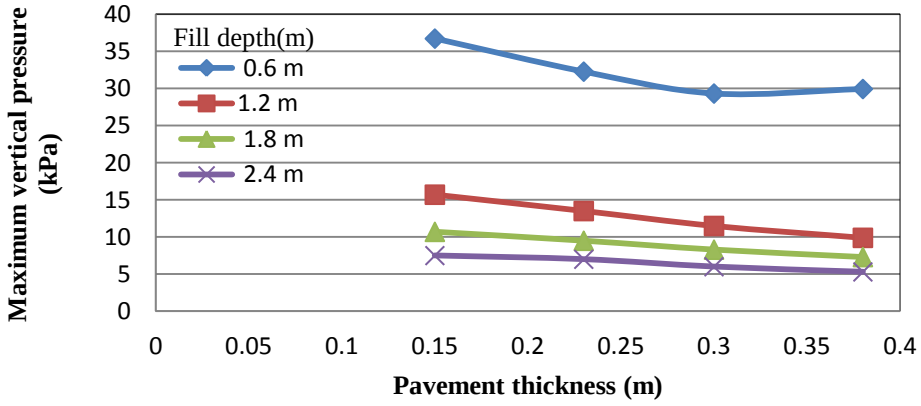

(c) Span =5.4 m

FIGURE 5.20 Variation of the maximum vertical pressure on the culvert with the asphalt pavement thickness at different fill depth and culvert span

5.4.2 Effect of Fill Depth

Figures 5.21 and 5.22 show the variations in the vertical pressure distributions on the culvert along and perpendicular to the culvert axis with the fill depth at different asphalt pavement thickness. These figures clearly indicate that the intensity of the vertical pressure on the culvert decreased gradually with the increase in the fill depth. A similar trend was observed for the culverts with spans of 1.8 m and 5.4 m. However, the locations of the maximum vertical pressures were not consistent for all fill depths. Along the culvert axis, the maximum vertical pressure was located below the wheel load for the case with 0.6 m fill but at the middle of the axle load for the case with1.2 m or more fill depth. Along the culvert span, the locations of the maximum vertical pressures were either at the middle of the axle load or at the edge of the culvert wall.

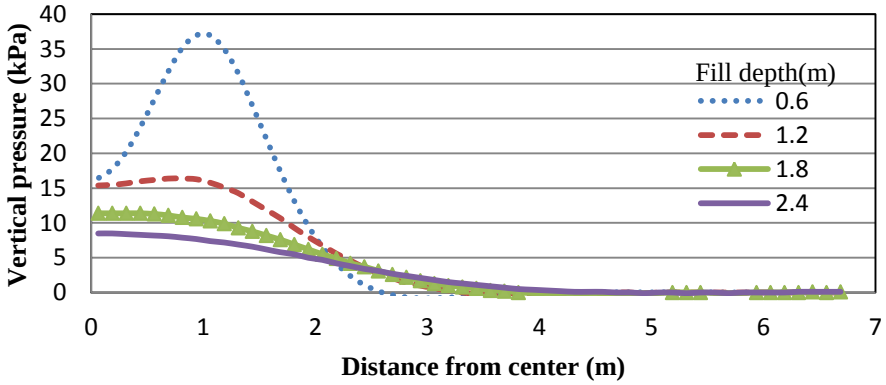

(a) Asphalt pavement thickness = 0.15 m

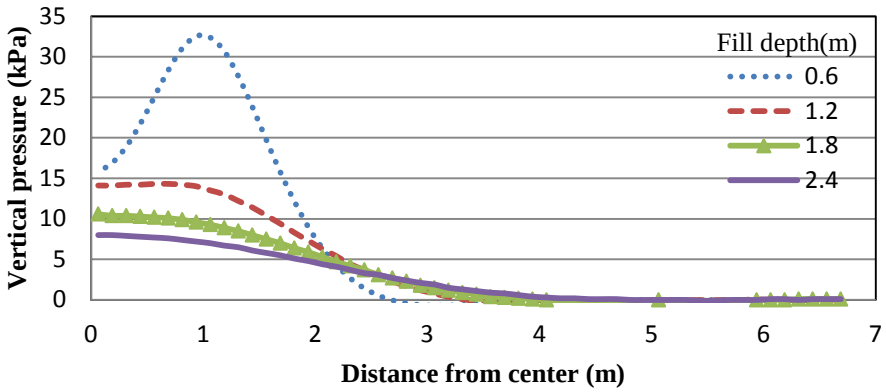

(b) Asphalt pavement thickness = 0.23 m

FIGURE 5.21 Vertical pressure distribution on culvert slab along the culvert axis at different fill depth and asphalt pavement thickness (culvert span =3.6 m)

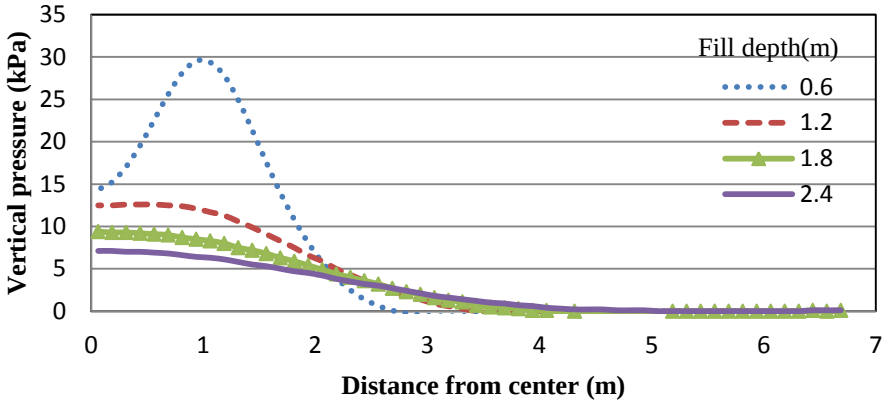

(c) Asphalt pavement thickness = 0.30 m

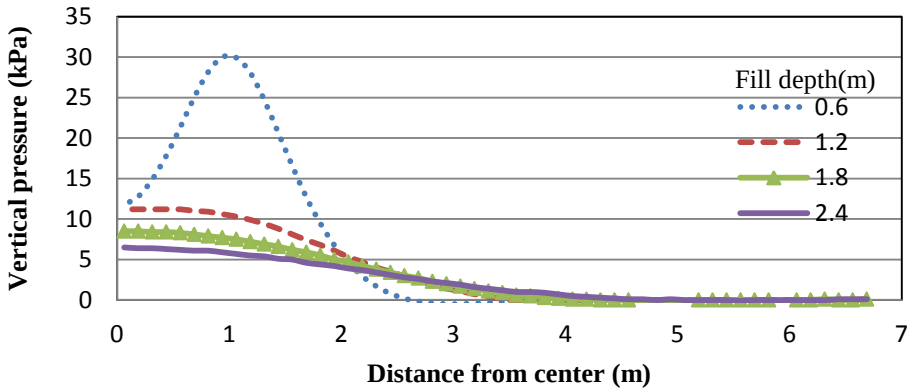

(d) Asphalt pavement thickness = 0.38 m

FIGURE 5.21 Vertical pressure distribution on culvert slab along the culvert axis at different fill depth and asphalt pavement thickness (culvert span =3.6 m) (continued)

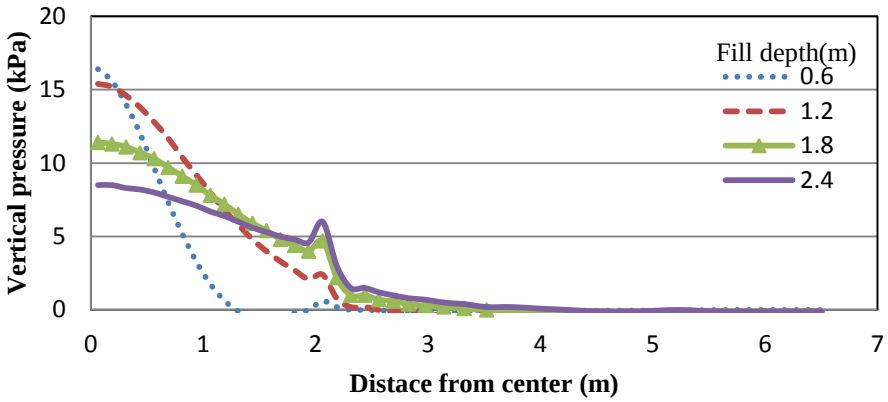

(a) Asphalt pavement thickness = 0.15 m

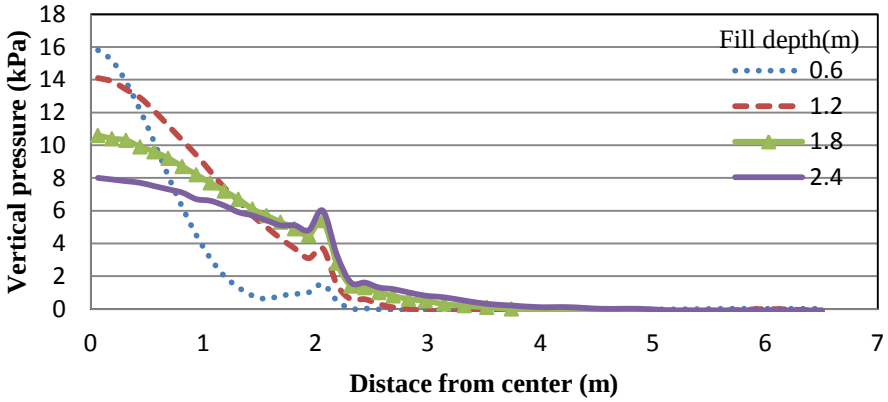

(b) Asphalt pavement thickness = 0.23 m

FIGURE 5.22 Vertical pressure distribution on culvert slab perpendicular to the culvert axis at different fill depth and asphalt pavement thickness (span = 3.6 m)

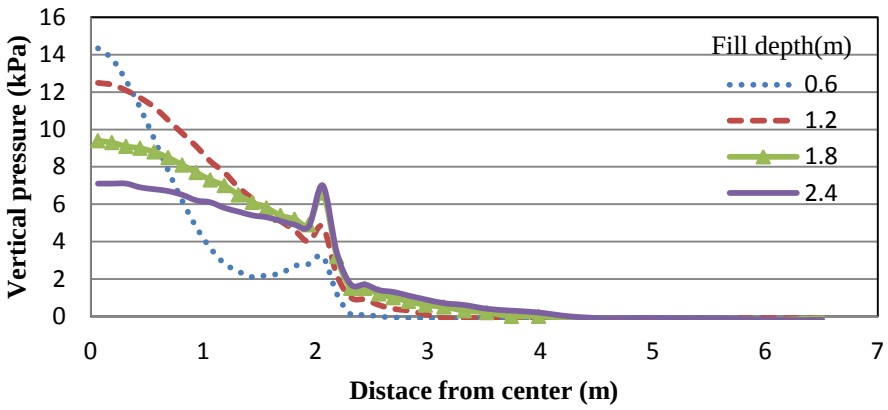

(c) Asphalt pavement thickness = 0.30 m

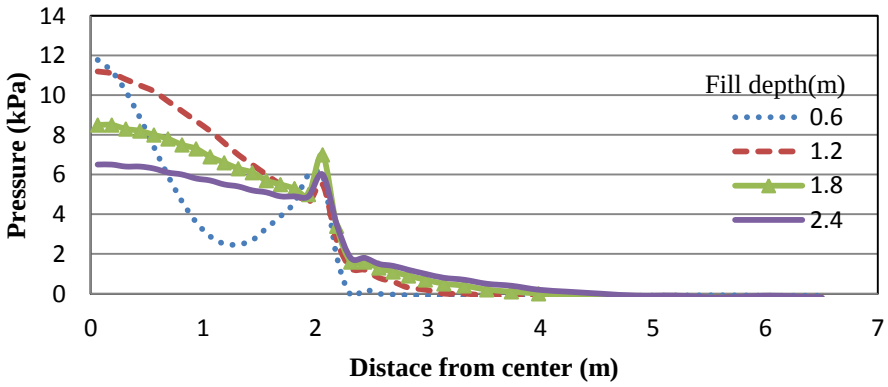

(d) Asphalt pavement thickness = 0.38 m

FIGURE 5.22 Vertical pressure distribution on culvert slab perpendicular to the culvert axis at different fill depth and asphalt pavement thickness (span = 3.6 m) (continued)

Figure 5.23 shows the variations of the maximum vertical pressures on the culverts with different span, fill depth, and asphalt pavement thickness. It is shown that the change of the maximum vertical pressure with the fill depth was higher at a low fill depth and the rate of the change gradually decreased at a higher fill depth. This similar trend was observed for each pavement thickness.

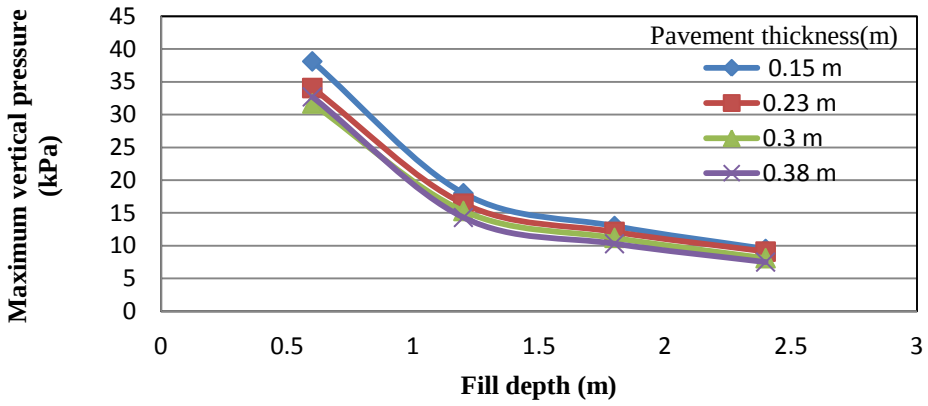

(a) Span = 1.8 m

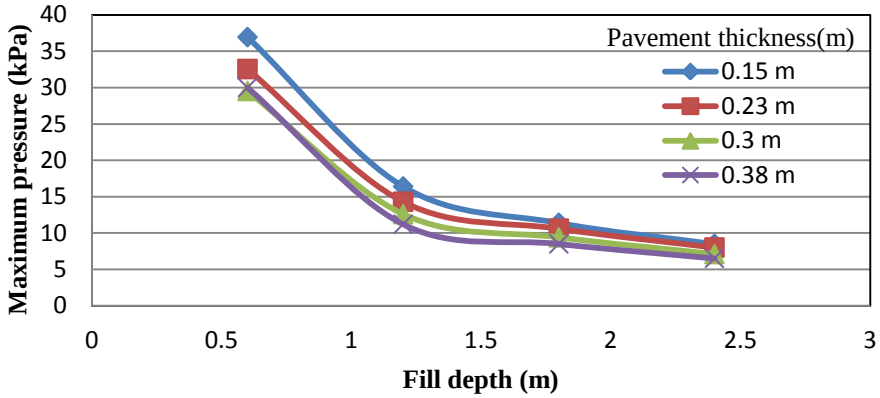

(b) Span = 3.6 m

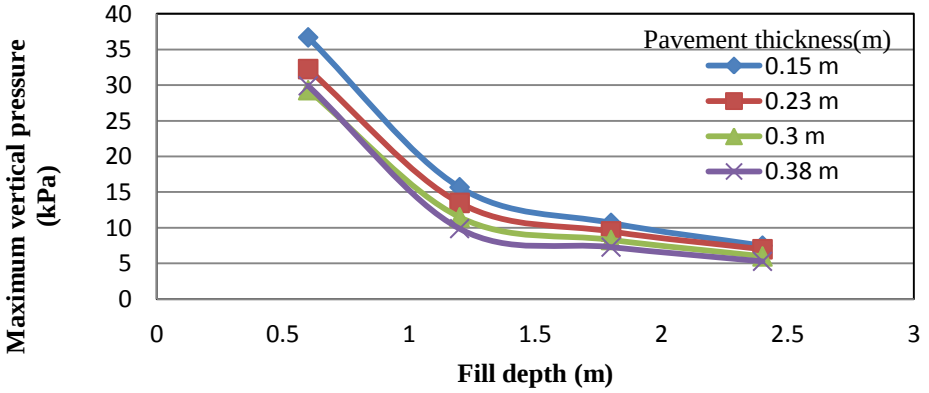

(c) Span = 5.4 m

FIGURE 5.23 Variation of the maximum vertical pressure on the culvert with different span, fill depth, and asphalt pavement thickness

5.4.3 Effect of Span

Figure 5.24 shows the variation of the vertical pressure distribution on the culvert along the culvert axis with the span at the fill depth of 1.2 m and different asphalt pavement thickness. Figure 5.25 shows the variation of the vertical pressure distribution on the culvert along the culvert axis at different fill depth and the pavement thickness of 0.25 m. These figures clearly indicate that the intensity of the vertical pressure on the culvert decreased gradually with the increase of the culvert span.

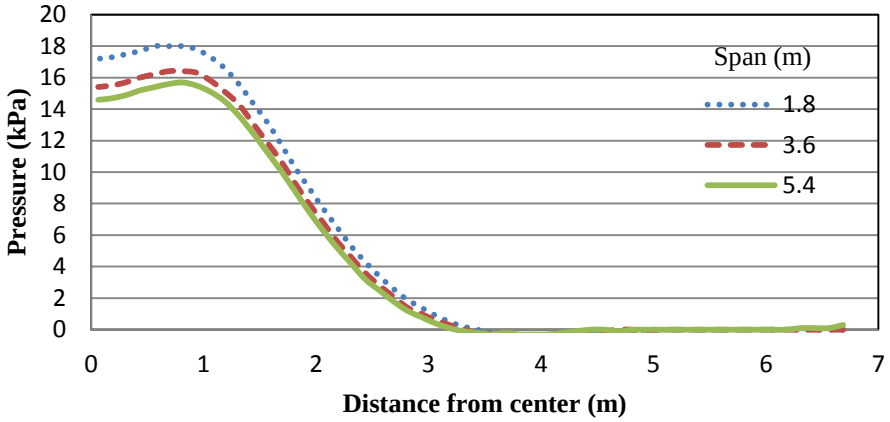

(a) Asphalt pavement thickness = 0.15 m

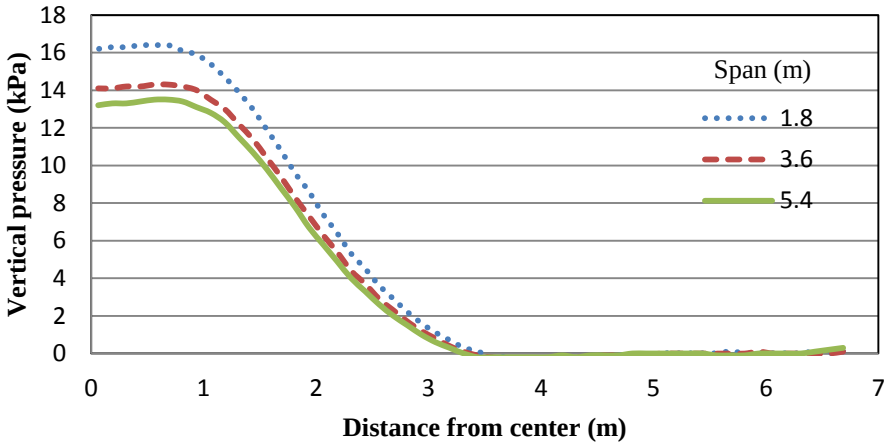

(b) Asphalt pavement thickness = 0.23 m

FIGURE 5.24 Vertical pressure distribution on the culvert along the culvert axis at different span and asphalt pavement thickness (fill depth = 1.2 m)

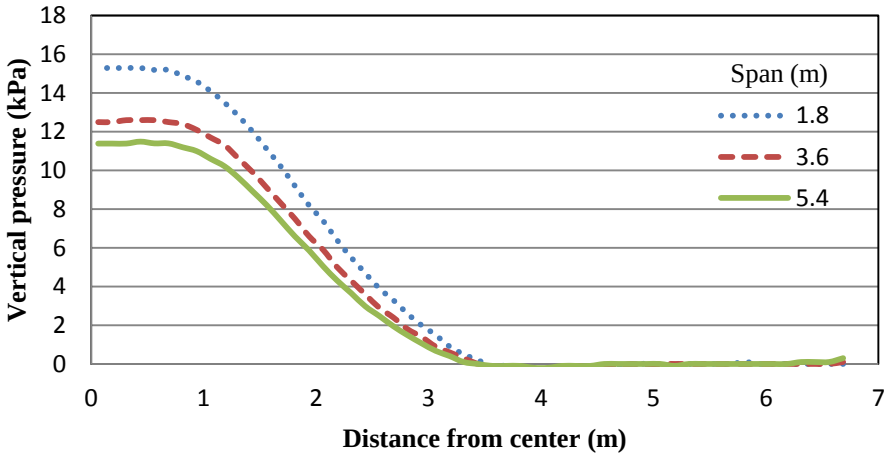

(c) Asphalt pavement thickness = 0.30 m

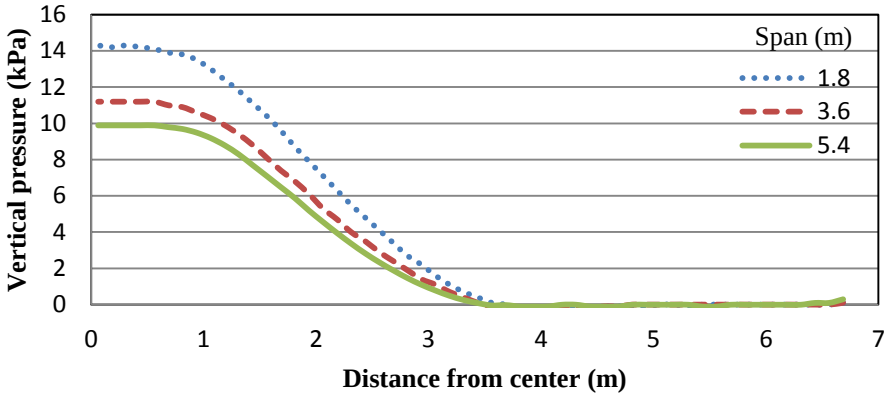

(d) Asphalt pavement thickness = 0.38 m

FIGURE 5.24 Vertical pressure distribution on the culvert along the culvert axis at different span and asphalt pavement thickness (fill depth = 1.2 m) (continued)

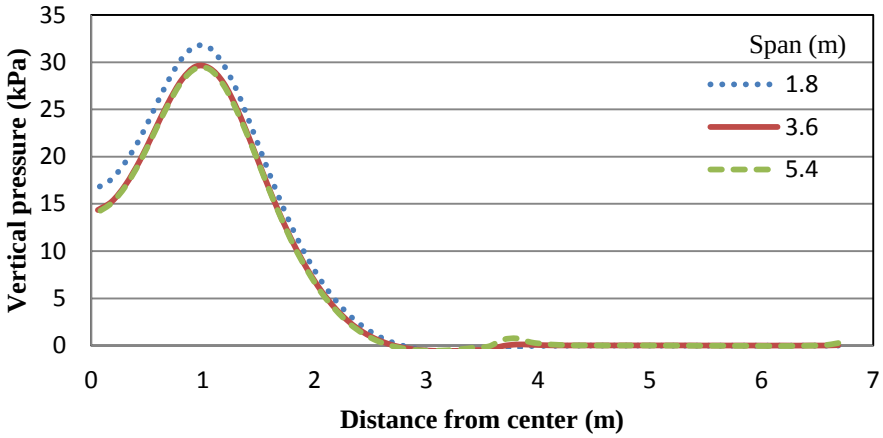

(a) Fill depth = 0.6 m

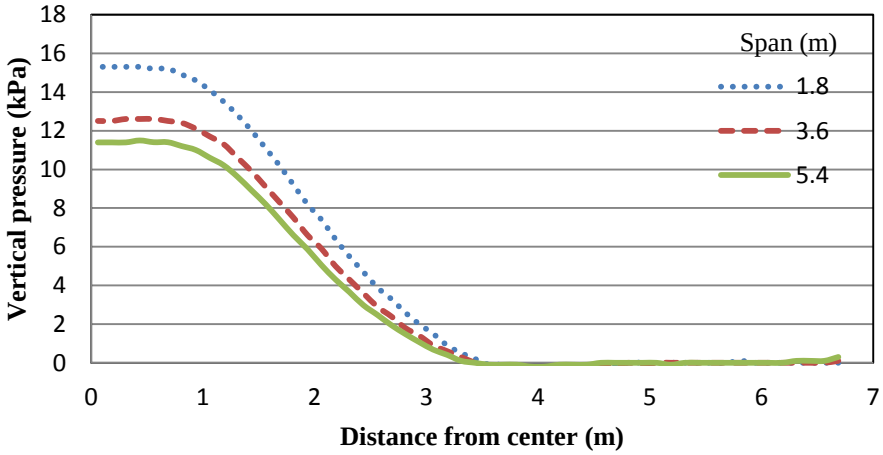

(b) Fill depth = 1.2 m

FIGURE 5.25 Vertical pressure distribution on the culvert along the culvert axis at different span and fill depth (asphalt pavement thickness = 0.30 m) (continued)

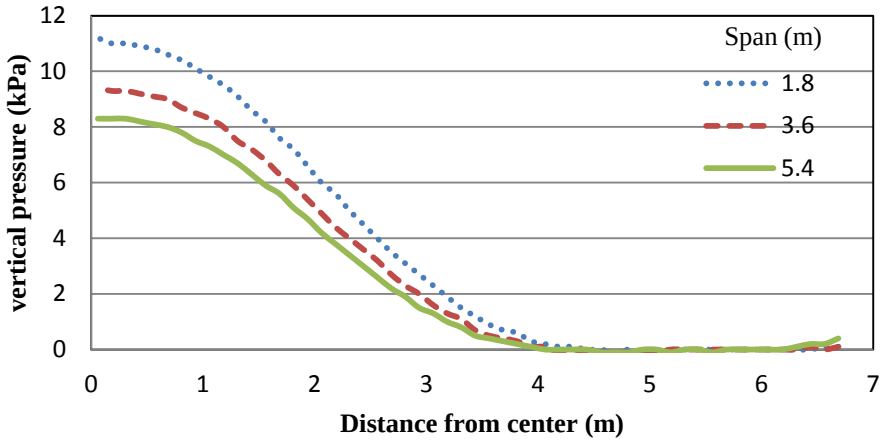

(c) Fill depth = 1.8 m

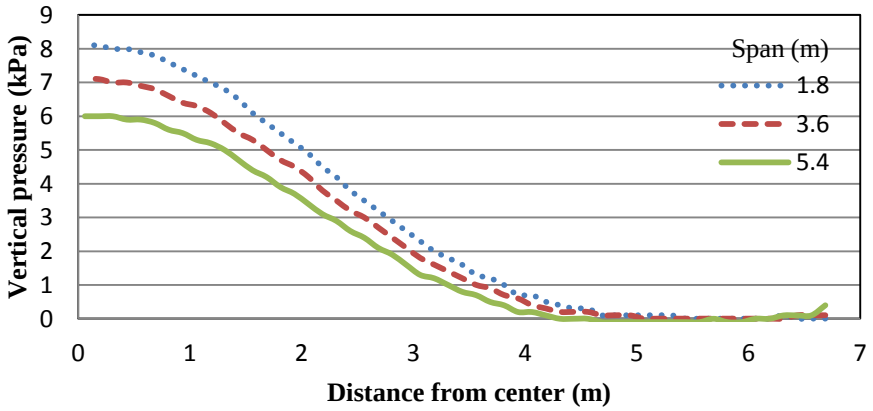

(d) Fill depth = 2.4 m

FIGURE 5.25 Vertical pressure distribution on the culvert along the culvert axis at different span and fill depth (asphalt pavement thickness = 0.30 m)

Figure 5.26 shows the variation of the maximum vertical pressure on the culvert with the span at different fill depth and asphalt pavement thickness. The figure shows that the change in the culvert span had more effect on the vertical pressure distribution at a low fill depth. The vertical pressure on the culvert increased with the decrease in the span. At the lower fill depth the

change in the vertical pressure when the span was varied from 1.8 m to 3.6 m was more significant than that when the span was varied from 3.6 m to 5.4 m. At the higher fill depth, however, the rate of change for the maximum vertical pressure with the span was uniform over all spans considered.

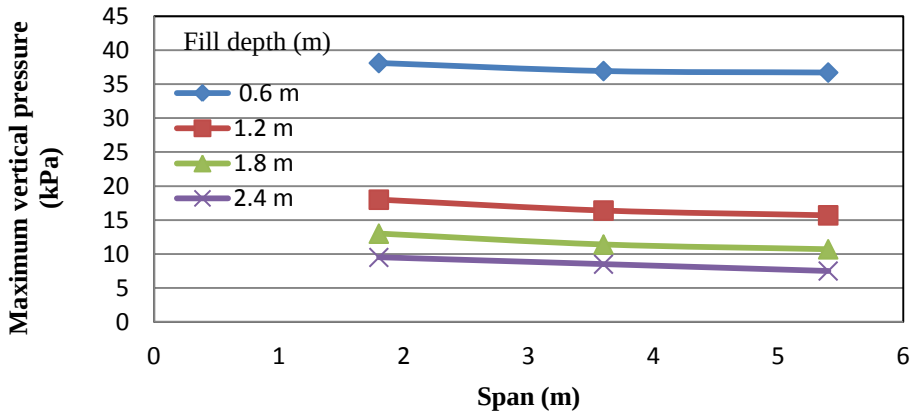

(a) Asphalt pavement thickness = 0.15 m

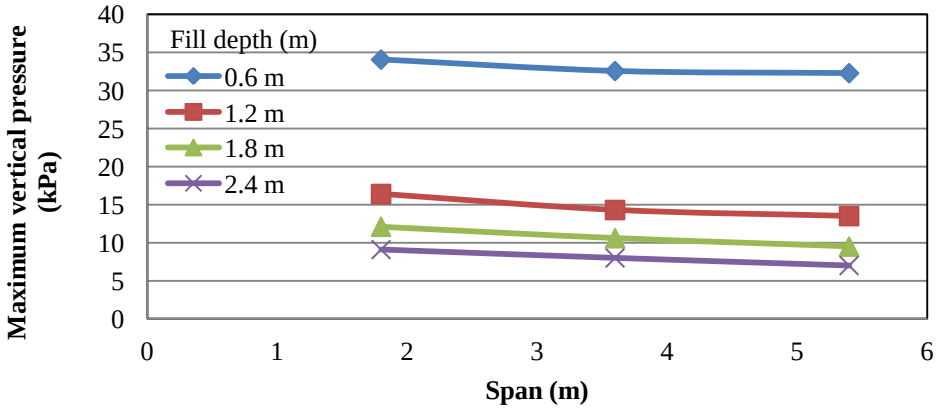

(b) Asphalt pavement thickness = 0.23 m

FIGURE 5.26 Variation in the maximum vertical pressure on the culvert with the span at different fill depth and asphalt pavement thickness

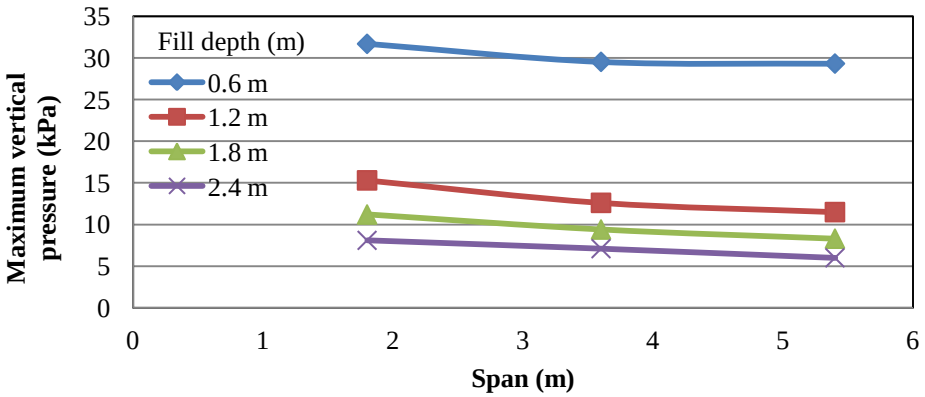

(c) Asphalt pavement thickness = 0.30 m

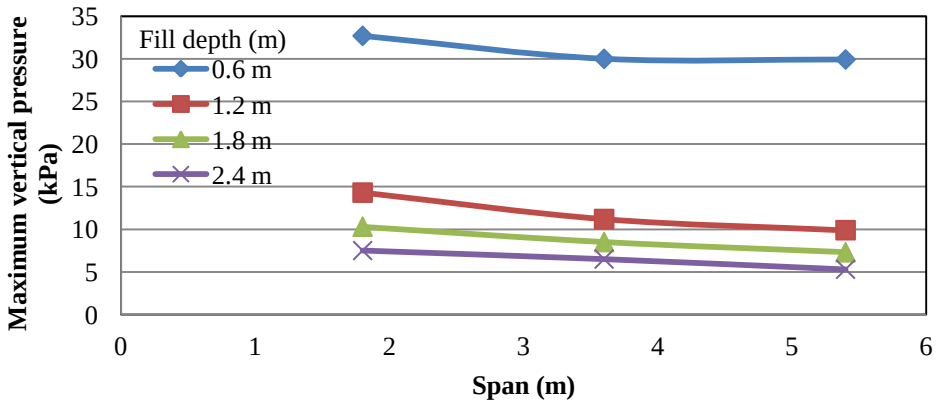

(d) Asphalt pavement thickness = 0.38 m

FIGURE 5.26 Variation in the maximum vertical pressure on the culvert with the span at different fill depth and asphalt pavement thickness (continued)

Since the thickness of the top slab used in the numerical model for all the three culvert spans was same, the culverts with a larger span were more flexible than those with a smaller span thus having more deflections as shown in Figure 5.27. The deflections might have affected the magnitudes of the vertical pressure on the culverts with a larger span. To investigate this effect, a separate model was created for a 5.4 m span culvert under a 1.2 m fill depth and a 0.15 m thick

pavement by doubling the top slab thickness (i.e., 0.50 m) as the original thickness. Figure 5.28 shows the distributions of the vertical pressure along the culvert axis for the 1.8 m span culvert and the 5.4 m span culverts with 0.25 m and 0.50 m thick top slabs. It is clearly shown that the increase of the slab thickness increased the vertical pressure on the culvert and the increased vertical pressure for the larger span was closer to that for the smaller span. In practice, thicker top slabs are always used to reduce deflections for larger span culverts. Therefore, it is conservative not to consider the vertical pressure reduction due to the increase of the culvert span.

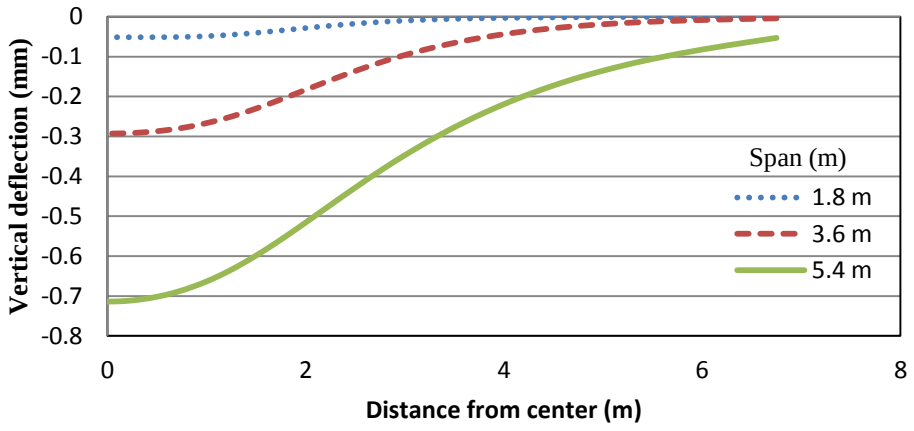

FIGURE 5.27 Deflection of slab at different span

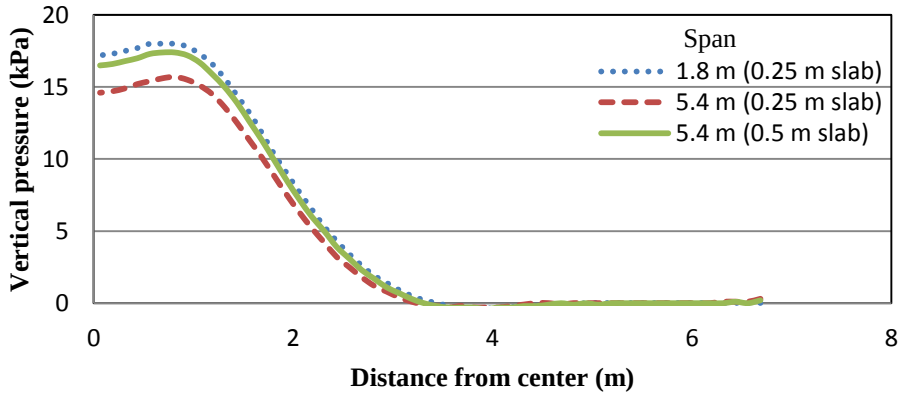

FIGURE 5.28 Deflection of slab at different span

5.4.4 Summary

The distribution of the vertical pressure due to a wheel load on the top slab of the low-fill box culvert under a flexible pavement was investigated using the 3D finite difference method in FLAC3D. Three key influence factors including the pavement thickness, fill depth, and culvert span, were considered. Before this parametric study, the finite difference model was verified against the field test data. The following conclusions can be made based on the parametric study:

1) The intensity of the vertical pressure on the top slab of the culvert gradually decreased as the increase of the asphalt pavement thickness because the wheel load was distributed over a wider area.
2) The intensity of the vertical pressure gradually decreased with the increase of the fill depth over the culvert also because the wheel load was distributed over a wider area.
3) The location of the maximum vertical pressure was below the wheel load when the fill depth was 0.6 m. However, the maximum vertical pressure was located below the middle of the axle load at the fill depth of 1.2 m and larger.
4) The vertical pressure on the top slab of the culvert decreased with the increase of the culvert span. The influence of the span was more at a lower fill depth. The rate of change in the vertical pressure on the top slab of the culvert with the span decreased with the increase of the culvert span.

5.5 Comparison with AASHTO Pressure Distribution

5.5.1 Rigid Pavement

The maximum vertical pressure on the culvert obtained by the numerical method for each case can be compared with the average vertical pressures using the formulae in the AASHTO LRFD code (2007) and AASHTO Standard Specifications (1992). The AASHTO LRFD code (2007) suggests two methods for the pressure distribution depending on the type of fill material, i.e., the H distribution and the 1.15 H distribution as discussed in section 2.3.2, in which H is the fill depth. Tables 5.1 to 5.3 show the comparison of the calculated vertical pressures with the LRFD H distribution, the LRFD 1.15 H distribution, and the distribution specified by the AASHTO Standard Specification respectively. Figure 5.29 compares the calculated vertical pressure by the numerical method and the AASTHO distribution methods for the culverts with a span of 1.8 m. Tables 5.1 to 5.3 and Figure 5.29 all show that the AASTHO distribution methods over-predicted the maximum vertical pressure as compared with the numerical method. It is shown that the AASHTO LRFD code calculated the higher vertical pressure than the AASHTO Standard Specification. The difference in the calculated vertical pressures between the numerical method and the AASHTO distribution method decreased with the increase of the fill depth.

TABLE 5.1 Comparison of the calculated vertical pressures by the numerical method and the LRFD H distribution method

Fill depth (m)	Pavement thickness (m)	Maximum pressure from numerical method (kPa)			Average pressure by LRFD H distribution (kPa)	Pressure difference (%)		
		Culvert span (m)				Culvert span (m)		
		1.8	3.6	5.4		1.8	3.6	5.4
0.6	0.2	16.4	10.98	10.19	73.5	348	569	621
	0.25	15.4	9.2	8.83	73.5	377	699	732
	0.3	14.61	8.1	8.5	73.5	403	807	765
	0.35	16.9	16.18	16.81	73.5	335	354	337
1.2	0.2	10.9	7.8	5.92	27	148	246	356
	0.25	9.6	6.5	4.7	27	181	315	474
	0.3	8.6	5.8	3.64	27	214	366	642
	0.35	8	5	2.82	27	238	440	857
1.8	0.2	7.2	6	4.7	16.4	128	173	249
	0.25	6.3	5.2	3.8	16.4	160	215	332
	0.3	5.6	4.5	3.5	16.4	193	264	369
	0.35	5.4	3.9	2.7	16.4	204	321	507
2.4	0.2	5.2	4.7	3.7	11	112	134	197
	0.25	4.7	4.1	3.1	11	134	168	255
	0.3	4.4	3.8	2.7	11	150	189	307
	0.35	3.9	3.2	2.3	11	182	244	378

TABLE 5.2 Comparison of the calculated vertical pressures by the numerical method and the LRFD 1.15 H distribution method

Fill depth (m)	Pavement thickness (m)	Maximum pressure from numerical method (kPa)			Average pressure by LRFD 1.15 H distribution (kPa)	Pressure difference (%)		
		Culvert span (m)				Span (m)		
		1.8	3.6	5.4		1.8	3.6	5.4
0.6	0.2	16.4	10.98	10.19	61.5	275	460	504
	0.25	15.4	9.2	8.83	61.5	299	568	596
	0.3	14.61	8.1	8.5	61.5	321	659	624
	0.35	16.9	16.18	16.81	61.5	264	280	266
1.2	0.2	10.9	7.8	5.92	22.4	106	187	278
	0.25	9.6	6.5	4.7	22.4	133	245	377
	0.3	8.6	5.8	3.64	22.4	160	286	515
	0.35	8	5	2.82	22.4	180	348	694
1.8	0.2	7.2	6	4.7	13.6	89	127	189
	0.25	6.3	5.2	3.8	13.6	116	162	258
	0.3	5.6	4.5	3.5	13.6	143	202	289
	0.35	5.4	3.9	2.7	13.6	152	249	404
2.4	0.2	5.2	4.7	3.7	9	73	91	143
	0.25	4.7	4.1	3.1	9	91	120	190
	0.3	4.4	3.8	2.7	9	105	137	233
	0.35	3.9	3.2	2.3	9	131	181	291

TABLE 5.3 Comparison of the calculated vertical pressures by the numerical method and the AASHTO Standard Specifications

Fill depth (m)	Pavement thickness (m)	Maximum pressure from numerical method (kPa)			Average pressure by AASHTO Standard Specification (kPa)	Difference (%)		
		Culvert span (m)				Span (m)		
		1.8	3.6	5.4		1.8	3.6	5.4
0.6	0.2	16.4	10.98	10.19	62.4	280	468	512
	0.25	15.4	9.2	8.83	62.4	305	578	607
	0.3	14.61	8.1	8.5	62.4	327	670	634
	0.35	16.9	16.18	16.81	62.4	269	286	271
1.2	0.2	10.9	7.8	5.92	16.8	54	115	184
	0.25	9.6	6.5	4.7	16.8	75	158	257
	0.3	8.6	5.8	3.64	16.8	95	190	362
	0.35	8	5	2.82	16.8	110	236	496
1.8	0.2	7.2	6	4.7	8.8	22	47	87
	0.25	6.3	5.2	3.8	8.8	40	69	132
	0.3	5.6	4.5	3.5	8.8	57	96	151
	0.35	5.4	3.9	2.7	8.8	63	126	226
2.4	0.2	5.2	4.7	3.7	5.4	4	15	46
	0.25	4.7	4.1	3.1	5.4	15	32	74
	0.3	4.4	3.8	2.7	5.4	23	42	100
	0.35	3.9	3.2	2.3	5.4	38	69	135

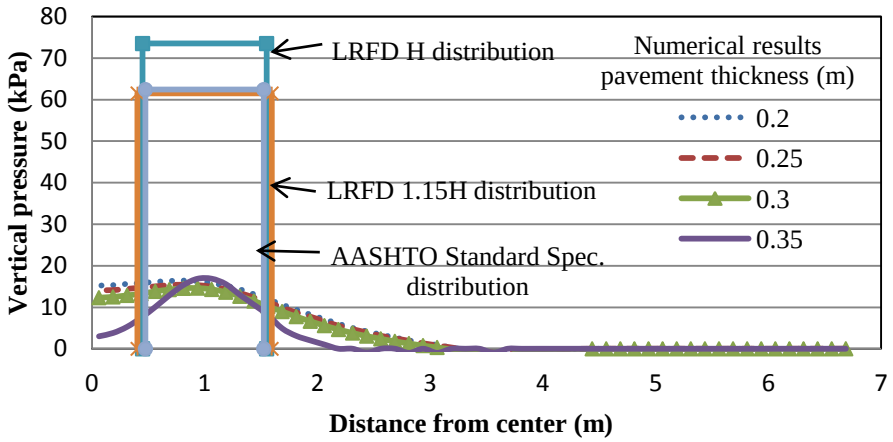

(a) Fill depth = 0.6 m

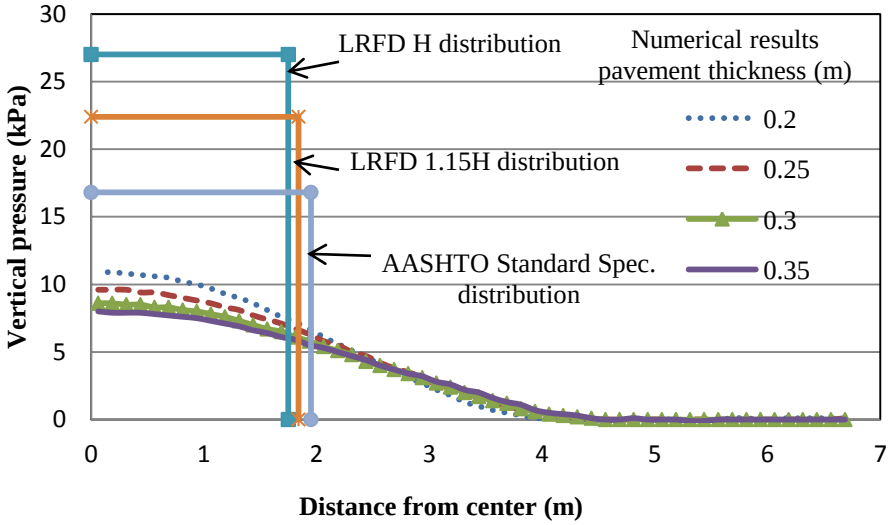

(b)Fill depth = 1.2 m

FIGURE 5.29 Comparison of the calculated pressures by the numerical method and the AASHTO distribution methods for the culvert with the 1.8 m span

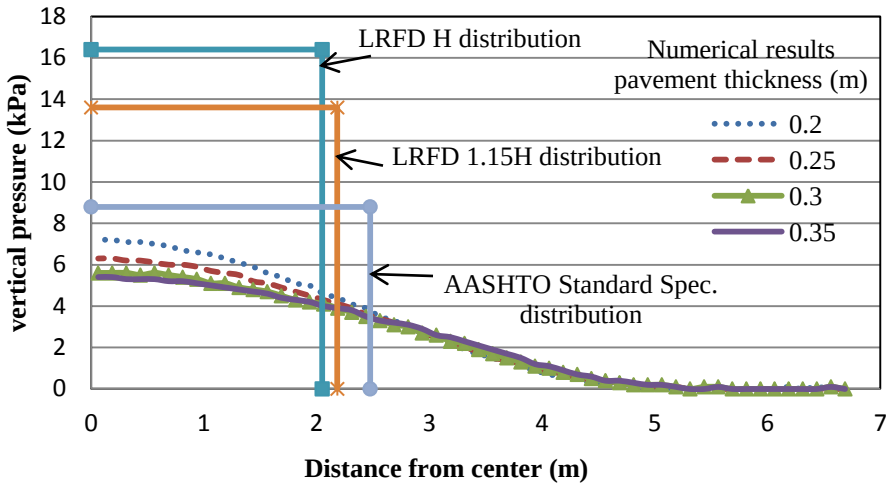

(c) Fill depth = 1.8 m

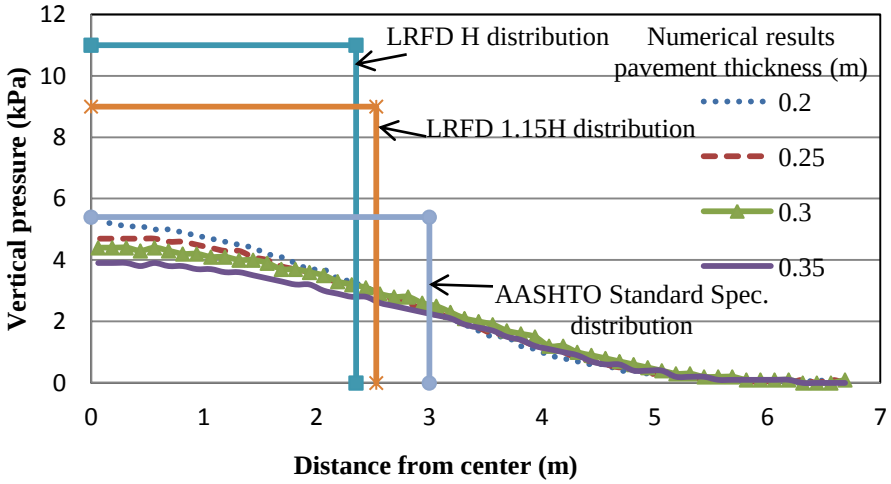

(d) Fill depth = 2.4 m

FIGURE 5.29 Comparison of the calculated pressures by the numerical method and the AASHTO distribution methods for the culvert with the 1.8 m span (continued)

5.5.2 Flexible Pavement

The maximum vertical pressure on the culvert obtained by the numerical method for each case can be compared with the average vertical pressures using the formulae in the AASHTO LRFD code (2007) and AASHTO Standard Specifications (1992). The AASHTO LRFD code suggests two methods for the pressure distribution depending on the type of fill material, i.e., the H distribution and the 1.15 H distribution as discussed in section 2.3.2, in which H is the fill depth. Tables 5.4 to 5.6 show the comparison of the calculated vertical pressures with the LRFD H distribution, the LRFD 1.15 H distribution, and the distribution specified by the AASHTO Standard Specification respectively. Figure 5.30 compares the calculated vertical pressure by the numerical method and the AASTHO distribution methods for the culverts with a span of 1.8 m. Tables 5.4 to 5.6 and Figure 5.30 all show that the AASTHO distribution methods over-predicted the maximum vertical pressure as compared with the numerical method at fill depths up to 1.2 m. However, at higher fill depth, the AASHTO distribution methods predicted the maximum vertical pressure similar to or less than the pressure predicted by numerical method. It is shown that the AASHTO LRFD code calculated the higher vertical pressure than the AASHTO Standard Specification. The difference in the calculated vertical pressures between the numerical method and the AASHTO distribution method decreased with the increase of the fill depth.

TABLE 5.4 Comparison of the calculated vertical pressures by the numerical method and the LRFD H distribution method

Fill depth (m)	Pavement thickness (m)	Max. pressure from numerical method (kPa)			Average pressure by LRFD H distribution (kPa)	Pressure difference (%)		
		Culvert span (m)				Span (m)		
		1.8	3.6	5.4		1.8	3.6	5.4
0.6	0.15	38.12	36.94	36.72	73.5	93	99	100
	0.23	34.05	32.55	32.27	73.5	116	126	128
	0.3	31.69	29.53	29.32	73.5	132	149	151
	0.38	32.7	30	29.93	73.5	125	145	146
1.2	0.15	18	16.4	15.7	27	50	65	72
	0.23	16.4	14.3	13.5	27	65	89	100
	0.3	15.3	12.6	11.49	27	76	114	135
	0.38	14.3	11.2	9.89	27	89	141	173
1.8	0.15	13	11.4	10.7	16.4	26	44	53
	0.23	12.1	10.6	9.5	16.4	36	55	73
	0.3	11.2	9.4	8.3	16.4	46	74	98
	0.38	10.3	8.5	7.3	16.4	59	93	125
2.4	0.15	9.5	8.5	7.5	11	16	29	47
	0.23	9.1	8	7	11	21	38	57
	0.3	8.1	7.1	6	11	36	55	83
	0.38	7.5	6.5	5.3	11	47	69	108

TABLE 5.5 Comparison of the calculated vertical pressures by the numerical method and the LRFD 1.15 H distribution method

Fill depth (m)	Pavement thickness (m)	Max. pressure from numerical method (kPa)			Average pressure by LRFD 1.15 H distribution (kPa)	Pressure difference (%)		
		Culvert span (m)				Span (m)		
		1.8	3.6	5.4		1.8	3.6	5.4
0.6	0.15	38.12	36.94	36.72	61.5	61	66	67
	0.23	34.05	32.55	32.27	61.5	81	89	91
	0.3	31.69	29.53	29.32	61.5	94	108	110
	0.38	32.7	30	29.93	61.5	88	105	105
1.2	0.15	18	16.4	15.7	22.4	24	37	43
	0.23	16.4	14.3	13.5	22.4	37	57	66
	0.3	15.3	12.6	11.49	22.4	46	78	95
	0.38	14.3	11.2	9.89	22.4	57	100	126
1.8	0.15	13	11.4	10.7	13.6	5	19	27
	0.23	12.1	10.6	9.5	13.6	12	28	43
	0.3	11.2	9.4	8.3	13.6	21	45	64
	0.38	10.3	8.5	7.3	13.6	32	60	86
2.4	0.15	9.5	8.5	7.5	9	-5	6	20
	0.23	9.1	8	7	9	-1	13	29
	0.3	8.1	7.1	6	9	11	27	50
	0.38	7.5	6.5	5.3	9	20	38	70

TABLE 5.6 Comparison of the calculated vertical pressures by the numerical method and the AASHTO Standard Specifications

Fill depth (m)	Pavement thickness (m)	Max. pressure from FLAC3D (kPa)			Average pressure by AASHTO Standard Specification (kPa)	Pressure difference (%)		
		Culvert span (m)				Span (m)		
		1.8	3.6	5.4		1.8	3.6	5.4
0.6	0.15	38.12	36.94	36.72	62.4	64	69	70
	0.23	34.05	32.55	32.27	62.4	83	92	93
	0.3	31.69	29.53	29.32	62.4	97	111	113
	0.38	32.7	30	29.93	62.4	91	108	108
1.2	0.15	18	16.4	15.7	16.8	-7	2	7
	0.23	16.4	14.3	13.5	16.8	2	17	24
	0.3	15.3	12.6	11.49	16.8	10	33	46
	0.38	14.3	11.2	9.89	16.8	17	50	70
1.8	0.15	13	11.4	10.7	8.8	-32	-23	-18
	0.23	12.1	10.6	9.5	8.8	-27	-17	-7
	0.3	11.2	9.4	8.3	8.8	-21	-6	6
	0.38	10.3	8.5	7.3	8.8	-15	4	21
2.4	0.15	9.5	8.5	7.5	5.4	-43	-36	-28
	0.23	9.1	8	7	5.4	-41	-33	-23
	0.3	8.1	7.1	6	5.4	-33	-24	-10
	0.38	7.5	6.5	5.3	5.4	-28	-17	2

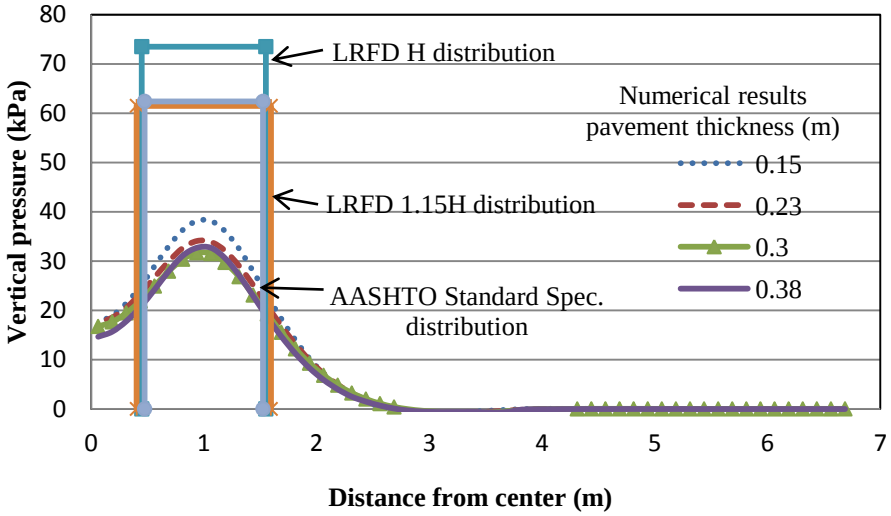

(a) Fill depth = 0.6 m

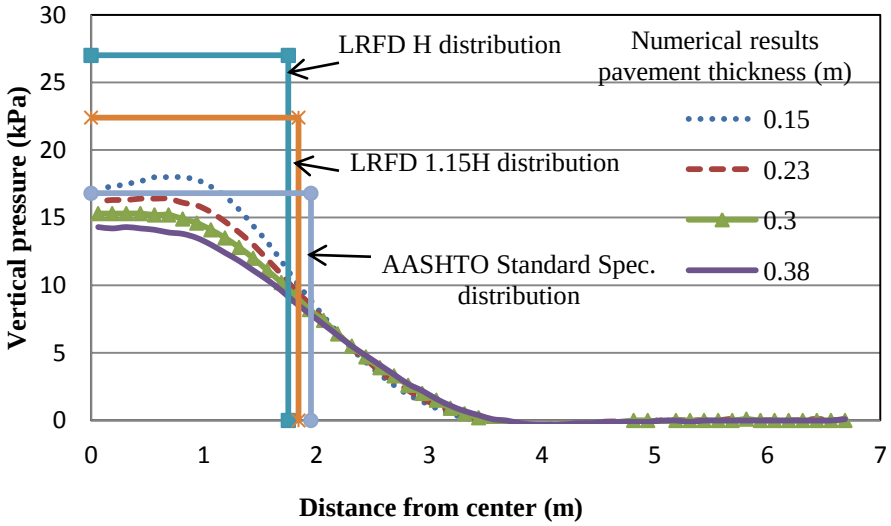

(b) Fill depth = 1.2 m

FIGURE 5.30 Comparison of the calculated pressures by the numerical method and the AASHTO distribution methods for the culvert with the1.8 m span

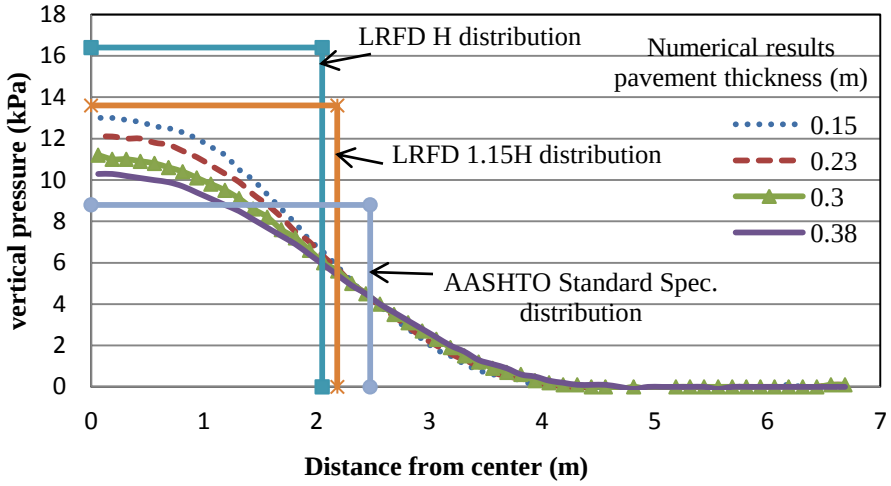

(c) Fill depth = 1.8 m

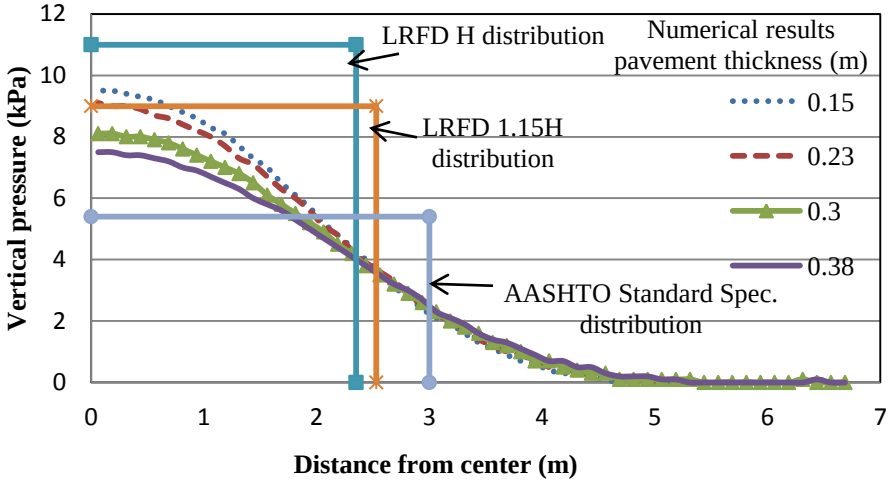

(d) Fill depth = 2.4 m

FIGURE 5.30 Comparison of the calculated pressures by the numerical method and the AASHTO distribution methods for the culvert with the1.8 m span (continued)

5.5.3 Summary

From the comparison of the calculated vertical pressures by the numerical method and the AASHTO distribution methods, the following conclusions can be drawn:

1) The current AASHTO pressure distribution methods are overly conservative for the wheel load distribution on a low-fill box culvert under a rigid pavement. The difference in the calculated vertical pressure decreased with the increase of the fill depth.
2) For the culvert under a flexible pavement, the current AASHTO pressure distribution methods calculated higher vertical pressures than those by the numerical method for the fill depth up to 1.2 m. The difference in the calculated vertical pressures by the numerical method and the AASHTO distribution methods decreased with the increase of the fill depth and became small at the fill depths 1.8 and 2.4 m.
3) At all the fill depths considered, the calculated pressure by the AASHTO LRFD code was higher than that by the AASHTO Standard Specification. At the higher fill depth and the wider span, the calculated pressure by the AASHTO Standard Specification closely matched with that by the numerical method.

Chapter 6 Proposed Simplified Methods for Pressure Distribution

6.1 Introduction

From the parametric study presented in Chapter 5, it became clear that the magnitude of the vertical pressure on the top slab of a low-fill box culvert under pavements (rigid and flexible pavements) due to wheel loads depends on the pavement type, pavement thickness, and fill depth. The current AASHTO LRFD code and Standard Specifications over-predict the vertical pressure on the culvert due to the fact that the effect of the pavement is not considered. Simplified methods were developed in this study to estimate the vertical pressures under rigid and flexible pavements. The development of the simplified methods is presented in this chapter.

6.2 Development of Simplified Methods

6.2.1 Culvert under Rigid Pavement

The fill above the culvert considered in this study consisted of concrete pavement, cement-treated base course, lime treated subgrade, and natural subgrade. Each layer distributes the vertical pressure at a different distribution angle. Giroud and Han (2004) suggested an approximate solution for the vertical pressure distribution angle from a base course to a subgrade based on Burmister's theoretical solution (Burmister, 1958) as follows:

$$tan\alpha_1 = tan\alpha_0 \left[1 + 0.204\left(\frac{E_{bc}}{E_{sg}} - 1\right)\right] \tag{6.1}$$

where α_1= pressure distribution angle in the base course,

α_0 = reference pressure distribution angle for a uniform medium defined by $E_{bc}=E_{sg}$,

E_{bc}= modulus of elasticity of base course,

E_{sg}= modulus of elasticity of subgrade.

In this proposed simplified model the vertical pressure distribution angles from the concrete pavement to the cement-treated base course, from the cement-treated base course to the lime-treated subgrade, and the lime-treated subgrade to the natural subgrade were determined by Equation 6.2, which is a modification of Equation 6.1:

$$tan\alpha_1 = tan\alpha_0 \left[1 + 0.204 \left(\frac{E_1}{E_2} - 1\right)\right] \quad (6.2)$$

where E_1 = elastic modulus of the pavement layer under consideration,

E_2 = elastic modulus of the underlying layer.

The angle, α_0, which is the reference pressure distribution angle for a uniform medium, was taken as 27^o (i.e., 2:1 distribution). The vertical pressure distribution angle from the natural subgrade to the culvert was taken as 27^o too. The elastic moduli used in the calculation of the pressure distribution angles were similar to the elastic moduli used in the parametric study in Chapter 5. Table 6.1 shows the distribution angle calculated based on the simplified model and the elastic modulus of each layer.

TABLE 6.1 Distribution angle for each pavement layers

Pavement layer	E_1 (MPa)	E_2 (MPa)	Distribution angle,α_1 (^{o})
Concrete pavement	24545	5171	42.0
Cement-treated base	5171	310	64.5
Lime-treated subgrade	310	12	71.7

In Table 6.1, the elastic modulus E_2 used for the calculation of the distribution angle in the lime-treated subgrade is the elastic modulus of the natural subgrade, which was 12 MPa. Figure 6.1 shows the schematic of the vertical pressure distribution on the culvert under a rigid pavement. The distributed area is determined by the distribution angle method as shown in Figure 6.1. In Figure 6.1, a represents the length of the rectangular distribution area on the top slab of the culvert along the culvert axis due to a single wheel load and can be determined as follows:

$$a = t_l + 2\left(h_1 \tan\alpha_1 + h_2 \tan\alpha_2 + h_3 \tan\alpha_3 + h_4 \tan\alpha_4\right) \tag{6.3}$$

where a = length of the distributed area by one single wheel load,

t_l = length of the tire footprint,

h_1, h_2, h_3, and h_4 = thicknesses of concrete pavement, cement-treated base, lime-treated subgrade, and natural subgrade, respectively,

α_1, α_2, α_3, and α_4 = distribution angles between concrete pavement, cement-treated base, lime-treated subgrade, and natural subgrade.

Since there are the same distributions in the perpendicular direction to the culvert axis, the width of the distributed area in the perpendicular direction is a - (t_l – t_w), where t_w is the width of the tire footprint. The length of the combined distribution area by the two wheel loads can be determined as follows:

$$b = a + s \tag{6.4}$$

where b = length of the combined distribution area,

s = spacing of the two wheel loads.

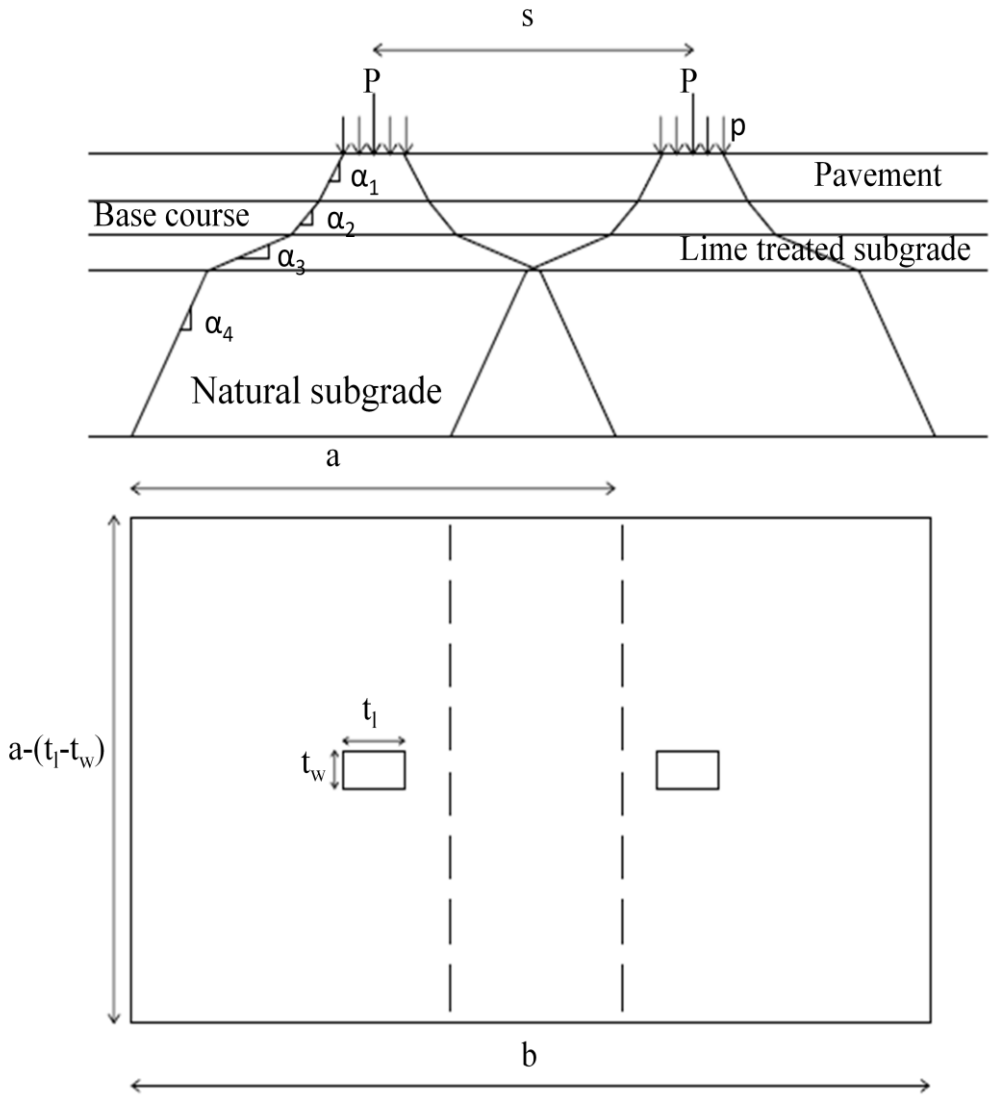

FIGURE 6.1 Vertical pressure distribution under a rigid pavement

Considering the rigidity of the concrete slab, the slab is assumed to act as a rigid foundation to carry the applied loads and distribute a uniform vertical pressure onto the culvert. The magnitude of the pressure can be determined by dividing the total loads from both wheels by the total distribution area as follows:

$$p_c = \frac{2P}{b(a - t_1 + t_w)} \tag{6.5}$$

where p_c = distributed pressure on the top of the culvert.

Therefore, the proposed distribution model distributes the vertical pressure wheel loads on the top slab of a low-fill box culvert under rigid pavement as shown in Figure 6.2.

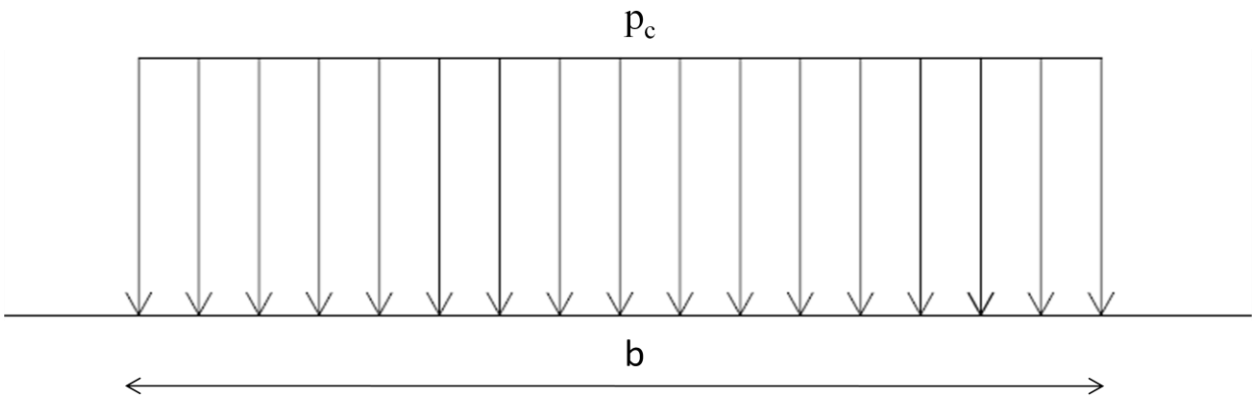

FIGURE 6.2 Distributed pressure on the top slab of the culvert under a rigid pavement

6.2.2 Culvert under Flexible Pavement

The fill above the culvert considered in this study consisted of asphalt pavement, lime treated subgrade, and natural subgrade. Each layer distributes the vertical pressure at a different distribution angle. In this proposed simplified model the vertical pressure distribution angles from the asphalt pavement to the lime-treated subgrade, and the lime-treated subgrade to the natural subgrade were determined by Equation 6.2. The angle, α_0, which is the reference pressure distribution angle for a uniform medium, was taken as 27^o (i.e., 2:1 distribution). The vertical pressure distribution angle from the natural subgrade to the culvert was taken as 27^o too. The elastic moduli used in the calculation of the pressure distribution angles were similar to the

elastic moduli used in the parametric study in Chapter 5. Table 6.2 shows the distribution angle calculated based on the simplified model and the elastic modulus of each layer.

TABLE 6.2 Distribution angle for each pavement layers

Pavement layer	E_1 (MPa)	E_2 (MPa)	Distribution angle,α_1 (^{o})
Asphalt concrete	1827	310	45
Lime-treated subgrade	310	12	71.7

In Table 6.2, the elastic modulus E_2 used for the calculation of the distribution angle in the lime-treated subgrade is the elastic modulus of the natural subgrade, which was 12 MPa. Figure 6.3 shows the schematic of the vertical pressure distribution on the culvert under a flexible pavement. The distributed area is determined by the distribution angle method as shown in Figure 6.3. In Figure 6.3, a represents the length of the rectangular distribution area on the top slab of the culvert along the culvert axis due to a single wheel load and can be determined as follows:

$$a = t_l + 2\left(h_1 \tan\alpha_1 + h_2 \tan\alpha_2 + h_3 \tan\alpha_3\right) \tag{6.6}$$

where a = length of the distributed area by one single wheel load,

t_l = length of the tire footprint,

h_1, h_2, and h_3 = thicknesses of asphalt pavement, lime-treated subgrade, and natural subgrade, respectively,

α_1, α_2, and α_3 = distribution angles between asphalt pavement, lime-treated subgrade, and natural subgrade.

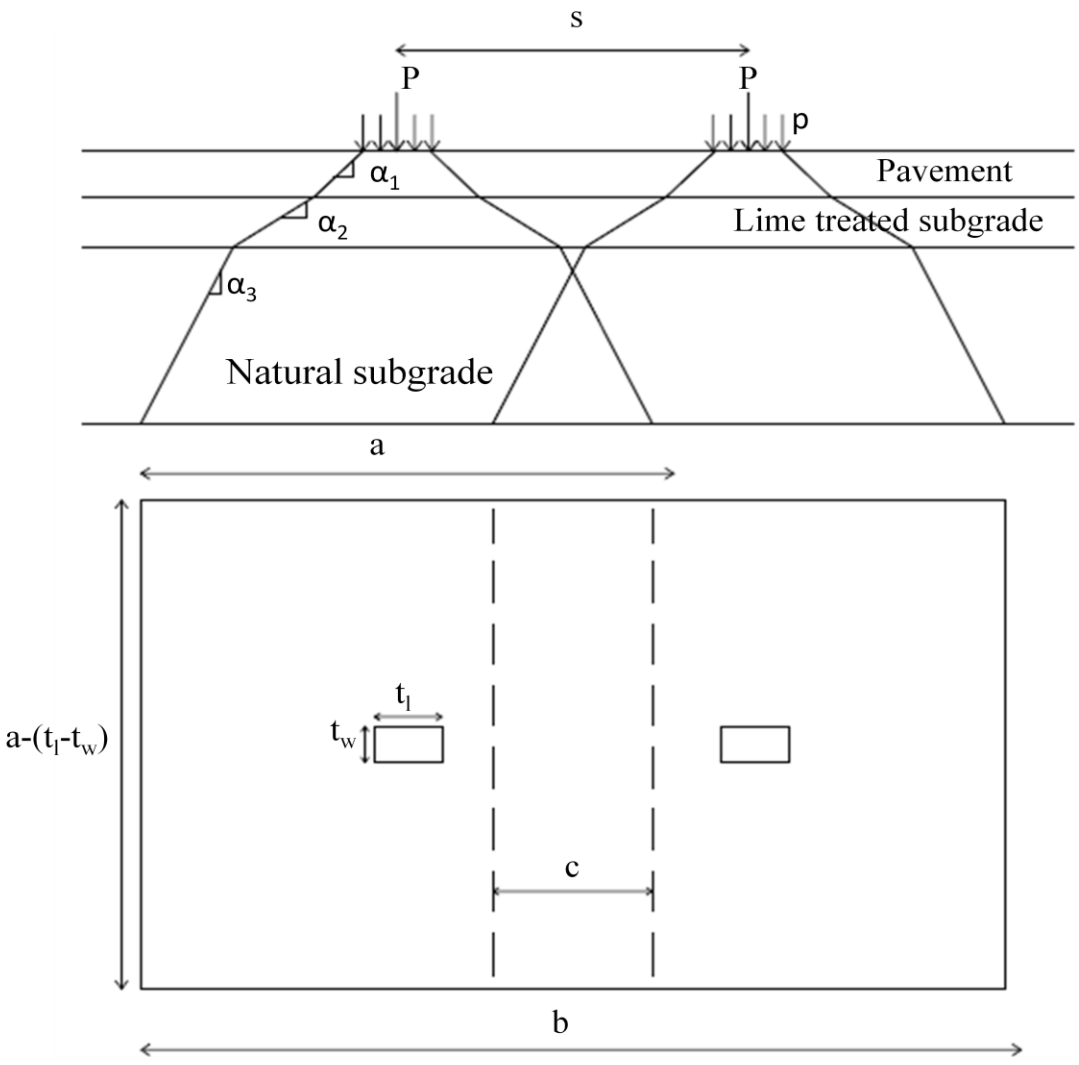

FIGURE 6.3 Vertical pressure distribution through flexible pavement layers

Considering the flexibility of the asphalt surface layer, the surface layer is assumed to carry the applied wheel loads and distribute a uniform vertical pressure independently onto the culvert. The uniform vertical pressure is

$$p_{c1} = \frac{P}{a(a - t_l + t_w)} \tag{6.7}$$

where p_{c1} = distributed vertical pressure by an individual wheel load.

Within the overlapped area, the vertical pressure on the top slab of the culvert can be determined using the superposition of the pressures due to two individual wheels, i.e.,

$$p_{c2} = 2p_{c1} \tag{6.8}$$

where p_{c2} = distributed vertical pressure within the overlapped area. The overlapped length is

$$c = \frac{2a - b}{2} = \frac{a - s}{2} \tag{6.9}$$

where c = overlapped length of the distributed areas by two wheel loads.

Therefore, the proposed pressure distribution model for the two wheel loads on the flexible pavement over the top slab of a low-fill box culvert is shown in Figure 6.4.

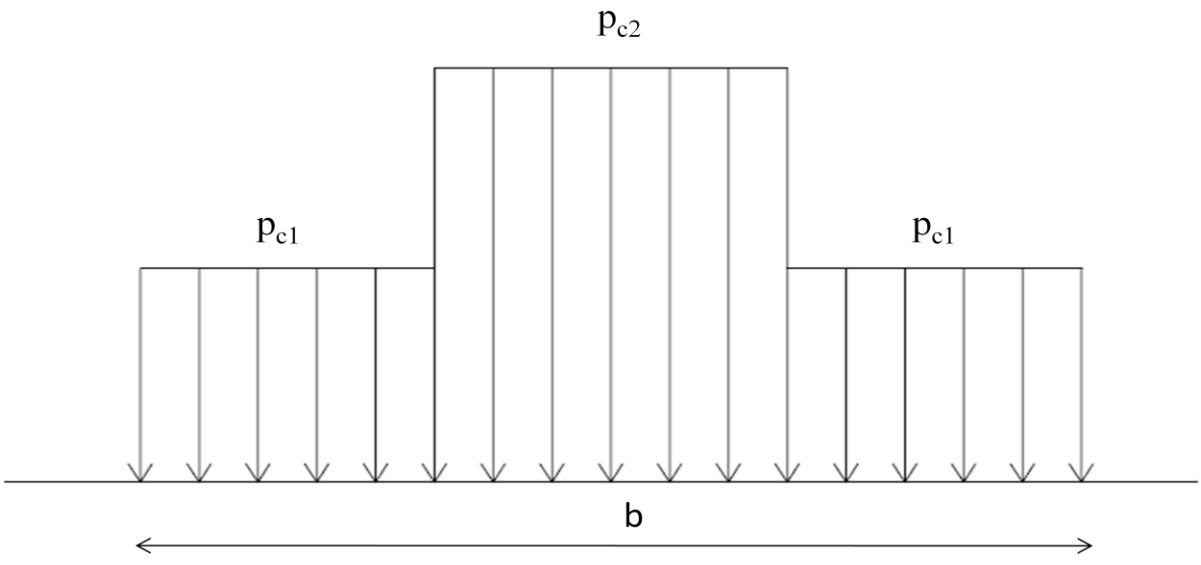

FIGURE 6.4 Distributed pressure on the top slab of the culvert under a flexible pavement

6.3 Comparison of Calculated Vertical Pressures

6.3.1 Culvert under Rigid Pavement

The average pressure on the culvert under a rigid pavement was calculated using the simplified distribution method described in Section 6.2.1. The calculated pressure can be compared with the maximum pressure computed by the numerical model as discussed in Chapter 5. As discussed in Chapter 5, the maximum vertical pressure on the culvert in the small span (1.8 m) was higher than those in the large span (3.6 m and 5.4 m) with the same top culvert slab thickness. Within the increase of the top slab thickness, the maximum vertical pressure on the culvert in the large span approached to that of the small span. Therefore, it is conservative to compare the maximum vertical pressure calculated by the numerical method based on the culvert with a small span. Table 6.3 shows the vertical pressures calculated by the proposed simplified method and the numerical model for the 1.8 m span. Clearly, the vertical pressures calculated by the proposed simplified method match those by the numerical method well. The distribution methods in the AASHTO LRFD code and Standard Specifications significantly overestimated the maximum pressures especially on the culverts with fill depths less than 1.2 m. The difference became smaller when the fill depth increased.

TABLE 6.3 Pressure from simplified and numerical method

Fill depth (m)	Pavement thickness (m)	Vertical pressure (kPa)			
		Numerical method	Simplified method	AASHTO LRFD H distribution	AASHTO standard specification distribution
0.6	0.2	16.4	15.9	62.4	73.5
	0.25	15.4	15.5	62.4	73.5
	0.3	14.61	15.0	62.4	73.5
	0.35	16.9	14.6	62.4	73.5
1.2	0.2	10.9	10.7	16.8	27
	0.25	9.6	10.5	16.8	27
	0.3	8.6	10.2	16.8	27
	0.35	8	10.0	16.8	27
1.8	0.2	7.2	7.7	8.8	16.4
	0.25	6.3	7.6	8.8	16.4
	0.3	5.6	7.5	8.8	16.4
	0.35	5.4	7.3	8.8	16.4
2.4	0.2	5.2	5.9	5.4	11
	0.25	4.7	5.8	5.4	11
	0.3	4.4	5.7	5.4	11
	0.35	3.9	5.6	5.4	11

6.3.2 Culvert under Flexible Pavement

Pressure on the culvert under flexible pavement was calculated using the simplified distribution method described in Section 6.2.2. The calculated pressure was then compared with the maximum pressure magnitude calculated from FLAC3D numerical model. Table 6.4 shows the pressure distribution from proposed simplified method closely predicted the pressure calculated from FLAC3D numerical model. The estimated pressure using the simplified method is very close to the pressure calculated from the FLAC3D numerical model for span 1.8 m and relatively higher for span 3.6 m and 5.4 m. It is also because of the decreased stiffness of the top slab of the culvert used in the FLAC3D at higher spans. The reason for decreased pressure at higher

span is described in Section 6.3.1 for culvert under rigid pavement. This is also true for the culvert under flexible pavement. Therefore, the proposed simplified method can also be used to predict the pressure for culverts under flexible pavement with span greater than 1.8 m.

TABLE 6.4 Pressure from simplified and numerical method

Fill depth (m)	Pavement thickness (m)	Vertical pressure (kPa)			
		Numerical method	Simplified method	AASHTO LRFD H distribution	AASHTO standard specification distribution
0.6	0.2	38.1	38.8	62.4	73.5
	0.25	34.1	35.7	62.4	73.5
	0.3	31.7	33.3	62.4	73.5
	0.35	32.7	30.9	62.4	73.5
1.2	0.2	18.0	22.1	16.8	27.0
	0.25	16.4	20.7	16.8	27.0
	0.3	15.3	19.7	16.8	27.0
	0.35	14.3	18.6	16.8	27.0
1.8	0.2	13.0	14.2	8.8	16.4
	0.25	12.1	13.5	8.8	16.4
	0.3	11.2	13.0	8.8	16.4
	0.35	10.3	12.4	8.8	16.4
2.4	0.2	9.5	9.9	5.4	11.0
	0.25	9.1	9.5	5.4	11.0
	0.3	8.1	9.2	5.4	11.0
	0.35	7.5	8.8	5.4	11.0

6.4 Summary

Simplified methods were developed in this study to predict the vertical pressure on a culvert under a rigid or flexible pavement. Three conclusions can be drawn from this development:

1) In the case of the culvert under a rigid pavement, the total wheel load can be distributed uniformly over the combined area with the extremities of the areas by individual wheels.

The calculated vertical pressures by the simplified method were in good agreement with the maximum vertical pressure by the numerical method.

2) In the case of the culvert under a flexible pavement, the vertical pressure within the overlapped area can be obtained by the superposition of the pressures due to individual wheels. The calculated vertical pressures by the simplified method were in good agreement with the maximum vertical pressure by the numerical method.
3) The distribution methods in the AASHTO LRFD code and Standard Specifications significantly overestimated the maximum pressures especially on the culverts with fill depths less than 1.2 m if a rigid or flexible pavement existed.

Chapter 7 Conclusions and Recommendations

This chapter summarizes the research work carried out in this study, draws the conclusions based on the experimental and numerical results, and makes recommendations for future research.

7.1 Summary of Research Work

This research addressed the improved load distribution for low-fill box structures under rigid and flexible pavements. The objective and scope of this study were outlined in Chapter 1. Chapter 2 included a comprehensive literature review of the research work relevant to this study along with the classification of box culverts, description and requirements of load rating methods and its requirements and constitutive models for geomaterials.

The load distribution on the top slab of the culvert depends largely on the depth of fill above the culvert, the type and the thickness of the pavement (rigid or flexible) over the culvert, and the span of the culvert. Therefore, this study was focused on the effect of pavements on the distribution of the wheel load over the top slab of the culvert.

Chapter 3 reported two flied tests carried out on the culverts under rigid and flexible pavements. The culverts were subjected to static and moving traffic loadings. The deflections of the top slabs of the culverts were monitored during both tests. Earth pressures were monitored in an unsurfaced section under static loading. Laboratory tests were carried to determine the properties of the pavement layers including the concrete, asphalt, base, and subgrade, and backfill soil obtained from the field. The culvert responses and material properties were used to validate the numerical model created in FLAC3D in Chapter 4.

Chapter 5 presents a parametric study carried out to investigate the effects of different influence factors (i.e., type of pavement, pavement thickness, depth of fill, and culvert span) on the pressure distribution. The material properties used in the parametric study were similar to those used in the validation of the models in Chapter 4. The pressure distribution over the top slab of the culvert due to a wheel load was monitored along the culvert axis and perpendicular to the culvert axis. In addition, the pressure distribution obtained from the numerical method was compared with that in the current AASHTO guidelines. In Chapter 6, simplified methods were developed to estimate the vertical pressures under rigid and flexible pavements.

7.2 Conclusions of Research

7.2.2 Culvert under Rigid Pavement

The following conclusions can be drawn from the parametric study carried out to investigate the distribution of the wheel load on the culvert under a rigid pavement considering the influence of pavement thickness, fill depth, and span of the culvert.

1) The magnitude of vertical pressure on the top slab of the culvert gradually decreased as the pavement thickness increased due to the distribution of the wheel load over a wider area.
2) The magnitude of vertical pressure decreased gradually with an increase of the fill depth over the culvert. The rate of pressure reduction with the fill depth was higher at a small fill depth. The effect of the traffic load on the culvert was higher at a low fill depth and gradually decreased with an increase of the fill depth.
3) The distribution of the vertical pressure at the fill depth of 0.6 m was characterized by a peak pressure under the wheel load and the pressure in the middle of the axle was smaller

than the peak pressure. Under such a fill depth, there was little interaction between the distributed pressures by wheel loads. However, when the fill depth was increased to 1.2 m and greater, the peak pressure was located in the middle of the axle. The interaction between the distributed pressures by wheel loads was developed at the fill depth of 1.2 m and greater.

4) The vertical pressure on the top slab of the culvert decreased with the increase of the culvert span. The influence of the span was more at a lower fill depth. The rate of change in the vertical pressure on the top slab of the culvert with the span decreased with the increase of the culvert span. The increase of the slab thickness increased the maximum vertical pressure on the culvert.
5) The current AASHTO guidelines for the pressure distribution are overly conservative for a wheel load on a low-fill box culvert under a rigid pavement. The current AASHTO guidelines estimated much higher pressure than that obtained by the numerical method down to a fill depth of 1.2 m. The AASHTO guidelines are still conservative for a rigid pavement with fill depths of 1.8 and 2.4 m. However, their difference decreased with an increase of the fill depth. Therefore, the wheel load distribution used by the AASHTO guidelines in load rating of a culvert under a rigid pavement would give a lower rating factor since the pressure distribution is conservative. The rating factor of a low-fill culvert can be significantly increased if the effect of the rigid pavement is considered in load rating.
6) At all fill depths considered, the pressure distribution from the AASHTO LRFD code (2007) was higher than that from the AASHTO Standard Specification (1992). At a

higher fill depth and a wider span, the pressure distribution from the AASHTO Standard Specification closely matched that from the numerical method.

7) In the case of the culvert under a rigid pavement, the total wheel load can be distributed uniformly over the combined area with the extremities of the areas by individual wheels. The calculated vertical pressures by the simplified method were in good agreement with the maximum vertical pressure by the numerical method.

7.2.3 Culvert under Flexible Pavement

The following conclusions can be drawn from the parametric analysis carried out to study the distribution of the wheel load on the culvert under flexible pavement under the influence of pavement thickness, fill depth, and span of the culvert.

1) The magnitude of vertical pressure on the top slab of the culvert gradually decreased as the pavement thickness increased due to the distribution of the wheel load over a wider area.
2) The magnitude of vertical pressure decreased gradually with an increase of the fill depth over the culvert. The rate of pressure reduction with the fill depth was higher at a small fill depth. The effect of the traffic load on the culvert was higher at a low fill depth and gradually decreased with an increase of the fill depth.
3) The distribution of the vertical pressure at the fill depth of 0.6 m was characterized by a peak pressure under the wheel load and the pressure in the middle of the axle was smaller than the peak pressure. Under such a fill depth, there was little interaction between the distributed pressures by wheel loads. However, when the fill depth was increased to 1.2 m and greater, the peak pressure was located in the middle of the axle. The interaction

between the distributed pressures by wheel loads was developed at the fill depth of 1.2 m and greater.

4) The vertical pressure on the top slab of the culvert decreased with the increase of the culvert span. The influence of the span was more at a lower fill depth. The rate of change in the vertical pressure on the top slab of the culvert with the span decreased with the increase of the culvert span.

5) For the culvert under a flexible pavement, the current AASHTO pressure distribution methods calculated higher vertical pressures than those by the numerical method for the fill depth up to 1.2 m. The difference in the calculated vertical pressures by the numerical method and the AASHTO distribution methods decreased with the increase of the fill depth and became small at the fill depths 1.8 and 2.4 m. Therefore, the wheel load distribution used by the AASHTO guidelines in load rating of a culvert under a flexible pavement would give a lower rating factor since the pressure distribution is conservative. The rating factor of a low-fill culvert can be increased if the effect of the flexible pavement is considered in load rating.

6) At all fill depths considered, the pressure distribution from the AASHTO LRFD code (2007) was higher than that from the AASHTO Standard Specification (1992). At a higher fill depth and a wider span, the pressure distribution from the AASHTO Standard Specification closely matched that from the numerical method.

7) In the case of the culvert under a flexible pavement, the vertical pressure within the overlapped area can be obtained by the superposition of the pressures due to individual wheels. The calculated vertical pressures by the simplified method were in good agreement with the maximum vertical pressure by the numerical method.

7.3 Future research

This research investigated the effect of the pavement type (rigid or flexible), pavement thickness, fill depth, and span on the load distribution for load rating of low-fill box structures. Future research is needed to address the following issues:

1) Field tests needed to be carried out by installing pressure cells under the pavement section to study the effect of the pavement on the pressure distribution on the top of the culvert. The field data will help verify the numerical results obtained in this research.
2) The numerical analysis done in this study was only on single-cell culverts. The effect of multiple cells should be investigated in the future.
3) The elastic moduli of the pavement layers and the backfill soil were kept constant. A future study is needed to evaluate the effects of the elastic moduli of the pavement layers and the backfill soil.
4) In this study soil was modeled as an elastic material. An advanced soil model may be used to verify the numerical results obtained in this study.
5) This study was carried out by assuming the unyielding foundation condition. A future study is needed to study the effect of a yielding foundation on the pressure distribution on culverts.

References

Abdel-Karim, A. M., Tadros, M. K., and Benak, A. J. (1993). "Structural response of full-scale concrete box culvert." *Journal of Structural Engineering*, 119(11), 3238-3254.

American Association of State Highway Officials (AASHO). (1949). *Standard specifications for highway bridges*, Washington DC.

American Association of State Highway Officials (AASHO). (1993). *Guide for design of pavement structures*, Washington DC.

American Association of State Highway and Transportation Officials (AASHTO). (1992). *Standard specifications for highway bridges*, Washington DC.

American Association of State Highway and Transportation Officials (AASHTO). (2007). *AASHTO LRFD bridge design specifications*, Washington DC.

American Association of State Highway and Transportation Officials (AASHTO). (2011). *The manual for bridge evaluation*, Washington DC.

American Society for Testing and Materials (ASTM D854). (2010). *Standard test method for specific gravity of soil solids by water pycnometer*.

American Society for Testing and Materials (ASTM D4318). (2005). *Standard test methods for liquid limit, plastic limit, and plasticity index of soils.*

American Society for Testing and Materials (ASTM D4767). (2011). *Standard test method for consolidated undrained triaxial compression test for cohesive soils.*

American Concrete Institute (ACI). (2011). *Building code requirements for structural concrete, ACI 318.*

Awwad, E. E. (2000). "Finite element analysis of concrete box culverts." *Computing in Civil and Building Engineering, Proceedings of the Eight International Conference, ASCE,* 1051-1053.

Bennett, R.M., Wood, S.M., Drumm E.C., and Rainwater, N.R. (2005). "Vertical loads on concrete box culverts under high embankments." *Journal of Bridge Engineering,* 10(6), 643-649.

Bloomquist, D.G., and Gutz, A.J. (2002). "Design live loads on box structures." *Report No. BC 354, RPWO # 47-Part 2,* University of Florida, 83p.

Burmister, D.M. (1958). "Evaluation of pavement systems of the WASHO road test by layered system method," *Bulletin 177,* Highway Research Board, 26-54.

Chajes, M.J., and Shenton III, H.W. (2005). "Using diagnostic load tests for accurate load rating of typical bridges." *Metropolis and Beyond Proceedings of the 2005 Structures Congress and the 2005 Forensic Engineering Symposium*, New York, 1-11

Dasgupta, A., and Sengupta, B. (1991). "Large-scale model test on square box culvert backfilled with sand." *Journal of Geotechnical Engineering,* 117(1), 156-161.

Delaware Department of Transportation. (2005). *Bridge design manual*.

Federal Highway Administration (FHWA). (1995). "Recording and coding guide for the structure inventory and appraisal of the nation's bridges." *Report No.FHWA-PD-96-001,* Washington DC, 78p.

Fernando, N.S.M., and Carter, J.P. (1998). "Elastic analysis of buried pipes under surface patch loadings." *Journal of Geotechnical and Geoenvironmental Engineering,* 124(8), 720-728.

Gardner, M. P., and Jeyapalan, J. K. (1982). "Preliminary analysis of the behavior of reinforced concrete box culverts." Report No. *FHWA/TX-82/50+326-1,* Texas Transportation Institute (TTI), Arlington, Texas 157p.

Giroud, J.P. and Han, J. (2004). "Design method for geogrid-reinforced unpaved roads, Part I theoretical development." *ASCE Journal of Geotechnical and Geoenvironmental Engineering,* 130(8), 776-786.

Iowa Department of Transportation, Office of Bridges and Structures. (2005). *Bridge design manual.*

Jaramilla, B., and Huo, S. (2005). "Looking to load and resistance factor rating." *FHWA-HRT-05-006,* Federal Highway Administration (FHWA), Public Roads, Jul/Aug, 69(1), 65p.

Kang, J., Parker, F., Kang, Y., and Yoo, C.H. (2008). "Effects of frictional forces acting on sidewalls of buried box culverts." *International Journal for Numerical and Analytical Methods in Geomechanics,* 32(3), 289–306.

Kansas Department of Transportation. (2011). *Design manual,* Volume III - Bridge section.

Katona, M. G., and Vittes, P. D. (1982). "Soil-structure analysis and evaluation of buried box-culvert designs." *Transportation Research Record,* 878, Transportation Research Board, Washington DC, 1-7.

Kim, K., and Yoo, C. H. (2005). "Design loading on deeply buried box culverts." *Journal of Geotechnical and Geoenvironmental Eng.,*131(1), 20-27.

Lade, P.V. (2005). "Overview of constitutive models for soils." *Geo-Frontiers 2005 Congress, Calibration of Constitutive Models (GSP 139),* Austin, Texas, USA, 1-34.

Lawson, W. D., Wood, T. A., Newhouse, C. D., and Jayawcikrama, P. W. (2009). *Culvert rating guide,* Texas Department of Transportation.

Lawson, W. D., Wood, T. A., Newhouse, C. D., and Jayawcikrama, P. W. (2010). "Evaluating existing culverts for load capacity allowing for soil-structure interaction." *Report No. 0-5849-1,* Texas Department of Transportation, 303p.

McGrath, T. J., Liepins, A. A., and Beaver J. L. (2005). "Live load distribution widths for reinforced concrete box sections." *Transportation Research Record,* Transportation Research Board, Washington, DC, 99–108.

Moore, I.D., and Brachman, R.W. (1994). "Three-dimensional analysis of flexible circular culverts." *Journal of Geotechnical Engineering,* 120(10), 1829-1844.

National Cooperative Highway Research Program (NCHRP). (2011). "A comparison of AASHTO bridge load rating methods." *Report No. 700,* Transportation Research Board, Washington DC, 93p.

National Cooperative Highway Research Program (NCHRP) (2010). "Recommended design specifications for live load distribution to buried structures." *Report No. 647,* Transportation Research Board, Washington DC,75p.

Oswald, C. J. (1996). "Analysis of reinforced concrete culvert considering concrete creep and shrinkage." *Transportation Research Record,*1541, Transportation Research Board, Washington DC, 120-126.

Pang, S., Fernando, N.S.M., and Carter, J.P. (1998). "Elastic analysis of buried pipes under surface patch loadings." *Journal of Geotechnical and Geoenvironmental Engineering,* 125(12), 1104-1105.

Rund, R. E., and McGrath, T. J. (2000). "Comparison of AASHTO standard and LRFD code provisions for buried concrete box culverts." *ASTM special publication,* http://books.google.com/books.

Sandford, T. C. (2010). "Soil-structure interaction of buried structures."*A2K04: Committee on Subsurface Soil-Structure Interaction,* University of Maine, 6p.

Schulz, J.L, Commander, B., Goble, G.G, and Frangopol D.M. (1995). "Efficient field testing and load rating of short-and medium-span bridges." *Structural Engineering Review,* 7(3), 181-194.

Seling, E.T. (1988). "Soil parameters for design of buried pipelines." *Pipeline Infrastructure: Proceedings of the Conference,* Boston, Massachusetts, 99-116.

Shivakumar, B. (1999). "Load rating and permit review using load and resistance factor philosophy." *Structural Engineering in the 21st Century: Proceedings of The 1999 Structures Congress*, 288-291.

Sun, L., Hopkins, T.C., and Beckham, T. L. (2011). "Long-term monitoring of culvert load reduction using an imperfect ditch backfilled with geofoam." *Transportation Research Record,* 2212, 56-64.

Sidney, M., Young, J.F., and Darwin, D. (2003). *Concrete*, 2nd edition, Prentice Hall, 644p.

Tadros, M.K. (1986). "Cost-effective concrete box culvert design." *Research report*, FHWA, Nebraska Department of Roads and Nebraska University, 422p.

Tadros, M. K., Benak, J. V., and Gilliland, M. K. (1987). "Soil pressure on box culverts." *ACI Structural Journal*, 86 (4), 439-450.

Tadros, M. K., and Benak, J. V. (1990)."Load distribution on box culverts." *Report No. NE-DOR-R 89-1,* FHWA, Nebraska Department of Roads and Nebraska University, 232p.

Vaslestad, J., Johansen, T. H., and Holm, W. (1993). "Load reduction on rigid culverts beneath high fills: long-term behavior." *Transportation Research Record,* 1415, Transportation Research Board, Washington DC, 58-68.

Yang, M. Z. (1997). "Influence of compaction effort on earth pressure on a box culvert." *9th International Conference on the Assoc. for Computer Methods and Advances in Geomechanics*, Wuhan, China, 2021-2026.

Yang, M. Z. (1999). "Measurement of earth pressures on concrete box culverts under highway embankments." *Proceedings of the 1998 Field Instrumentation for Soil and Rock*, 87-100.

Yoo, C.H., Parker, F., and Kang J. (2005). "Bedding and fill heights for concrete roadway pipe and box culverts." *Research report,* Highway Research Center, Auburn University, Alabama, 245p.

Yost, J. R., Schulz, J.L., and Commander, B.C. (2005). "Using NDT data for finite element model calibration and load rating of bridges." *Metropolis and Beyond Proceedings of the 2005 Structures Congress and the 2005 Forensic Engineering Symposium,* New York, 21-29.